STUDIES IN PHOTOIONISATION

by

John Paul Maier

A thesis presented for

the degree of

Doctor of Philosophy

at the

University of Oxford

Faculty of Physical Sciences

Balliol College,
Oxford.

BODLEIAN LIBRARY OXFORD
DEPOSITED
THESIS
2·5·73

November, 1972.

ABSTRACT

The studies in photoionisation in molecules presented in this thesis were accomplished by the technique of Photoelectron Spectroscopy. The gaseous molecules are irradiated by photons of discreet energy ($h\nu$), sufficient to eject electrons, and through the analysis of the kinetic energies (E_n) of the photoelectrons the ionisation energies (I_n) can be determined from Einstein's photoelectric equation

$$E_n = h\nu - I_n$$

Ionisation phenomena and the means of relating the information to electronic structure and dimensional changes are discussed. The techniques used to study electronic processes in the vacuum ultra-violet are outlined and the advantages, limitations in the experimental aspects and interpretation of data compared. The features of significance in photoelectron spectroscopy are discussed both from the theoretical and experimental viewpoint. The instrumental development since the initial work in the early sixties is reviewed and the experimental criteria outlined. The modifications carried out in conjunction with this work and the experimental details are presented.

In the lowest ionisation process in phosphine and phosphorous trifluoride an extensive vibrational progression is discernible. The sufficiently high quality data allows a detailed discussion of the geometry of these ions, barriers to inversion and potential functions. The analysis suggests that the ground ionic state of phosphorous trifluoride is very probably strictly planar, while that of phosphine is pyramidal with a very small barrier to inversion. The higher ionisation energies are discussed in view of the spectral detail and a molecular orbital scheme.

In the study of steric inhibition of resonance in substituted benzenes, it is shown that through the correlation of Π-energy levels in series of related molecules, electronic and steric effects can be separated and the relative importance of the latter estimated.

In biphenyls an empirical correlation between certain bands in the spectra and dihedral angle is noted and its use in conformational studies emphasised.

The variation of the photoelectron Π-ionisation energies in biphenyls, phenyl ethylenes, anilines, phenols and related molecules is rationalised on a semi-quantitative basis by a Hückel-type theory based on the interaction of semi-localised Π-MOs. The dihedral angles in sterically hindered, or rigidly held, phenyl ethylenes and anilines can then be inferred. The validity of the semi-empirical treatment is demonstrated by the success in reproducing the photoelectron data.

Discussion of the Franck-Condon envelopes gives support to the assignment of the Π-MOs, indicating geometrical changes. In the anilines the deduction is that nitrogen is non-planar.

Features of interest in the individual molecules are also discussed. Correlation diagrams are used extensively to illustrate the trends, choice of basis set parameters, and to summarise the assignments.

ACKNOWLEDGEMENTS

I wish to thank Dr. D.W. Turner for his supervision, encouragement and especially for many stimulating discussions throughout.

I also wish to thank Professor R.E. Richards, F.R.S. and Professor F.S. Dainton, F.R.S. for research facilities in the Physical Chemistry Laboratory, Oxford, and finally the Science Research Council for a Research Studentship.

TABLE OF CONTENTS

		page
Acknowledgements		2
Publications		6
Introduction		7
CHAPTER I	IONISATION PHENOMENA	9
1.1	Ionisation and Electronic Structure	9
1.2	Franck-Condon Principle	12
1.3	Correlation of Band Shapes, Vibrational Frequency Changes and Bonding Character	13
1.4	Dissociative Ionisations	17
1.5	Autoionisation	18
1.6	Double Ionisation	18
1.7	Absorption Spectroscopy in the Vacuum U.V.	19
1.8	Electron Impact Techniques	20
1.9	Photon Impact Techniques	24
1.10	Penning Ionisation	26
1.11	Positive Ion Impact	28
1.12	Photoelectron Spectroscopy	29
1.13	Ion Fluorescence	31
1.14	X-ray Photoelectron Spectroscopy	33
1.15	Auger and X-ray Emission Spectroscopy	34
CHAPTER II	PRINCIPAL FEATURES OF PHOTOELECTRON SPECTROSCOPY	37
2.1	Photoionisation Cross-Sections	37
2.2	Angular Distribution of Photoelectrons	40
2.3	Autoionisation	44
2.4	Forbidden Processes	47
2.5	Franck-Condon Factors and Vibrational Fine Structure	48
2.6	Structureless Bands	50
2.7	Vibronic and Spin-Orbit Structure	50

page

2.8 Multiplet Splitting 52

2.9 Predissociation 53

2.10 Interpretation of P.E. Spectra 55

CHAPTER III EXPERIMENTAL AND INSTRUMENTATION 56

3.1 Vacuum System 56

3.2 Light Sources 58

3.3 Electron Energy Analysers 61

3.4 Detection, Recording and Calibration of Photoelectrons 68

3.5 Experimental Details Associated with Chapters IV-VII 69

RESULTS AND DISCUSSION 71

CHAPTER IV PHOSPHINE AND PHOSPHOROUS TRIFLUORIDE MOLECULAR IONS 72

4.1 Ground States of the Phosphine and Phosphorous Trifluoride Ions... $^2A_1$ 72

4.2 First Excited State of the Phosphine Ion... ^2E 81

4.3 Higher Ionisation Potentials of Phosphorous Trifluoride 83

CHAPTER V BIPHENYLS 88

5.1 Introductory Remarks on Chapters V-VII 88

5.2 Outline of Related Studies on Biphenyls 88

5.3 Results 89

5.4 Discussion 92

5.5 Discussion of Individual Cases 114

CHAPTER VI PHENYL ETHYLENES 125

6.1 Outline of Related Studies 125

6.2 Results 127

6.3 Discussion 136

		page
CHAPTER VII	ANILINES, PHENOLS AND RELATED COMPOUNDS	146
7.1	Outline of Related Studies	146
7.2	Results	147
7.3	Discussion	158
7.4	Concluding Remarks on Chapters V-VII	165
APPENDIX		166
REFERENCES		169

PUBLICATIONS

Most of the work reported in this thesis is also included in the following papers:-

"Photoelectron Spectroscopy and the Geometry of the Phosphine and Phosphorous Trifluoride Molecular Ions" by J.P. Maier and D.W. Turner, J.C.S. Faraday II, 1972, 68, 711.

"Some Physical and Analytical Topics in Photoelectron Spectroscopy" by J. Daintith, R. Dinsdale, J.P. Maier, D.A. Sweigart and D.W. Turner, Molecular Spectroscopy, Institute of Petroleum, 1971.

"Steric Inhibition of Resonance Studied by Molecular Photoelectron Spectroscopy", Part I, "Biphenyls" by J.P. Maier and D.W. Turner, Discuss.Faraday Soc., 1972, 54.

Part II, "Phenyl Ethylenes" by J.P. Maier and D.W. Turner, in press, J.C.S. Faraday II, 1972.

Part III, "Anilines, Phenols and Related Compounds" by J.P. Maier and D.W. Turner, submitted to J.C.S. Faraday II, 1972.

INTRODUCTION

In atoms and molecules many important electronic processes occur in the vacuum u.v. region (~2 - 2000 Å). The study of these phenomena is of fundamental importance in the understanding of structure and bonding.

The pioneering work of Schumann and Lyman in the vacuum u.v. opened the area to a variety of experimental techniques. Investigation of absorption and emission spectra gave the initial insight of atomic and molecular structure. Initial development was relatively slow; vacuum conditions are necessary as air is strongly absorbing in this region and thus experimental difficulties arise. Progress then escalated, spurred on partly by the advent of sophisticated theories of structure requiring experimental evidence, and partly by technological advancement. The latter was appreciably enhanced as a consequence of atmospheric, space and plasma research, where the importance of electronic phenomena was appreciated. Specific absorption processes were studied using photon and electron impact techniques, and a wealth of information was forthcoming. However, much of the data was complex and seldom interpreted unambiguously.

The work presented in this thesis is concerned with the study of photoionisation of molecules using u.v. radiation by the technique of photoelectron spectroscopy. P.E. spectroscopy is a new method in the field of vacuum u.v. research and has the advantage of being free from secondary effects; only direct ionisation, and possibly autoionisation, processes are studied. Ionisation energies of the deeper orbitals can be obtained directly as well as often fine detail of ionic structure. In turn, the P.E. data can be correlated with experiments involving additional electronic processes and with theoretical models and calculations.

In Chapter I, ionisation phenomena, methods for investigation of the latter, and the information available are discussed. In Chapter II the important theoretical and experimental aspects, as well as the fine detail and subtleties of the data obtained by P.E. spectroscopy are presented. Chapter III reviews the experimental development, the instrumental and technical details of the P.E. spectrometer used and the experimental modifications carried out in conjunction with the work described in Chapters IV to VII.

CHAPTER I

IONISATION PHENOMENA

The possibilities of different modes of excitation leading to ionisation are large, especially for polyatomic molecules, and the more important processes are tabulated below. These are referred to in the subsequent text.

TABLE 1

a.	$AB + E \longrightarrow AB^{+} + e$	Direct ionisation
b.	$AB + E \longrightarrow A^{+} + B + e$	Direct dissociative ionisation
c.	$AB + E \longrightarrow AB^{*} \longrightarrow AB^{+} + e$	Autoionisation
d.	$AB + E \longrightarrow AB^{++} + 2e$	Double ionisation
e.	$AB + E \longrightarrow A^{+} + B^{-}$	Ion pair formation

The energy (E) can be supplied by photons. (hν), electrons (e), metastable atoms and molecules (M^{*}), and even positive ions (M^{+}). In the discussion of the electronic processes photoionisation in particular is considered for convenience and simplicity. The alternative modes of energy supply are referred to further on.

I.1 Ionisation and Electronic Structure.

In the direct ionisation process (1a) where the photons of energy (hν) cause ionisation of electrons, whose ionisation energies (I.E.s) are less than hν , the excess energy is converted to kinetic energy and is partitioned by the resulting ion and the photoelectron. By conservation of momentum, the electron acquires virtually all the excess kinetic energy. In the least favourable case of hydrogen the error is only

~ 1 in 10^4. According to Einstein's Photoelectric Law

$$E = \tfrac{1}{2} mv^2 = h\nu - I_i$$

where E = kinetic energy of the photoelectron and I_i = ith I.E. An idealised photoionisation process is illustrated in Fig.1a. The molecule has three filled energy levels with I.E.s less than $h\nu$. In this case the groups of photoelectrons obtained with three discreet values of kinetic energy correspond to the ionic configurations as shown. Thus in general, provided that $h\nu$ is large enough, all occupied energy levels can be represented by a group of photoelectrons.

It is useful to link the I.E.s with orbital energy levels, as above. This link is provided in a theorem by Koopmans,[1.] which equates the negative of the orbital energy to the I.E. in closed shell molecules when the orbital energies are calculated by the Hartree-Fock self-consistent field (HFSCF) method. There are three approximations in the use of this link and it is important to be aware of these. Koopmans' theorem ignores reorientation energy, i.e. essentially assumes that the orbitals are the same in the ion and molecule. This results generally in a calculated I.E. which is a few eV too high. Fortunately, the correlation energy energy neglect is of similar magnitude (less in ion than molecule) but of opposite sign and thus the two tend to cancel. The latter is an inherent effect in the HFSCF method, as instantaneous correlation of electron motions is neglected. There is also a relativistic correction which is necessary, though this only becomes really important for inner shell electrons. Thus the theorem is generally practicable, but when levels are close in energy the defects outlined can well cause an "inversion". The now classic example is of the $A^2\Pi_u$ and $X^2\Sigma_g^+$ energy levels of nitrogen.[2.] In most cases use of Koopmans' theorem leads to estimates of I.E.s 2-10% too large, but can nevertheless provide a rough order of states. The applicability of Koopmans' theorem

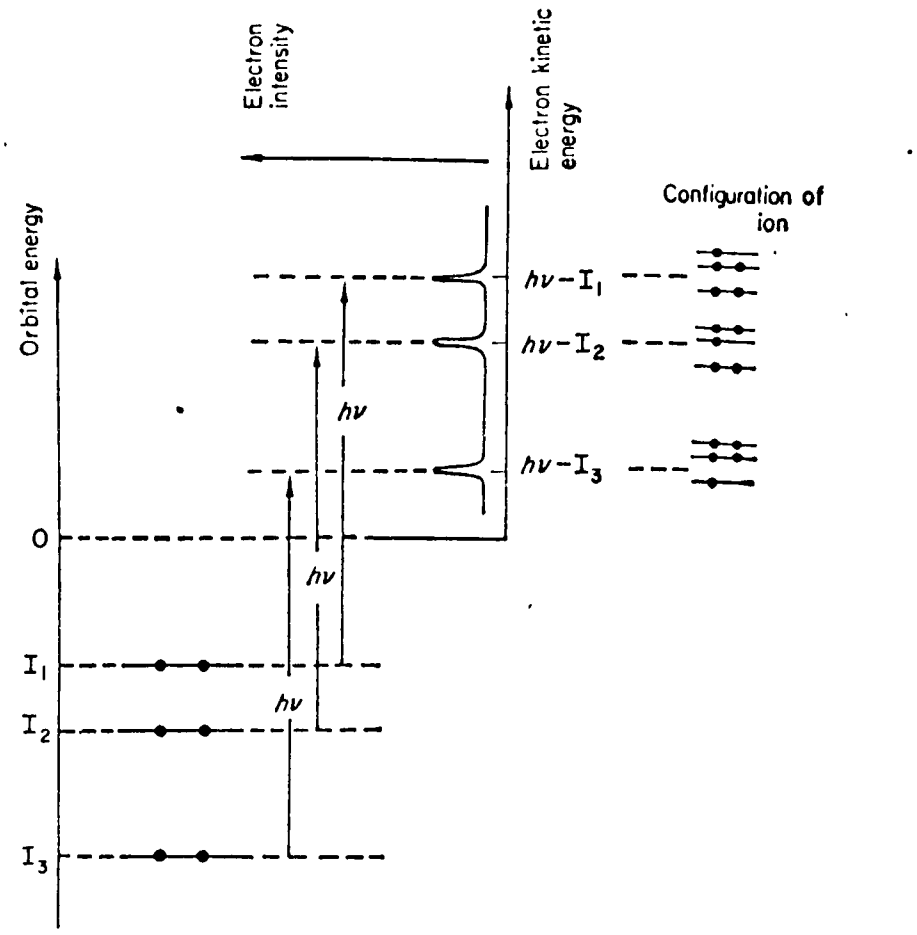


Fig. Ia Idealised photoionisation process

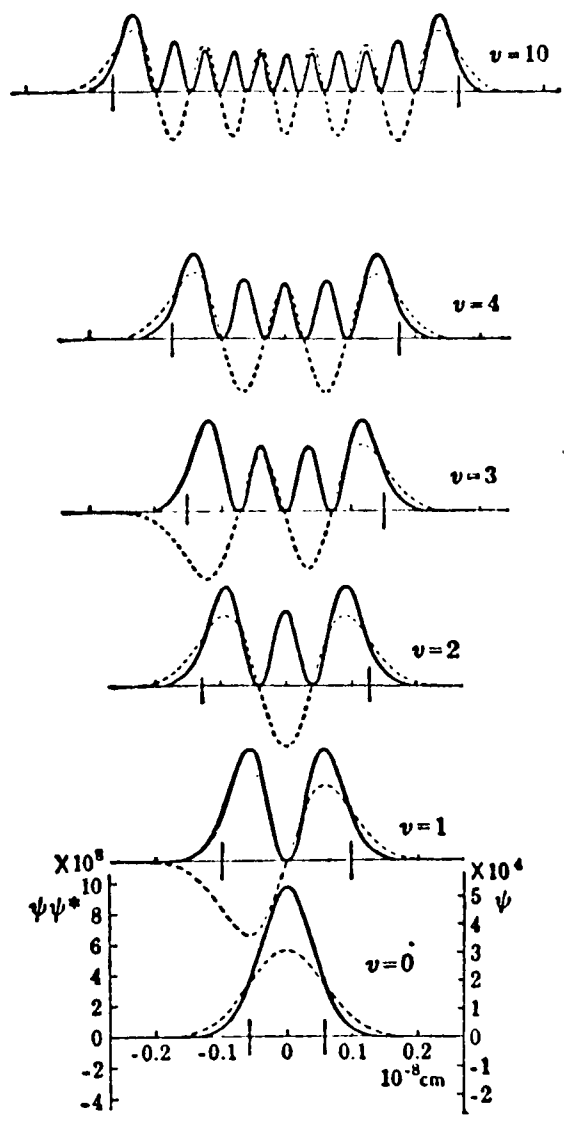


Fig. Ib Eigenfunctions and probability distribution of a harmonic oscillator

has been discussed in detail by Richards.[3] For practical reasons calculations on large molecules are of the semi-empirical nature and it is generally hoped to minimise the "defects" in use of Koopmans' theorem through the use of empirical parameters.

1.2 Franck-Condon Principle.

In the ionisation process described, charges of vibrational (ΔE_{vib}) and rotational (ΔE_{rot}) energy can also be involved. The "excess" energy carried off by the electron is then

$$E = h\nu - I_i - \Delta E_{vib} - \Delta E_{rot}.$$

Thus in the idealised case in Fig. Ia, each band of electrons will have an energy spread determined by the vibrational and rotational transitions. The vibrational intensity distribution (or band profile) can be interpreted largely by consideration of the Franck-Condon principle.

The original semi-classical formulation of Franck[4] can be stated succinctly as "electronic transition occurs in the time which is short compared to the time of vibrational motion." This then suggests that the most probable transitions are vertical. This was put on a more rigorous basis by Condon.[5] The wave-mechanical formulation of the Franck-Condon principle rests on the assumption that the variation of the electronic transition moment ($\underline{R}_e$) is slow with internuclear distance (r) and hence can be replaced by an average value ($\underline{R}_e^{av}$). Then in the Born-Oppenheimer approximation[6]

$$\underline{R}_{v'v''} = \underline{R}_e^{av} \int \Psi_{v'} \Psi_{v''} dr$$

The transition probability ($P_{v',v''}$) and therefore the intensity is proportional to the square of the integral (overlap integral) over the product

of the vibrational eigenfunctions of the two states, i.e.,

$$P_{v',v''} \alpha \left[\int \psi_{v'} \psi_{v''} \, dr \right]^2$$

The square of the overlap integral is usually referred to as the Franck-Condon factor.

In an equilibrium system the population of a state of energy E_n above the lowest energy state is dependent on the Boltzmann factor, i.e.,

$$\alpha \exp(-E_n/kT)$$

as kT at room temperature is $\sim 200 cm^{-1}$, excited electronic states are never thermally populated, lowest vibrational levels of the ground state to a few per cent at the most, and a large number of rotational levels of the zeroth vibrational level. Thus the main part of an electronic band will be due to transitions from the lowest vibrational level of the ground state of the molecule. Though a number of rotational levels will be populated, details of the rotational wave function are not important in comparatively low resolution spectroscopy as of concern here. This will result merely in the broadening of the vibrational component of the band.

In the lowest vibrational state, $\psi_{v''}$ has its maximum at the equilibrium distance (Fig. Ib), while for all other vibrational levels there is a maximum just inside the turning point and smaller maxima in between. Typical eigenfunctions and probability density distributions are shown in Fig. Ib. Thus, the consequence of the quantum mechanical formulation of the Franck-Condon principle is that the most probable electronic transitions are the vertical ones as here the overlap integrals have their maximum values. This corresponds to the shaded portion in Fig. 2. Outside this region there is the possibility of transitions to other vibrational levels as the wave functions approach zero asymptotically,

however these are not significant in view of inherent experimental signal:noise statistics. With the aid of Fig. 2 some ionisation processes are discussed in terms of the Franck-Condon principle. The electronic states are represented by the potential energy function depicted; in diatomics this is the potential curve while in polyatomics potential surface.

1.3 Correlation of Band Shapes, Vibrational Frequency Changes and Bonding Character.

The process $\tilde{X} \leftarrow X$ (Fig. 2) corresponds to the instance where the potential functions are very much alike in both electronic states, as is the case in ionisation of a non-bonding electron. By definition, this implies little dimension change and consequently the overlap integral is largest for the $0 \leftarrow 0$ transition and considerably smaller for all other v'. The vibrational intensity distribution, shown alongside (RHS) is very similar to ionisation in atoms and the kinetic energy distribution of the electrons would be in this case:

$$h\nu - I_i - \Delta E_{v' \leftarrow o} \quad \text{where } v' = 0 \longrightarrow 3$$

If the potential function in the ionic state ($\tilde{A}$) differs appreciably from the ground molecular state (X), the situation depicted by the $\tilde{A} \leftarrow X$ transition occurs. This corresponds to the ionisation of a strongly bonding electron and if the normal co-ordinate (abscissa) represents an internuclear distance (r, as shown), the equilibrium bond length $r_{e'}$ will be longer than $r_{e''}$. The Franck-Condon region falls on the repulsive part of the curve (or surface) so that higher vibrational levels will be populated. In this particular case, the overlap integral has its maximum value at $v' = 4$ and the intensity of the other vibrational transitions (RHS) is governed by their respective Franck-Condon factors. The vertical I.E. corresponds to the most probable transition, the $4 \leftarrow 0$. The $0 \leftarrow 0$ transition is defined as adiabatic.

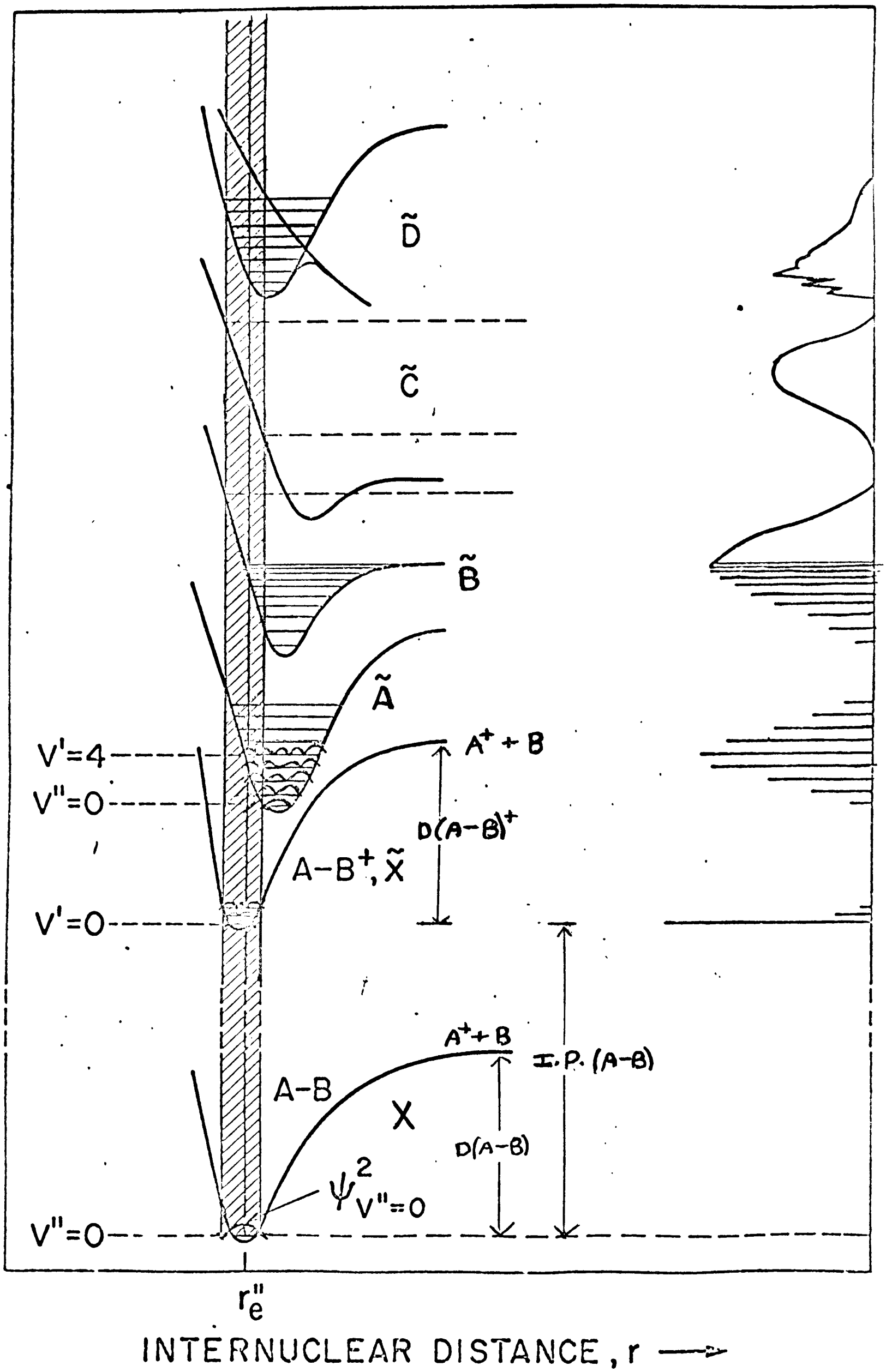


Fig. 2 Significance of potential energy curves in ionisation

The removal of an antibonding electron (in case of Fig. 2 $r_e' < r_e''$) will result in a vibrational envelope similar to that in the $\tilde{X} \leftarrow X$ transition rather than the $\tilde{A} \leftarrow X$; the antibonding effect is of much smaller magnitude.

As well as the Franck-Condon envelope a vibrational frequency change is the function of the normal co-ordinate change. Thus the comparison of vibrational frequencies, when discernible, in the ionic state with the ground molecular state values, will in general give a further indication of the bonding character of the electron removed. The energies of the vibrational levels ($E_{v'}$) are usually represented as

$$E_{v'} = (v' + \tfrac{1}{2})\, h\omega - (v' + \tfrac{1}{2})^2\, h\omega x + \ldots\ldots$$

where v' = vibrational quantum number, x = anharmonicity constant, ω = vibrational frequency = $\frac{1}{2\pi}\,(k/\mu)^{\frac{1}{2}}$. k = force constant, μ = reduced mass. As k is a measure of the curvature of the potential well at the equilibrium distance, it is indirectly a measure of the bond dissociation energy. If a non bonding electron is removed on ionisation, there will be little change in k and hence ω. Thus in the transition $\tilde{X} \leftarrow X$ the vibrational frequencies ω' and ω'' will be essentially the same. If a bonding electron is removed, k' and ω' for the ion should be less than k'' and ω'' for the ground state of the molecule. Consequently in the process $\tilde{A} \leftarrow X$ the vibrational frequency will be appreciably reduced. Conversely, on removal of an antibonding electron, ω' is usually slightly greater than ω''. In polyatomics where a multidimensional surface is required to describe the electronic states and vibrational motions, dimensional changes are not necessarily restricted to one parameter, and these correlations have to be treated with care. Nevertheless, in practice such notions can normally be used as a good guide to bonding character.

In the Born-Oppenheimer approximation there are no restrictions on the changes in the quantum number (Δv) of totally symmetric

vibrations in an electronic transition.[7] For non-totally symmetric vibrations Δv must be even and bands with $\Delta v = \pm 2, \pm 4, \ldots\ldots$ will be very weak compared to $\Delta v = 0$. If vibronic interactions are strong there will be a relaxation of these selection rules (see Chapter II).

1.4 Dissociative Ionisations.

In the $\tilde{B} \leftarrow X$ transition (Fig. 2), part of the Franck-Condon allowed region is to the potential surface above the dissociation continuum. This can also occur when there is a very large dimensional change. The band (RHS) usually shows a convergence of vibrational levels merging into the continuum. Above the dissociation limit the energy of the ejected electron is not quantised and the result is a continuous spectrum.

A case of dissociative ionisation (predissociation, Table Ib), is represented by the $\tilde{C} \leftarrow X$ process. Transitions take place to a purely repulsive surface and smooth featureless band is obtained. The band profile represents in essence the shape of the $\Psi_{v''} = o$ wave function as no discreet vibrational levels are populated. The excess energy is partitioned between the fragments.

The last process considered in Fig. 2 is the ionising transition $\tilde{D} \leftarrow X$; predissociation by curve crossing. If the two eigenfunctions have the same symmetry the non-crossing rule applies.[6] There will be a perturbation of the wave functions and effectively two new potential surfaces will be formed (as shown in Fig. 2). Below the perturbation discreet vibrational levels will be populated, while above, ionisation into non-quantised continuum occurs. Below the perturbation broadening of the vibrational levels takes place; the inherent ion instability leads to a spectral line broadening of magnitude $h\tau^{-1}$ (uncertainty principle). The scope of curve crossings and combinations of processes is considerable particularly for polyatomics with large numbers of surfaces, and these are discussed comprehensively by Herzberg.[8-10]

1.5 Autoionisation.

In an autoionisation process (Table Ic) ionisation occurs, not by a direct transition to the ionic state, but via an initial superexcited neutral state, possibly a Rydberg state, followed by a radiationless decay to the ionic state. The initial excitation can only occur at discreet value of the incident energy, corresponding to the energy required to populate the excited state. Thus the energy of the ejected electron will be equal to the energy difference between the ground molecular and the ionic state. The derived vibrational profile can be radically different to that which would be obtained by direct ionisation. In Chapter II examples of the latter in autoionisations detected by P.E. spectroscopy are discussed in more detail.

1.6 Double Ionisation.

The simultaneous removal of two electrons (Table Id) from a molecule is expected to become important for incident energies greater than $\sim$ 30eV.[11.] However, for large molecules where the first I.E. can be around 6eV, double electron process could take place even with He 584 Å(21.22eV) radiation and certainly likely to some extent with He 304 Å(40.81eV) for example.

Processes that can occur after initial ionisation, Auger, and fluorescence are discussed in conjunction with their experimental techniques at the end of this Chapter.

TECHNIQUES USED IN THE STUDY OF IONISATION PHENOMENA

The energy associated with ionisation processes is large since complete charge separation is involved and thus even the first I.E.s are much larger than the bond energies. Such relatively high energy necessary is supplied by physical means by different agents mentioned

previously. Correspondingly, the methods, and results, differ depending on the particular parameter(s) followed in the experiment.

1.7 Absorption Spectroscopy in the Vacuum U.V.

Observation of absorption spectra was the earliest technique in the study of direct excitation processes. Essentially, continuum radiation dispersed by a vacuum monochromator is passed through the vapour of the substance and is then allowed to strike a photographic plate. The exposure is reduced at wavelengths corresponding to an absorption process. In general the spectra are complex as all possible excitation processes can take place. However, when the absorption bands can be fitted to a Rydberg series, very accurate I.E.s are obtained. Rydberg states correspond to the excitation of an electron to successively higher outer unfilled orbitals, with increasing quantum number n, and converging in the limit to the continuum (i.e. ionisation). The general expression for a Rydberg series is

$$\nu_n = \nu_\infty - \frac{R}{(n - \Delta)^2}$$

where ν_∞ = I.E., R = Rydberg constant, ν_n = frequency of the absorption line and $(n - \Delta)$ = effective quantum number. As there is some penetration of the core electron cloud by the excited electron, the magnitude of the defect, and often type of orbital, are reflected in Δ. Generally, a large Δ of 0.9 - 1.2 is associated with s - orbitals, a Δ of 0.3 - 0.5 with p, and Δ of $\leqslant$ 0.1 with d orbitals.[10.]

The technique has proved particularly important for small molecules, especially for non bonding electrons which give nearly atomic Rydberg series. The extension to complex molecules is difficult; there are many types of electrons, and many types of excitation processes are possible. The Rydberg bands associated with the ionisation of inner electrons are almost invariably autoionised as a result of which they are too broad and

diffuse to allow extrapolation to the appropriate ionisation limit. This very much limits the study to the first I.E. The development and applications of absorption spectroscopy in the vacuum u.v. have been the subject of many reviews.[12,13].

1.8. Electron Impact Techniques.

The early experiments of Franck and Hertz demonstrated the use of electrons as an energy source in electronic processes. The difficulty lay with the interpretation of the data, molecular excitation and ionisation were not distinguished.

In mass-spectrometric appearance potential measurements, a variable energy electron beam is employed in conjunction with a mass spectrometer to determine the ion current. The source of the electrons is an electrically heated filament of tungsten, tantalum or thoriated irridium. The energy of the electron beam is defined by a potential gradient before the ionisation region. Thus, an ionisation efficiency curve can be obtained for molecular and fragment ions from the ion current and electron energy. In fig.3a a typical efficiency curve is shown.[13]. However, there are difficulties in the extrapolation of the curve to the threshold to determine the ion appearance potential.[14].

It was realised that there are differences in threshold behaviour for different fundamental processes. Theoretical treatment[15]. shows that the cross - section variation with energy for direct ionisation is proportional, or nearly so, to E^{n-1}, where E is the energy above the threshold, and n is the number of electrons leaving the collision complex. In Fig. 3b the theoretical and the experimentally observed functions are shown. In general, there is agreement with the equation. Thus there is inherent advantage in photon impact as the onsets are steep and well defined. It is worth noting, that the threshold laws are essentially time dependant and for, say, an autoionisation process an intermediate law may hold if

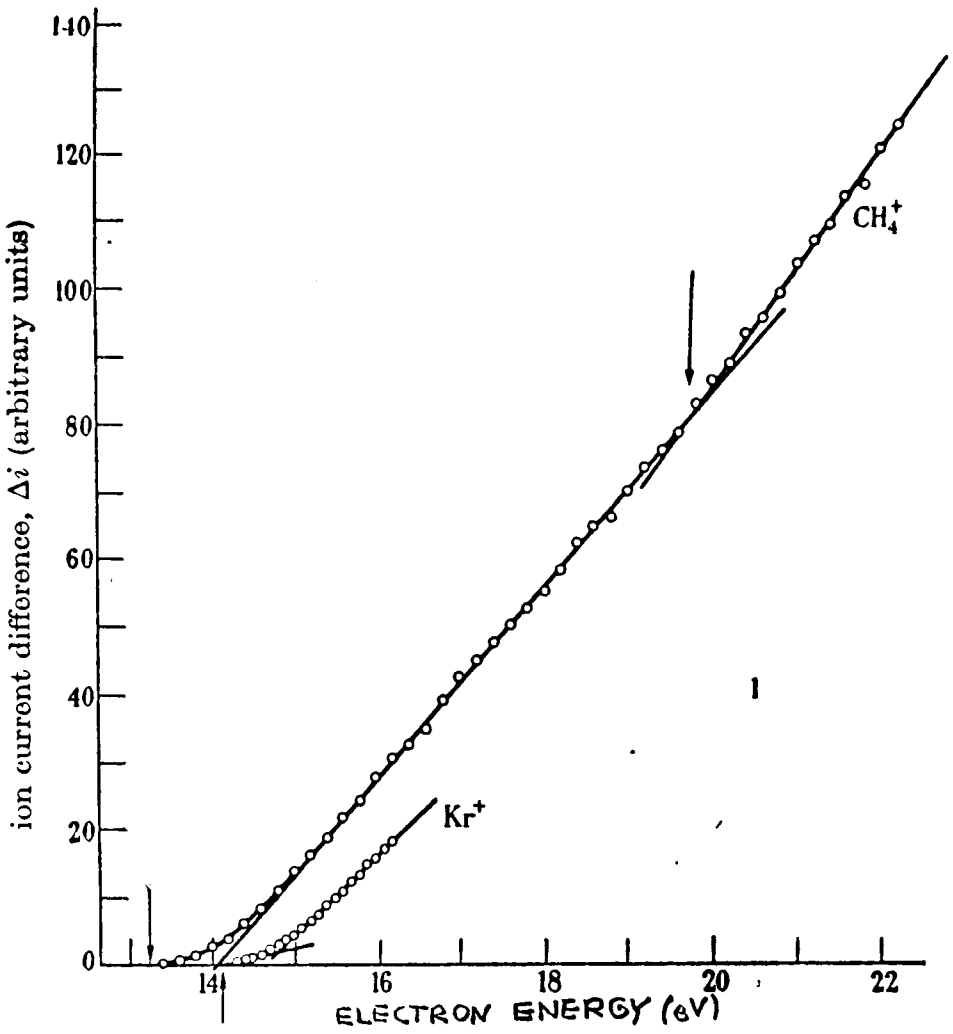


Fig.3a Electron impact ionisation efficiency curve, Ref. 13

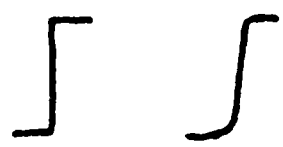
Theor. Expt.	Theor. Expt.	Theor. Expt.	Theor. Expt.
			
1) Negative ion formation by electron impact. $A + e \rightarrow A^-$	1) Photo-ionisation. $A + h\nu \rightarrow A^+ + e$	1) Ionisation by electrons. $A + e \rightarrow A^+ + 2e$	1) Double ionisation by electrons. $A + e \rightarrow A^{++} + 3e$
2) Photo-excitation. $A + h\nu \rightarrow A^*$	2) Excitation by electrons. $A + e \rightarrow A^* + e$	2) Double photoionisation $A + h\nu \rightarrow A^{++}$	

Fig. 3b Theoretical and experimental threshold laws

its life time approaches direct ionisation ($\sim 10^{-15}$ sec. c.f. auto-ionisation where the electron usually leaves the complex after 10^{-12}-10^{-13} sec.). Regarding selection rules it can be expected that they are less restrictive for electron impact than for photon, because of the additional electron available for the transfer of spin and orbital angular momentum.[16.]

In Fig. 3a the critical potentials are indicated in changes in the slope of the curve. However, as this is a threshold technique the breaks in the curve occur also for autoionisation transitions, as is the case shown here when the break at 19.5 eV cannot be the second I.E. of methane which is known to be at $\sim$22 eV. In determining inner ionisation energies by measuring increase in ion current with increase of incident energy, at energies of autoionising states there is a large increase of ion current which usually obscures the increase in ion current corresponding to the ionisation of inner orbitals.

The major experimental problem is the energy spread of the electron beam and a number of approaches have been employed to combat this. Energy dispersion analysers, electrostatic and magnetic (Chapter III), have been used frequently to define the spread. Alternatively, in the retarding potential difference (R.P.D.) technique developed by Fox,[17.] only the higher energy portion of the quasi-Maxwellian energy distribution is used.

In Electron Impact Energy Loss Spectroscopy developed by Lassettre and co-workers[18.] the scattered electrons are analysed. A monochromatic beam of electrons, energy selected by an electrostatic analyser, is passed through the gaseous sample (or at solid surface) and the scattered electrons are again electrostatically analysed. Electron losses correspond to excitation processes to molecular and ionic states. Electron loss spectra are particularly suitable for the investigation of Rydberg and autoionising transitions because of the extensive incident energy range available. In Fig. 4 a recent spectrum is reproduced indicating the

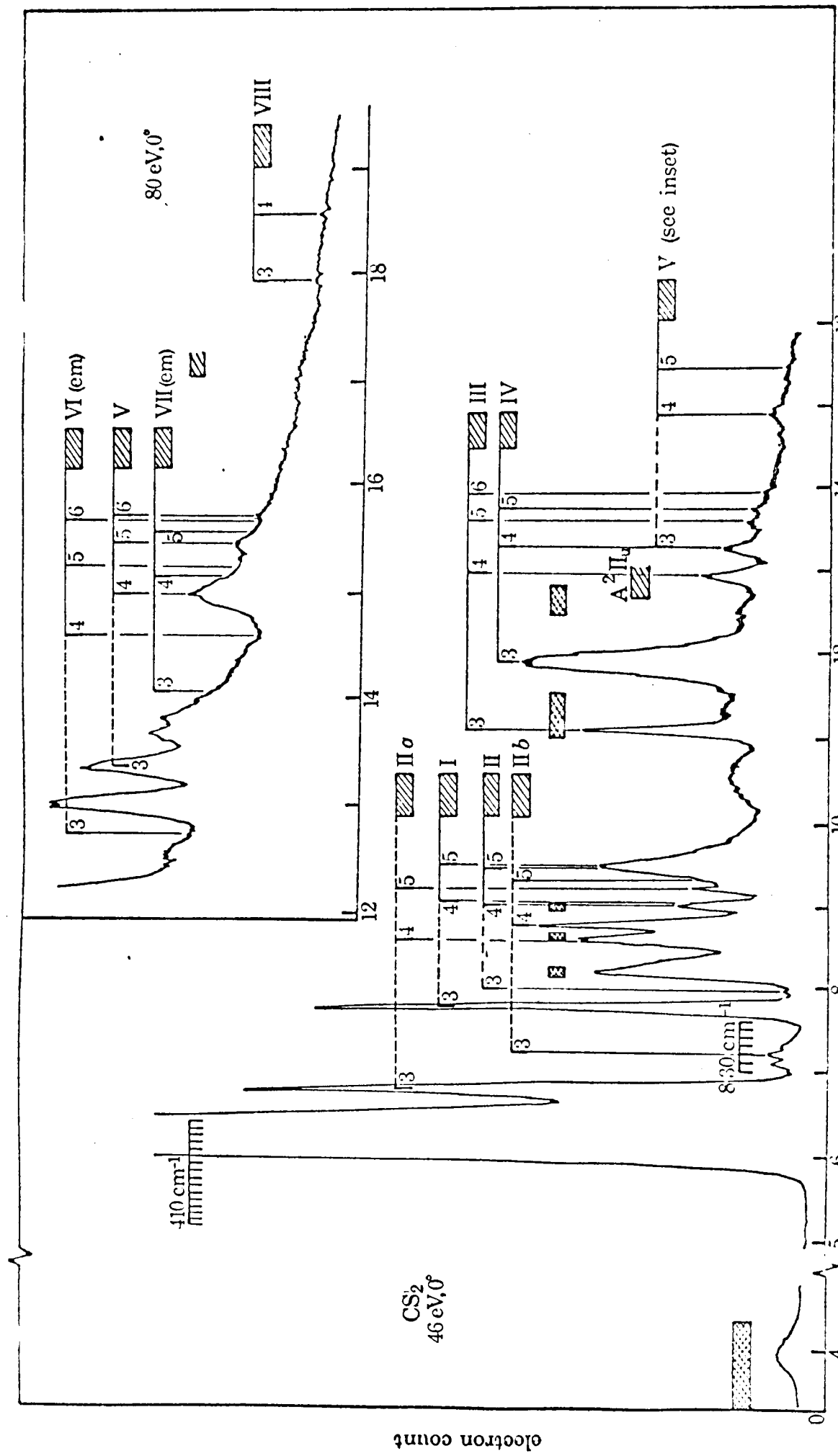


Fig. 4 Electron impact energy loss spectrum of CS_2, Ref. 19

complexity.[19] The spectra are very similar to optical absorption spectra except that optically forbidden transitions are observed (vide supra). The instrumental advances and electron energy analysers in electron impact techniques have been comprehensively reviewed by Klemperer.[20]

1.9 Photon Impact Techniques.

Although it is easier to obtain a sufficient flux at a chosen energy in the vacuum u.v. for electrons than photons, the unfavourable threshold function and experimental energy spread often make photon impact techniques more attractive.

In a technique developed by Watanabe,[21] the first I.E. can be accurately and unambiguously determined. The energy of the exciting radiation ($h\nu$) is exactly defined by the monochromator setting and the intensities of the incident and transmitted light, after interaction with the sample, are reflected in the photomultiplier currents, I_o and I respectively. The ion current (i) produced in the absorption chamber is also measured. The photoionisation efficiency (Y) is given by

$$Y \propto \frac{i}{I_o - I}$$

where i is proportional to the number of ions formed, while $I_o - I$ is proportional to the number of photons absorbed. Thus a plot of Y against incident wavelength will rise sharply at the first I.E. (Fig. 5a). The technique is very accurate for the latter, but for higher I.E.s auto-ionisation is again dominant, as is always the case with a threshold technique.[22]

Total absorption cross-section (σ_t) can be obtained from the Beer-Lambert Law,

$$I = I_o \exp(-n\sigma_t x)$$

where n = number of molecules cm^{-3}, x = the path length, by the plot

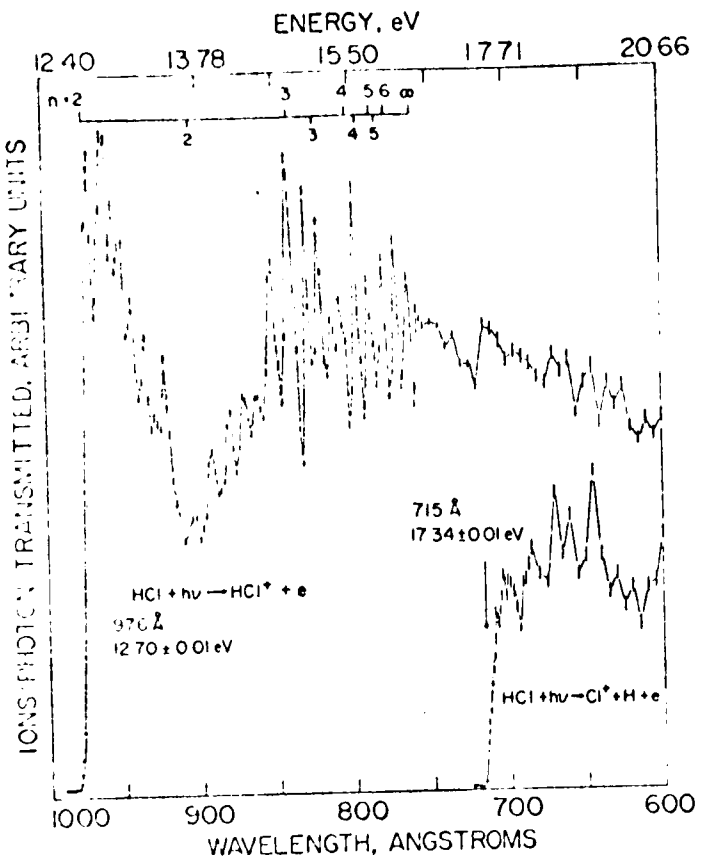


Fig. 5a Photoionisation yield curve, Ref. 22

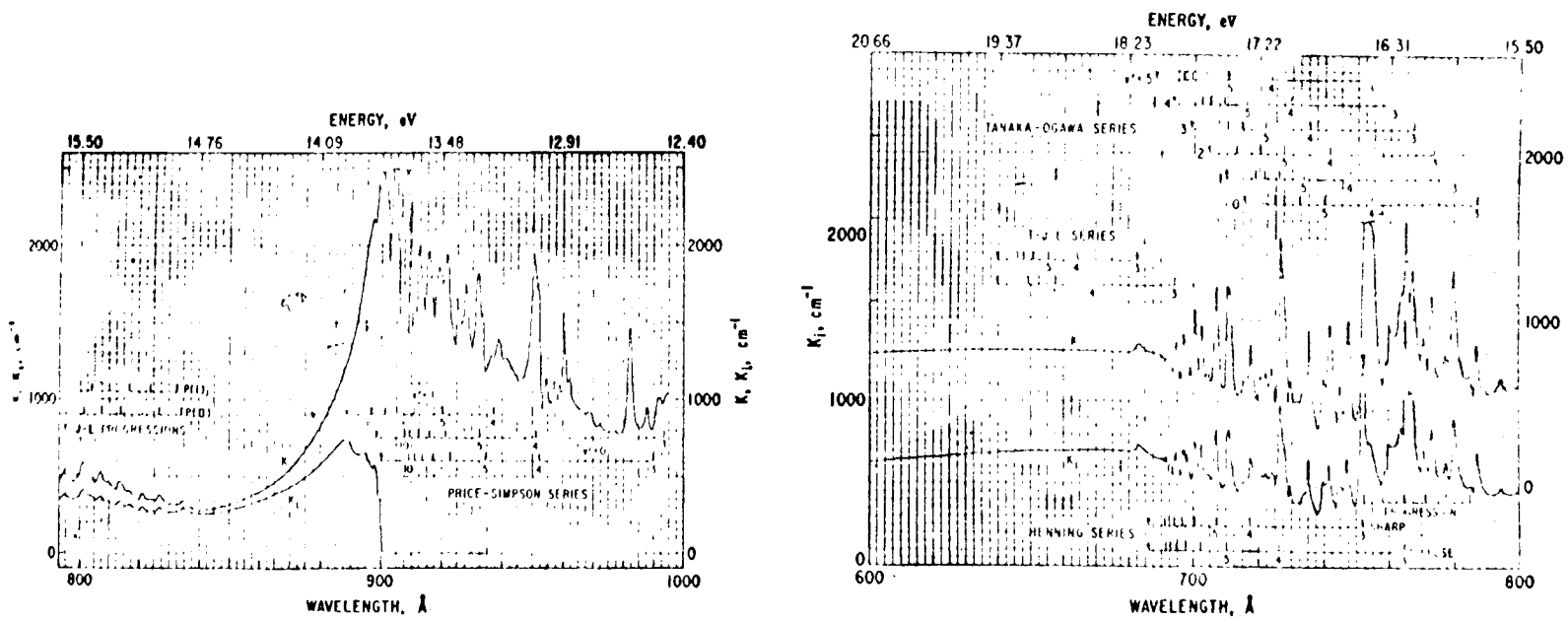


Fig. 5b Absorption and ionisation coefficients of CO_2, Ref. 23

of $\log_e I/I_o$ against pressure. As not all the photons are concerned in ionisation

$$\sigma_t = \sigma_i + \sigma_d$$

where σ_i = ionisation cross-section, σ_d = cross-section for other processes. The yield Y is then defined

$$Y = \frac{\sigma_i}{\sigma_t}$$

and as the rate of production of ions $\alpha Y(I_o - I)$, the ion current is proportional to

$$e \frac{\sigma_i}{\sigma_t} I_o \left[1 - \exp(-n\sigma_t x) \right]$$

In practice, the apparatus is calibrated with a gas of known cross-sections and then σ_i determined for other gases.[23.] In Fig. 5b typical σ_i and σ_t curves are shown. The σ_t curve is essentially the same as an absorption photograph except that resolution is lower but intensity has been recorded. The σ_i gives information on autoionisation and dissociation. As with electron impact, combination with a mass spectrometer allows the direct study of formation and breakdown of ions. Photoionisation yields with mass analysis are obtained. A recent review covers all the aspects of photoionisation and mass analysis detail.[24.]

I.10 Penning Ionisation.

The ionisation of atoms and molecules by long-lived excited neutral species (M^*) is known as Penning ionisation,[25.] i.e.

$$AB + M^* \longrightarrow AB^+ + M + e$$

The excited species are usually metastable rare gas atoms. These are produced by a low energy electron beam in a low pressure of the rare gas. For example, with helium, 2^1S and 2^3S states are so obtained with energies of 19.81 and 20.61eV respectively. The energy of the ejected electrons are analysed in a similar fashion to that in P.E. spectroscopy (Chap.III) and gives essentially the same information. As in the latter, the number of autoionising states accessible is limited by the

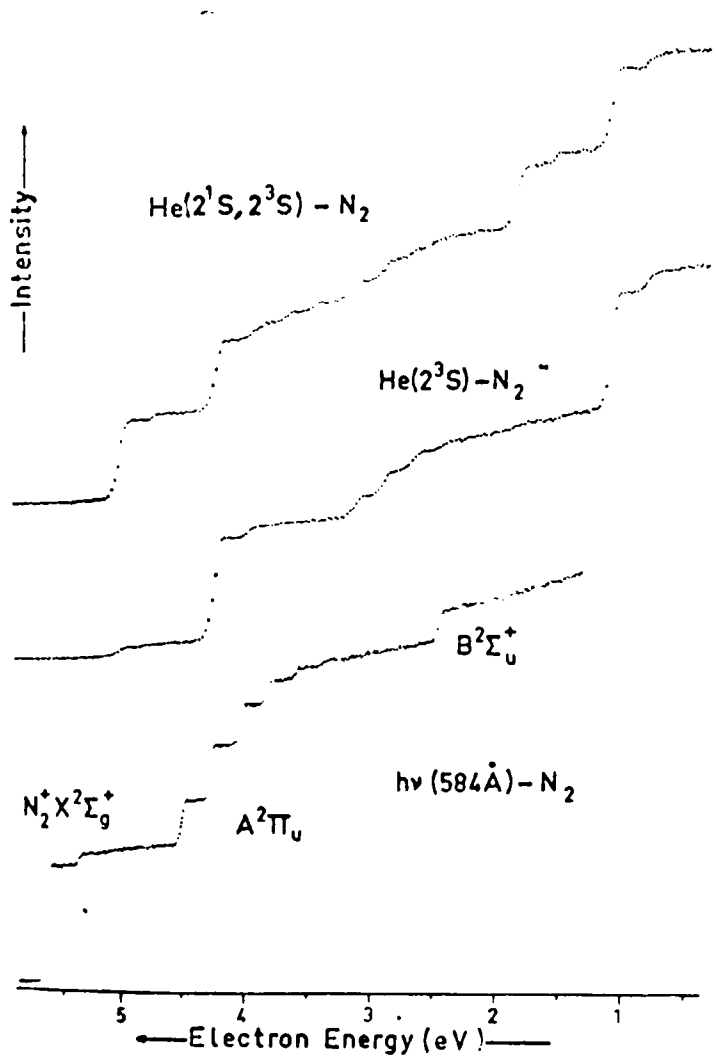


Fig. 6 Photoelectron and Penning electron spectra for the system He - N_2, Ref. 26

discreet energy of the ionisation agent. However, there are differences which arise from the excitation mechanisms. It has been found that the population of electronic states are generally different (Fig. 6), while relative populations of the vibrational states in each electronic state are very nearly equal.[26] The transition collision complex is relatively long lived, 10^{-13}sec. (c.f. 10^{-18}sec. for photons) and the transition therefore may not be strictly vertical. Nevertheless, there is generally good agreement of vertical I.E.s with P.E. data suggesting that the Franck-Condon principle is still operative. In Penning ionisation, associative ionisation can occur,

$$AB + M^{*} \longrightarrow AB\,M^{*} + e$$

and lead to the study of states inaccessible by photoionisation.

The technique can also be used to detect long lived excited molecular states, as has been demonstrated for nitrogen.[27] An interesting feature of the Penning process is that through the use of particles of different spin, the spin conservation rule could be examined.

I.11 Positive Ion Impact

Ion-molecule and charge exchange processes have been studied in double mass spectrometers. Ions are generated in the first section by an ion gun, are mass analysed, and then the chosen primary ion beam is retarded before entering the collision chamber of the second sector. The product ions are again mass analysed. Ionisation of the target molecules may only occur when the recombination energy of the ion is close to the I.E. of the neutral molecule; the cross-section falls rapidly for "excess" energy difference. From the intensity of the incident and emitted ion beams, the ionisation cross sections, fragment appearance potentials and also a few inner I.E.s have been obtained.[28]

1.12 Photoelectron Spectroscopy.

In the ionisation process (Table I) using photons as the excitation, the measurement of the electron kinetic energy distribution is known as photoelectron spectroscopy. There is a natural division dependant on the energy of the ionising radiation, either utilising u.v. photons or soft X-rays. The two branches were also developed independently. In this section the technique using photons in the u.v. is considered.

The technique was first described by Vilesov and co-workers[29.] and independently by Turner and Al-Jobury,[30.] in 1961. Vilesov et al used a continuum source in conjunction with a vacuum monochromator and a LiF window to isolate the ionisation chamber. The window limited the wavelength to $> 1040\text{Å}$ ($\sim$ IleV) the LiF cut-off. Turner used a windowless system by relying on differential pumping to isolate the lamp from the ionisation region. Using undispersed radiation from a helium discharge lamp, a much greater photon flux was obtained, and the ionisation energy was extended to 21.22 eV. Both groups used a cylindrical retarding grid system for electron analysis in their initial work. The instrumental development and progress since the initial break-through are discussed in Chapter III.

The electron kinetic energy (E) is exactly defined, at time of ionisation by

$$E = h\nu - I_i - \Delta E_{vib} - \Delta E_{rot} \pm \Delta E_{trans}.$$

The additional term included (ΔE_{trans}) represents the translational energy contribution (see Chap.III). Thus the equation can be utilised to determine the I.E.s (I_i) of all the electrons with energy above the energy of the radiation used, i.e. with He Iα above -21.22 eV. In Fig. 7 a P.E. spectrum obtained with the retarding grid instrument is shown, the steps represent the adiabatic I.E.s, and a corresponding differential spectrum obtained with a high resolution deflecting field instrument.

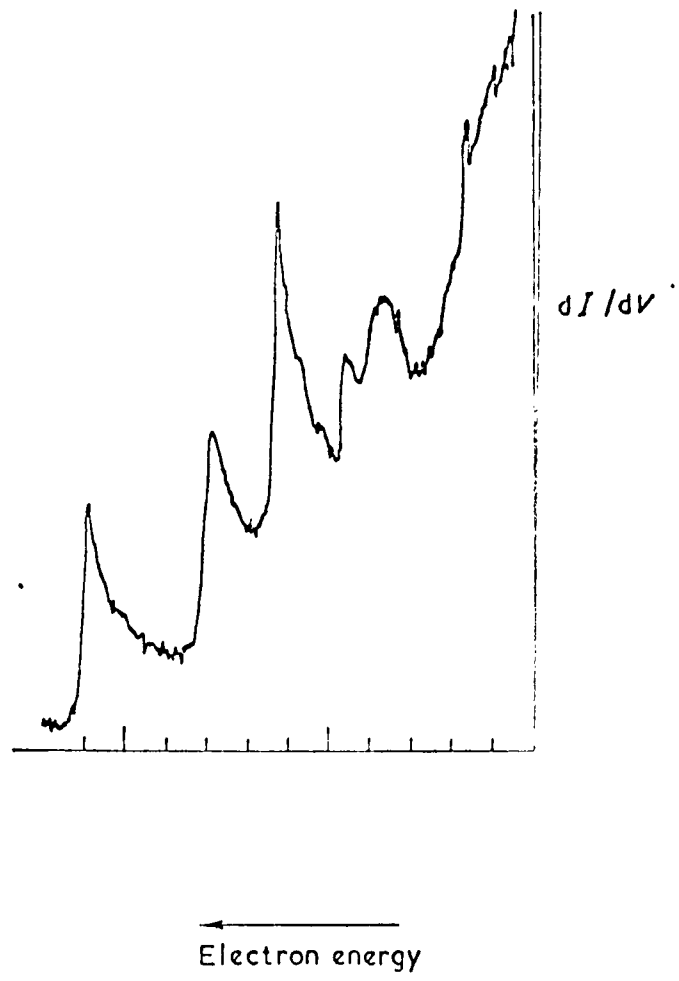


Fig.7a Photoelectron spectrum of CS_2 obtained with retarding cylindrical grids, Ref. 90c

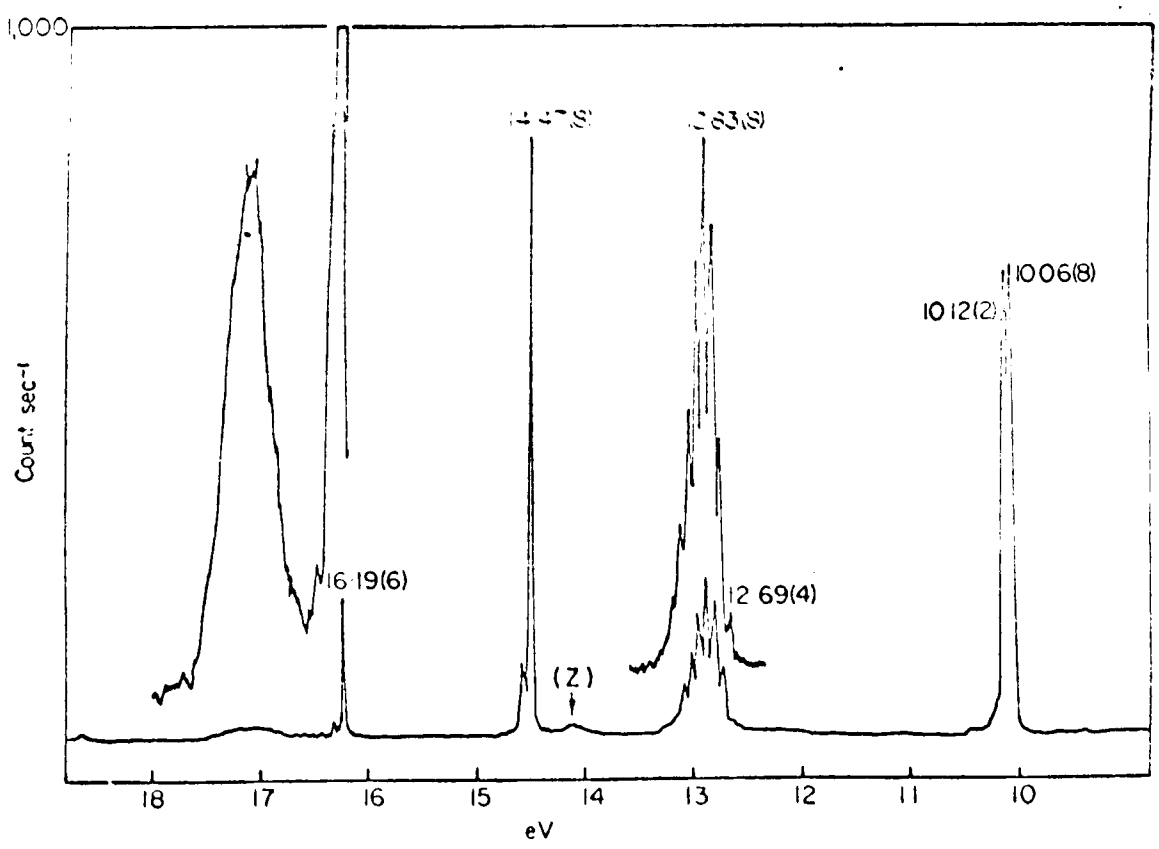


Fig. 7b Photoelectron spectrum of CS_2 obtained with 127° electrostatic cylindrical grids, Ref. 47.

In P.E. spectroscopy the only processes of concern are those liberating electrons; direct ionisation and possibly autoionisation. As a fixed quantum of radiation ($h\nu$) is used as source of excitation, the process is a non-threshold one. Thus autoionisation which is a resonance phenomenon will be relatively rare especially with the higher energy sources and can anyway be easily detected by a mere change of the energy of the line source. Conversely, autoionisation can be readily studied by using continuum sources and a monochromator in conjunction with the P.E. apparatus.[31.] The information available and the theoretical aspects concerned intimately with P.E. spectroscopy are discussed more fully in the following Chapter (II).

A modification of the technique, labelled as photoionisation resonance spectroscopy, has been described by Villarejo and co-workers.[32.] A variable photon wavelength is obtained from a monochromator and the flux of the zero kinetic energy photoelectrons analysed as a function of the wavelength of the photons. In this mode of operation, all autoionising surfaces which cross over directly the ionic state will be detected through the release of the zero energy electrons.

Other recent developments are aimed towards photoelectron-mass ion coincidence measurements. The experiment involves linking specific ions with selected photoelectrons (and vice versa). Separate mass analysers have been employed, attached to the P.E. spectrometer,[33.] alternatively the same electrostatic cylindrical condenser analyser has sufficed for the analysis of electrons by energy dispersion and mass ions by time of flight.[34.]

I.13 Ion Fluorescence.

In the de-excitation of ionic states in the valence band, sometimes fluorescent radiation is emitted. Fig. 8a shows schematically a hypothetical example of the production of fluorescence and photoelectrons

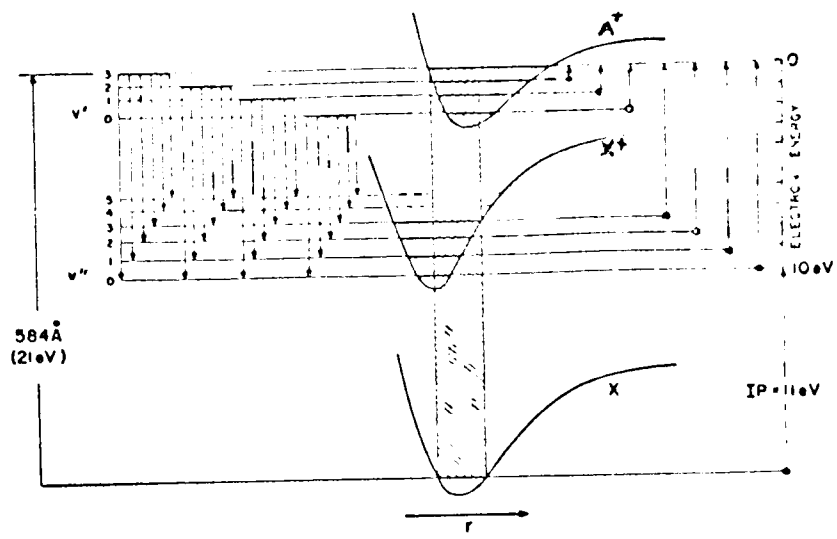


Fig. 8a Hypothetical example of the production of fluorescence and photoelectrons owing to absorption of 584 Å radiation

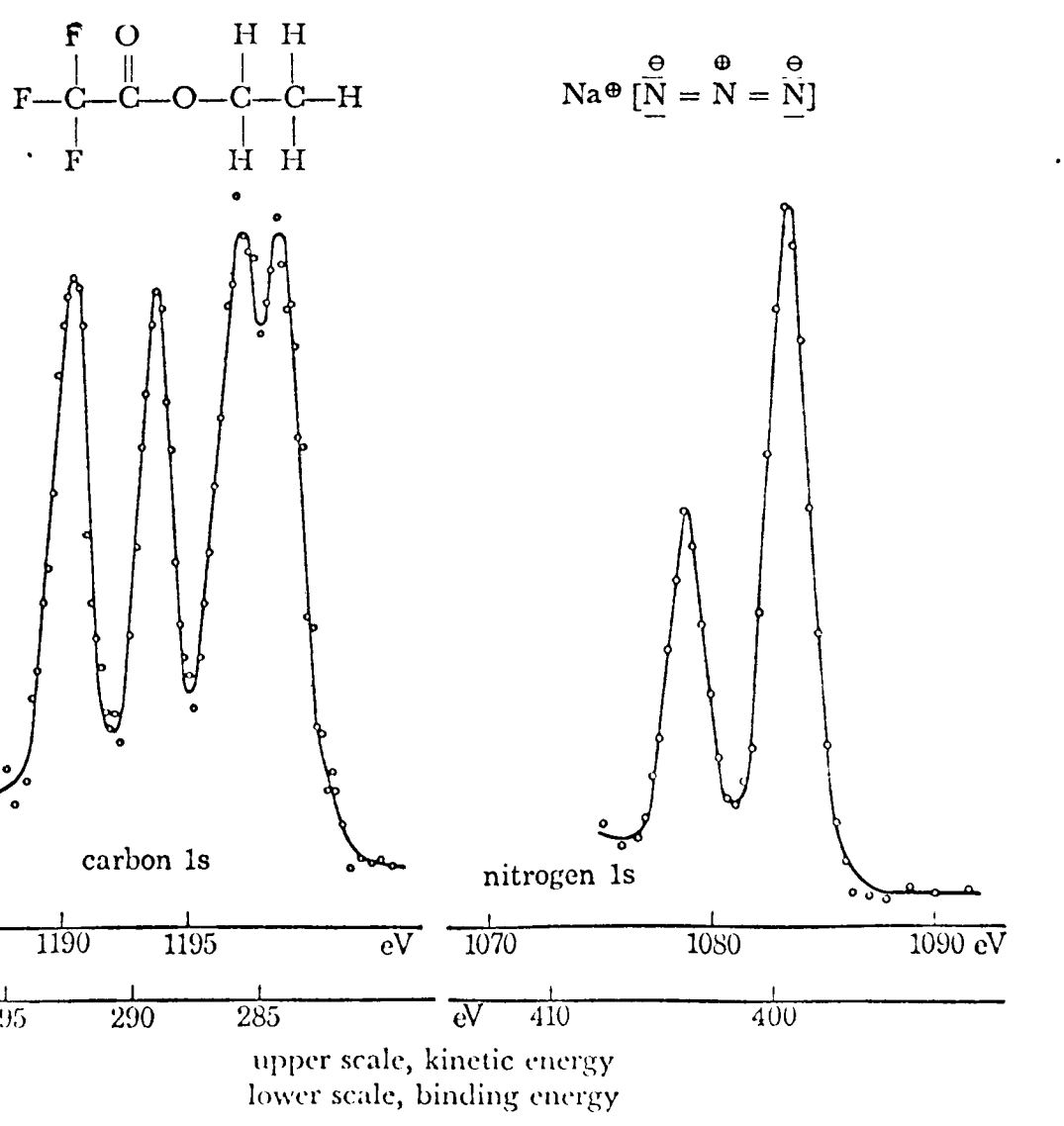


Fig. 8b Photoelectron spectra obtained with X-ray photons, Ref. 43c

on irradiation with He 584 Å. The absorption of radiation leads to the formation of the first excited state of the ion ($\tilde{A}$) which can decay to the ground ionic state ($\tilde{X}$) with emission of fluorescent radiation; the lifetime of the decay is $\sim 10^{-8}$ sec. Thus if the ionic state $\tilde{A}$ is relatively long lived, fluorescent radiation should be observed.

The method of exciting fluorescent radiation by using a monochromatic beam of vacuum u.v. radiation is advantageous. In conventional gas discharge ion emission spectra the internal energy distribution is not known. Judge and co-workers[35.] observed fluorescence from molecular ions excited by photons by combining two monochromators. In a recent approach the He 584 Å resonance line is used as source of excitation.[36,37.]

The consideration of P.E. and ion fluorescence data is most beneficial. When the P.E. spectra show by the presence of well defined vibrational fine structure that long-lived ($\sim 10^{-12}$ sec.) ionic states are formed, fluorescence may be expected. The I.E.s obtained from the P.E. spectra will define precisely the energy of the fluorescent transition. Fluorescent transitions are subject to selection rules and thus the interplay of the data from the two processes can assist in the symmetry assignment of the orbitals. Such is a case in hexafluorobenzene where the fluorescence unambiguously shows that the second band in the P.E. spectrum is Πa_{2u}.[37.] In Chapter II the more detailed example is considered (HBr^{+}). Other techniques in the determination of structures of molecular ions are discussed in a review by Herzberg.[38.]

1.14 X-ray Photoelectron Spectroscopy.

The techniques was developed by a transition from the initial work on a β-ray spectroscopy to the use of X-rays as a source of radiation. The development and progress, which ran parallel to u.v. region, are contained in two monographs by the pioneers in this field, Siegbahn and co-workers.[39-40.]

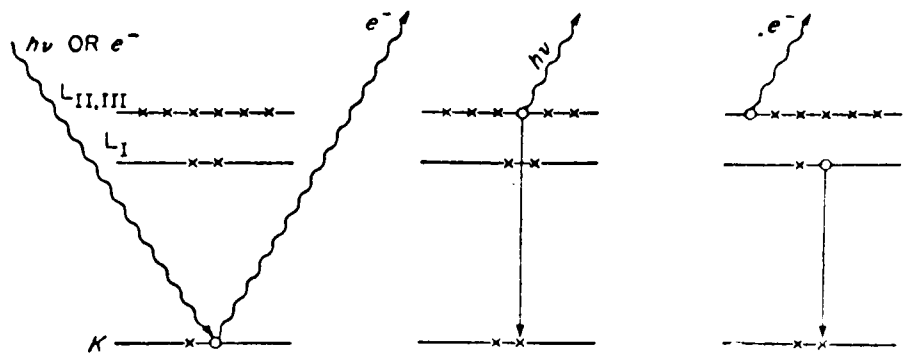
In principle all electrons from the core to the valence shell can be studied. However, the use of X-rays poses additional problems, in particular low ionisation cross-sections in the valence region and an inherent line width of the X-ray line (see Chap.II). The studies have shown that core electron lines are characteristic of the atom in the molecule and are subject to chemical shifts dependent on chemical environment (Fig. 8b). Such work on the free molecules has resulted in large number of models of chemical shifts correlated with calculations of varying approximations.[41.] In the valence shell, up to the present time, fine detail is largely elusive due to the natural line width of the X-ray line. Nevertheless, comparison of P.E. band intensities, excited by X-rays and u.v. sources has shown to be informative (see Chap. II). A large proportion of the X-ray work has been concerned with surface phenomena and this is discussed elsewhere.[42.]

1.15 Auger and X-ray Emission Spectroscopy

When a vacancy is produced in an inner shell, the excited ion can relax by one of two processes; radiative transition or Auger emission. The latter is a radiationless process in which the hole (say K shell) is filled by an electron from a higher shell (say L) with simultaneous ejection of another electron (say M). In this case the Auger process is designated as KLM. A KKM type process is referred to as a Coster-Kronig one. In the KLM Auger process the electron which goes away into the continuum carries away discrete amount of energy equal to the difference between the initial and final states i.e.

$$E_{Auger} \sim E_K - E_L - E_M$$

In lighter elements the yield of an Auger process is high while the X-ray yield is low. As the atomic number increases the former yield decreases, the latter yield increases. At the atomic number around 33 the 50% probability point occurs after which there is a cross over.[43.]



PHOTOIONIZATION $E_K = h\nu - E$ (PHOTOELECTRON)
FLUORESCENCE $E_K - E_L = E$ (X RAY)
AUGER $E_K - E_L - E_L' = E$ (AUGER)

Fig. 9a Schematic representation for processes that form the basis of photoelectron, fluorescence and Auger spectroscopy

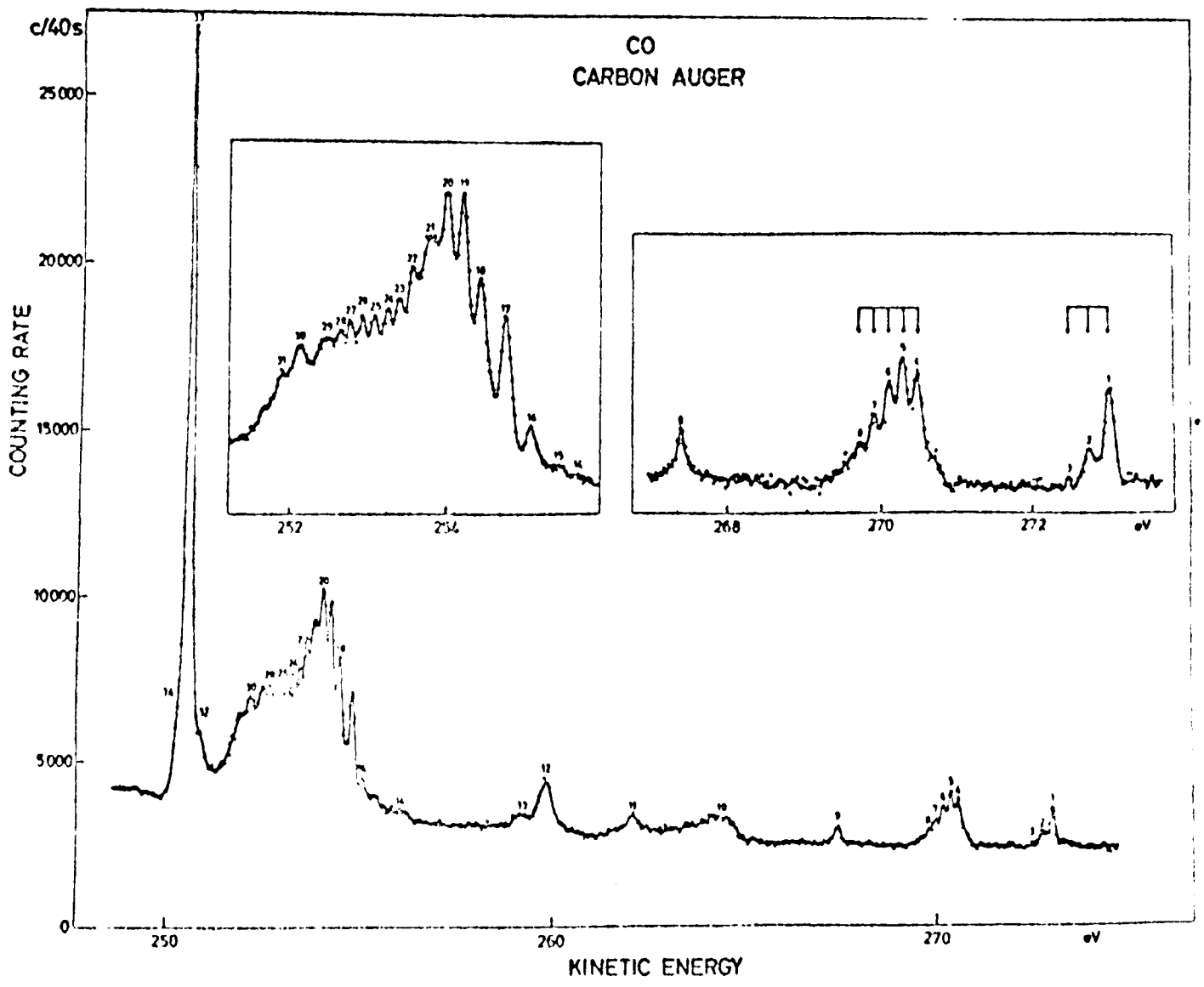


Fig. 9b Carbon Auger and autoionisation electron spectrum from CO excited by electron impact. Insets are vibrational and autoionisation and lines and Auger vibrational lines, Ref. 45

In the radiative relaxation, the X-ray which is emitted is classified according to the orbital in which the primary vacancy was created.[44] An advantage in the study of this process is that the transition is subject to selection rules, $\Delta l = \pm 1$, $\Delta j = \pm 1, 0$. Unfortunately, the actual intensity is a function of variety of factors and therefore the interpretation is by no means clear cut. In Fig. 9a the processes discussed are schematically summarised. In Auger and X-ray emission the resolution is largely governed by the inherent widths of the levels concerned in the transition. The narrowest Auger line observed so far is .18 eV (in CO) and this is sufficient to observe vibrational fine structure (Fig. 9b).[45] Experimentally, both processes can be induced by X-ray or electron beam bombardment. The advantage of the latter is that more electrons than photons can be generated and with surface studies electrons can be focused on a very small area; however, X-ray radiation is less damaging. Usually, when the X-ray emitted is induced by electron impact it is referred to as X-ray emission, if by X-ray photons, as fluorescence. When X-rays are used to study Auger spectra, the photoelectron spectra are obtained at the same time (and vice versa). In the latter the energy of the Auger lines is of course independent of the incident X-ray and therefore easily identifiable. Both techniques are particularly suitable for surface study and elemental analysis.[44,46]

CHAPTER II

PRINCIPAL FEATURES OF PHOTOELECTRON SPECTROSCOPY

The P.E. spectra display a wealth of detail not only in yielding accurate ionisation energies which in themselves are of paramount importance, but also in the shapes and intensity of bands, and fine structure when discernible. In order to comprehend the information available, theoretical aspects of photoelectron emission, of electronic structure and experimental limitations have to be appreciated. In this Chapter the former features of relevance are discussed, while the experimental side is the subject of the following Chapter.

BAND INTENSITIES

In broad terms, the intensity of the P.E. band is a function of the photon wavelength, angular distribution of the photoelectrons and the nature of the orbital. Detailed consideration of these criteria in molecules is only now starting to reach momentum experimentally and theoretically, as it has been realised that the variation of photoionisation cross-sections and angular distribution of photoelectrons can be used as a diagnostic tool in the assignment of P.E. spectra.

2.1 Photoionisation Cross-Sections.

In P.E. spectroscopy where discreet photon energy is used as source of excitation, it has been realised qualitatively that relative intensities of the P.E. bands often reflect, to some extent, the degeneracy of the subshell ionised.[47] This has been shown semi-quantitatively to be reasonable under certain assumptions and included open-shell cases.[48] In essence, this rests on the assumption that

the photoionisation cross-sections are much alike. Thus it is only really meaningful when the orbitals are similar in nature, in I.E. and not too near the threshold. For example, calculations of relative Π - electron cross-sections for ionisation of planar hydrocarbons show that the computed cross-sections are very nearly constant of all the Π - electrons in the molecule and in all the hydrocarbons considered.[49.] Thus when relative intensities are used in conjunction with, say, multiplet splitting, it is reasonable. On the other hand, in, say, methane, the degeneracy argument would suggest that the intensity of the a_1 and t_2 band should be in the ratio of $\sim$ 1:3. However, in the P.E. spectra excited by He II (40.81 eV) and Al Kα (1486 eV) photons the experimental ratios are $\sim$1;7 and$\sim$3:1 respectively. The problem is that the cross-section rises abruptly at the threshold and then decreases in a way dependent on the orbital.[50.] In methane, however, the a_1 and t_2 orbitals are inherently different, the former is solely 2s and latter 2p. Thus the use of relative intensities as criteria of assignment has to be treated with care.

Experimentally, P.E. is practically the only method available for the determination of partial photoionisation cross-sections and the latter have been determined for atoms, and for small molecules, mainly diatomic.[51.] In Fig.10a the complex nature of the cross-sections is evident.[31.]

Calculations of photoionisation cross-sections are difficult. Accurate wavefunctions of the ground state are necessary, though more of a problem is the true form of the continuum wavefunctions which are not known for any polyelectronic species. Up to now the few detailed calculations for molecules have been concerned with relative cross-sections. In one approach, the intensity of the valence shell bands, excited by X-rays were calculated.[52.] The wavefunction of the outgoing electron was represented by plane waves as the kinetic energy is high

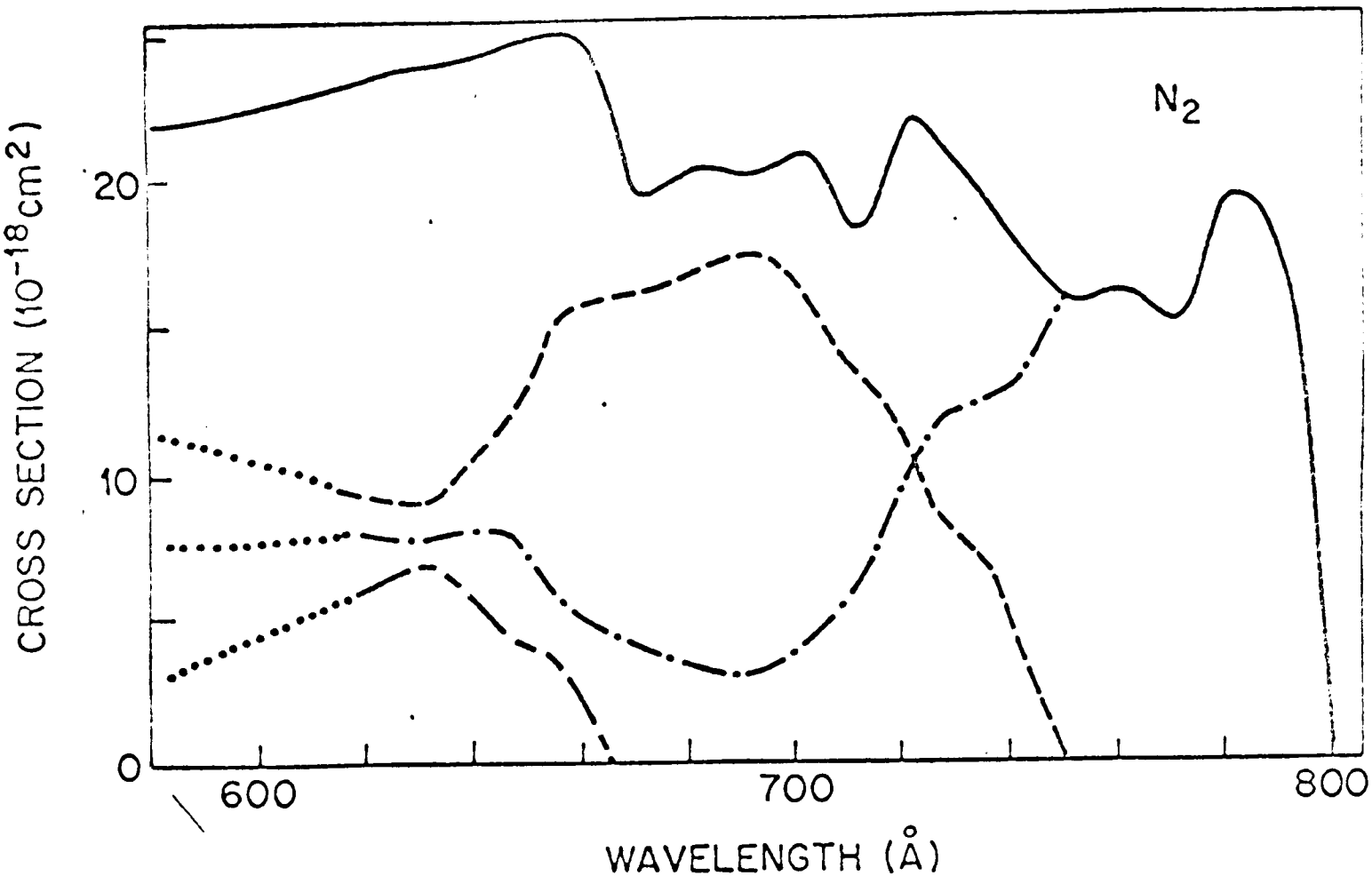


Fig. 10a Total photoionisation cross-section and individual orbital cross-sections (dashed lines) as a function of wavelength for nitrogen Ref. 31.

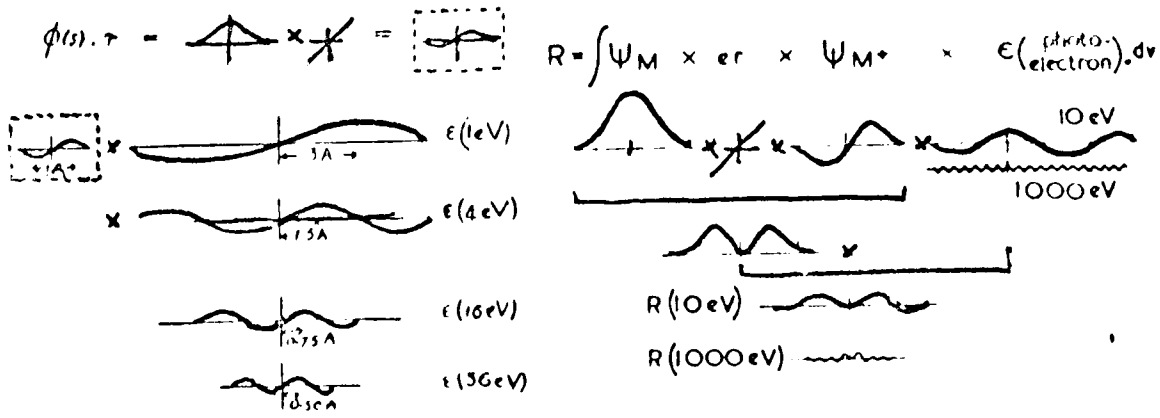


Fig. 10b Diagrammatic illustration of features of importance in the photoionisation of an electron, p-type (LHS) and s-type (RHS) Ref. 55.

enough. Cross-sections determined for the rare gases were correlated with gross atomic populations obtained from ab initio calculations were used as standards to evaluate the relative intensity for number of small molecules. In the u.v. region, calculated photoionisation cross-sections of linear molecules also showed good agreement with experimental data and qualitative rules were suggested.[53] The experimental and theoretical work is summarised by Lohr.[54]

Price and co-workers have discussed the variation of photoionisation cross-sections in view of the P.E. spectra excited by He I, He II and X-rays.[55] In Fig. 10b the qualitative argument is reproduced, based on simple overlap considerations, indicating the reason for the low cross-sections of the valence shells using X-rays. Fig.11a shows the general fall off of the $\sigma 2p/\sigma 2s$ ratio with increase of energy of the outgoing photoelectron. The variation of this ratio has been investigated in detail,[56] in agreement with these qualitative notions. The changes can be used diagnostically in band assignment. The MO with predominant p or s character shows corresponding changes (Fig. 11a). Similar considerations can be applied to intensity variation of bands, due to symmetry and size variation. (Fig. 11b). For example, this helps to assign the complex fine structure in HCN, where the near degeneracy of the $p\sigma$ and $p\pi$ orbitals prevents identification from the He I P.E. spectrum alone. Another example worth mention are the halogen ($p\pi$) bands in halogenated aromatics which can be identified by the drastic reduction in the intensity of the band with He II compared to He I P.E. spectra.

For the inner shell orbitals, the cross-section remains approximately constant in different molecules and atoms in the molecules, and a semi-quantitative use of the band intensities is often made.[40]

2.2 Angular Distribution of Photoelectrons.

To determine true photoionisation cross-sections the electrons have

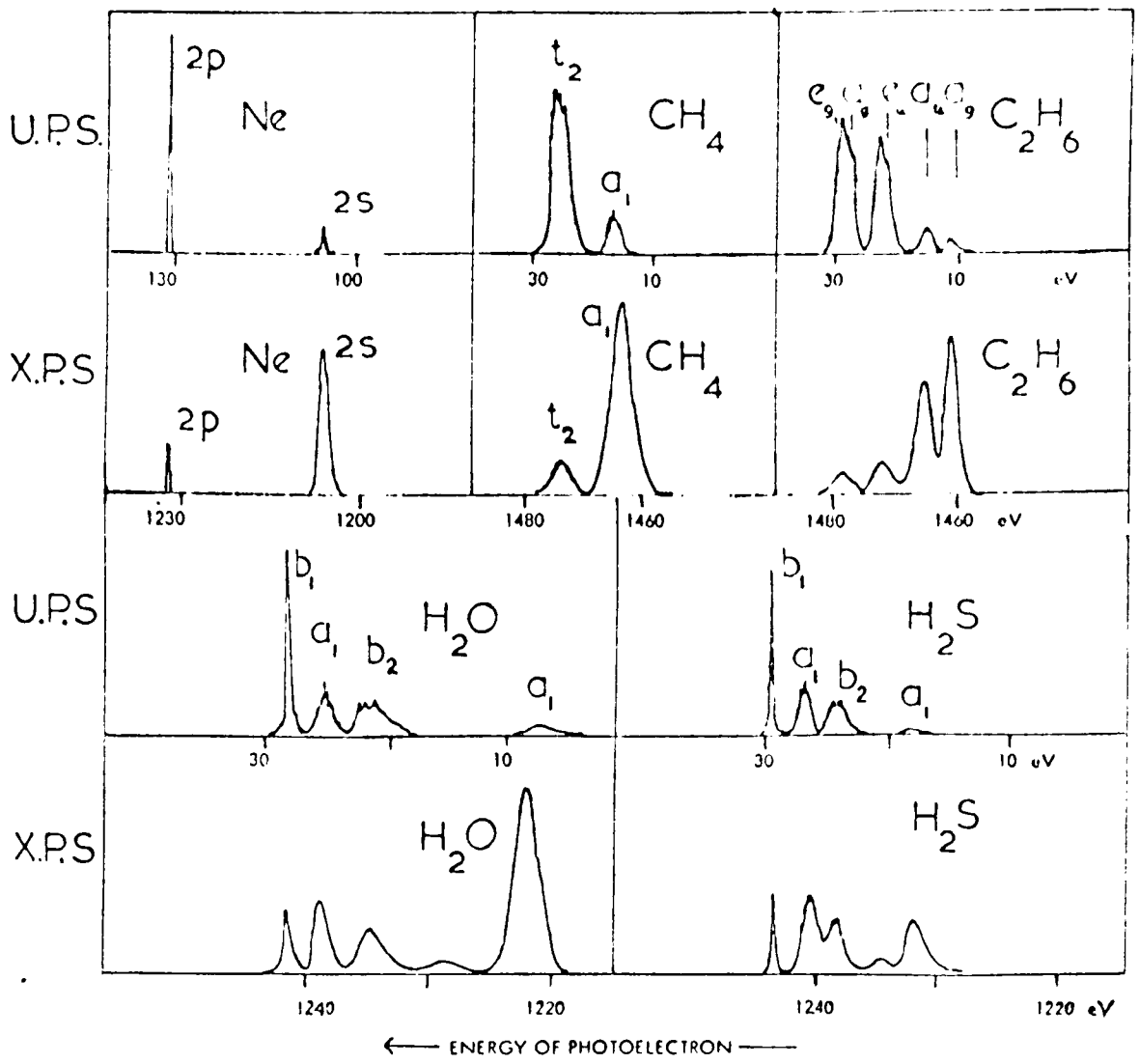


Fig. IIa Change in relative intensities of bands from p- and s-type orbitals with ionising photons of low and high energy Ref. 55.

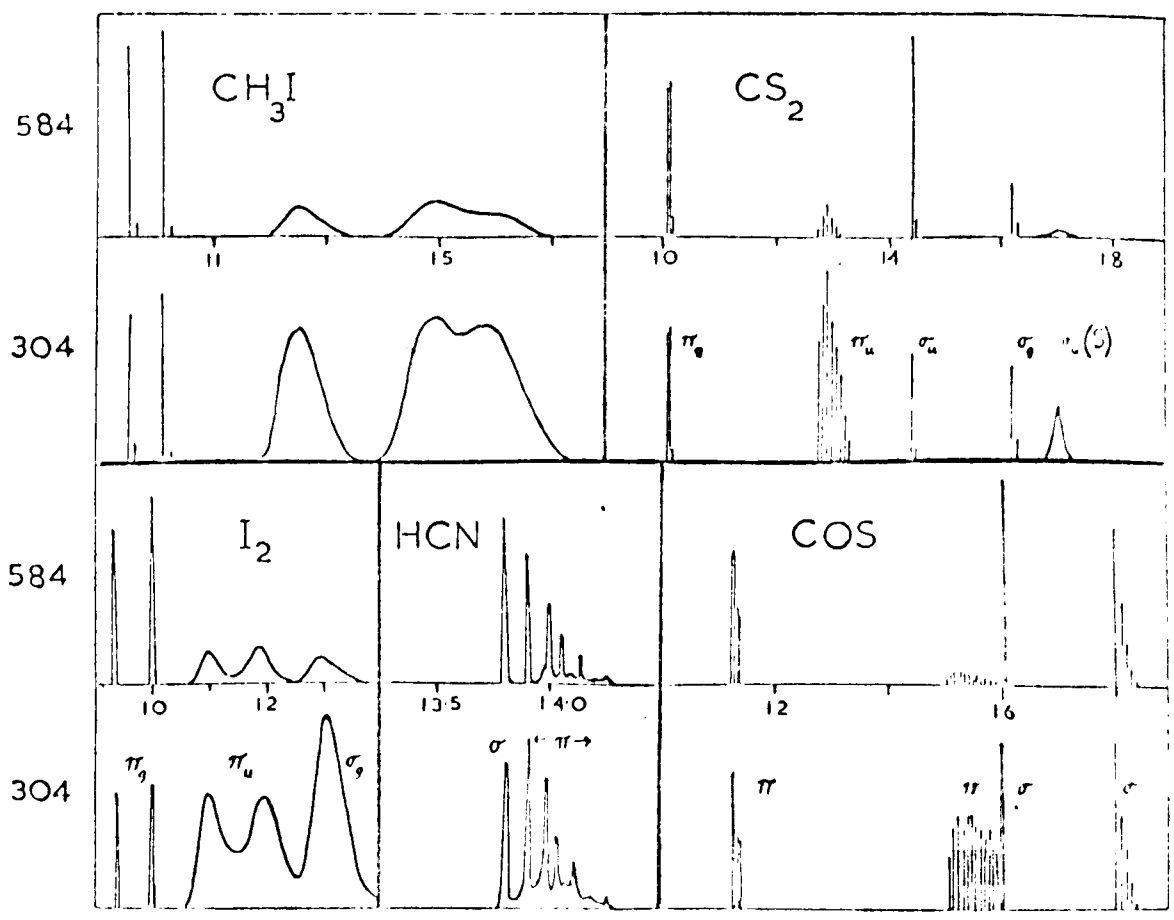


Fig. IIb Changes in relative intensities in going from 584 Å - 304 Å irradiations Ref. 55.

to be analysed either over 4π radians or the angular distribution must be known. The latter is more practical as most high resolution analysers accept electrons only close to a normal to the direction of propagation of the photon beam.

Photoelectrons have an angular intensity distribution because they are ejected in preferred directions; the axis of propagation is defined in theory by the plane of polarisation of radiation; experimentally as the radiation is unpolarised by the photon beam.

In the one-electron treatment, Bethe gave an expression for the intensity (I) distribution in terms of the angular dependence, for electric-dipole induced transition for plane polarised radiation.[57.] This has been generalised to many-electron atoms,[58.] and diatomics.[59.] The general equation of the asymmetry parameter (β) is

$$I(\alpha) = \frac{\sigma_T}{4\pi} \left[1 + \frac{\beta}{2} (3\cos^2\alpha - 1)\right]$$

where α is the angle between the axis of polarisation and the direction of propagation of the electron, σ_T is the total cross-section and β varies from -1 to +2; in the case of $\beta = 0$ isotropic distribution is obtained.

For unpolarised radiation,[60.] as is the case experimentally, theoretical treatments give the general form

$$I(\Theta) \alpha\ 1 + \frac{\beta}{2} \left(\frac{3}{2}\sin^2\theta - 1\right)$$

where θ is the angle between the directions of propagation of the radiation and of the photoelectron. More general equations for the angular distribution at any degree of polarisation has been treated by Samson.[51.] At an angle of $54^o\ 44'$, with respect to the three axes of the co-ordinate system, the distribution of the electrons is completely independent of the degree of polarisation of the ionising radiation and β.

Experimentally this has been exploited to determine true branching ratios.[61.]

The asymmetry parameter β depends on the energy of the photoelectron and the nature of the MO. In atomic systems, β values lead to information of the initial state of the electron. For example, for a S-type orbital $\beta = +2$ and the intensity has a $\sin^2\theta$ dependence. In molecules the angular momentum is not a good quantum number and symmetry has to be considered. Data on molecules are few as yet, and routine determination of reliable angular parameters is only forthcoming recently; previous results were conflictory.[62.] The early experiments used retarding spherical grids,[51,63.] workers now favour the double focusing deflection analysers.[64.] The angle (θ) is varied by rotating the light source,[62.] alternatively two multipliers are used for simultaneous detection at two angles utilising the inherent double focusing of the hemispherical analyser.[34.]

In a recent study of halomethanes, β variation was correlated, to some extent, with population density and atomic angular parameters.[65.] Preliminary data on azobenzenes also suggest diagnostic trends.[34.] Another interesting result is that the vibrational peaks in the $X\ ^2\Sigma_g^+$ state of nitrogen show angular dependence, suggestive of a breakdown of the Born-Oppenheimer approximation.[62.] In the $H_2^+ \leftarrow H_2$ transition, angular distribution study of photoelectrons from different rotational transitions[66.] show a difference in β values for the $\Delta N = 0$ and $\Delta N = 2$ (N = rotational quantum number); in agreement with theoretical work of Sichel.[67.]

In cross-section and angular distribution studies anomalous results will be obtained when perturbations due to autoionisation process and configuration interaction arise.

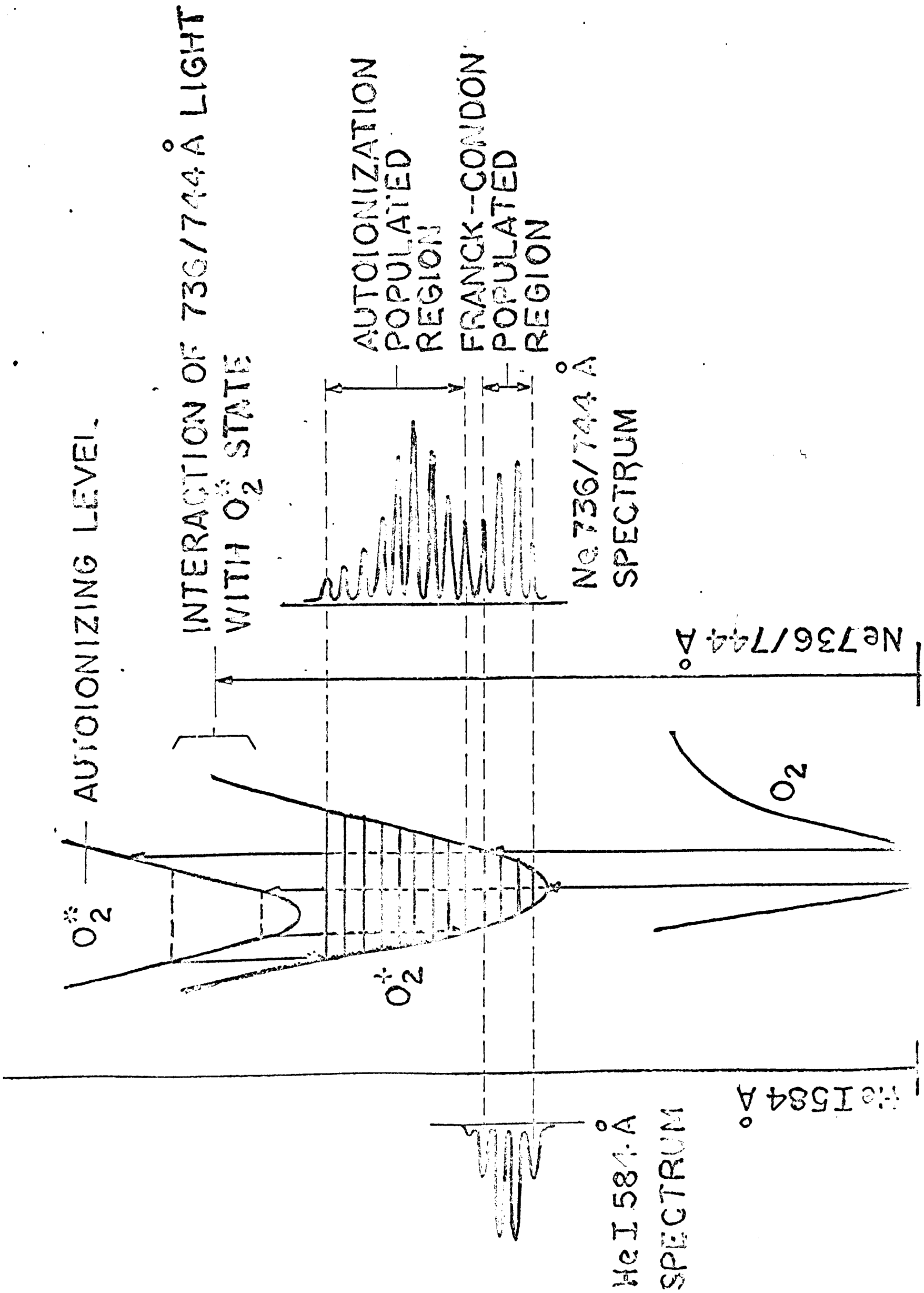
2.3 Autoionisation

In P.E. spectroscopy direct ionisation into the continuum is dominant, in contrast to threshold techniques where the high probability autoionisation processes obscure most details of inner valence orbitals. However, in P.E. spectroscopy if the autoionisation process does take place (Table 1c) this will lead to the same ionic configuration that could be reached directly. As this is a resonance phenomenon, the energy of the monochromatic photon beam must correspond with the energy of the super-excited bound or dissociating neutral state (M^*), which has the right symmetry to interact with the product of the wavefunction of the lower ionised state and its photoelectron.

The now classical case of autoionisation in P.E. spectroscopy is of oxygen.[68] The profile of the first band in the spectrum excited by He I radiation differs considerably to that excited by Ne I radiation. In Fig. 12 the autoionisation process (with Ne I) is diagrammatically rationalized. When this sort of perturbation occurs, the Franck-Condon factors can be altered considerably, though this can be advantageous when the Franck-Condon region is effectively extended. In the case of oxygen, the distribution of calculated Franck-Condon factors agrees well with experimental.[69]

The ionic states of the valence shell are located in the I.E. $\sim$ 8 - 25eV range and thus using lower energy photon lines, such as H_2, A, Ne (Chapt. III), there is likelihood of coincidence of the resonance line with the Rydberg bands converging to the excited states of the ion. Even with He584Å radiation, therefore, autoionisation is quite possible and the work of Price shows[55] that indeed autoionisation is a bit more widespread with He584Å than had hitherto been realised. In Fig. 13 the striking differences in band intensities in the He I and He II P.E. spectra are attributed to autoionisation. The use of the latter radiation is advantageous in this respect as very few

Fig.12 Schematic diagram illustrating the direct and autoionising processes for the ionisation process in oxygen



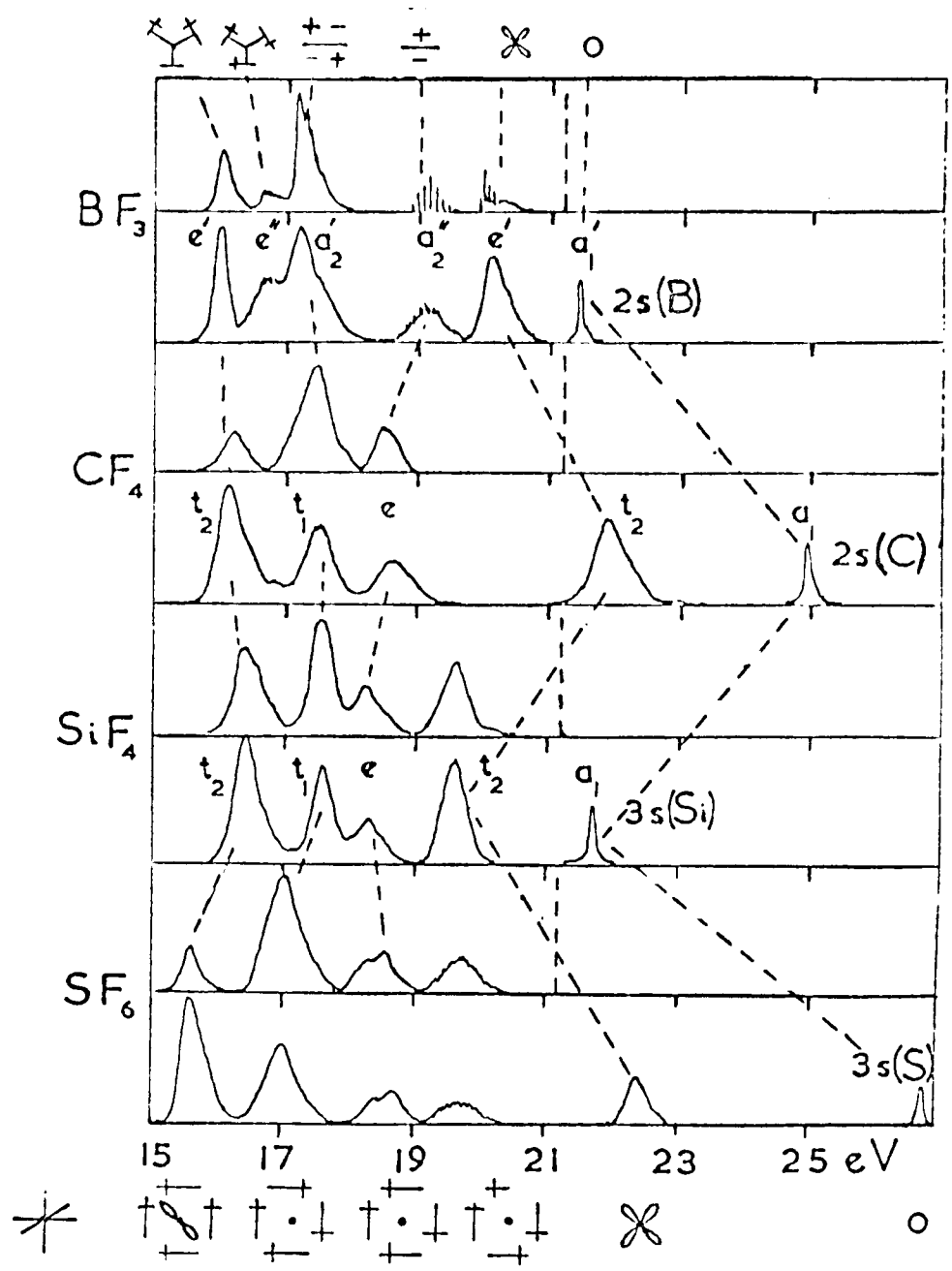


Fig. 13 Photoelectron spectra of XF_n molecules with 584 Å and 304 Å irradiation

molecules have Rydberg bands of valence electrons at this wavelength.

Selective autoionisation can be used to an advantage as the process is subject to selection rules and this may be used to identify the symmetry of the states concerned by correlation with optical and electron impact data.[55].

2.4 Forbidden Processes.

The interaction between a molecule and a photon is described by a one-electron operator and thus only those ionic states which differ from the neutral state by one MO will be allowed in the first approximation. However, if electron correlation is included, through configuration interaction (CI) for example, "forbidden" transitions inaccessible normally by a one-electron process may be partially allowed.[70,71]. An example is the production of the $C^2\Pi_u$ state of O_2^+ which is formally forbidden. Through CI intensity can be "borrowed" from the allowed transition to the $A^2\Pi_u$ state.[70]. The calculations suggest that the latter should have approximately a third of the statistically expected intensity and this is indeed borne out experimentally.[72]. Similarly, the two electron transition to the $C^2\Sigma_u^+$ state of N_2^+ has been detected at 25.3eV; the intensity is "borrowed" from the allowed transition to the $B^2\Sigma_u^+$ state at 18.8eV through CI.[73].

In the P.E. spectra excited by X-ray photons, multielectron excitations are much more common. These are known as "shake-up" and "shake-off" processes, though the mechanism of these is the subject of controversy.[74]. In the u.v. region the only known case of simultaneous ionisation and excitation is the $He^+2s \longleftarrow He\ 1s^2$ process occurring at 65.4eV.[75].

BAND SHAPES AND FINE STRUCTURE

The general principles in the correlation of band shapes and

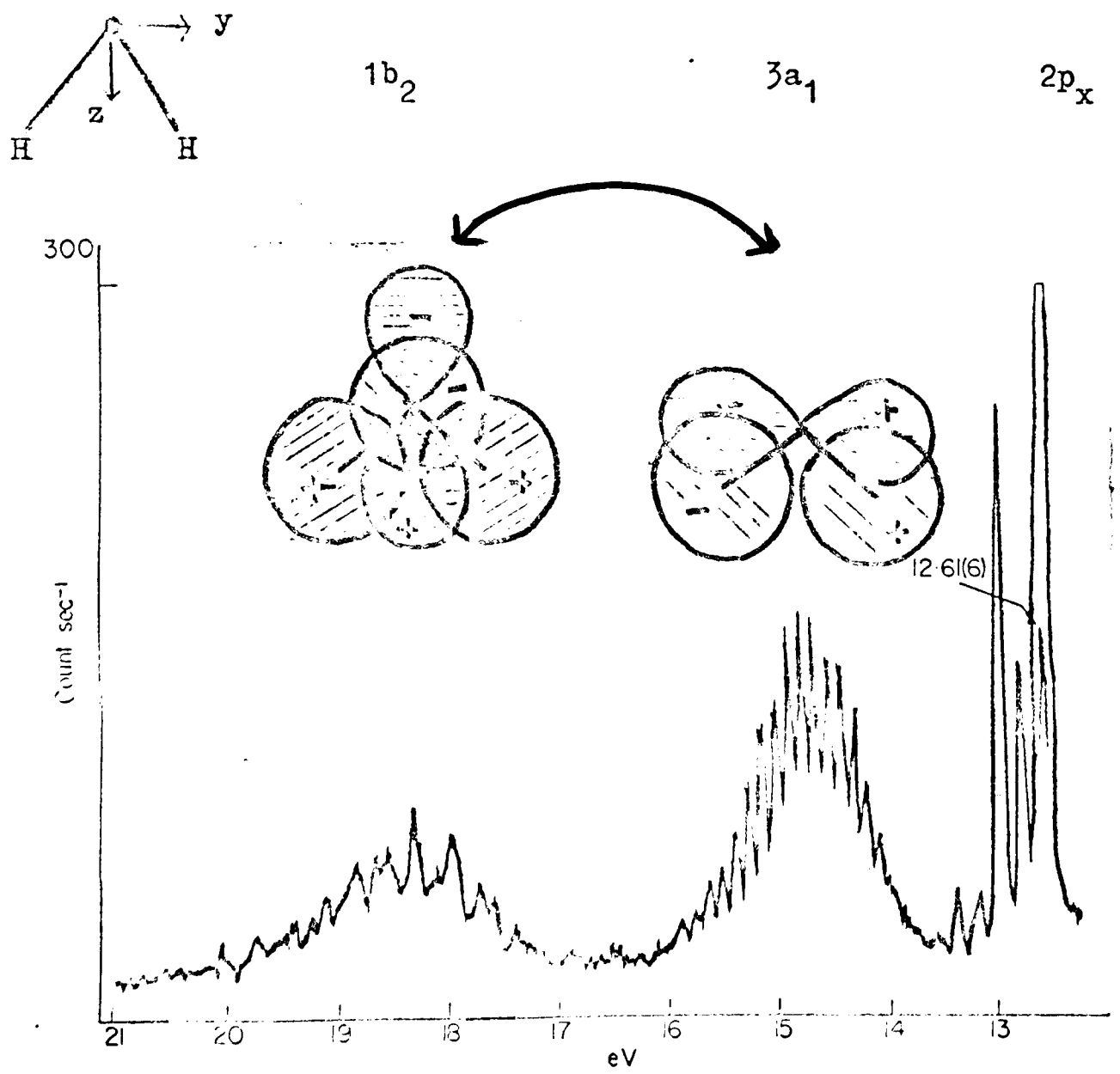
vibrational frequency change with geometry changes and bonding characteristics of the orbital concerned in the ionisation were discussed in the previous chapter. In P.E. spectroscopy these factors often give as much information as the energy of the process (I.E.), particularly in small molecules where vibrational fine structure is discernible.

2.5 Franck-Condon Factors and Vibrational Fine Structur

The P.E. spectrum of water (Fig. 14) beautifully exemplifies the points discussed in 1.2.[76.] The band shapes reflect the dimensional changes on ionisation and the vibrational modes excited and the frequency change relative to the ground molecular state reflect the bonding characteristics between the particular atoms. These features support directly the simple MO scheme shown; the data is diagrammatically summarised in Fig. 14. The experimental Franck-Condon factors can be compared with calculated ones as function of the dimensional parameters to deduce the ionic geometry. This has been done with several small molecules.[77.]

In polyatomic molecules, Turner showed[47.] that empirical relations used in optical spectroscopy, linking inter-nuclear distance and vibrational frequency, can be extended to cover vibrational bands observed in P.E. spectra. A reasonable fit is obtained for w''/w' and $I_v - I_a$ (I.E.s) for many polyatomics. This has practical significance, as the derived relationships can assist to identify vibrational modes excited in cases of doubt.[78.]

In the absence of rotational analysis in electronic transitions, arguments as above present practically the only means of discussion of the bonding characteristics. In high resolution P.E. spectra, in some cases, there is asymmetrical broadening of vibrational peaks by rotational envelopes. This can yield information of the relative dimensional change. In brief, bond length increase leads to a diverging P-branch



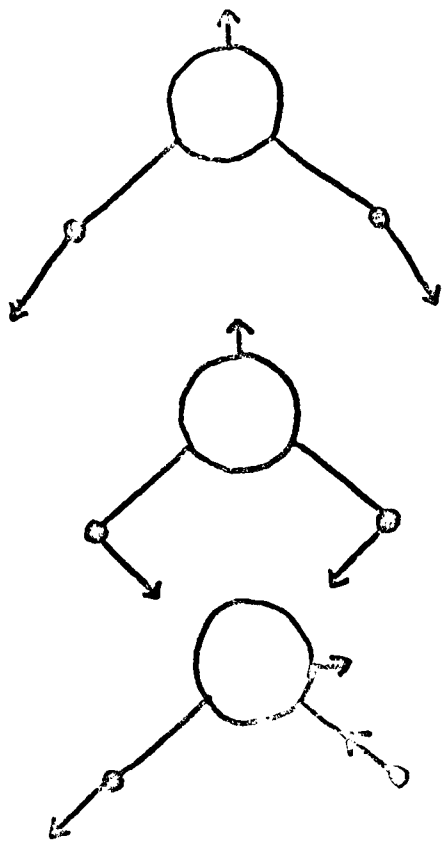


Fig.14. Photoelectron spectrum of water, molecular orbitals and vibrational frequencies.

and an R-branch converging to a band head. This will give rise to a "tail" on the vibrational components on the low I.E. side. In hydrogen, where in fact some of the rotational transitions are resolved, this is readily perceived (Fig. 15a).[79.]

2.6 Structureless Bands.

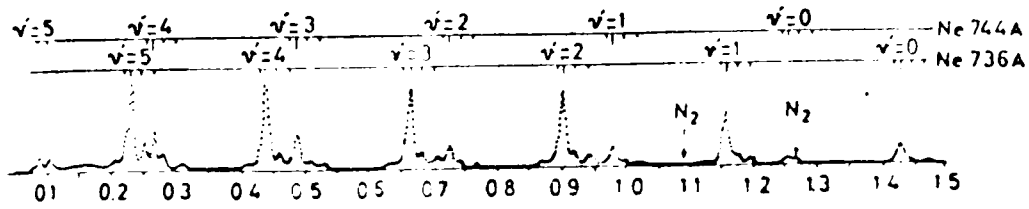
In large molecules few of the bands have distinct vibrational fine structure discernible. Large numbers of vibrational (and rotational) modes can be excited which overlap, so that an apparent continuum is obtained, though in some cases transitions may take place to a repulsive state. Nevertheless, the profile of the Franck-Condon envelope can be used as an indication of geometry change (see Chapters V-VII).

2.7 Vibronic and Spin-Orbit Structure.

In non-linear molecules in degenerate states there is always at least one non-totally symmetric normal co-ordinate that causes splitting of the potential function so that the potential maxima are not in the symmetrical position. The consequence of the Jahn-Teller theorem[80.] is that on ionisation the different electronic states, arising from the distortion, will be accessible and a modified Franck-Condon envelope may be obtained.

Methane was the first unequivocable example of a Jahn-Teller distortion detected by P.E. spectroscopy.[81.] Ionisation of an electron from the t_2 orbital leads to a treble maximum in the first band. The initial triple degeneracy is removed as result of the distortion and the three energetically different processes observed, correspond to the transitions to the surfaces of the resultant electronic states. Many other molecules show the Jahn-Teller distortion in the P.E. spectra.[82.]

In a few instances, the vibronic fine structure discernible has provided unambiguous assignment of the electronic state.[83.] Conversely,



(a)

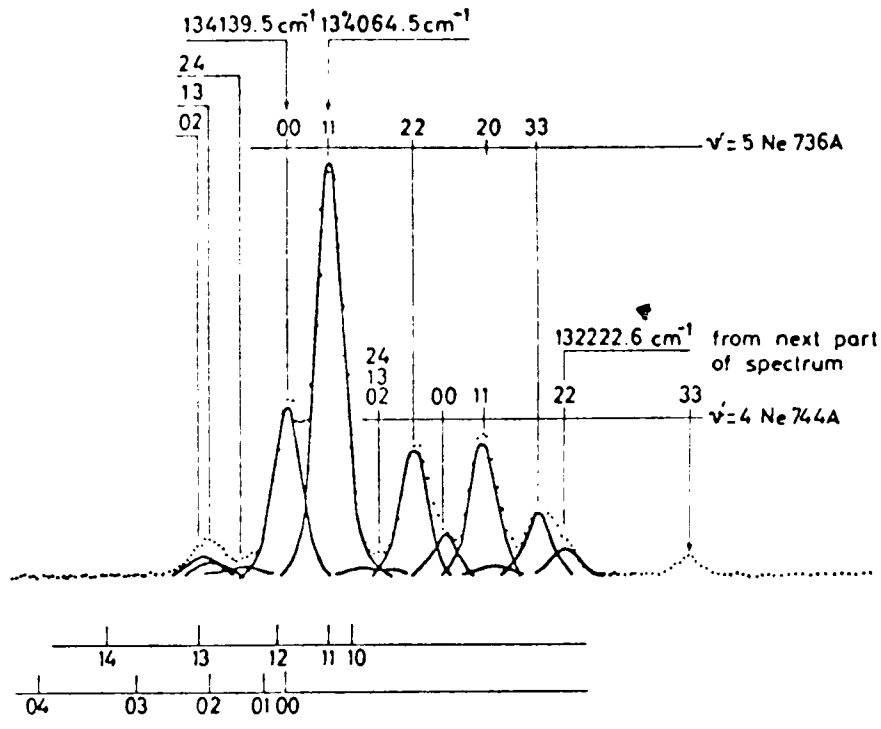


Fig. 15a Photoelectron spectrum of H_2 observed with Ne source Ref. 79

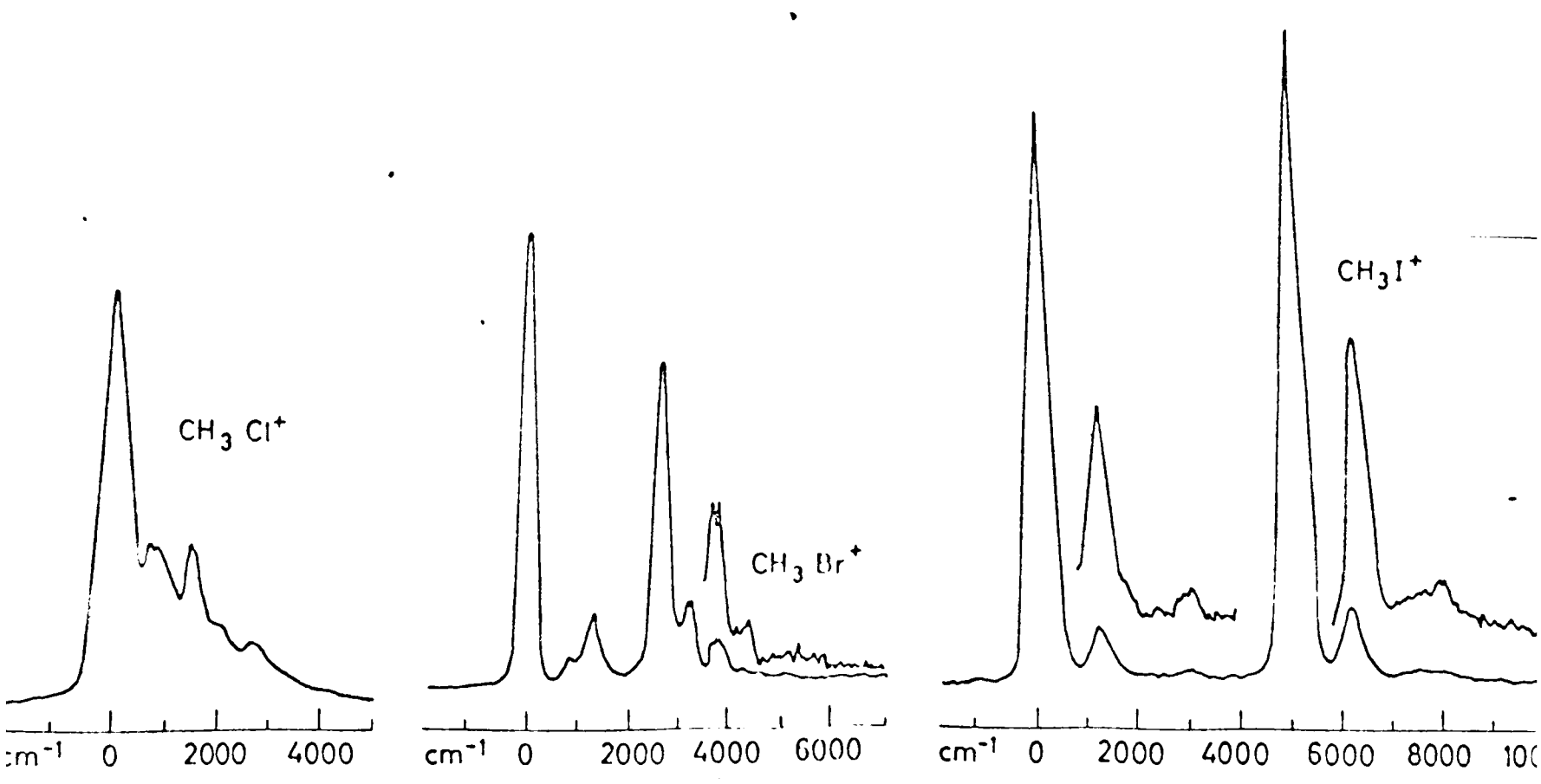


Fig. 15b First bands in the He I photoelectron spectra of methyl halides

in analysis of vibrational fine structure, the presence of non-totally symmetric modes is often an indication of vibronic effects. Likewise,, the presence of the double maxima has been used as support in assignment of degenerate orbitals; the magnitude of the splitting is proportional to the "bonding power" of the electrons involved. In linear molecules, the first order Jahn-Teller term vanishes and the corresponding vibronic perturbation (second order) is known as the Renner-Teller effect.[84.] This has been observed in water and probably hydrogen cyanide ions.[47.]

Multiplet fine structure arising from spin-orbit (S-O) interaction is often discernible in the P.E. spectra, particularly with the presence of heavy atoms.[85.] This is very useful in spectral assignment as it indicates orbital degeneracy, and the magnitude of the splitting can be used as a sensitive probe of the electronic environment. The magnitude of the splitting depends on the atomic number and the localisation characteristics of the degenerate orbital in question.[86.] Molecule ion states susceptible to S-O splitting will at the same time be to Jahn-Teller forces; large S-O effect quenches the latter.[10.] This is illustrated in the P.E. spectra (Fig. 15b) of the methyl halides.[47.] In their doublet spin ionic states the electronic spin angular momentum (Σ) interacts with the electronic angular momentum (Λ), resulting in two energetically different states ^2E characterised by the total angular momentum quantum number $\Omega = \frac{3}{2}, \frac{1}{2}$. In CH_3Cl^+ a complex profile is obtained due to competition between the S-O and Jahn-Teller forces, while in CH_3I^+ the S-O interactions quench the vibronic coupling.

In the P.E. spectra excited by X-rays, resolution limits the fine structural detail discernicle mainly to S-O splitting in the core shells, which is often of magnitude of 10eV or more.[87.]

2.8 Multiplet Splitting.

In open-shell molecules additional electronic interactions need

consideration. Ionisation of inner valence electrons will result in the formation of triplet and singlet states as consequence of quantum mechanical exchange interaction of the odd electrons. Such exchange splitting can be seen in the P.E. spectrum of NO_2.[47.] If, additionally, the odd electrons possess angular momentum, different term states will also be obtained. An example is provided by NO.[47.]

2.9 Predissociation

Photoelectron spectral line broadening, governed by the uncertainty principle, is of magnitude $h\tau^{-1}$. When an unstable ion is formed (e.g. predissociated), with lifetime comparable to the time of molecular vibration, broadening, or complete absence of vibrational peaks is observed. In the P.E. spectra broadening, followed by breaking off of vibrational fine structure is often used as evidence for curve crossing.[47.] The appearance potentials of fragment ions often fit well with the I.E. near the break-off point. However, in correlating P.E. data with mass spectrometric details the time scale must be kept in perspective, as in the latter the ions are studied usually after $\sim 10^{-6}$ sec.

It is interesting to consider the predissociation in HBr^+ as detected by a complementary study with P.E. spectroscopy[47.] and ion fluorescence.[36.] In the P.E. spectrum (Fig. 16a) the band associated with the $\tilde{A}\,^2\Sigma^+$ state, shows broadening in V' = 4 vibrational peak, the subsequent peaks become diffuse and fine structure breaks off near 16eV. This is attributed to predissociation by the interaction of the $^2\Sigma^+$ potential curve with the a $^4\Pi$ repulsive curve leading to fragmentation into the ions. The P.E. spectral evidence suggests that the curve crossing occurs between V' = 3 and V' = 4. Fluorescence of the allowed transition

$$\tilde{A}\ ^2\Sigma^+ \longrightarrow \tilde{X}\ ^2\Pi_\Omega \quad \Omega = \frac{3}{2}, \frac{1}{2}$$

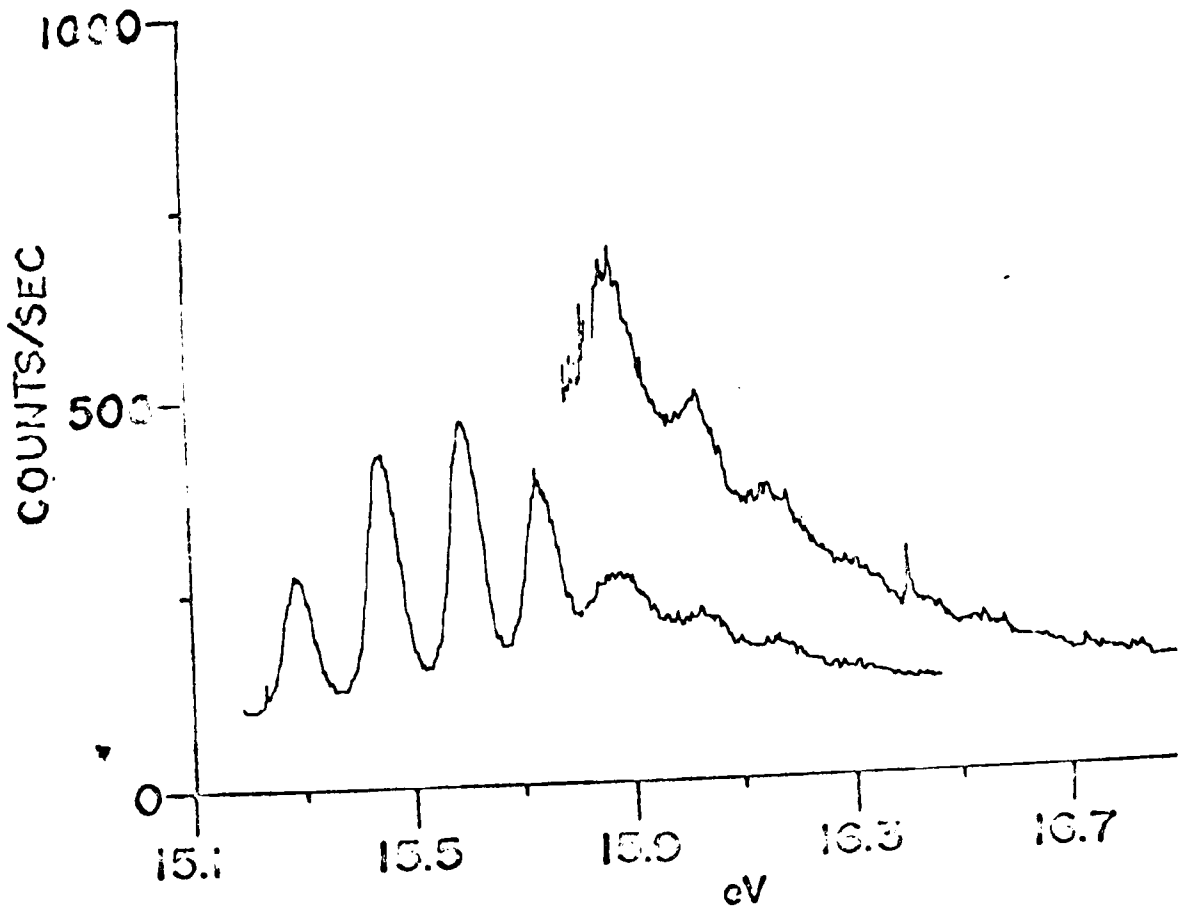


Fig. 16a Photoelectron spectrum of the $\tilde{A}^2\Sigma^+$ state of HBr^+

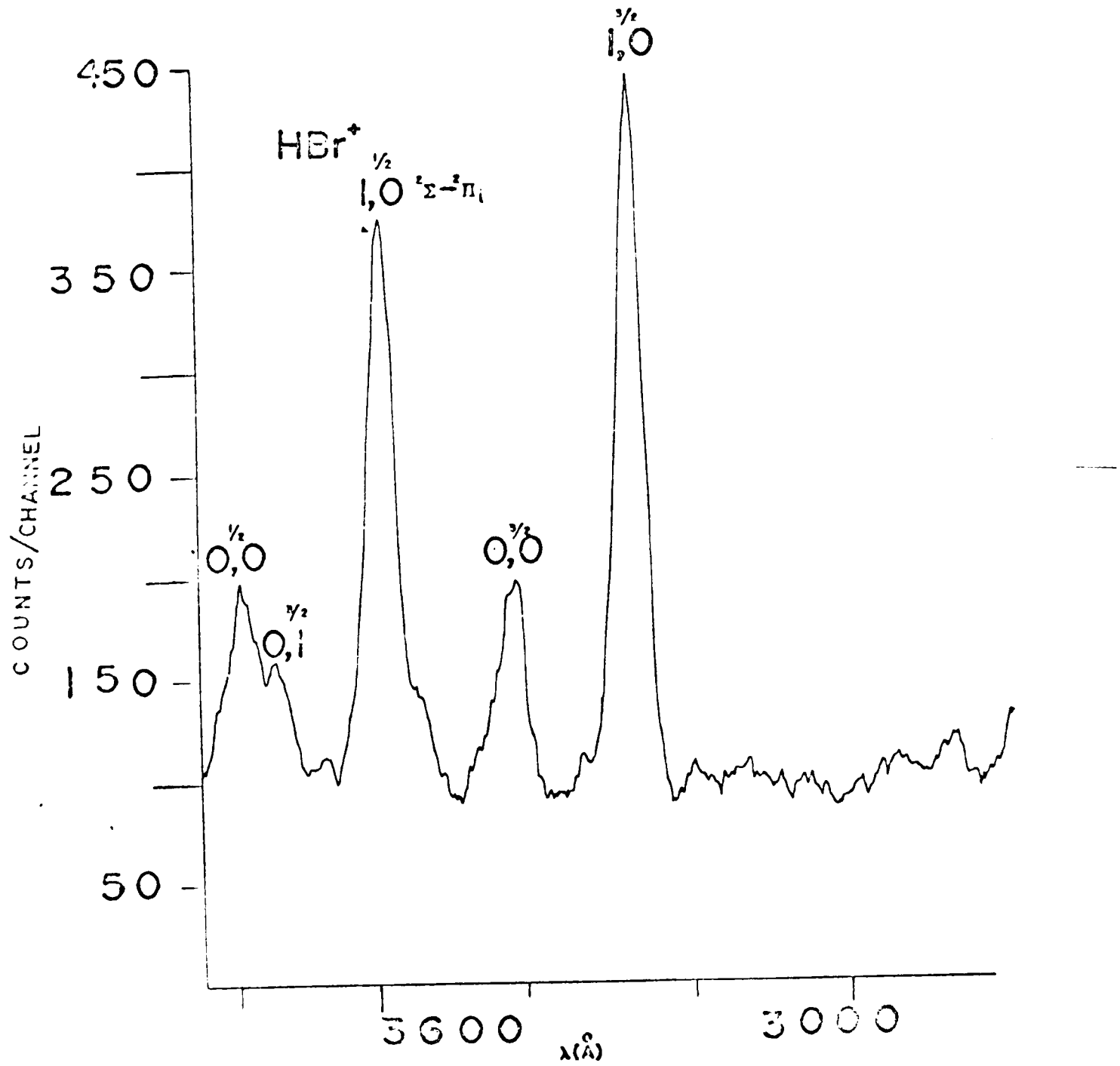


Fig. 16b Fluorescence photoionisation of HBr^+ $\tilde{A}^2\Sigma^+ - \tilde{X}^2\Pi$

is only observed from V' = 0 and V' = 1 level of the $^2\Sigma^+$ state, even though the P.E. spectra show significant population of vibrational levels up to V' = 5. However, an emission spectrum is a much more sensitive test of predissociation indicating in this case that levels $V' \geq 2$ must be predissociated.

2.10 Interpretation of P.E. Spectra.

The fine structural detail and subtleties discussed above, when discernible, help appreciably in the interpretation of the P.E. bands. In addition, the experimental I.E.s can be compared with orbital energies from quantum mechanical calculations. The prolific data forthcoming in the past decade has regenerated interest in MO calculations and particularly emphasised the deficiencies of the various approximations.

For complete assignment, a priori determination of the 3N - 6 dimensional energy profile of the molecule in its ground state and for the ion in all its different electronic states is necessary. Though, ab initio calculations are becoming more widespread, for large molecules they are still impractical. Thus semi-empirical methods of the CNDO, MINDO, Extended Hückel still thrive. Their application in P.E. spectroscopy has been reviewed by Worley.[88]

The interpretation of the P.E. spectra based solely on calculations is neither reliable nor satisfactory, although as a supplemental tool they are often useful. A satisfactory and often the only means, especially in larger molecules, of interpreting the P.E. spectra is through trends in a series of closely-related molecules. These can be correlated with other physicochemical data and fitted in a convenient, and hopefully useful, scheme. There are now many such successful correlations both in the inorganic and organic fields.[47,89]

CHAPTER III

EXPERIMENTAL AND INSTRUMENTATION

Since the initial exploratory work of Turner[30.] in u.v. and Siegbahn[39.] in the X-ray region, all aspects of the photoelectron spectrometer have been improved. The interest generated has resulted in the rapid development of light sources, adaptation of numerous electron analysers and several commercial spectrometers. The basic instrumentation for P.E. spectroscopy using u.v. photons and soft X-rays is essentially the same, though specific features may change depending on the emphasis of the study.

3.1 Vacuum System

The essential features of the vacuum system of the spectrometer used in this work are shown in Fig. 17. A pressure of $\sim 10^{-6}$ torr can be maintained by means of a rotatory pump and an oil diffusion pump. This pressure is adequate for gaseous, but not for surface study where a pressure better than 10^{-9} torr is necessary. The working main chamber pressure is limited to $\sim 5 \times 10^{-4}$ torr by the channel multiplier. The volatile sample inlet pressure is normally up to $\sim .3$ torr, that of the helium $\sim .1$ torr in the light source. The pressure differential is maintained by a fast pumping system, slits, and narrow bore inlet tubes. Solid samples used in this work were inserted directly to the proximity of the ionisation chamber via a vacuum lock (Fig. 17) on the end of a steel probe sliding through o-rings. The principle of the operation is that a subsidiary pumping port is available so that samples may be inserted without disruption of vacuum; the seal is kept by o-rings. The sample could be heated up to the desired temperature via an internal electrical filament in the probe. When involatile samples

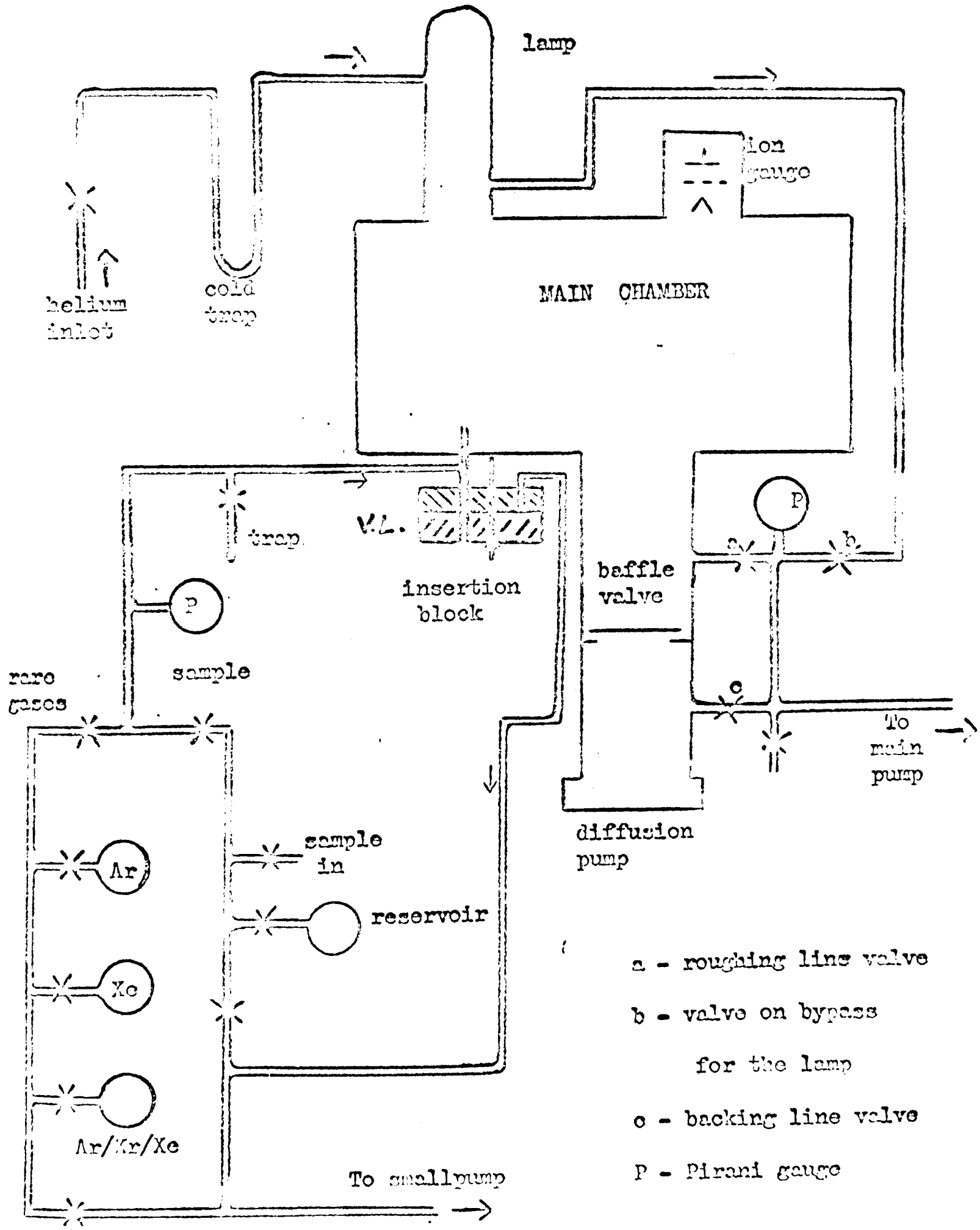


Fig. 17 Vacuum system of the spectrometer

were studied the whole vacuum chamber was maintained at $\sim 70^{\circ}$, to reduce surface contamination, particularly important in the ionisation chamber.

3.2 Light Sources.

The source of energy of concern here is photons, alternatives such as electrons and excited metastables were mentioned in Chap.I. The distinction between u.v. and X-ray P.E. spectroscopy is a natural one; the energy of the excitation radiation used in the former is usually < 60eV and in the latter > 1000eV.

The majority of the work in the u.v. has utilised the He Iα (21.22eV) emission line,[47] corresponding to the process

$$He(1s^2 \ldots {}^1S_0) + e \longrightarrow He^*(1s2p \ldots {}^1P_1) + e \xrightarrow[584\text{Å}]{h\nu} He(1s^2 \ldots {}^1S_0) + e$$

The emission is usually generated by a high voltage DC discharge through helium in a capillary[90] and sometimes by microwave excitation.[13,91] The helium is purified by passage through charcoal (or zeolite) trap at liquid nitrogen temperature. However, even if the helium is pure satellite lines of the He I series are present; the ratios depend on experimental conditions. The most intense, He Iβ (537Å) usually occurs to an extent of a few per cent. In addition, a small percentage of impurity lines, particularly H_2Ly and NI, can often be detected.[92] These complications must be appreciated when analysing P.E. spectra and can lead to errors in the interpretation.

He IIα (40.81eV) sources have been constructed for routine use in P.E. spectroscopy.[11,68] The emission is the fluorescence of the helium ion

$$He(1s^2 \ldots {}^1S_0) + e \rightarrow He^{+*}(2s \ldots {}^2P_{\frac{1}{2}}) + 2e \xrightarrow[304\text{Å}]{h\nu} He^+(1s \ldots {}^2S_{\frac{1}{2}}) + 2e$$

In brief, the emission is enhanced by low helium pressure, fast differential pumping and high current density. The photon energy of 40.8leV offers the advantage of the extension of the ionisation range. However, complete "removal" of the He I radiation is troublesome, but can be achieved using thin films (or plug gas) as filter.[93.]

The resonance lines of other rare gases are also used,[47.] especially when the lower kinetic energy of the ejected electron is advantageous in the resolution problem. Hydrogen Lyman and nitrogen I lines can also be useful in this respect. In Table 2 the wavelengths of the more important emission lines used, are given.[12.]

TABLE 2

Resonance Line	λ(Å)	eV
He Iα	584.3*	21.22
He Iβ	537.0	23.09
He IIα	303.8*	40.81
He IIβ	256.3	48.37
Ne I	735.9*	16.85
	743.7	16.67
AI	1048.2*	11.83
	1066.7	11.62
N_2 I	1135.0	10.92
H_2 Lyα	1215.7	10.20

* Raie ultime

The use of synchrotron radiation,[94.] whose continuum extends through the vacuum u.v. coupled to a monochromator is an exciting proposition though not yet practical due to large loss of intensity.

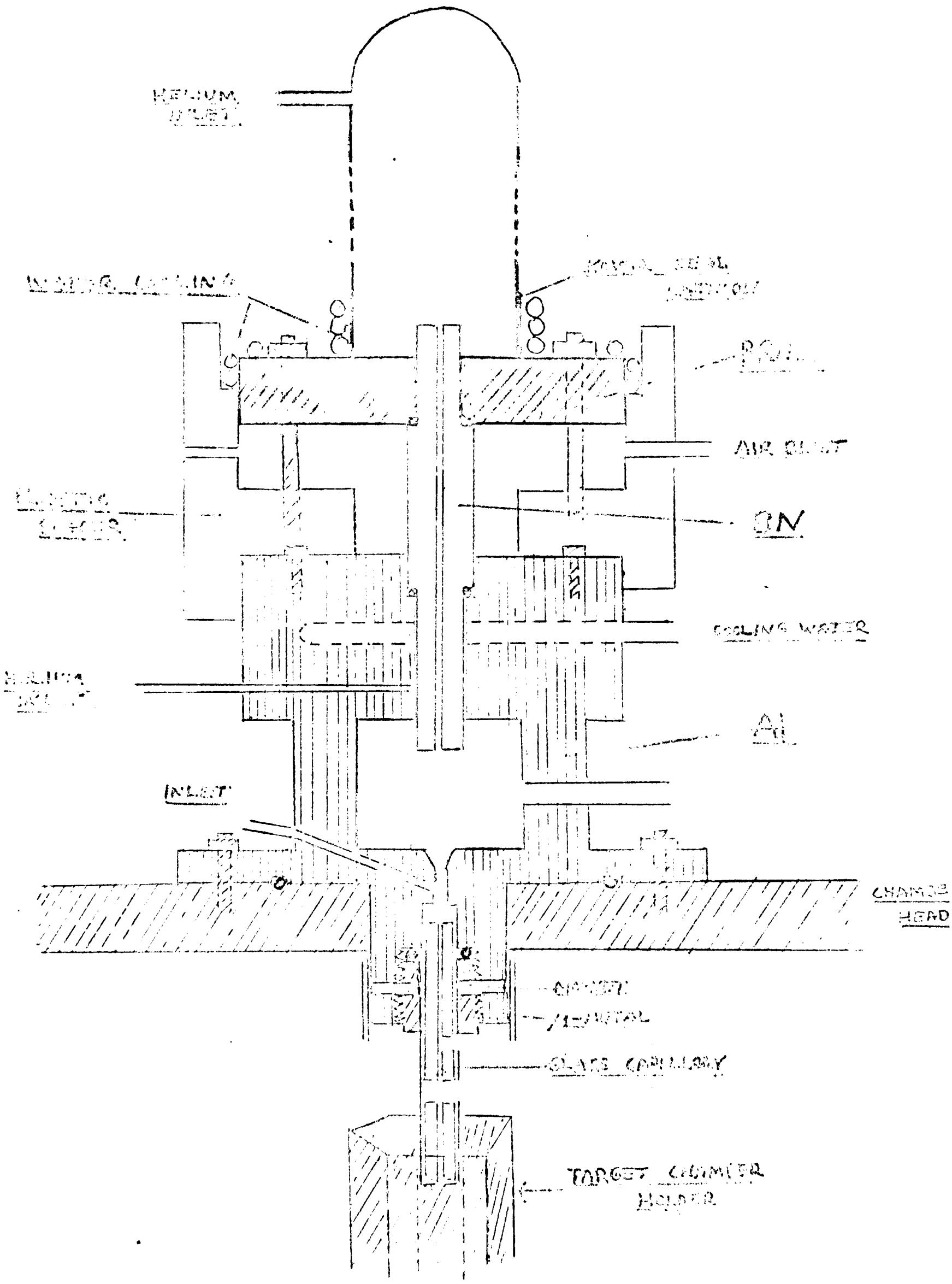


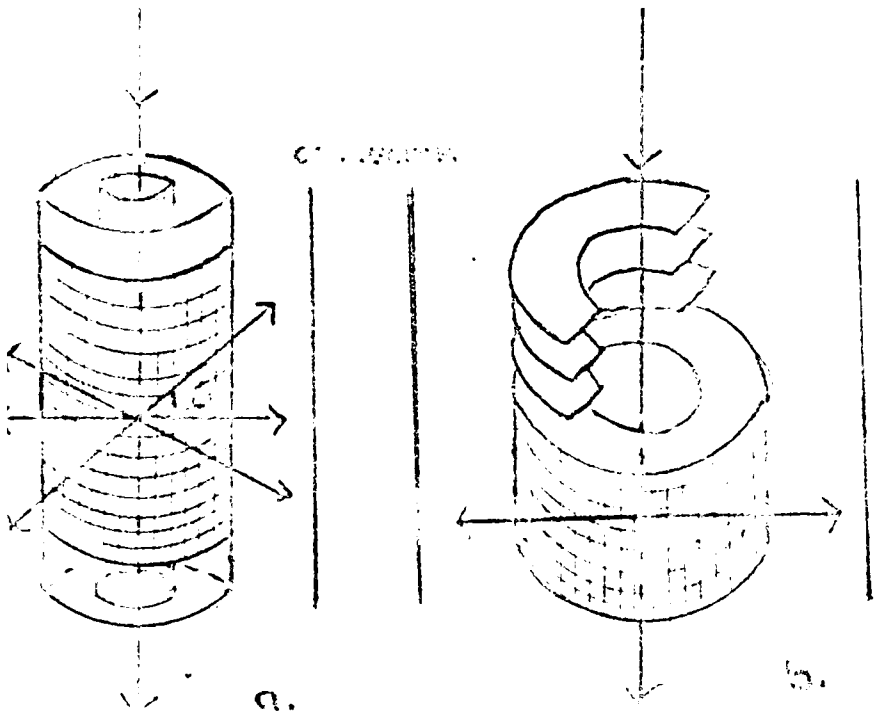
Fig. 18 Cross-section of the light source and collimating system

In the X-ray region, most convenient sources up to now are the K_α lines of Mg (1253.6eV) and Al (1486.6eV); lower Na (1041.0eV) and higher, up to Ag (22162.9eV), lines are available.[45.] Sources in the intermediate range, such as YMζ (132.3eV) are being developed.[95.]

The P.E. spectra presented in this thesis, were obtained using a modified DC capillary discharge light source designed and built to give higher He I flux and also He II. A schematic cross-section is shown in Fig. 18. The lamp differs from the one reported by Turner earlier[96.] in that the quartz capillary was replaced by boron nitride (10cm long 1mm internal diameter) and additional ports were provided to allow reliable operation with lower helium pressures without accumulation of impurities. Depending on the helium flow rate and pressure gradient, the lamp would emit either He I free from He II resonance line or up to c.a. 1:1 He II/He I ratio. lower pressure favours the latter condition.

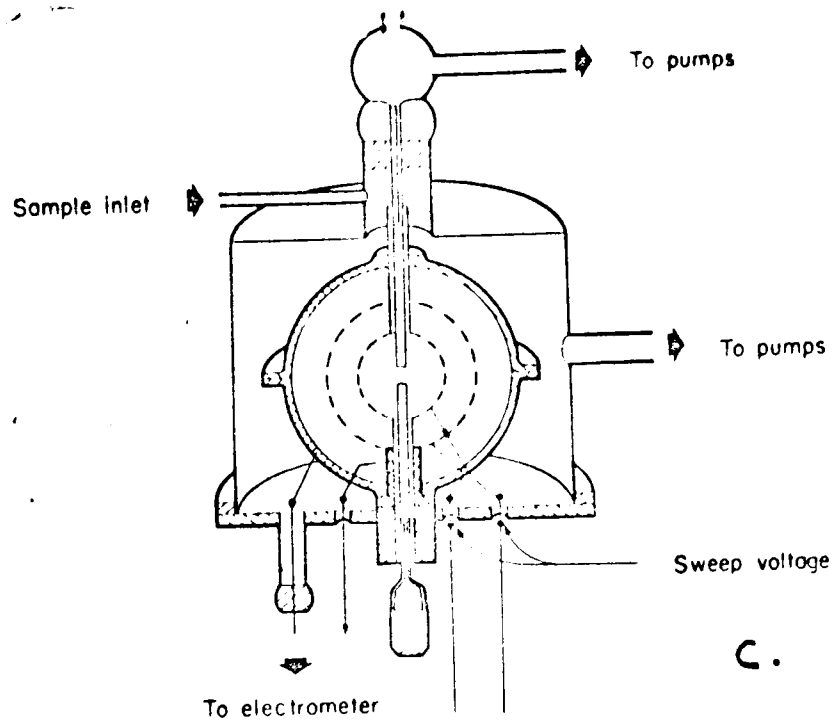
3.3 Electron Energy Analysers.

The initial photoelectron spectrometers utilised electrostatic retarding fields for electron energy analysis. Both Turner[30.] and Vilesov[29.] used a cylindrical retarding system (Fig. 19a). In this arrangement the collimated light beam travels down the axis of the grids ionising the sample gas. The ejected electrons, drawn towards the collector, pass through the inner grid into the retarding field between the two grids. The energy analysis is achieved by change of the retarding field gradient between the grids. Thus for each ionisation a step is produced. However, the cylindrical analyser suffers from inherent lack of resolution because not all the electrons are ejected at right angles to the retarding field. This difficulty was overcome with slotted grids[68.] (Fig. 19b). The latter inhibit collection of electrons <u>not</u> at right angles to the axis. Alternatively, spherical grids[13,97.] (Fig. 19c) can be used as the full 4π solid angle is examined and all the ejected electrons are

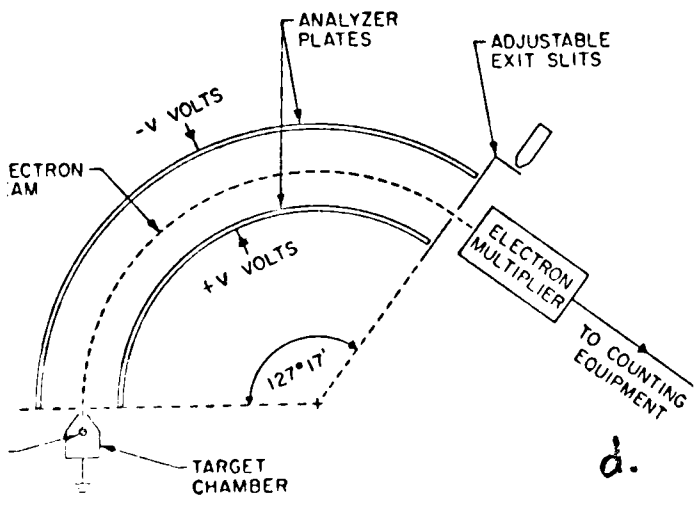


a.

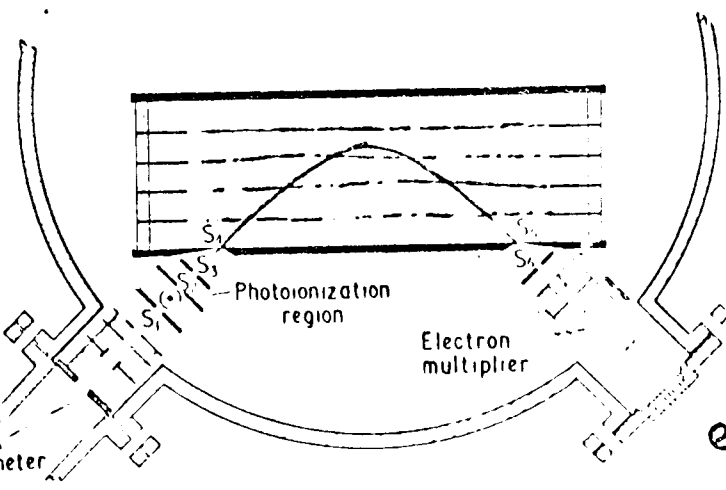
b.



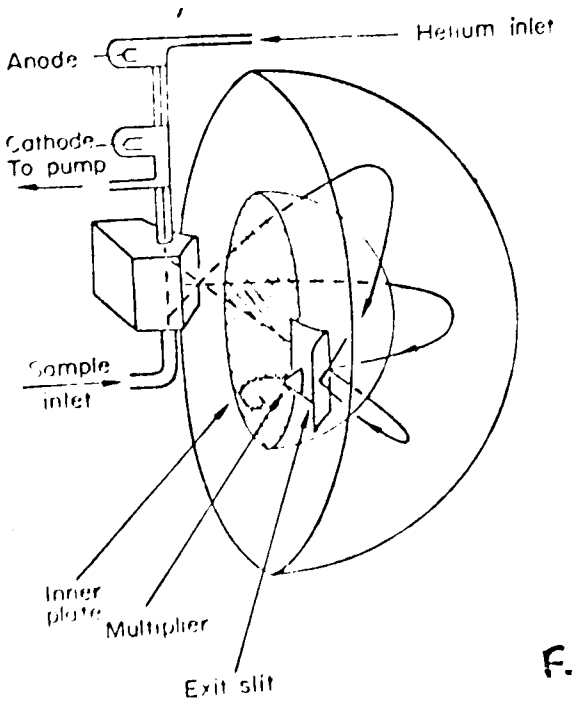
c.



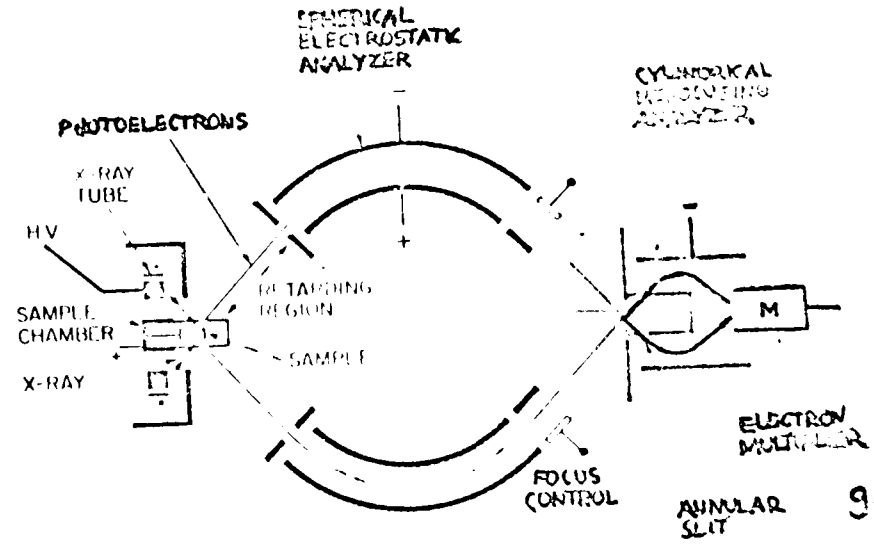
d.



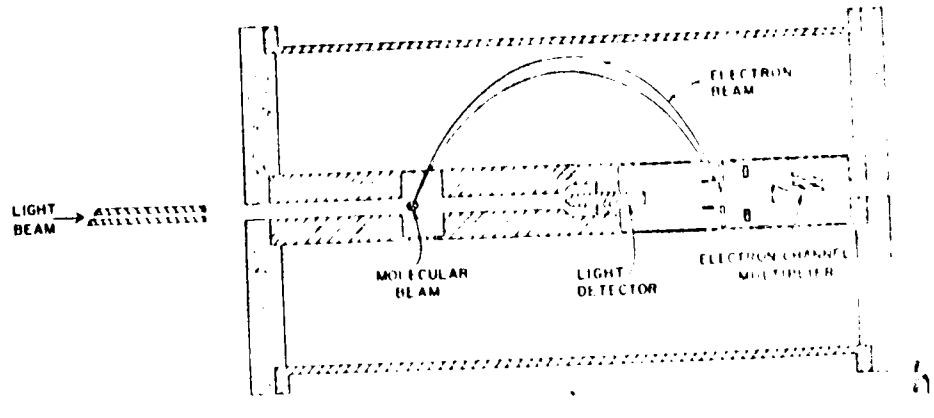
e.



f.



g.



h.

Fig. 19 Electron energy analysers used in photoelectron spectroscopy

at right angles to the retarding field. The resolving power achieved with these grid systems is of the order $E/\Delta E \sim 90$. (The experimental resolving power of a photoelectron spectrometer is usually defined as $E/\Delta E$, where ΔE is the full width at half-height of the photoelectrons of kinetic energy E.) The advantage of the grid analysers is that they are easy to make, and have a high collection efficiency due to the effective large solid angle. However, the crucial surface conditions, limited resolution and especially the integral spectrum obtained have put them out of favour for routine work. To produce a differential spectrum involves deterioration of the S/N ratio. In the study of fine structure the diff-ential spectrum is more revealing and thus the use of focusing deflection fields, either magnetic or electrostatic is advantageous. The electrons are analysed by energy dispersion.

A homogeneous magnetic field (180^{o}) analyser (momentum selector), with fixed slits used by Turner,[98] first demonstrated improve-ment in peak shape, and resolution, which was sufficient to observe vibrational fine structure on the P.E. bands. The major disadvantage was, however, the non-linear scale as it is a momentum scanning device. The advantage is its high collecting power and as the focusing field is external to the vacuum chamber it is suited to high temperature studies. Recent designs incorporate double focusing properties provided by an inhomogeneous magnetic field.[99]

The simplest electrostatic analyser is the $\pi/2^{\frac{1}{2}}$ ($127^{o}17'$) cylindrical sector (Fig. 19d) which was first used successfully in a P.E. spectrometer by Turner.[96] This is the energy selector used in this work and is illustrated in more detail in Fig. 20. Ionisation takes place in the target chamber (T) and some of the ejected photo-electrons pass through the slit into the analyser. The energy of the electrons is scanned by increase of the potential of the plates of the analyser (P_1, P_2) so that successively more energetic electrons are

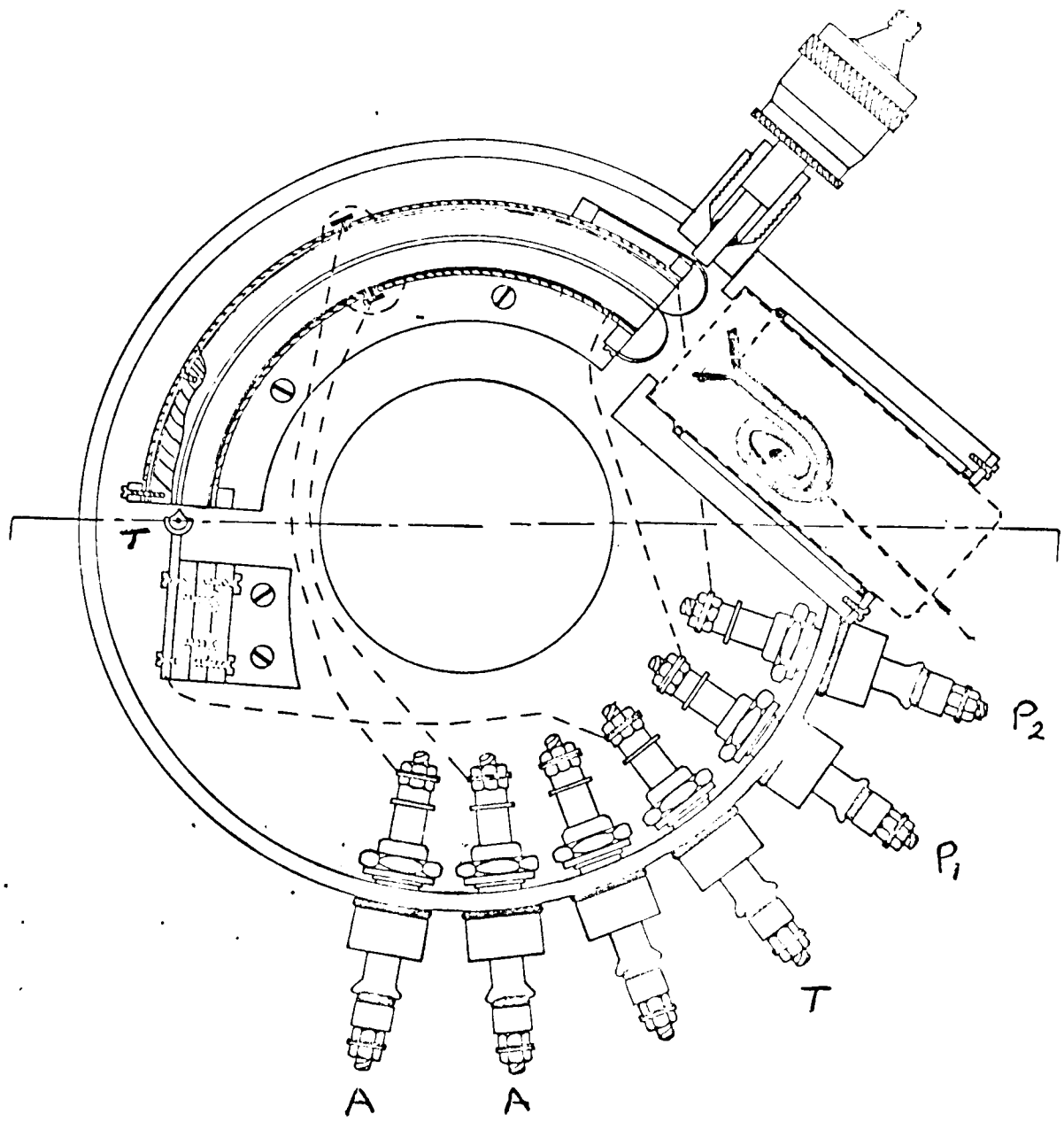


Fig. 20 127° sector electrostatic electron energy analyser

focused on the exit slit. At the angle of $127^{o}17'$ it can be shown that electron trajectories deviating but slightly from the circular orbit are refocused.[100.] A voltage difference of $2V_p$ applied to the plates focuses electrons (V_{el}), where

$$V_p = V_{el} \log_e \frac{r_1}{r_2}$$

r_1, r_2 are the radii of curvature of the outer and inner cylindrical plates respectively. The two aberration electrodes (A_1 and A_2), placed at mid-points of the plates, are swept simultaneously at opposite polarity to the corresponding plates (P_1 and P_2 respectively). This has the effect of focusing electrons deviating from the path outside the limits of refocusing criteria at $\pi/2^{\frac{1}{2}}$. The sweep circuit used is shown in Fig. 21.

As electron paths are influenced by magnetic fields, it is necessary to shield the electron beam from stray magnetic fields, especially earth's field. This is achieved by one or a combination of two techniques, Helmoltz coil system or paramagnetic shielding material as μ-metal. With the 127^{o} analyser described a set of horizontal and vertical Helmoltz coils is used. The current in the coils is adjusted for optimum resolution, accordingly the small residual field is beneficial. Another requirement for improvement of resolution is that surfaces near the electron beam be equipotential. The plates of the analysers, slits and target chamber are coated with colloidal graphite, for example. Such a surface has low reflection coefficient for slow electrons and is found to be as effective as gold in producing uniformity of potential. With these refinements resolving power $E/\Delta E \sim 500$ can be achieved with skill. A disadvantage of electrostatic deflecting field analysers is that intensity falls off roughly linearly with kinetic energy. This is especially serious for 0-3eV electrons and can be "compensated" by a suitable bias on the target chamber. Spectra obtained in this way are characterised

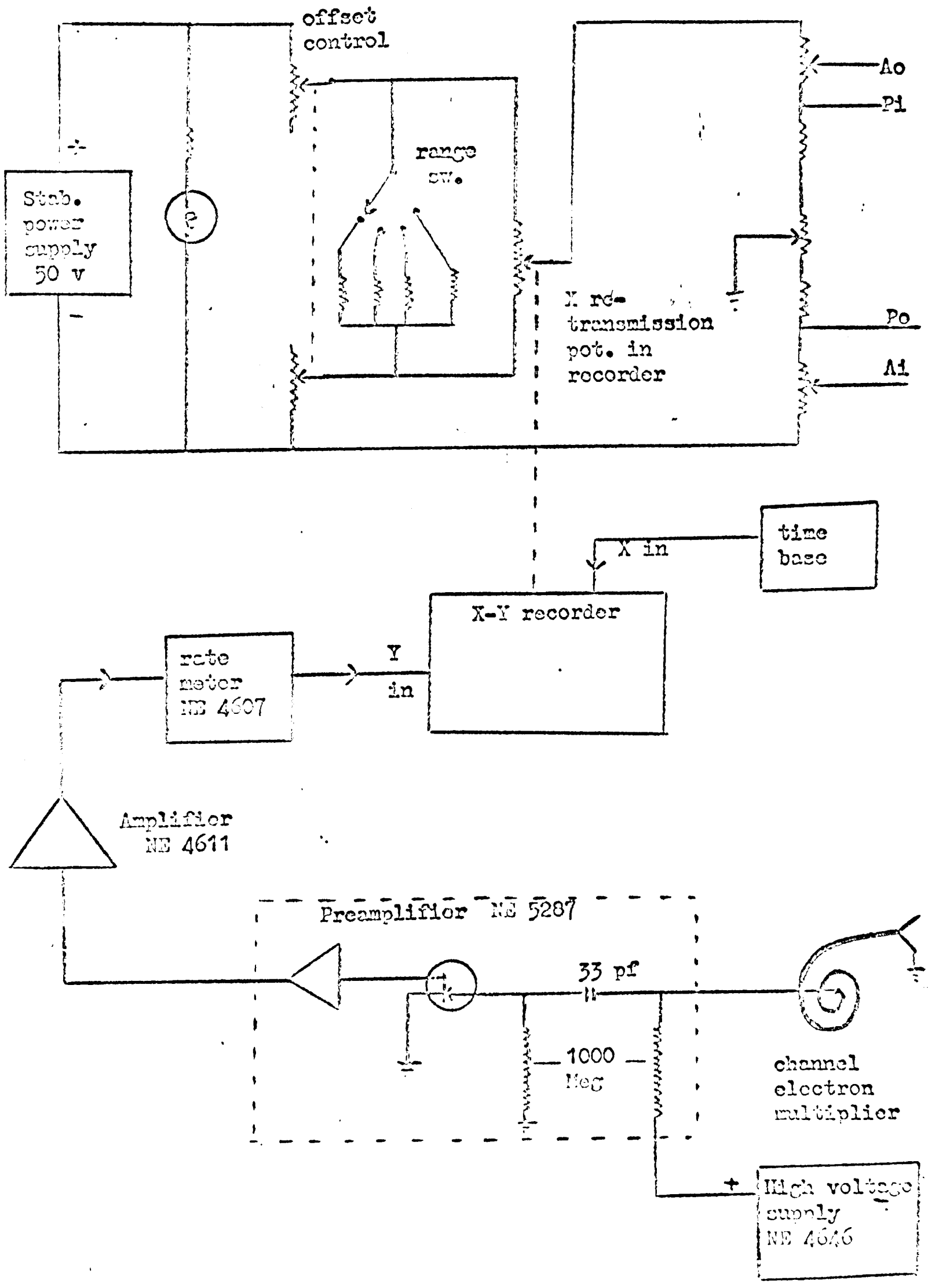


Fig. 21 Scanning and recording arrangement

by an intense peak at zero kinetic energy.

Another means of one-dimensional electrostatic focusing used in a P.E. spectrometer is with parallel plates (Fig. 19e).[101.] The electric field between the two plates causes electrons to travel in parabolic paths. Resolution comparable to the 127° cylindrical analyser can be obtained.

Recently double focusing spherical analysers have attracted widespread attention. In Fig. 19f a three dimensional view of a 180° hemispherical analyser is shown, illustrating the inherent double focusing properties.[102.] Various sectors from 157° x 60° to whole sphere are in use.[103.] In the electrostatic deflecting analysers, instrumental contribution to the line width (ΔE) depends on the energy (E) and thus ΔE is reduced by retardation of the electrons prior to analysis. This is important in X-ray work with high energy photoelectrons. A typical arrangement is shown in Fig. 19g.[45.]

Cylindrical mirror analyser (Fig. 19h) is the most recent adaptation,[104.] consisting of two concentric cylinders, with inherent double focusing. The electron optical properties have been found, theoretically up to now, superior to the hemispherical analyser.

At this stage it is appropriate to consider the problem of resolution briefly. The ultimate energy spread of the photoelectron bands is determined by experimental limits and fundamental factors. The latter depend on the lifetime of the ionic state and have been considered in the previous Chapter. The natural width of the exciting line increases rapidly with energy (as ν^3) and thus becomes important in the P.E. spectra excited by X-rays, e.g. Al K_α ~.9eV, c.f. ~ 10^{-7} eV for He I. This can be overcome by monochromatisation of the X-ray line and the unavoidable loss of intensity can be compensated for by dispersion compensation and a large multidetector system.[45.] In u.v. P.E.

spectroscopy, the limits are set essentially by thermal motion of the molecules and line broadening in the light source. The magnitudes have been discussed by Samson,[105] whose study shows that it should be possible to obtain a half width of 1meV with the He584Å emission line. The thermal motion of the target gas is the major experimental limitation up to now, in the absence of molecular beams. A resolution of ~ 5meV has been achieved,[106] approaching the theoretical limit. All the factors limiting resolution have been discussed comprehensively by Turner.[107]

3.4 Detection, Recording, and Calibration of Photoelectrons

In the grid instruments the transmitted electron current is measured by an electrometer (10^{-12} - 10^{-15} amps). Deflection type analysers use particle counters. A channel multiplier, ("channeltron") was used in conjunction with the 127° analyser in this work. These multipliers have been generally found preferable to the multistage box-grid type (Be-Cu) on grounds of reliability and robustness.

The signal from the electron multiplier is amplified and fed into the Y-axis of an X-Y recorder, while the X-axis is internally driven and used to vary the potential between the analyser plates. In u.v. P.E. spectroscopy, sufficient signal strength and low S/N ratio allows direct recording of the spectrum with an X-Y recorder. For He II and X-ray work, long counting times are often necessary and multichannel signal storrer is preferred.

In principle, the energy scale can be absolutely determined from the plate voltage (equation above). In practice, variations in surface potentials, space charge effects and magnetic fluctuations make this unreliable. Internal calibration is necessary, preferably by mixing the calibrant with the sample to compensate for sample region surface

charging phenomena.[37] Rare gases are used as accurate I.E.s are known spectroscopically (Table 3).

Table 3

	$^2P\frac{3}{2}$	$^2P\frac{1}{2}$
A	15.759eV	15.937eV
Kr	14.000eV	14.665eV
Xe	12.130eV	13.436eV

As there are difficulties in maintaining linearity of the energy scale, extrapolation is best avoided and additional "sharp" photoelectron peaks, as in methyl iodide (9.55 and 10.16eV) are used.[108]

Each spectrum is a continuous record of electron count rate, integrated over either 1, 3 or 10 seconds normally and plotted as function of kinetic energy. The spectra were obtained with a recording system which covered a maximum range of 10 eV at one setting. Vibrational fine structure when discernible was recorded with 5 or 10 fold expansion of the abscissa scale at lower speed and increased integration time. This also allowed more accurate calibration of energy. The absolute accuracy is .01eV or better.

3.5 Experimental Details Associated with Chapters IV-VII

The P.E. spectra of phosphine and phosphorous trifluoride were recorded under a working resolution of 0.02eV, or better, full width at half height for 5 eV electrons. Phosphine was prepared by pyrolysis of phosphorous acid under vacuum and purified by trap to trap distillation.[109]

The P.E. spectra of the substituted benzenes (Chaps. V-VII) were recorded under a resolution of .02-.05eV depending on the sensitivity

needed. All spectra were repeated until consistent. The samples were mostly commercial products, the remainder were prepared according to standard preparative techniques. Solid samples were vacuum sublimed and liquids were vacuum distilled prior to use. All the samples were thoroughly degassed. Purity was checked by n.m.r. and g.l.c. when in doubt.

Samples of 1-methylenebenzocycloalkanes and benzocycloheptane, g.l.c. purified, were kindly supplied by Professor T.G. Traylor, University of California, and benzoquinuclidine kindly by Professor B.M. Wepster, University of Delf.

RESULTS AND DISCUSSION

In the following Chapters, IV - VII, the P.E. data of the molecules studied are presented, analysed and discussed. In the first Chapter, the vibrational fine structure discernible allows a discussion of the geometry of phosphine and phosphorous trifluoride in their ground ionic states. The data is of sufficiently high quality to reveal subtleties, and lack of them, yielding information, on the barrier to inversion in the ions, and on the potential surfaces.

Chapters V - VII are concerned with the study of steric phenomena in benzene-type molecules. In the latter, the fine detail, as in Chapter IV is not discernible; nevertheless, the Franck-Condon profile can give indications of geometry changes especially in a series of topologically related molecules as is the case there. These are significant in that they are consistent with the spectral band assignment and the conformations.

The discussion is based on correlation of the ionisation energies of the series of related molecules, where steric effects vary over a wide range. The spectral pattern is rationalised in terms of a simple theoretical framework developed and the questions of steric hindrance and conformations discussed quantitatively.

CHAPTER IV

PHOSPHINE AND PHOSPHOROUS TRIFLUORIDE MOLECULAR IONS

4.1 Ground States of the Phosphine and Phosphorous Trifluoride Ions... $^2A_1$.

The adiabatic ionisation potentials (9.96$\pm$.01 and 11.57$\pm$.01eV of phosphine and phosphorous trifluoride respectively) are deduced from the first distinguishable vibrational transitions (indicated in Figs. 22 and 23, as O-O) and by extrapolation of the vibrational progressions in the region where it is well resolved. Although the value for phosphine is in very good agreement with the ionisation potential deduced from Rydberg series[110.] (9.98eV), it is difficult to exclude the possibility of an even lower adiabatic ionisation potential, as the first few transitions have a low probability associated with very adverse Franck-Condon factors. The same difficulty would also apply however, in assigning the Rydberg series components. It is often of interest to compare photoelectron with optical absorption spectra in those cases where the Rydberg states can be clearly identified and which approach the geometry of the ion. Close resemblance between Rydberg and photoelectron bands is often then found in respect of vibrational frequencies and Franck-Condon factors[111.] unless strong non Rydberg transitions or autoionisation processes intervene. In the case of the Rydberg states of phosphine[112.] difficulties arose, the bands were diffuse and weak, and consequently analysis of the progressions was not possible with any degree of certainty. In the present photoelectron study vibrational levels were sharply resolved in phosphine and phosphorous trifluoride ions, as can be seen in Figs.22 and 23.

There is a great similarity in the Franck-Condon envelopes of

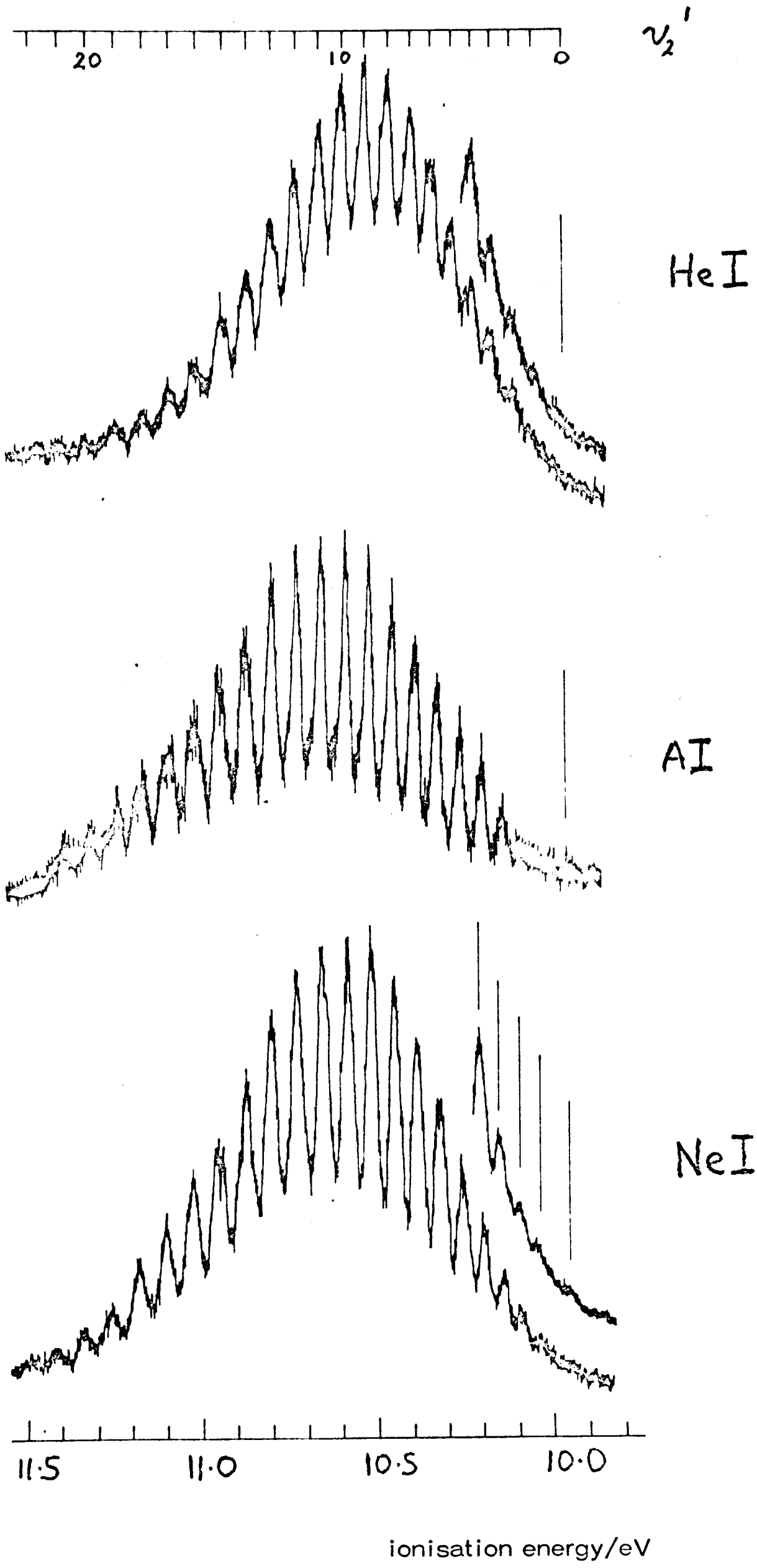


Fig.22 The highest energy photoelectron band in phosphine using the He I, Ne I and Al resonance lines

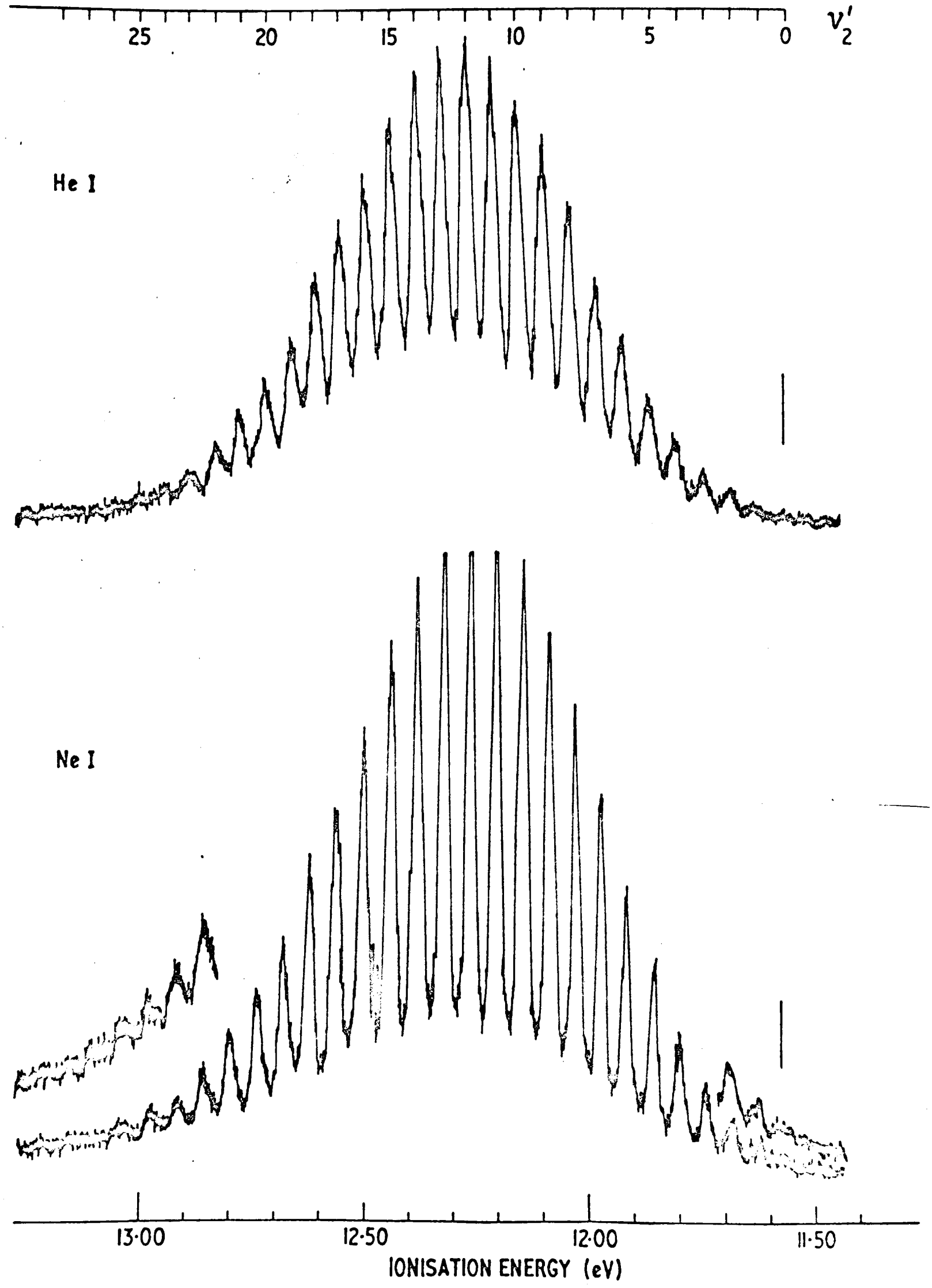


Fig. 23 The highest energy photoelectron band in phosphorous trifluoride usin the He I and Ne I resonance lines

the photoelectron bands in these two molecules. A very long vibrational progression in excited, with an interval of 530 ± 80 cm^{-1} (average from $v'=6$ to $v'=17$) in the phosphine ion, and 470 ± 80 cm^{-1} (average from $v'=5$ to $v'=20$) in the phosphorous trifluoride ion. If the ionisation does not reduce the three-fold symmetry, the only totally symmetrical mode of the correct magnitude possible is the symmetrical out-of-plane bending mode ν_2. The ground state values are 992 and 487 cm^{-1} respectively.[10.] Excitation of ν_2 is expected for a transition involving a large change of interbond angle from that in the molecule. This is in accord with a change in the height of the inversion barrier which would follow ionisation of an electron from the phosphorous "lone-pair" orbital. In phosphine this is the $5a_1$ molecular orbital (in phosphorous trifluoride the $8a_1$) localised on the phosphorous atom with 71% 3p and 17% 3s P character (35% 3p P and 35% 3s P in phosphorous trifluoride).[113.] These are expected to be the most weakly bound orbitals.

Transitions take place from the zeroth vibrational level of the ground state (double on account of inversion but with a splitting far too small to be detected here; calculated in phosphine to be of the order 10^{-4} cm^{-1} and smaller in phosphorous trifluoride)[9.] into the Franck-Condon allowed region of the ground ionic state. As no staggering is observed in the extensive vibrational progressions, if the ionic state is pyramidal with all the ionisation taking place to levels below the barrier, this barrier will have to be much higher than the extent of the Franck-Condon envelope ($1\frac{1}{2}$ eV). If this was not the case some irregular perturbation of the higher vibrational levels would be apparent. In the phosphorous trifluoride ion the vibrational spacing over the whole progression observed is constant. If the approach to inversion barrier resembles initially some anharmonic potential functions (e.g. Morse curve) with a high dissociation limit, near the energy minimum we would expect some similarity in the behaviour of the vibrational levels. However, the

potential functions of diatomic molecules with dissociation limits over 10 eV are such that even in the relatively small region at the bottom of the well, which is of relevance here, convergence of the vibrational levels is readily seen.[114.] (It is worthwhile to note that taking the average value of the corresponding split vibrational levels in the ground state of the ammonia molecule, as actually observed,[115.] considerable convergence does take place). Such a high barrier to inversion is unrealistic from our knowledge of the AB_3 molecules. Calculations indicate that the barrier in the ground molecular state of phosphorous trifluoride is only some 2eV high;[116.] in phosphine only 1.7 eV, as calculated by an ab initio method.[117.] In phosphine the interbond angle depends quite markedly on the relative energies of the 2e and $5a_1$ molecular orbitals, and the removal of an electron from the $5a_1$ orbital would be expected to increase the interbond angle,[118.] with a decrease in the barrier height.

From the preceding argument, therefore, the $^2A_1$ ionic states of phosphine and phosphorous trifluoride* should be either planar or very nearly so (i.e. pyramidal with a very small barrier to inversion). In the P.E. spectrum of the phosphine ion in the ground ionic state (Fig.22) there is broadening of the lower vibrational levels which can not be accounted by the inherent $E/\Delta E$ variation of the analyser alone. Comparison of the first band in the phosphine spectrum with the second band in the P.E. spectrum of water (H_2O^+ $^2A_1$ ionic state)[76.] reveals a marked resemblance. The bending mode is strongly excited in both, and each shows a marked divergence of the latter members of the series (vide infra). In the $^2A_1$ states of H_2O^+ the considerable complexity in the early vibrational transitions arises from a strong Renner effect giving a slightly non-linear ion. The implication of the similarity is that phosphine ion in the $^2A_1$ state is slightly non-planar. The influence of the double minimum in the potential surface is greatest for the lowest vibrational levels in both cases. The Ne I spectrum (Fig. 22) shows all

*However, it is impossible to exclude the possibility of a parabolic potential function for the phosphorous trifluoride ion with ionisation taking place below the barrier and work regarding this possibility is in process.

the vibrational transitions including the transition provisionally assigned as O-O. As well as the broadening of the early members of the progression the first two members are not only more "smeared-out" than the rest but there is also a considerably different vibrational interval between the $v'=0$ and $v'=1$ levels (approximately $1\frac{1}{2}$ times the rest of the progression). This can also be seen in the He I spectrum (Fig. 22). A quantitative application of the Franck-Condon principle[119.] to the phosphine absorption study of Walsh et al.[112.] indicates that the Rydberg states, and hence the ground ionic state, are near planarity. Since they observed no irregular spacings in the first few vibrational levels, the exactly planar geometry was inferred.

It is concluded that the ground state of the phosphine ion is pyramidal with a barrier to inversion of the order of a vibrational quantum in magnitude (i.e. c.a. 0.07eV).

The P.E. spectrum for the ammonia ion,[47.] known to be strictly planar,[120.] and phosphorous trifluoride in their ground ionic states show no perturbation of the early members of the vibrational levels compared to that in the phosphine ion, although the bands are otherwise very similar. It is therefore concluded that phosphorous trifluoride in the ground ionic state is very probably strictly planar. A Rydberg state of phosphorous trifluoride studied by Walsh et al.[112.] has been deduced to be non-planar. The present results for the ion suggest that the Rydberg state might also be planar and that the valence force treatment was misleading in this case.

In the phosphine ion the vibrational levels diverge quite considerably beyond the $v'=16$ level indicating that the anharmonicity constant x_{22} is positive ($v'_{20}-v'_{21}$ vibrational interval is approximately $650\ cm^{-1}$). The $v'=15$ and all the subsequent peaks are all somewhat broader (see Fig. 22). In the Ne I and Al spectra the higher wavelength

component of the doublet contributes to this broadening, though this is small as can be seen by comparing the contribution in the phosphorous trifluoride ion Ne I spectrum (Fig. 23). (The predominance of the lowest wavelength component of the doublet can be seen on the earlier vibrational transitions in the phosphine ion band where the 755Å, 1067Å, of Ne I and Al respectively, photoelectrons appear at the base of the subsequent peak). The broadening is also present in the He I spectrum and this may be due to short lifetime of the ion in the higher vibronic levels. In phosphorous trifluoride ion there is no detectable divergence.

The P.E. spectra of ammonia, phosphine, and phosphorous trifluoride are very similar for the ground ionic states. Nevertheless, an interesting comparison between the potential functions can now be made. In ammonia and phosphine ions x_{22} is positive; in the former there is no barrier to inversion at the bottom of the well, but the function has a shallow minimum, in the latter the observed vibrational pattern is also indicative of a potential surface with a "steeper wall" than that of a harmonic oscillator, but with a small "hump" resulting in the perturbation of the first few vibrational levels. In contrast to this the phosphorous trifluoride ion potential function is essentially that of a harmonic oscillator. The difference between phosphine and ammonia ions is not surprising. In the former there is a decrease of "H-H non-bonded repulsions" compared to the latter, and in phosphine d orbitals are available. Their participation need only be small as they can partially stabilise by $3p_{\Pi}$ $-3d_{\Pi}$ overlap the 2e orbitals in C_{3v} symmetry only, tending to favour pyramidalisation rather than planarity. Calculations including a d orbital basis do indicate some involvement.[113,121] Thus it may be expected for ammonia to have a larger interbond angle than phosphine ion (states being planar and non planar respectively).

Descending the group Vb series, the calculated barrier to inversion is greater in arsine and stibine than in phosphine;[116] therefore a more

TABLE 4

Observed ionisation potentials* (eV) and calculated eigenvalues (eV) of the two highest occupied molecular orbitals of phosphine

Orbital	Calculated			Experimental *	
	(a)	(b)	(c)	(d)	(e)
$5a_1$	-10.9	-10.0	-10.0	$10.58 \pm .01$	$10.59 \pm .02$
2e	-14.7	-13.7	-13.0	$13.50 \pm .05$	$13.6 \pm .1$

* Vertical ionisation potentials

(a) Ref.121 (b) Ref.113 (c) Ref.124 (d) present work
(e) Ref.123.

TABLE 5

Adiabatic ionisation potentials (eV) and observed vibrational frequencies (cm^{-1})

Electronic State	Electronic Configuration	Adiabatic ionisation potential	Observed vibrational frequencies			
			a	b	c	d
Ground molecular state[10]			$\nu_1(a_1)$	$\nu_2(a_1)$	$\nu_3(e)$	$\nu_4(e)$
$^1A_1$	$(1a_1)^2(2a_1)^2(1e)^4(3a_1)^2$ $(4a_1)^2(2e)^4(5a_1)^2$		2323	992	2328	1122
$^2A_1$	..... $(2e)^4(5a_1)^1$	$9.96\pm.01$	-	530 ± 80	-	-
^2E	..... $(2e)^3(5a_1)^2$	$12.40\pm.02$	1610 ± 80	-	-	810 ± 80

a. P-H totally symmetric stretching mode.
b. P-H totally symmetric out-of-plane bending mode.
c. Doubly degenerate asymmetric stretching mode.
d. Doubly degenerate asymmetric bending mode.

extensive perturbation in the vibrational fine structure is anticipated and the possibility of a change of vibrational spacing in the P.E. spectra when the barrier is a few quanta in magnitude in the ground states of the ions. Such effects have been observed.[122.]

4.2 First Excited State of the Phosphine Ion.....^2E

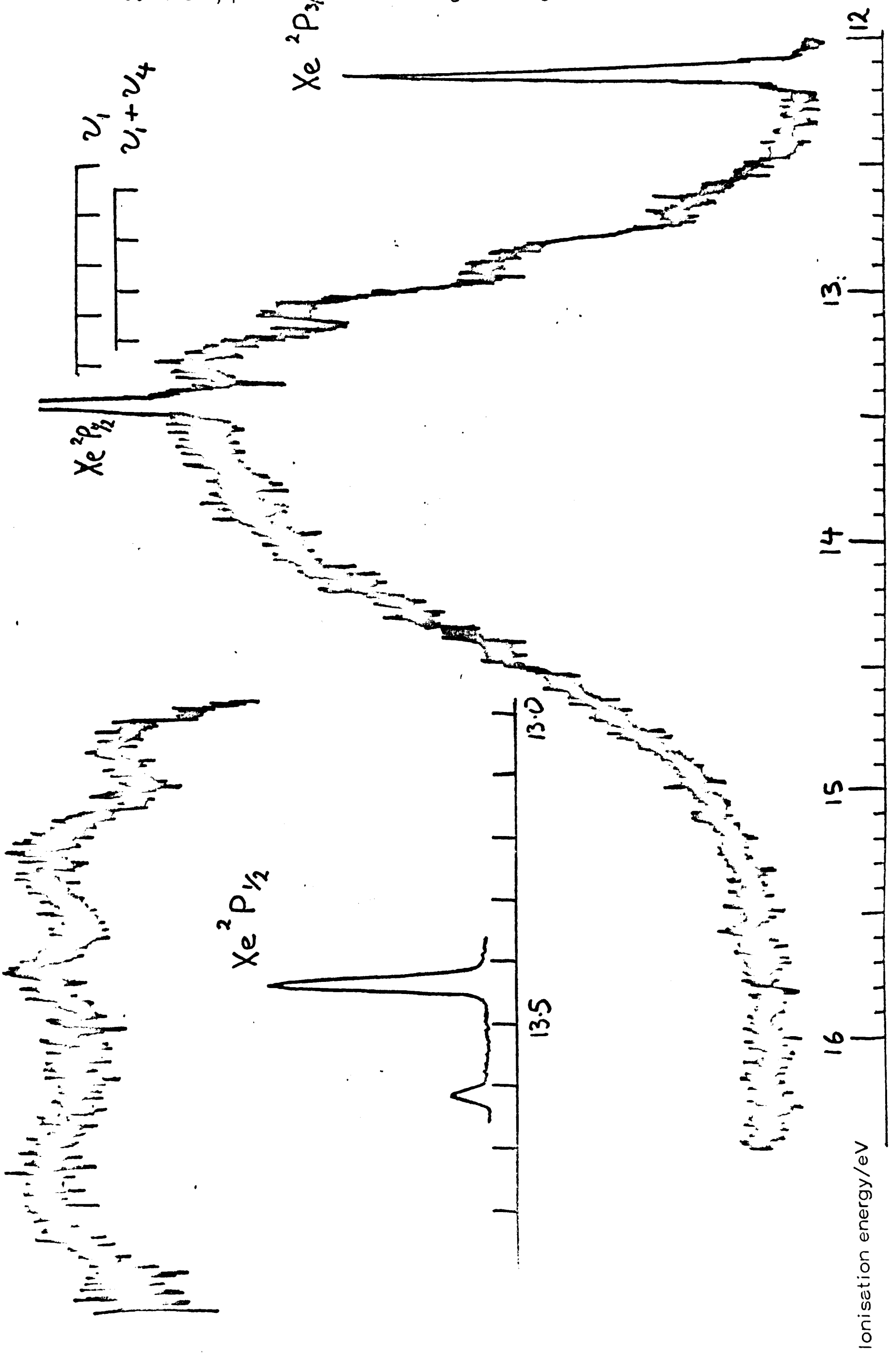
The second band (Fig. 24) has a very broad Franck-Condon envelope (c.a. 2eV) with distinguishable vibrational fine structure on the high electron energy part only. Two vibrational progressions detectable are the totally symmetric stretching vibration $\nu_1(a_1)$ and the doubly degenerate $\nu_4(e)$ vibration. Several vibrational levels in each are discernible; both frequencies are considerably reduced in magnitude relative to the ground state values (Table 5).

These observations indicate that the ionised electron originates from a bonding orbital, as is expected for the 2e molecular orbital, which provides a major contribution to the P-H bonds.[113.] This assignment is further substantiated by the relative areas of the first and second bands (1:2) reflecting the degeneracies of the orbitals concerned.

All the vibrational components are rather broad and at $13.4 \pm .1$eV there is a discontinuity in the electron flux and a breaking off of the vibrational progressions (Fig. 24 inset), near the appearance potential of the fragment ion PH_2^+ of $13.2 \pm .2$eV as measured by electron impact.[127.] Thus, the P.E. data suggests that the ^2E state of PH_3^+ is predissociated by repulsive curve crossing just above the $v'=4$ level to give PH_2^+.

The band has a typical Jahn-Teller contour as is expected for a ^2E state[80.] where the ion is inherently unstable in orbitally degenerate state, the degeneracy being removed by distortion to lower symmetry by means of vibronic interactions. The two maxima are separated by approximately .45 eV; the magnitude is comparable to the "splittings"

Fig.24 Second photoelectron band in phosphine using He I resonance line. Inset, portion of the same region using Ne I resonance line.



observed in the P.E. spectra of degenerate states of other simple molecules (c.f. methane, ammonia[47].).

4.3 Higher Ionisation Potentials of Phosphorous Trifluoride.

The vertical ionisation potentials listed in Table 6 were measured from the He I and He II photoelectron spectra (Figs. 25 and 26 respectively). The agreement with previously observed P.E. spectral values of other workers is good. The assignment of the various bands is generally well agreed on, although discrepancy does arise in the relative ordering of the $1a_2$ and 6e molecular orbitals. The eigenvalues calculated by an ab initio procedure are a little high.[113.] However, the Koopmans' theorem ionisation potentials calculated by non-empirical calculations have been shown to be uniformly too high in the valence shell, and if one reduces the calculated values by an empirical factor, satisfactory correlation is obtained.[111,128.] The P.E. spectrum using He 304Å as the ionising source, was obtained up to an ionisation energy of 28eV. This reveals one further ionisation potential, at $22.55 \pm .05$eV, which is assigned to the $6a_1$ molecular orbital. This is a predominantly P-F bonding orbital. The value agrees quite well with the calculated eigenvalue if the latter is empirically reduced (Table 6). The He II spectrum gives a new relative intensity distribution. This indicates once more, that care has to be exercised when assigning P.E. spectra solely on the intensity ratio. There is a marked decrease in the relative intensity of the $8a_1$ molecular orbital when using the 304Å resonance line instead of the 584Å. Similar intensity changes with the two resonance lines have been noticed with other molecules studied, often indicating an orbital predominantly p in character. The second band, in contrast, shows a marked increase in intensity when the higher energy ionising source is used.

Use of the higher ionisation energy source avoids some of the

TABLE 6

Observed ionisation potentials* (eV) and calculated eigenvalues (eV) of trifluorophosphine

Orbital	Calculated		Experimental*		
	(a)	(b)	(c)	(d)	(a)
$8a_1$	-12.6	$12.27^{+}_{-}.01$	12.28	12.3	12.3
6e	-18.2	$15.88^{+}_{-}.02$	15.89	15.9	16.3
$1a_2$	-17.8	$16.30^{+}_{-}.05$	16.29		15.8
5e	-19.6	$17.46^{+}_{-}.02$	17.35	17.4	17.5
$7a_1$	-21.0	$18.60^{+}_{-}.05$	18.51	18.5	18.6
4e	-21.4	$19.50^{+}_{-}.05$	19.31	19.4	19.4
$6a_1$	-24.6	$22.55^{+}_{-}.05$			

* Vertical ionisation potential

(a) Ref.125 (b) Present work (c) Ref.82 (d) Ref.126

Fig. 25 He I photoelectron spectrum of phosphorous trifluoride

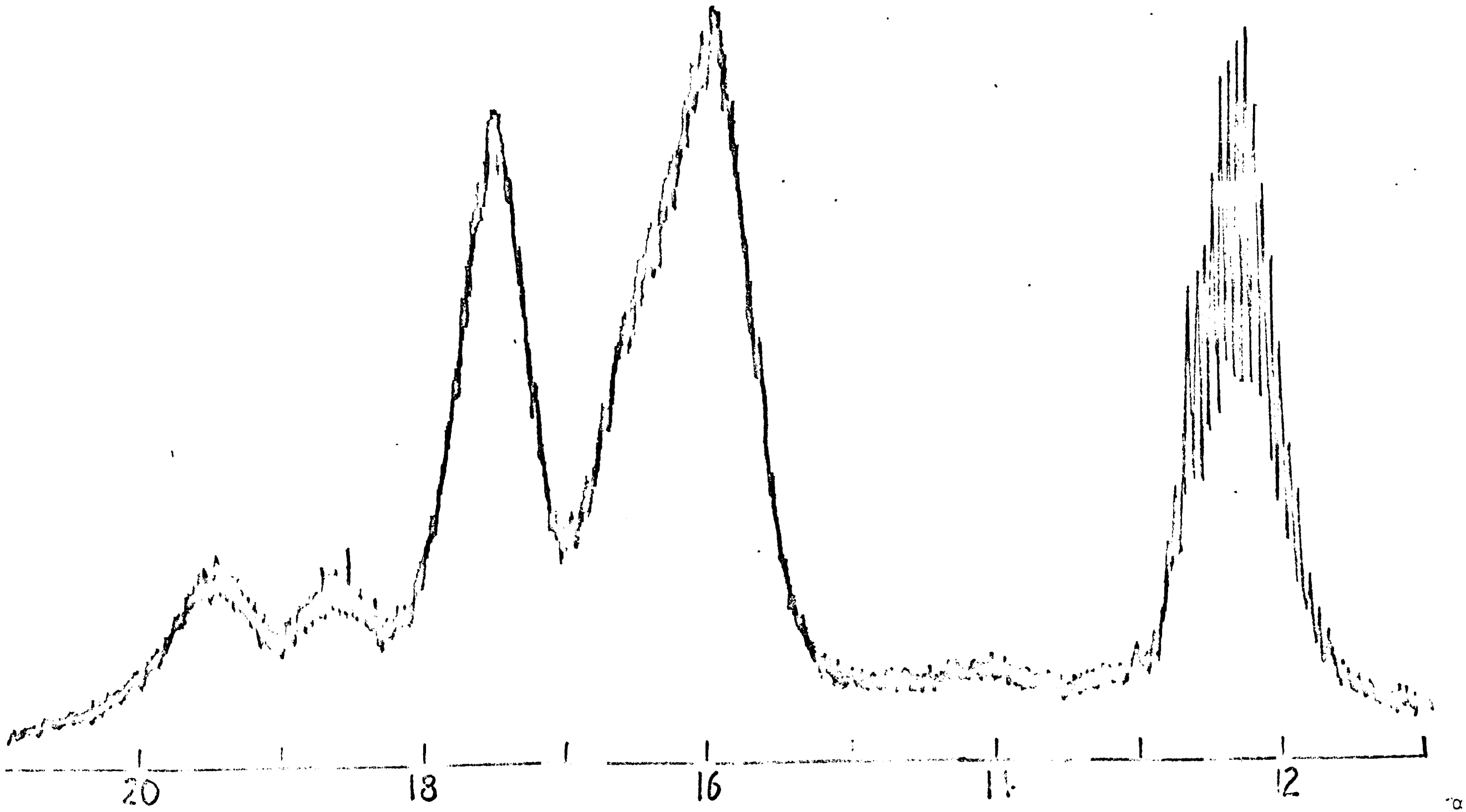




Fig. 26 He II photoelectron spectrum of phosphorous trifluoride

distortion in the relative intensity distribution, as all the photoelectrons have similar high kinetic energy. This is apparent on comparison of the two spectra in question, especially in the 18-21eV ionisation energy region where the analyser discriminates most when using He I. The relative intensity of bands at 18.6 and 19.5 eV under He II conditions (c.f. He I) does tend to support the assignment made previously on the basis of the He I spectra, i.e. $7a_1$ and 4e respectively.

CHAPTER V

BIPHENYLS

5.1 Introductory Remarks on Chapters V-VII.

Nearly every experimental technique of molecular structure determination has been applied with varying success to the question of "steric hindrance" in chemistry; a unifying concept brought in to explain irregular or unusual changes in some experimental observation associated mainly with the presence of bulky substituents. Aromatic molecules, especially, lend themselves well to investigation of this phenomenon, since the resultant changes in conjugation produce most marked deviations from "normal" behaviour. Such anomalies should be reflected by changes in the arrangement of the occupied energy levels of a series of related molecules. Thus photoelectron spectroscopy should be ideal for this purpose.

The consequences of steric interference and studies of relevance to the particular series discussed, are briefly reviewed at the beginning of the respective Chapters.

5.2 Outline of Related Studies on Biphenyls.

The importance of "through-space" steric effects was realised early from the study of stereoisomerism in biphenyls.[129] The latter provided for the first time a class of molecules exhibiting atropisomerism. Intramolecular steric effects were unequivocally demonstrated by the resolution of optically active ortho-substituted biphenyls. It was found that with four ortho substituents, if two are large, the two isomers can be isolated at room temperature; the rings cannot become coplanar nor rotate freely. In contrast, diphenic acid can racemize as the carboxylic

groups can slip past the ortho hydrogens quite easily. It was realised that the barrier to racemisation might vary widely and was highly steric in origin. From such studies the substituents were arranged according to their mutual interference.

Qualitative deductions about the magnitude of the dihedral angle between the planes of the two rings have been made on the basis of optical activity measurements,[130.] optical rotatory dispersion, and circular dichroism.[131.] Rather more quantitative inferences have been made on the basis of optical anisotropy of depolarised Rayleigh scattering.[132.] Again qualitative estimates of dihedral angle have been obtained from ^{1}H and ^{19}F n.m.r. chemical shifts.[133,134.] With this method information about the magnitude of the barrier to rotation could also be obtained. From the quantitative standpoint infra-red absorption[135.] and dipole moment measurement[136.] have been less satisfactory, though the latter have shown a tendency for cissoid arrangement of substituents in 2,2'-substituted biphenyls and transoid arrangement of the N atoms in 2,2'-bipyridyl.

The literature concerning u.v. absorption spectra of biphenyl is extensive. Several quantitative evaluations of the dihedral angle in substituted biphenyls on the basis of the wavelength shifts of the absorption bands have been carried out, recently by Suzuki, who also reviews the field.[137.]

Differences in conformation are also reflected systematically in certain other physical properties notably melting point, equilibrium constants of chemical reactions[138.] and gas-liquid chromatography retention times.[139.] In Table 8 the dihedral angle inferred from these different sources of information are summarised.

5.3 Results.

The spectra of all the biphenyls though showing many, and often

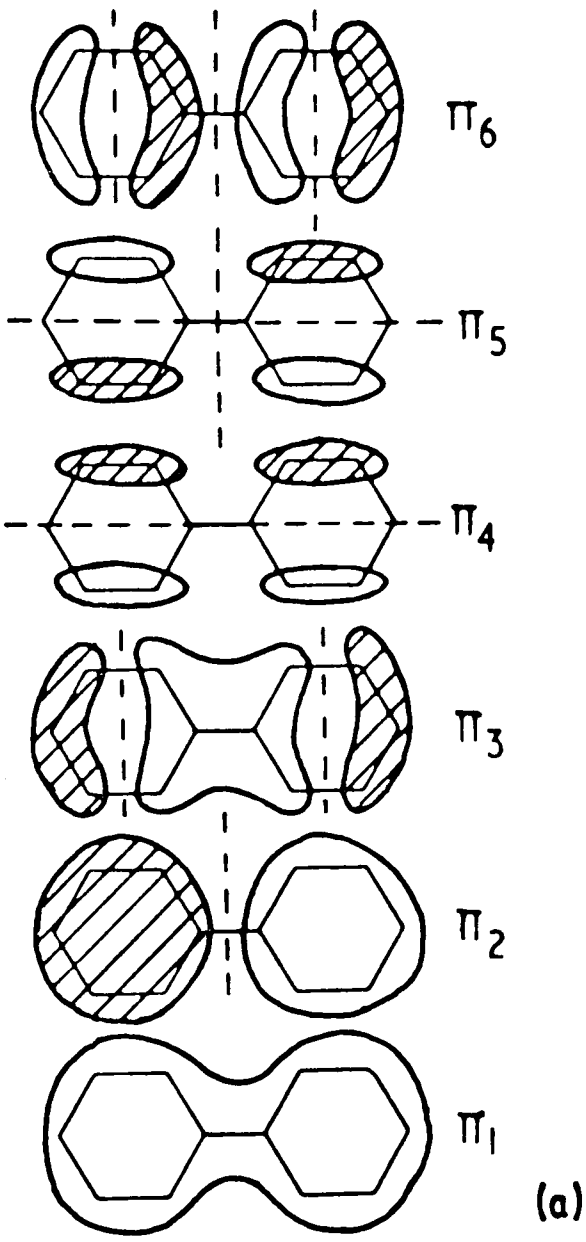
overlapping, bands can be seen to display certain common features. This is best perceived by the comparison of the spectra (Figs. 29-36). The range of I.E. from about 7.8 to 10.7 eV contains one group of bands whilst the others occupy the regions c.a. 11-13 eV and c.a. 13-17 eV. Each of these main features finds its counterpart in the spectrum of the corresponding benzene where these groups of electrons are associated with orbitals of the $\Pi_{2,3}$ (e_{2g} in benzene) and sigma type orbitals composed of "in-plane", "radially" and "tangentially" directed carbon 2p atomic orbitals.

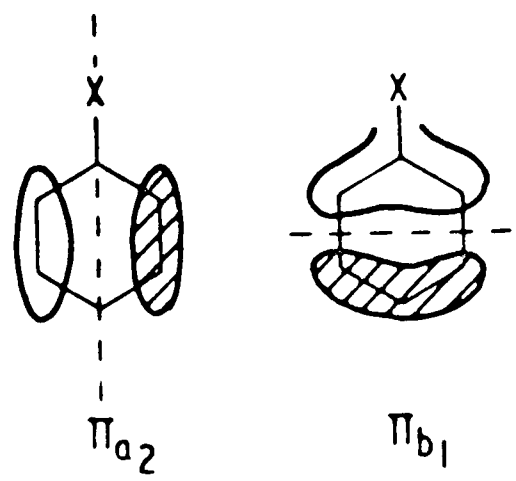
In Tables 9-11 the observed I.E. data are listed. In the Tables, (Chapters V-VII) band maxima are referred to as the vertical ionisation energies (I.E.s). It must be appreciated that in polyatomics where many vibrational modes are excited, the maxima do not necessarily correspond to the vertical I.E.s. In the text the maxima are referred to, as not all the adiabatic I.E.s are defined. The latter (band onsets) are listed in parentheses when defined in the P.E. spectra. The correlation diagrams (Figs. 38-42) summarise the assignments in the P.E. spectra.

5.4 Discussion.

In order to explain the P.E. spectra, each band must be associated with the formation of a radical cation corresponding to the ejection of a photoelectron from the appropriate MO. Of most concern here are the bands correlated with the pi MOs designated in Fig. 27a. In the P.E. spectra the first group of bands is associated with the MOs Π_i i=3 – 6.

Empirically there is a relationship between the separation of the bands 1 and 4 (vide infra), and the dihedral angle from the experimental data(Fig.28). The observed values of the dihedral angle as determined by electron diffraction[140]. (Table 7) form the basis of this correlation. The plot is linear. Clearly this might be used diagnostically to determine the dihedral angle in other biphenyls. In Table 8, the determined dihedral





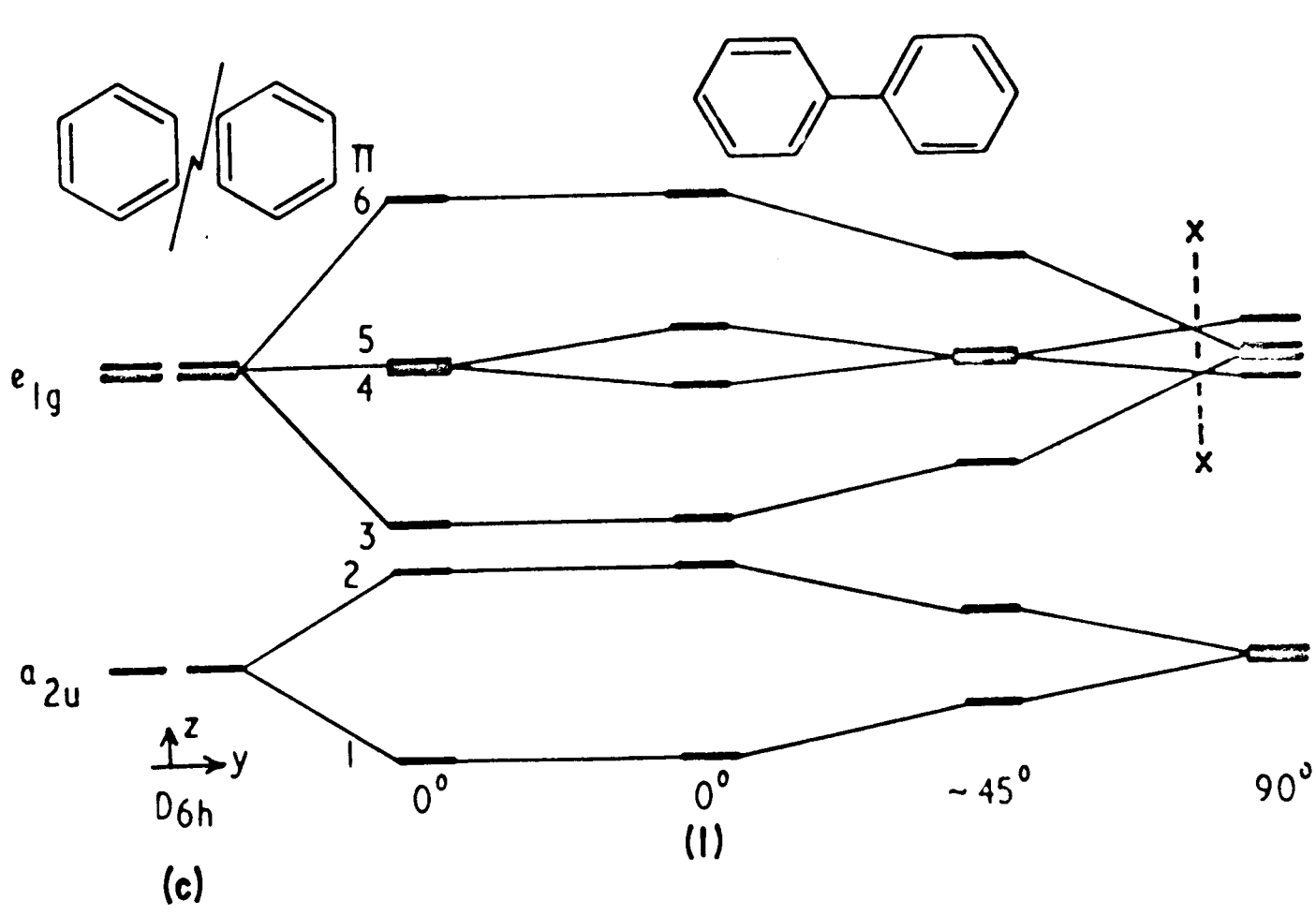


Fig.27 (a) Nodal properties of the pi-MOs of biphenyl. (b) Nodal properties of the upper pi-MOs of mono-substituted benzenes. (c) Interaction pattern on rotation of a phenyl ring in biphenyl (i) Including non-nearest neighbour interactions

TABLE 7

Experimental data defining the regression of Fig.28

	ΔE (eV) (a)	θ^o (b)
Fluorene	1.98	0
Biphenyl	1.46	45 ± 10, 42 ± 2 (i)
2-fluorobiphenyl	1.40	49 ± 5
2,2'-difluorobiphenyl	1.15	60 ± 5
Perfluorobiphenyl	0.90	70 ± 2 (ii)
2,2'-dibromobiphenyl	$0.7 \pm .1$	75 ± 10

(a) $\Delta E \equiv I_4 - I_1$ from P.E, data, Ref. 140

values $\pm$ .02 eV

(b) Electron diffraction data.

(i) Ref.141

(ii) Ref.143

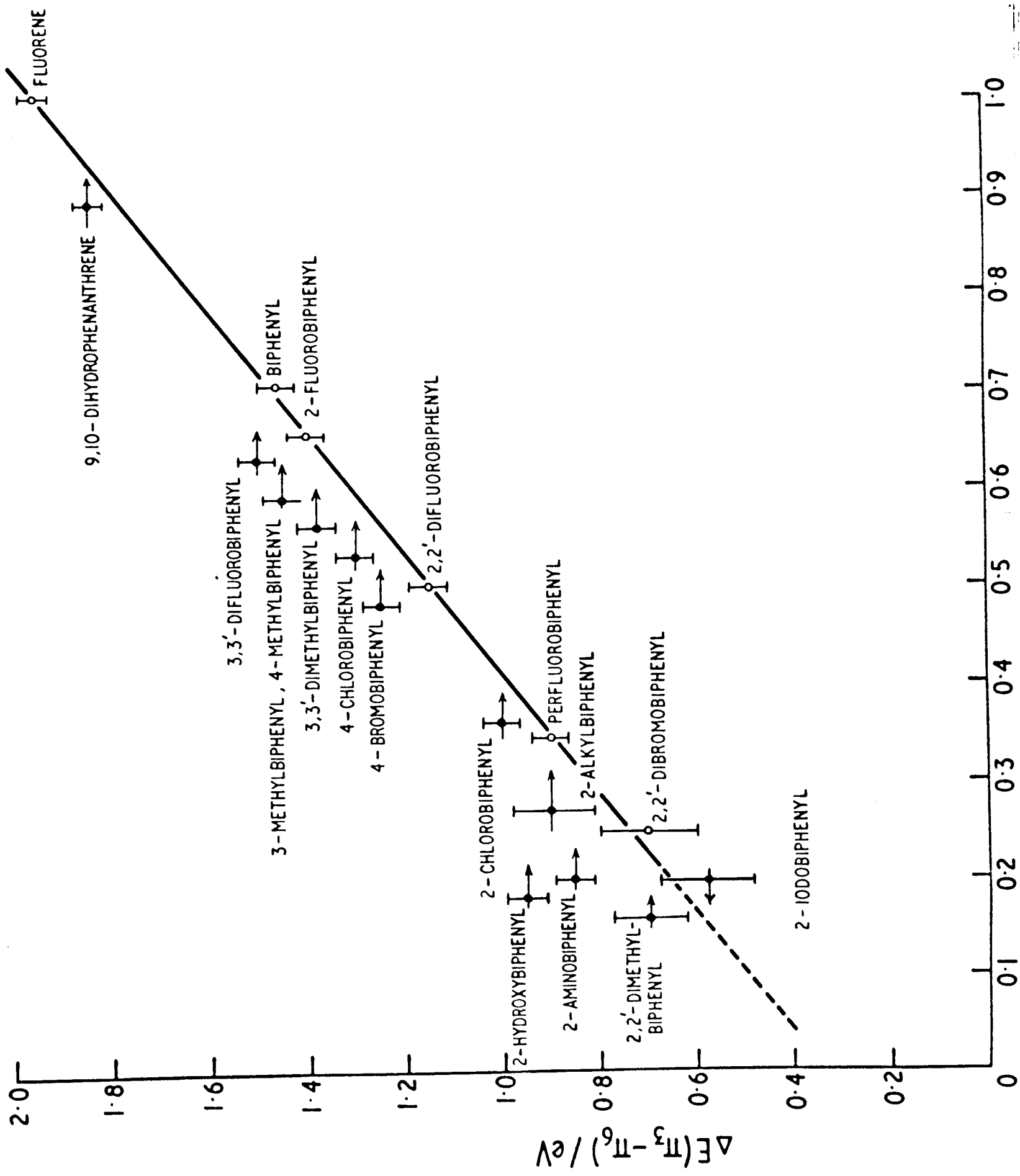


Fig.28 Plot of I_4-I_1 ($\equiv \Delta E$) against dihedral angles for biphenyls.
Coordinates from Table 7. ΔE from P.E. spectra

TABLE 8

Dihedral angles (θ) of substituted biphenyls

Biphenyl derivative	This work ΔE(eV)[a]	This work θ°[b]	Other workers Scale models[c][d]	Other workers Solution[C][d]
9,10-dihydro-phenanthrene	1.84	21	20	24
3,3'-difluoro	1.50	44		
3-methyl	1.45	46		
4-methyl	1.45	46	43	34
4-fluoro	1.45	46		
4,4'-difluoro	1.42	47		
4,4'-bromofluoro	1.40	49		
3,3'-dimethyl	1.38	49		
4-chloro	1.30	53		
4-bromo	1.25	55		22
2-chloro	1.00	66	66	48
2-hydroxy	0.95	68	52	50
2-methyl	0.90	70	72,62	58, 39
2-alkyl[e]	0.90 ± .1	70		61, 46
2-amino	0.85	71		
2,2'-dimethyl	0.70	78	72	70, 48
2-iodo	~.6 ± .1	82 ± 4		

(a) Values ± .02 eV

(b) Values ± 2°

(c) Ref. 137

(d) Ref. 132

(e) Alkyl=ethyl, n-propyl, iso-propyl, n-butyl

angle in other substituted biphenyls which were investigated are listed, and compared to values from scale models and previous estimates. In comparing the results obtained from the various techniques differences in the physical state of the molecules must be appreciated. Environment affects the conformation markedly;* cohesive forces are important. Using this empirical relationship, however, the conformation can be determined quickly and to above the same accuracy as is possible by electron diffraction.

The study of the electronic structure of biphenyls helps to clarify the much debated concept of conjugation versus non-bonded repulsions. The former pi-pi type interactions tend to keep the phenyl groups coplanar, the latter are least when the phenyl groups are more or less perpendicular. To get a realistic estimate of the potential surface it is necessary to include both. Such calculations predict the equilibrium geometry of biphenyl satisfactory,[142] however, in substituted biphenyls it is difficult to obtain an adequate function to represent the non-bonded interactions.[143] Thus with the introduction of different substituents in the ortho positions, this gives rise not only to twisting about the central bond (as a consequence of the non-bonded repulsions), but also marked electronic perturbation. The contribution of the latter is estimated by comparison with meta (and para) substituted biphenyls. On consideration of the effect of rotation on the pi-energy levels of an isolated biphenyl molecule, a qualitative interaction pattern as shown in Fig. 27c is obtained. This pattern is reproduced in the P.E. spectra (Figs.29-36). The Π_4, Π_5 MOs are predominantly invariant to rotation while the Π_3, Π_6 MOs reflect changes in conjugation.

---

*Footnote: X-ray diffraction indicates that biphenyl is planar in the solid phase; [140] electron diffraction finds an angle of 45° [140] (and 42°) [141]; in solution the value is intermediate depending on the solvent ~ $19\text{-}26^{\circ}$ [137] In view of the present data a dihedral angle of 45° fits appreciably better the regression than 42°.

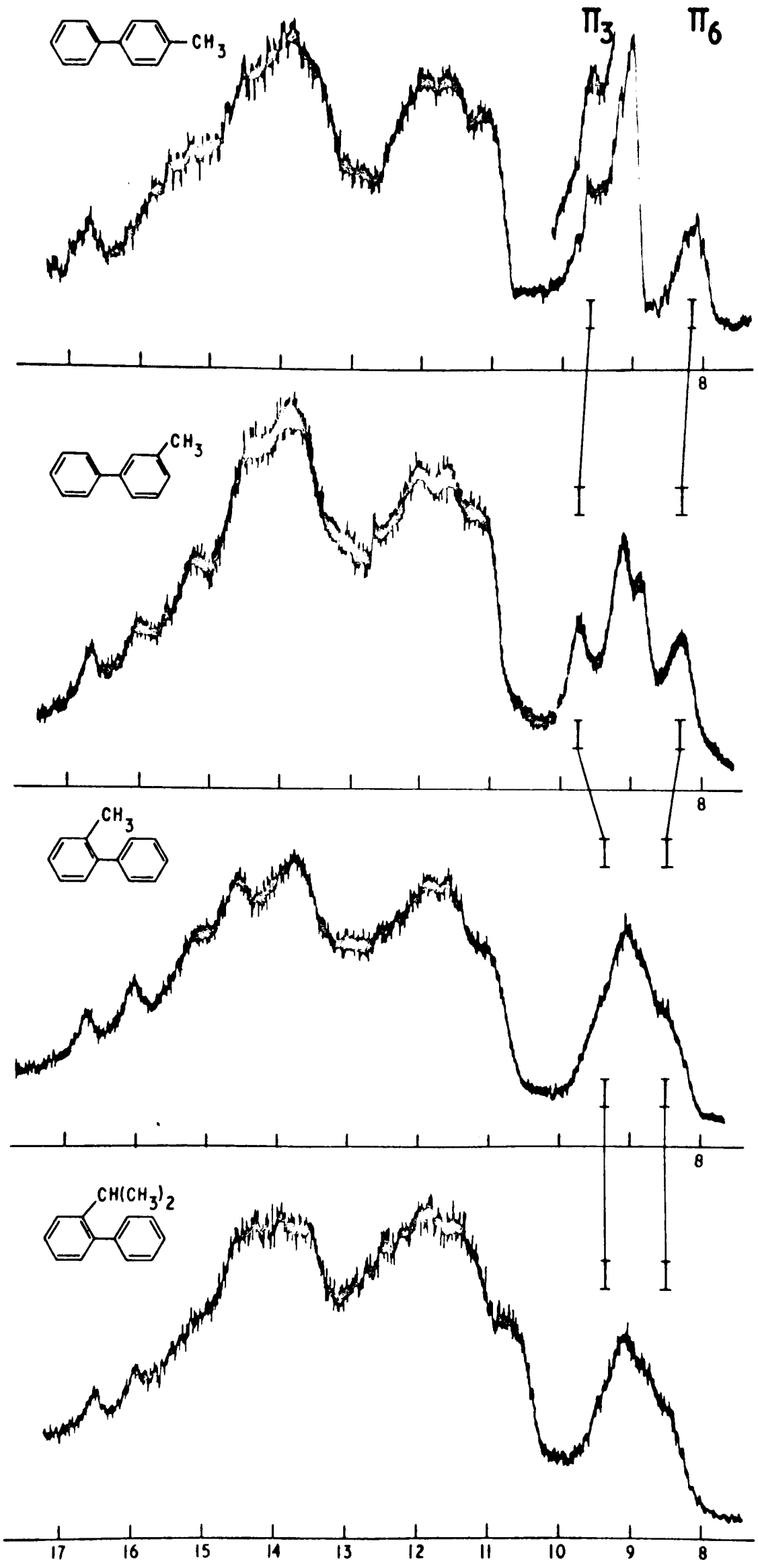


Fig.29 He I (21.22 eV) photoelectron spectra of substituted biphenyls and related molecules

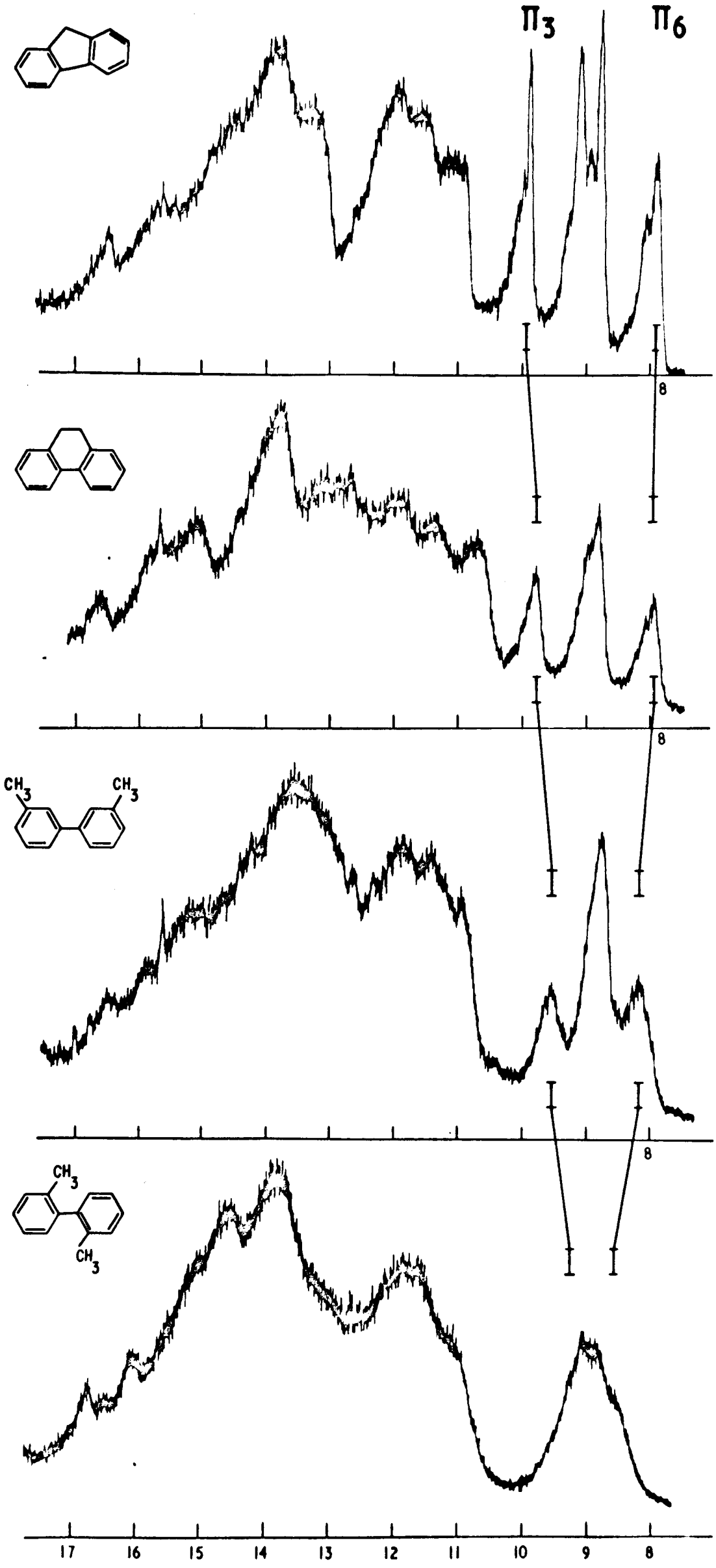


Fig.30 He I (21.22eV) photoelectron spectra of substituted biphenyls and related molecules

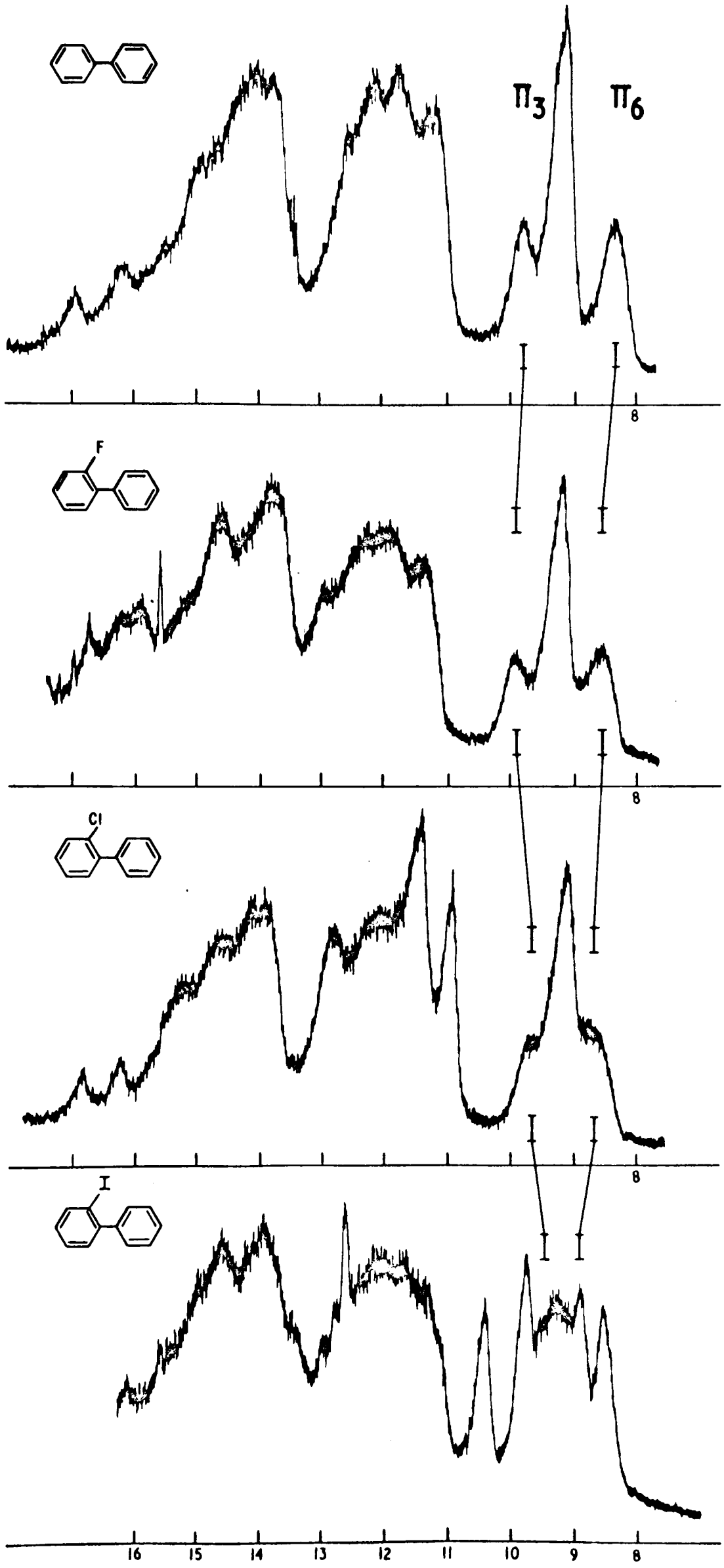


Fig.31 He I (21.22 eV) photoelectron spectra of substituted biphenyls and related molecules

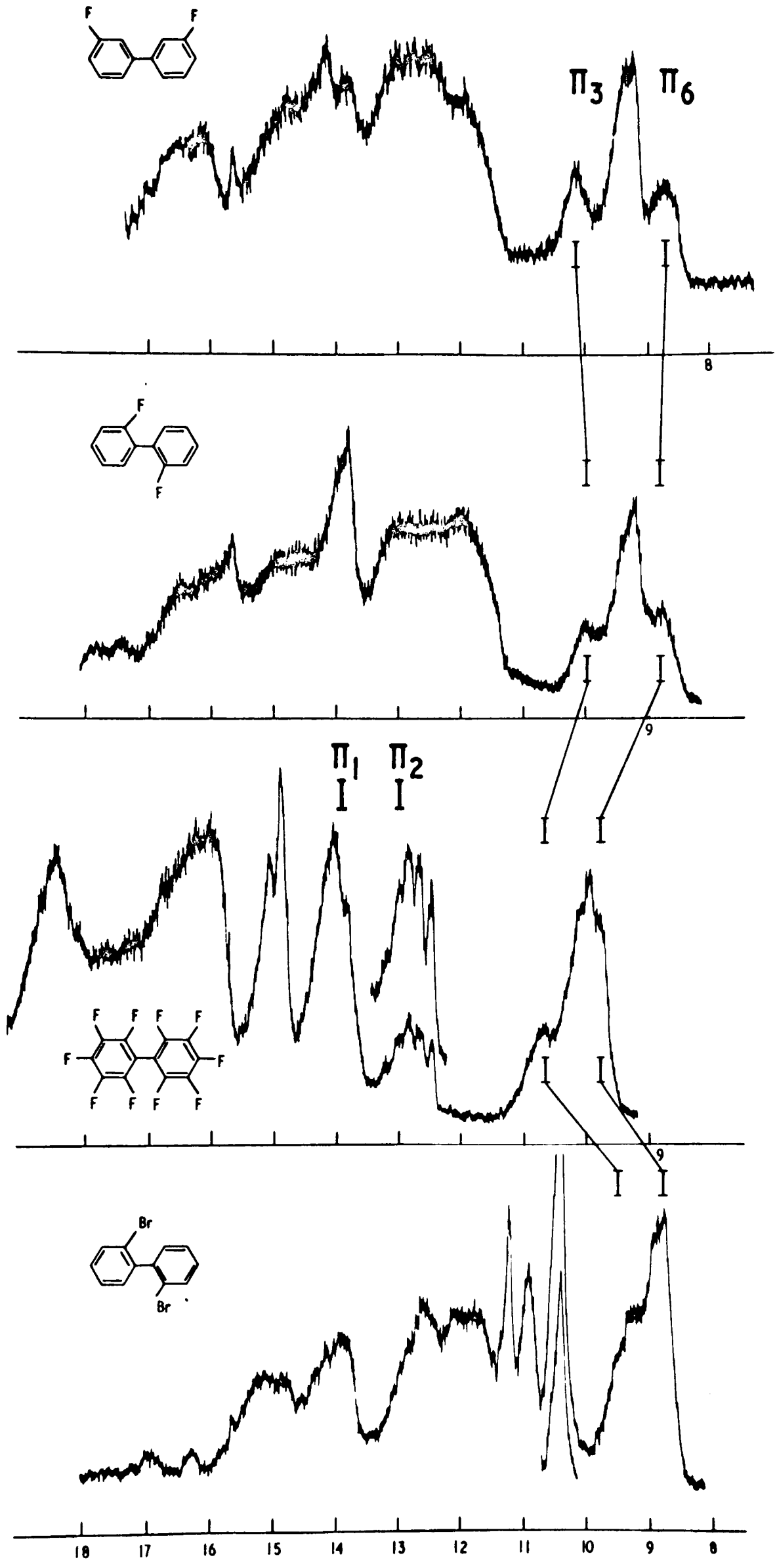


Fig.32 He I (21.22 eV) photoelectron spectra of substituted biphenyls and related molecules

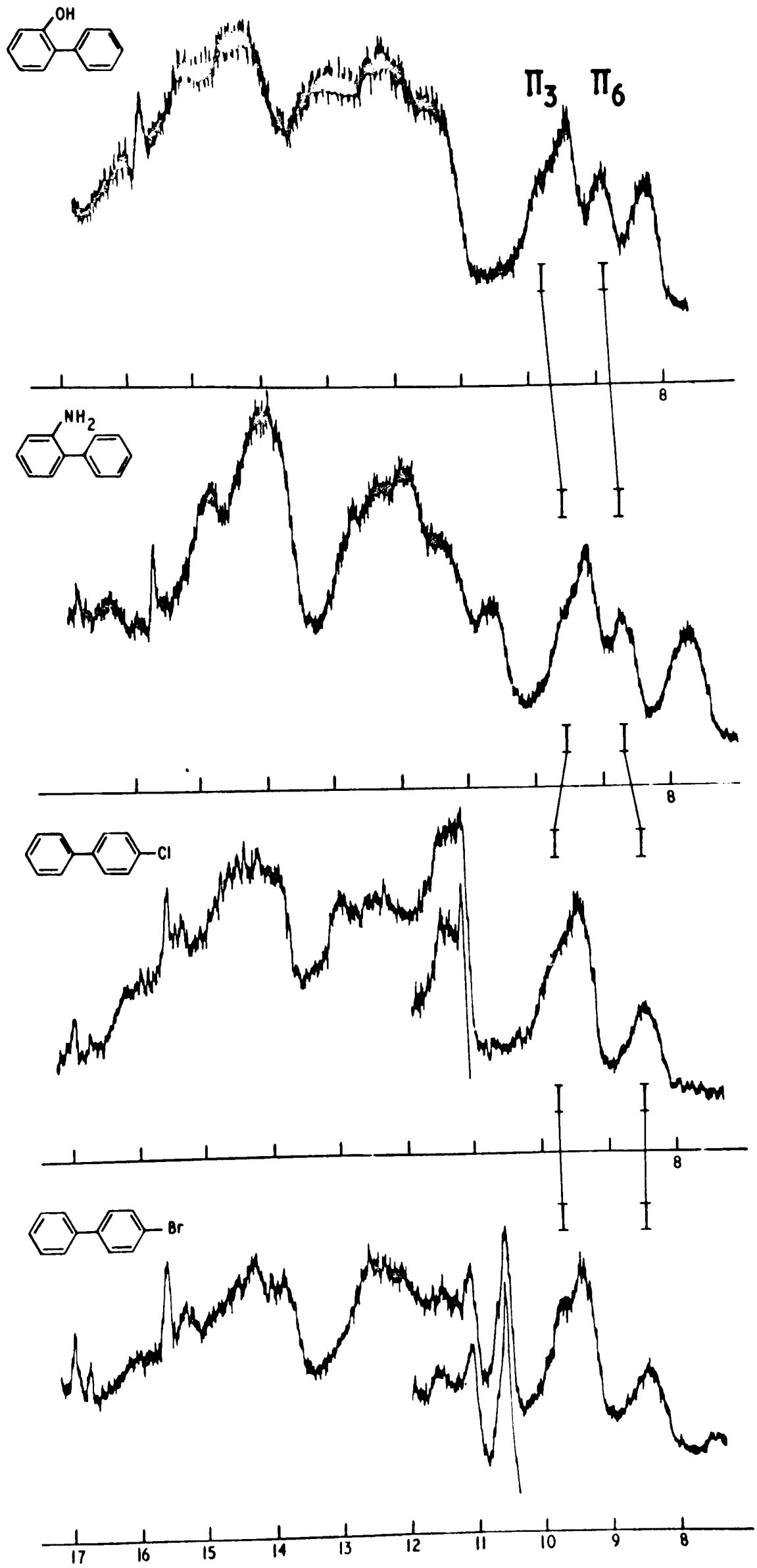


Fig. 33 He I (21.22 eV) photoelectron spectra of substituted biphenyls and related molecules

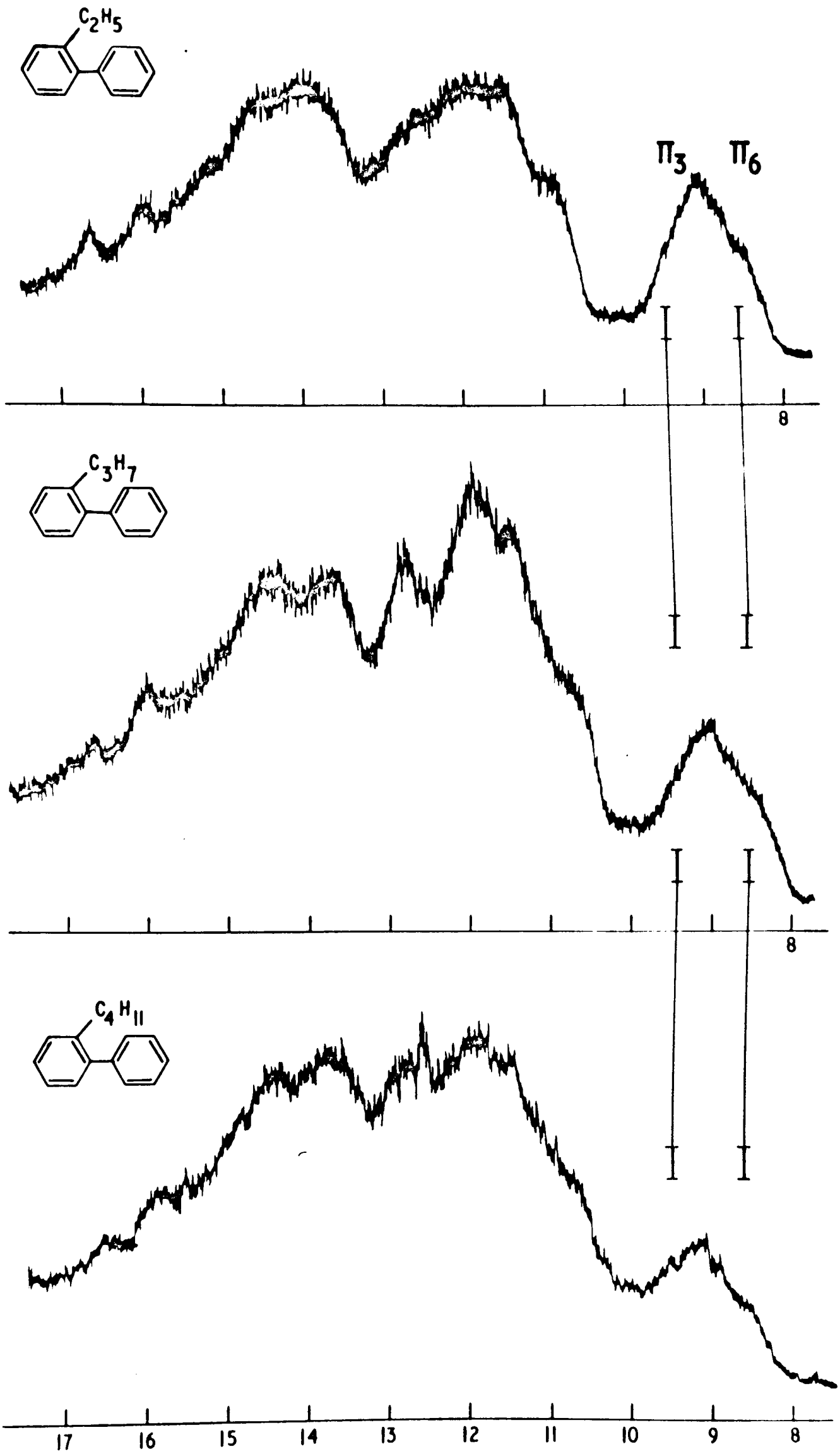


Fig.34 He I (21.22 eV) photoelectron spectra of substituted biphenyls and related molecules

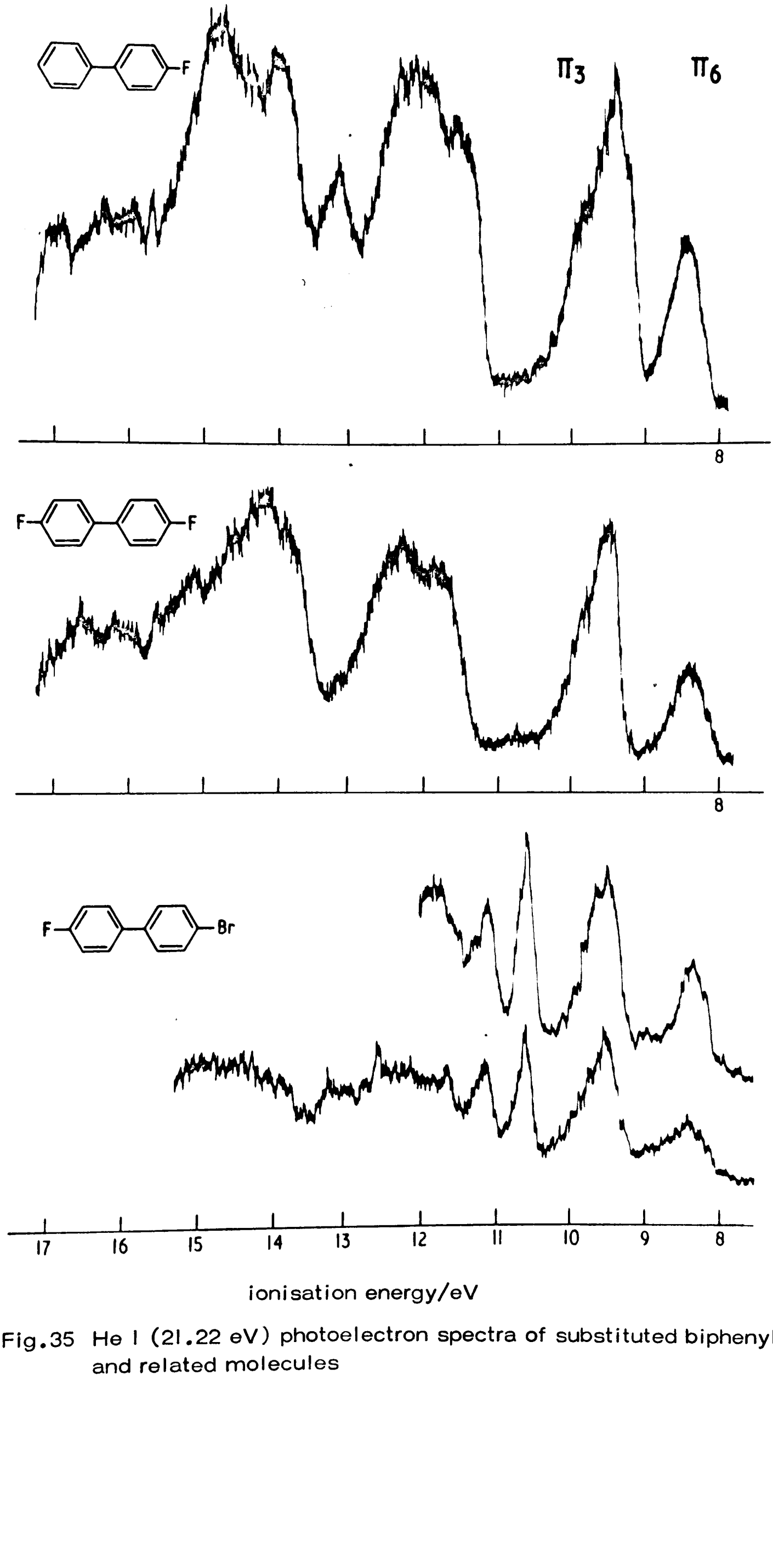


Fig.35 He I (21.22 eV) photoelectron spectra of substituted biphenyls and related molecules

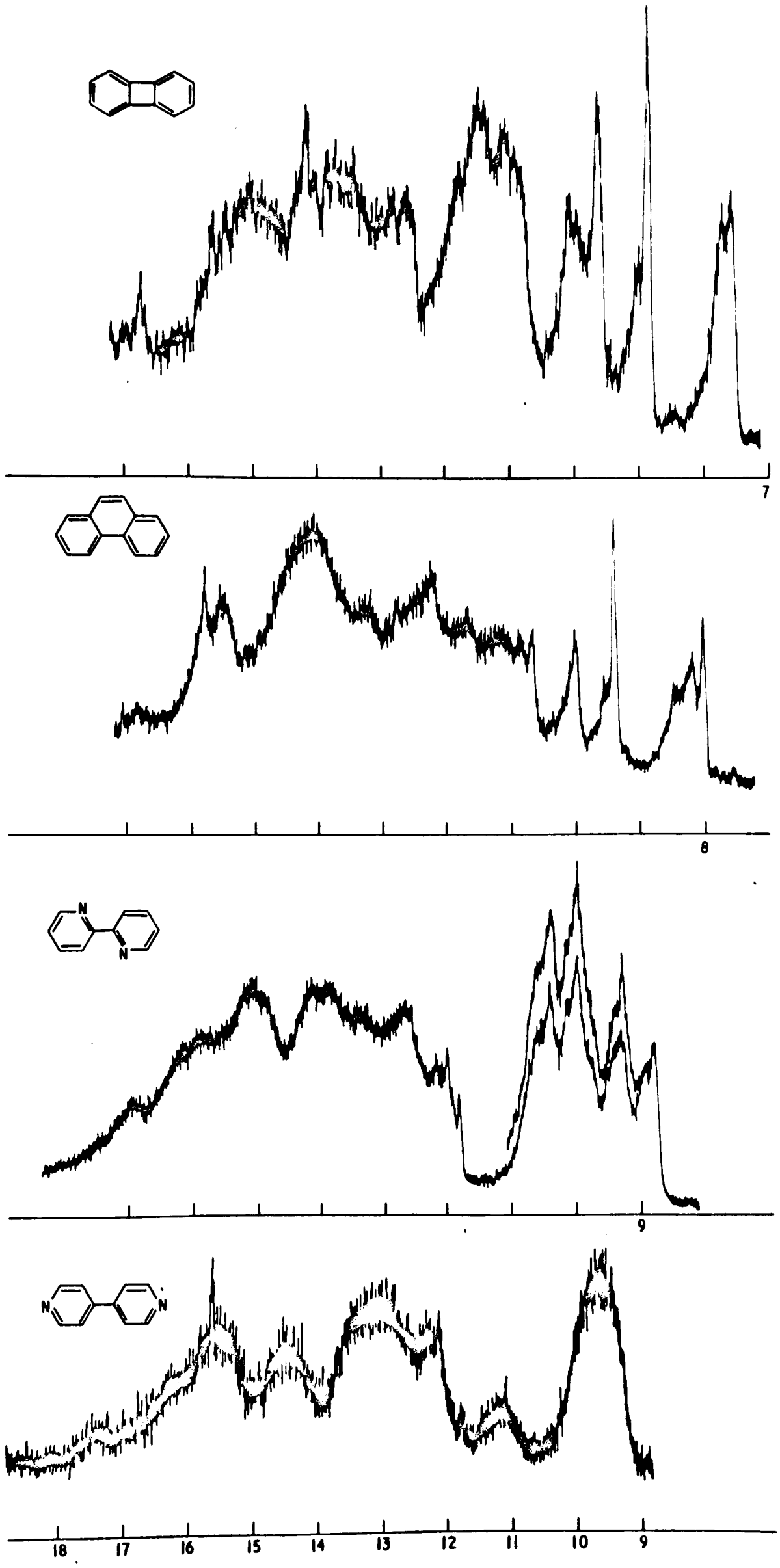


Fig.36 He I (21.22 eV) photoelectron spectra of substituted biphenyls and related molecules

TABLE 9

Observed ionisation energies (eV)

Biphenyl derivative	$I_1(\Pi_6)$	$I_{2,3}(\Pi_5, \Pi_4)$	$I_4(\Pi_3)$	I_5
9,10-dihydro-phenanthrene	7.96(7.55)	8.80(8.60),8.95	9.80(9.60)	10.7(10.35)
3,3'-dimethyl	8.15(7.85)	8.73,8.88	9.53	10.9(10.6)
2,2'-dimethyl	8.55(8.05)	8.80,9.00	9.25	11.1(10.5)
3-methyl	8.30(7.95)	8.90,9.10	9.75	11.2(10.75)
2-methyl	8.60(8.10)	8.85,9.10	9.50	11.1(10.55)
2-ethyl	8.55	8.85,9.10	9.45	10.9
2-n propyl	8.50	8.85,9.10	9.45	10.8
2-isopropyl	8.50	8.85,9.05	9.45	10.7
2-n butyl	8.50	8.90,9.05	9.40	10.9
4-methyl	8.15(7.80)	9.00(8.80),9.15	9.60	10.95(10.7)
3,3'-difluoro	8.70(8.35)	9.30,9.40	10.20	11.8(11.35)
2,2'-difluoro	8.85(8.35)	9.20,9.38	10.00	11.6(11.3)
2-fluoro	8.55(8.20)	9.18,9.35	9.95	11.4(11.0)
4-fluoro	8.35(8.00)	9.35(8.95),9.45	9.80	11.4(11.05)
4,4'-difluoro	8.38(8.00)	9.50(9.25)	9.80	11.7(11.3)

I_1 and I_4 values $\pm$ .02 eV, I_5 $\pm$ .1 eV

In Tables 9-11 the band onsets (adiabatic I.E.s) are listed in parentheses when defined in the P.E. spectra; $\pm$ .02 eV.

TABLE 10. Observed ionisation energies (eV)

Biphenyl	I_1	$I_{2,3}$	I_4	I_5	I_6	I_7
2-chloro	8.70(8.20)(π_6)	9.10,9.25(π_5,π_4)	9.70(π_3)	10.95($\pi_{X:}$)	11.42($\sigma_{X:}$)	11.6
4-chloro	8.46(8.10)(π_6)	9.43(9.10),9.56(π_5,π_4)	9.75(π_3)	11.18($\pi_{X:}$)	11.47($\sigma_{X:}$)	11.3
4-bromo	8.40(8.05)(π_6)	9.40(9.05)(π_5,π_4)	9.65(π_3)	10.50($\pi_{X:}$)	11.05($\sigma_{X:}$)	11.5
4,4'-bromofluoro	8.40(8.10)(π_6)	8.50,9.60(π_5,π_4)	9.80(π_3)	10.57($\pi_{X:}$)	11.10($\sigma_{X:}$)	11.80(11.5
2-hydroxy	8.25(7.80)(π_5)	8.90(π_6)9.45(π_4)	9.80(π_3)	11.3(10.8)($\pi_{X:}$)		
2-amino	7.70(7.28)(π_5)	8.70(8.30)(π_6),9.15(π_4)	9.50(π_3)	10.60(10.20) ($\pi_{X:}$)	11.2	
Perfluoro [(a)]	9.80(9.40)(π_6)	9.96,10.10(π_5,π_4)	10.70(π_3)	12.85(12.48) (π_2)	13.85(13.55) (Π_1)	14.03
2,2'-dibromo	8.75(8.40)(π_6)	8.85,9.20(π_5,π_4)	9.45(π_3)	10.42(:Br)	10.90(:Br)	11.22(:Br) [(c)]
2-iodo [(b)]	8.50(8.20)(π_5)	8.90(π_6)9.30(π_4)	9.50(π_3)	9.75(I_6)	10.40(Π_5^+)	11.3(10.9)
2,2'-bipyridyl [(d)]	8.58(8.35)	9.10,9.85	10.25	11.90(11.70) (π_2)	12.55	
4,4'-bipyridyl [(e)]	9.75(9.10)	11.20(10.80)(π_3)	12.30(11.85)			

(a) I_8 14.90(14.65), I_9 16.00(15.55), I_{10} 16.60, I_{11} 18.40

(b) Π_5^-, Π_5^+, see text

(c) I_8 12.0(11.8)

(d) $I_1 - I_4$ are the maxima of the first group of bands

(e) I_1 corresponds to the maximum of the first coalesced band, range of ionisation energies of the components $\pm$ .4 eV

TABLE 11

Observed ionisation energies (eV)

	Biphenyl				Fluorene	
	(a)	(b)	(c)		(a)	(b)
I_1	8.32 (7.95)	8.23	8.20	6	7.93	7.93
I_2	9.05 (8.80)	9.08	9.08	5	8.83	8.74
I_3	9.15			4	9.13	
I_4	9.80	9.76	9.70	3	9.91	
I_5	11.20(10.80)	11.02	11.02		10.95(10.70)	10.90

	Biphenylene		Phenanthrene		
	(a)	(b)	(a)	(b)	(d)
I_1	7.60	7.62	7.92	7.91	7.92
I_2	8.85	8.89	8.12		8.12
I_3	9.65	9.68	9.30	9.18	9.28
I_4	10.05	10.10	9.90	9.74	9.88
I_5	10.90(10.60)		10.60	10.71	10.64
I_6	11.1		10.77		

I_i (i = 1 - 4) values $\pm$ .02 eV

(a) This work

(b) Ref. 148

(c) Ref. 149

(d) Ref. 146

In substituted biphenyls the situation is analogous to substituted benzenes. In the latter the two-fold degeneracy of the $\Pi_{e_{2g}}$ orbital is removed and the resulting MOs have a maximum electron density and node at the point of substitution, i.e. Π_{b_1} and Π_{a_2} respectively (Fig. 27b). It is this property that leads to the additivity relationship in 1,4,disubstituted benzenes.[144.] In 1,2 and the complementary 1,3 disubstituted benzenes the perturbation on the Π_{b_1} MO (of the mono substituted) is the same as reflected by their I.E.s[145.] (of course excluding steric effects in the 1,2 cases). Similar considerations apply to the substituted biphenyls. Thus ortho and meta substituents cause a second order electronic perturbation on the Π_3 and Π_6 MO by through-bond coupling. Any other changes are steric in origin. In contrast the perturbation on Π_4, Π_5 MOs will be extensive but to the same extent in the ortho and meta compounds. The I.E.s of Π_4, Π_5 are the same in the ortho and meta biphenyls and are very similar to the I.E. of the Π_{b_1}, MO of the corresponding benzene. In para-substituted biphenyls, on the other hand, the values correlate with the Π_{a_2} MO. This is seen vividly in the correlation diagrams.

This is diagnostically important. The comparison of ortho substituted biphenyls with their meta counterparts allows the identification of the Π_4, Π_5 bands; whereas in the meta derivatives they are well defined in the P.E. spectra; in the ortho the first group of pi orbitals often coalesce in the P.E. spectra. From such a comparison it appears that the angle at which the crossover of Π_4 and Π_6 (and Π_3 and Π_5), x ... x in Fig. 27c, takes place greater than $\sim 80^{\circ}$.

For a more detailed discussion of the assignments a semi-empirical approach is used that can be readily extended to other systems. Examination of the P.E. spectra of the biphenyls indicates that the grouping of orbitals may be simpler than is suggested by more sophisticated MO methods. In the latter, for example extended Hückel and CNDO, it is well known that sigma orbitals seem consistently too high

in energy; an artefact of the approach. This is especially serious in the biphenyls where such calculations predict extensive pi-sigma mixing. The results obtained using the extended Hückel method, for example, showed no simple relationship between the pi-energy levels and the dihedral angle (see Appendix II).

In diacetylene, regarded as made up from two acetylene pi electron moieties, the separation in energy between the symmetric and anti-symmetric linear combinations of the individual group orbitals, π_1 π_2, is given by

$$\Delta E = \varepsilon(\pi_- - \pi_+) \text{ where } \pi_- = \frac{1}{\sqrt{2}}(\pi_1 - \pi_2)$$

$$\pi_+ = \frac{1}{\sqrt{2}}(\pi_1 + \pi_2)$$

Π-orbital photoelectron bands in many conjugated molecules (Table 12) can be treated in this way. A standard interaction parameter

$$B = \langle \Pi_i | H | \Pi_j \rangle = -1.2 \text{ eV} \qquad i, j \ni c = c,\ c \equiv c,\ c = o \text{ etc.}$$

at distance of 1.38Å between the linked carbon atoms of the two moieties is thus obtained. (In these cases of course, B is related to the standard Hückel resonance integral

$$\beta = \langle 2p_i | H | 2p_j \rangle$$

for the adjacent atomic orbitals i,j. i.e. $\beta = 2B$).

In biphenyl where large pi-pi interaction is expected between the levels which in the separated benzene rings would be degenerate, the extension of these ideas is straightforward. The maximum interaction will be when the two phenyl groups are coplanar, as in fluorene. It has been shown that in empirical calculations on pi-electron orbital energies the predominating parameter is the distance between the over-

TABLE 12

Splitting of levels (ΔE) found from Photoelectron Spectra of selected molecules

Compound	$\Delta E(eV)$ [1]	$r(\mathring{A})$ [2]
$HC\equiv C-C\equiv CH$	2.45	1.38
$NC\equiv C-C\equiv N$	2.46	1.38
$HC\equiv C-C\equiv N$	2.43	1.38
$H_2C=CH-CH=CH_2$ (t)	2.41	1.48
$H_2C=CH-C\equiv N$	2.40	1.44
$Ph.C\equiv CH$	2.21	1.42
$Ph.C\equiv CN$	2.20	1.42
$Ph.CH=CH_2$	2.07	1.48
Fluorene	1.98	1.48

1. $\Delta E = (\pi_- - \pi_+) = 2B$; vertical I.E.s used, $\pm$ .02 eV Refs.47,145.

2. r is the distance between the linked carbon atoms of the interacting moieties.

lapping AOs.[146] Thus it is interesting to note that assuming proportionality of B to the overlap integral,

$$B_r = \frac{S_r}{S_{1.38}} \; B_{1.38}$$

where $S_r = \langle 2p_i | 2p_j \rangle$, i,j separated by r (Å) a value of 2.0 eV is obtained at ~ 1.50 Å (mean in biphenyls) using Slater or SCF overlap integrals.* The observed splitting between the Π_3 and Π_6 levels in fluorene corresponding to ΔE defined, (vide infra) is 2.0 eV. The effective constancy of the B parameter indicates the utility of semi-localised MOs as basis sets in place of atomic orbitals.

In planar biphenyl the basis set are the semi-localised orthogonal pi-MOs of the phenyl moieties, i.e. $\Pi_{a_{2u}}$, $\Pi_{e_{1g}}$ (b_1) and $\Pi_{e_{1g}}$ (a_2) labelled as Ψ_1, Ψ_2 and Ψ_3 respectively, on the separated rings R and S. From its nodal properties Ψ_3 need not be included in the interaction scheme. The LCMO (linear combination of basis MO) are used as trial eigenfunctions in the variational treatment. Within the Hückel formalism and with experimental quantities for matrix elements: i.e. (see Appendix I)

$$\langle \psi_i | H | \psi_i \rangle = A_i$$

and

$$\langle \psi_i^R | H | \psi_i^S \rangle = \langle \psi_i^R | H | \psi_j^S \rangle = B, \quad i,j = 1,2$$

where A_i is the negative of the experimental I.E. of an electron ionised from the pi-MO ψ_i of benzene.

---

*Footnote: Standard Hückel calculations on planar biphenyl predict a splitting ΔE of $\sim .6\beta$, i.e. ~ 1.5 eV without correcting for the distance variation.

From the solution of the secular determinant*

$$\Delta E = \epsilon(\Pi_6 - \Pi_3) = 2B$$

In the non-planar case, using the relationship for off-diagonal elements B_θ

$$B_\theta = B \cos \theta$$

the dihedral angle (θ) being zero in the planar case. Ignoring pi-sigma mixing in non-co-planar molecules, it follows that

$$\Delta E = 2B \cos \theta$$

The form of the resultant MOs will be very much like Π_i ($i = 1-6$) depicted in Fig. 27a**. The first order interaction by direct "through-space" overlap gives a splitting of $2B \cos \theta$ between the MOs $\Pi_3 - \Pi_6$. The effect of Π_1 and Π_2 will be a second order perturbation on Π_3 and Π_6 respectively of $\frac{[B \cos \theta]^2}{A_1 - A_2}$ shift to higher energies. The magnitude of this latter perturbation is of the order $< .2$ eV. Consequently in the non-planar case where pi-sigma mixing should strictly be included, the sigma effect on $\Pi_3 - \Pi_6$ will be much smaller (but see Appendix I); not significant at this level of sophistication.

On the basis of this approach a linear regression between ΔE and $\cos \theta$ is expected, and the experimental plot is indeed such a relationship. The gradient is however ~ 1.7 and extrapolation to $\theta = 90^\circ$ produces a finite intercept. It is possible that the observed regression reflects the

---

*Footnote: The calculated orbital energies are related to the I.E.s assuming Koopmans' theorem.[1]

**The MOs arising from Ψ_3 i.e. $\Pi_4 \Pi_5$ do have their degeneracy removed to some extent, as is apparent from the P.E. spectra; this indicates that non-nearest neighbour interaction, i.e. 2-6', 2-2' type, can not be entirely neglected.

neglects, for example, of pi-sigma interaction, electron correlation, and interaction with antibonding orbitals. It would not be surprising to find a high degree of proportionality in such a related system between the various effects.[147.*]

This treatment also predicts that $\Delta E' = \varepsilon(\Pi_2 - \Pi_1) = 2B \cos\theta$.** Unlike ΔE this can not be tested as in the relevant region of the P.E. spectra there is considerable complexity due to overlap with sigma bands. Nevertheless, in one instance this splitting can be unambiguously measured; in perfluorobiphenyl (vide infra). In this case the splittings are $\Delta E \sim .9$ eV and $\Delta E' \sim 1.0$ eV. However, in most cases it would not be expected that this relationship is obeyed to such a degree as ΔE; the pi-sigma interaction can be considerable, especially in the presence of substituents.

The basis orbital parameters are summarised in Table 13 and the calculated values compared with the observed I.E.s. In substituted biphenyls the basis is the appropriate MO of the corresponding substituted benzene; Ψ_1 and Ψ_2 in ortho and meta biphenyls, Ψ_1 and Ψ_3 in para. The difficulties which arise are the matrix elements A_1. Even in benzene itself, the value of the I.E. of the $\Pi_{a_{2u}}$ MO is the subject of much controversy; values range from 11.5 - 12.2 eV. However, as pointed out above, this is only a second order correction to the energies of the Π_3, Π_6 MOs as can be seen in Table 13, where two alternative values for the parameter A_1 are used, the choice is not critical. For the non-zero off diagonal elements the value obtained from

---

* Footnotes: Including coefficients, as derived from Hückel MOs in the treatment, the first order interaction yields $\Delta E' = \frac{2}{3}B$ (c.f. $\Delta E = \frac{4}{3}B$).

** The ratio $\Pi_3 - \Pi_{4,5}$ to $\Pi_6 - \Pi_{4,5}$ in ortho and meta dialkyl biphenyls ($\theta = 0 - 80^{o}$) seems to be independent of the dihedral angle.

TABLE 13

Comparison of calculated and experimental ionisation energies (eV) for some biphenyls

Biphenyl	A_2	A_1	calculated Π_6	calculated Π_3	calculated Π_2	experimental $\frac{1}{2}(\Pi_3+\Pi_6)$	experimental $\frac{1}{2}(\Pi_4+\Pi_5)$
Biphenyl	9.3	12.1 11.5	8.35(8.32) 8.3	9.85(9.80) 9.8	11.55(11.20) 11.0	9.17	9.25
Fluorene	9.1	12.0 11.2	7.8(7.95) 7.8	9.8(9.90) 9.7	11.3(10.95) 10.6	8.92	8.98
9,10-dihydro-phenanthrene	9.1	12.0 11.2	7.9(7.96) 7.85	9.75(9.80) 9.7	11.35(10.70) 10.6	8.88	8.87
2,2'-dimethyl	9.1	12.0 11.2	8.7(8.55) 8.7	9.4(9.25) 9.4	11.7(11.1) 10.9	8.90	8.90
3,3'-dimethyl	9.1	12.0 11.2	8.25(8.15) 8.25	9.6(9.53) 9.65	11.5(10.9) 10.65	8.84	8.80
2,2'-difluoro	9.8	12.1 11.8	9.1(8.85) 9.1	10.2(10.00) 10.2	11.6(11.3) 11.4	9.42	9.29
3,3'-difluoro	9.8	12.1 11.8	8.8(8.35) 8.8	10.4(10.20) 10.4	11.6(11.4) 11.3	9.45	9.35
4,4'-difluoro	9.2	12.1 11.8	8.25(8.38) 8.25	9.75(9.80) 9.75	11.4(11.3) 11.25	9.07	9.40
Perfluoro	10.1	12.8	9.6(9.80)	10.5(10.70)	12.4(12.85)*	10.25	10.00

Values in parentheses are the corresponding experimental I.E.s

* Vertical I.E. (adiabatic ~2.5 eV),
Π_1 13.3 (13.85 vertical, 13.55 adiabatic)

the linear regression rather than B cos θ is utilised, in order to reproduce the experimental results as closely as possible. The agreement is generally good.

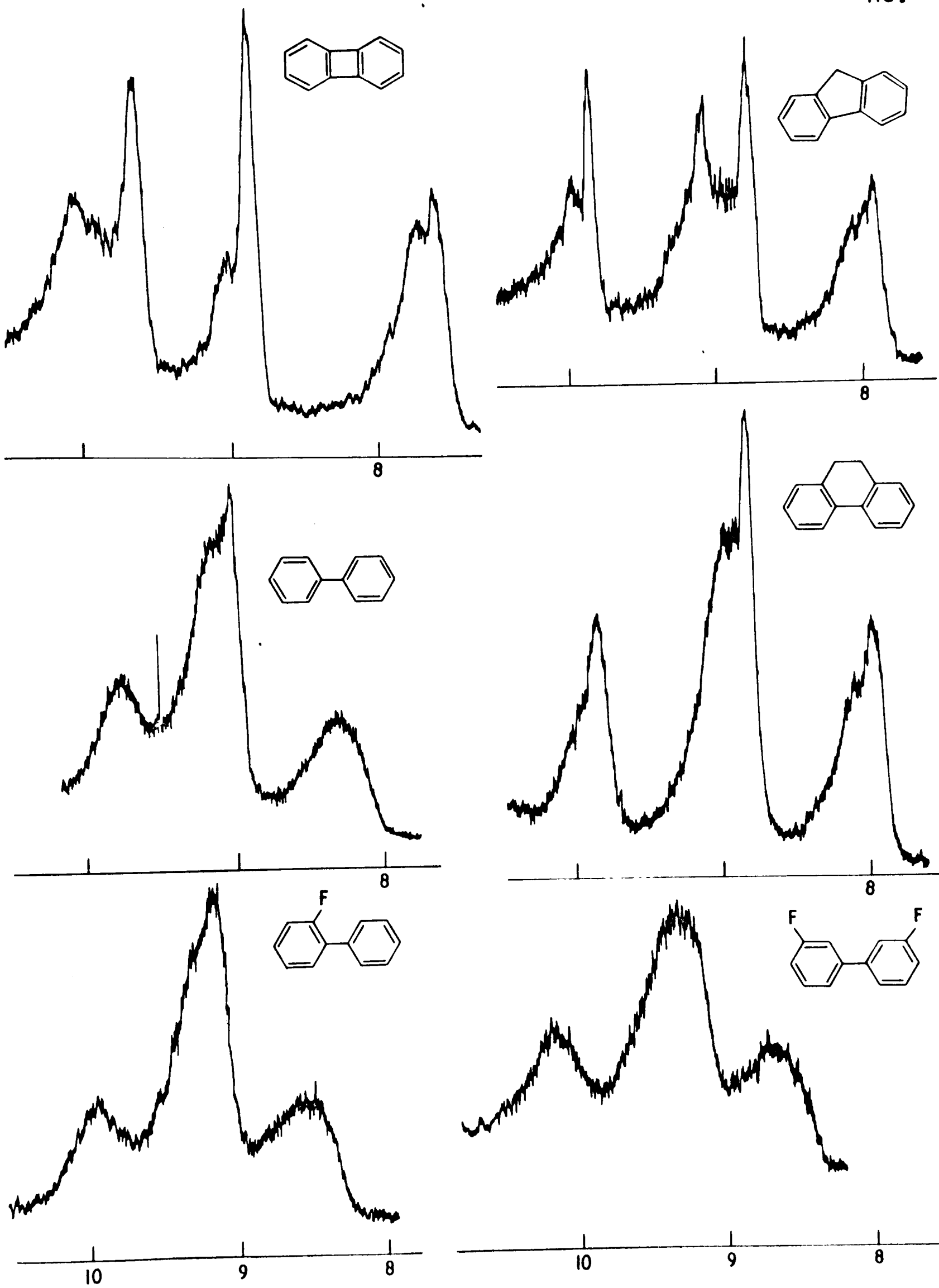
5.5 Discussion of Individual Cases.

In many small molecules changes of molecular geometry on ionisation are reflected by the form of the Franck-Condon envelopes of the P.E. bands.[47] In aromatic and polyatomic molecules, rigidity usually prevents much geometry change, as in bridged biphenyls where the two phenyl rings are rigidly held. In Fig. 37 some of the P.E. spectra are shown with the first four bands Π_i (i = 3 - 6) on expanded energy scale. It appears that the Franck-Condon envelopes are different for the rigidly held biphenyls to those which are free to rotate. For the former the O-O transition is prominent, for the latter the Franck-Condon envelope is rather broad; particularly for the Π_3 and Π_6 ionisations. This indeed would be expected as the Π_4, Π_5 MOs are largely invariant with rotation, unlike the former; and therefore one may expect their potential surfaces to be very similar in the ground and ionic states. Interestingly in u.v. spectra similar differences are observed between bridged and unbridged biphenyls.[137] Calculations on biphenyl cation[142] are in accord with such changes, indicating an angle of approximately 26^{o}.

Alkyl biphenyls

In ortho-alkyl biphenyls (Fig. 30) there is little change from methyl to isopropyl, n-butyl, in the splitting between the Π_3 and Π_6 ionisations. It seems that the additional methylene groups can adopt a favourable conformation without any increase in steric hindrance.

In fluorene and 9,10 dihydrophenanthrene the splitting between the second and third bands arise from the removal of the degeneracy of the Π_4, Π_5 MOs by direct interaction with the bridging methylene groups



ionisation energy/eV

Fig.37 He I (21.22 eV) photoelectron spectra of biphenyls, with first group of bands expanded

of correct symmetry.

Perfluorobiphenyl

In this molecule (Fig. 32) there is a striking relationship of the P.E. spectrum to that of hexafluorobenzene.[47.] In the latter, the second band is associated with the lower pi-MO, $\Pi_{a_{2u}}$. The highest sigma level, $3e_{2g}$, is at I.E. of 14.02 eV. Therefore in perfluorobiphenyl pi-sigma mixing will be minimized in the Π_1 and Π_2 levels as well. The band in the P.E. spectrum at 12.85 eV can only be associated with the Π_2 MO. The relative intensity of this band also suggests that it is associated with only one non-degenerate level. Under high resolution this band shows two vibrational progressions with vibrational intervals of $\sim$1400 and $\sim$ 400 cm^{-1}. The Franck-Condon factors, envelope, and magnitude of the vibrational quanta are almost identical to that in the $\Pi_{a_{2u}}$ band in hexafluorobenzene. These two vibrational progressions are assigned to the totally symmetric modes, stretch (ν'_1) and ring breathing (ν'_2); the ground state values being 1474 and 510 cm^{-1}. On the 15 eV band in perfluorobiphenyl the ν'_1 stretching vibrational quanta are prominent and the band bears a great resemblance to the fourth band in hexafluorobenzene, associated with fluorine atoms orbital in both molecules. The 14 eV band in perfluorobiphenyl may consist of two overlapping bands. There is a corresponding band in hexafluorobenzene at 14.02 eV; the $3e_{2g}$ sigma orbital. The shoulder on the band in perfluorobiphenyl (13.85 eV) is associated with the Π_1 MO. From this assignment the splitting ($\sim$1.0 eV) between the Π_1 and Π_2 levels (c.f. ΔE = .9 eV) is the result of direct interaction of the Ψ_1 basis orbitals on both rings. This is striking support for this simple approach.

Azabiphenyls

These are closly related to pyridine as are the biphenyls to benzene. The P.E. spectra are shown in Fig. 36. The P.E. spectrum of pyridine[47.]

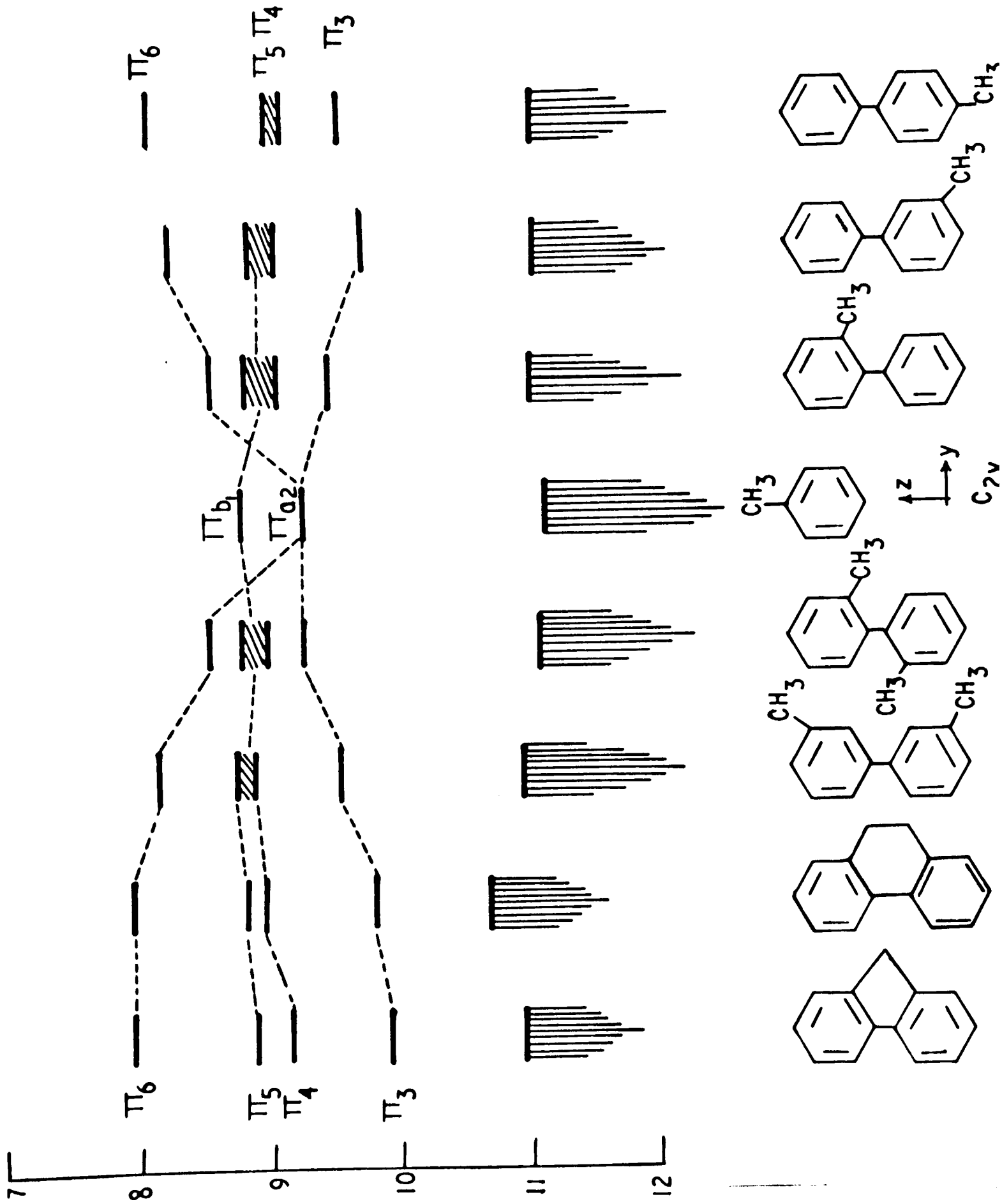


Fig. 38 Correlation of ionisation energies

has been of considerable interest and there is still uncertainty regarding the relative order of the two highest occupied orbitals, $la_2(\pi)$ and $lla_1(:N)$. It is agreed that the band at 10.5 eV relates to the ionisation of an electron from the $2b_1(\pi)$ MO (c.f. π_{b_1} in Fig. 27b). Thus in 4,4'bipyridyl the $2b_1$ orbitals will interact as the Ψ_2 basis orbitals in biphenyl to form Π_3 and Π_6 MO, with a splitting of 2B cos θ approximately about the 10.5 eV level. The la_2 orbitals (c.f. Ψ_3) will give rise to Π_4, Π_5 MOs. Thus the situation is analogous to biphenyl, but with an additional band arising from the in-plane $lla_1(:N)$ "lone-pairs". The first group of bands in the P.E. spectrum therefore arises from these five MOs; Π_4,Π_5 the degenerate nitrogen lone-pairs, and Π_6. The Π_3 MO is clearly identified as the second band at 11.9 eV. The splitting of ~1.4 eV indicates a dihedral angle of 45^{o} from the empirical plot. This agrees with electron diffraction.

In 2,2'-bipyridyl the $2b_1$ orbital assumes the role of Ψ_3 while the Π_3 and Π_6 MO arise from the main interaction of the la_2 orbitals (c.f. ψ_2). In this case the nitrogen lone-pairs may have their degeneracy removed to some extent by interaction via the sigma orbitals. This leads to a more comples first group of bands. In the correlation diagram (Fig. 40) a possible scheme is proposed. Previous structure studies indicate that the molecule is planar with a transoid conformation. The splitting $\Delta E \sim 1.8$ eV here also suggests a near planar conformation. The band with onset at 11.70 eV has two vibrational progressions discernible, with frequencies ~1600 and 800 cm^{-1}; similar vibrational quanta are excited on the pi bands in pyridine. This band is assigned to the Π_2MO

2-amino and 2-hydroxy biphenyls

The P.E. spectra compared with aniline and phenol respectively show that the lowest I.E. relates not to a Π_6 but to a Π_5-like MO (Fig. 41), very much like the π_{b_1} MO in the corresponding benzene. Of interest

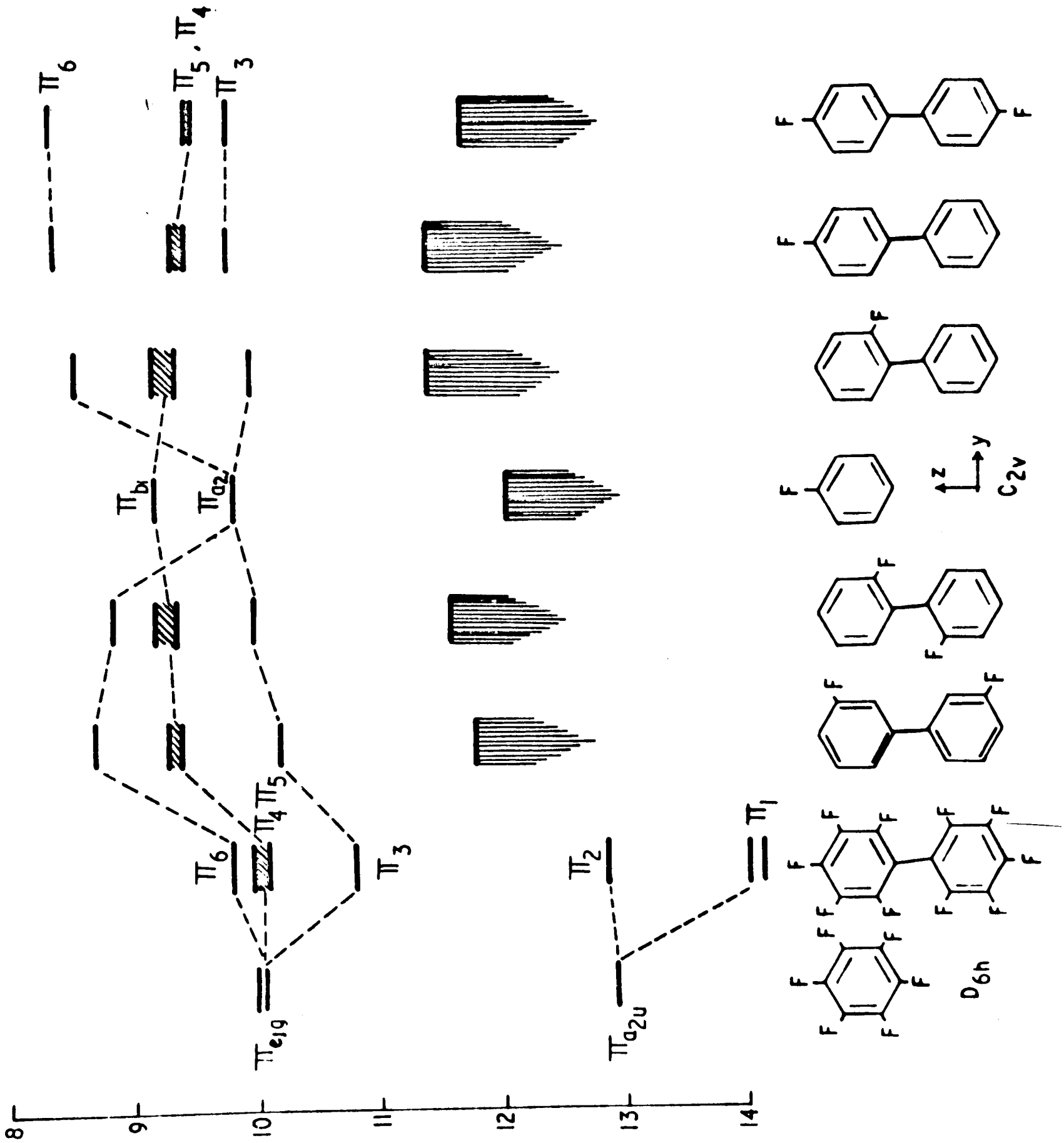


Fig.39 Correlation of ionisation energies

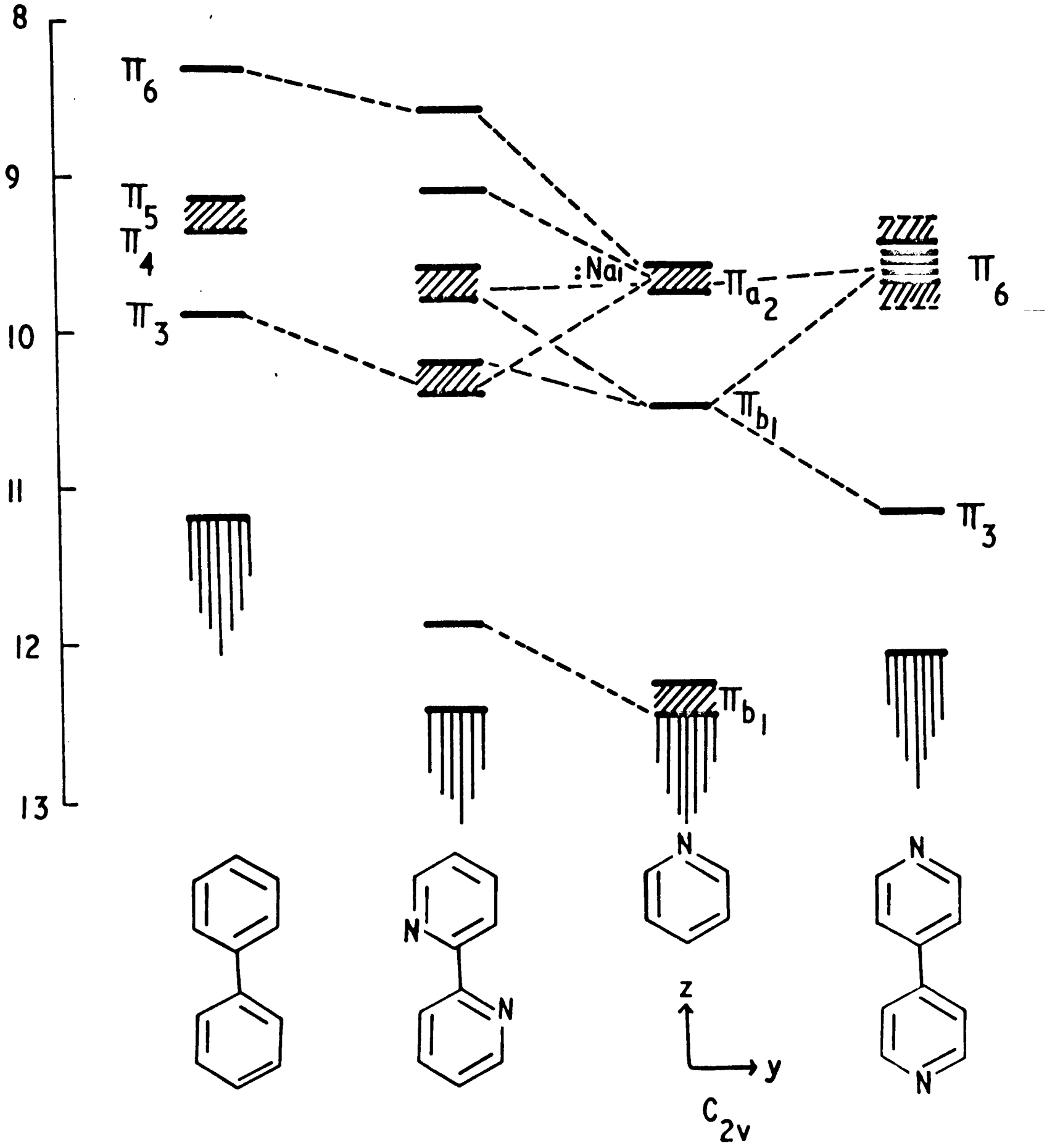


Fig.40 Correlation of ionisation energies

in these molecules is the conformation of the amino and hydroxy groups themselves, as steric strain could be relieved by the rotation of these groups from the position of maximum 2p-π interaction. One can identify in the P.E. spectra the levels associated with the nitrogen and oxygen "lone-pair" orbitals. From the examination of the steric effects in substituted anilines and phenols (Chap.VII) it can be deduced that in ortho-amino and hydroxy biphenyls no such rotation takes place but that the amino and hydroxy group orientation is as in aniline and phenol.

Iodobiphenyl

In the correlation diagram (Fig. 41), reproduction of the interaction pattern is only possible with the knowledge of the sequence of orbital energies in iodobenzene.[145.] The perturbation of the energy levels by π_{5p}-π mixing is extensive however. From the estimated ΔE, iodine is found to be the most effective blocking group of all the substituents studied.

Halobiphenyls

The splitting of the halogen "lone-pairs" seen earlier in the halobenzenes is again noticeable. In the case of 2,2' dibromobiphenyl this is not clearly defined. There seems to be appreciable interaction between the lone-pairs of the different bromine atoms. Similar effects are observed in the ortho-dihalobenzenes.[145.]

Phenanthrene and biphenylene

These are included as they can be compared to planar biphenyl. In view of the reactivity of the 9,10 double bond in phenanthrene, the P.E. spectrum may be tentatively interpreted as a planar biphenyl with a perturbing ethylene MO. Comparison with the P.E. spectrum of fluorene shows this similarity. The positions of π_3, π_5, π_6 bands are nearly the same. The first band in the P.E. spectrum of phenanthrene shows a

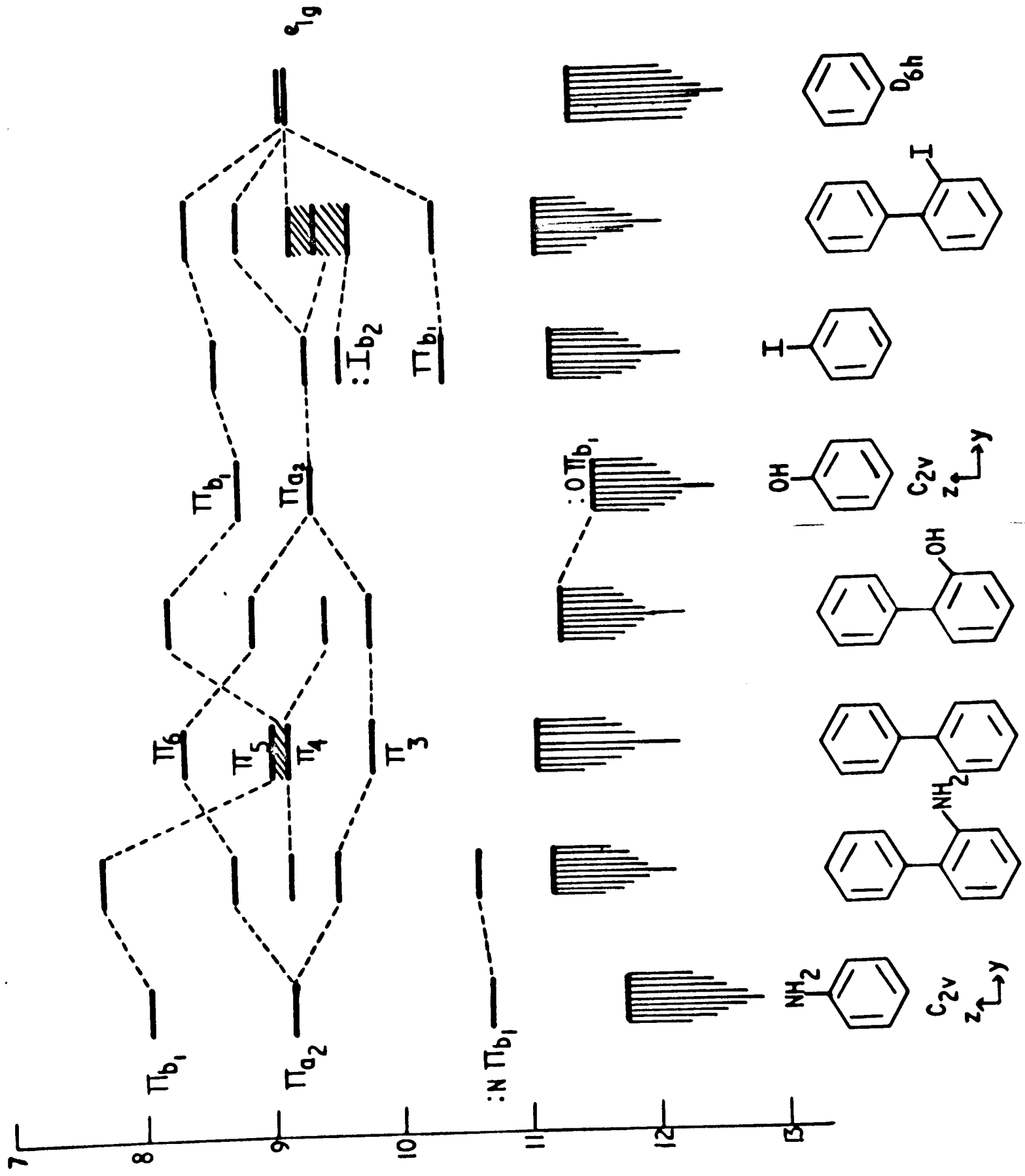


Fig.41 Correlation of ionisation energies

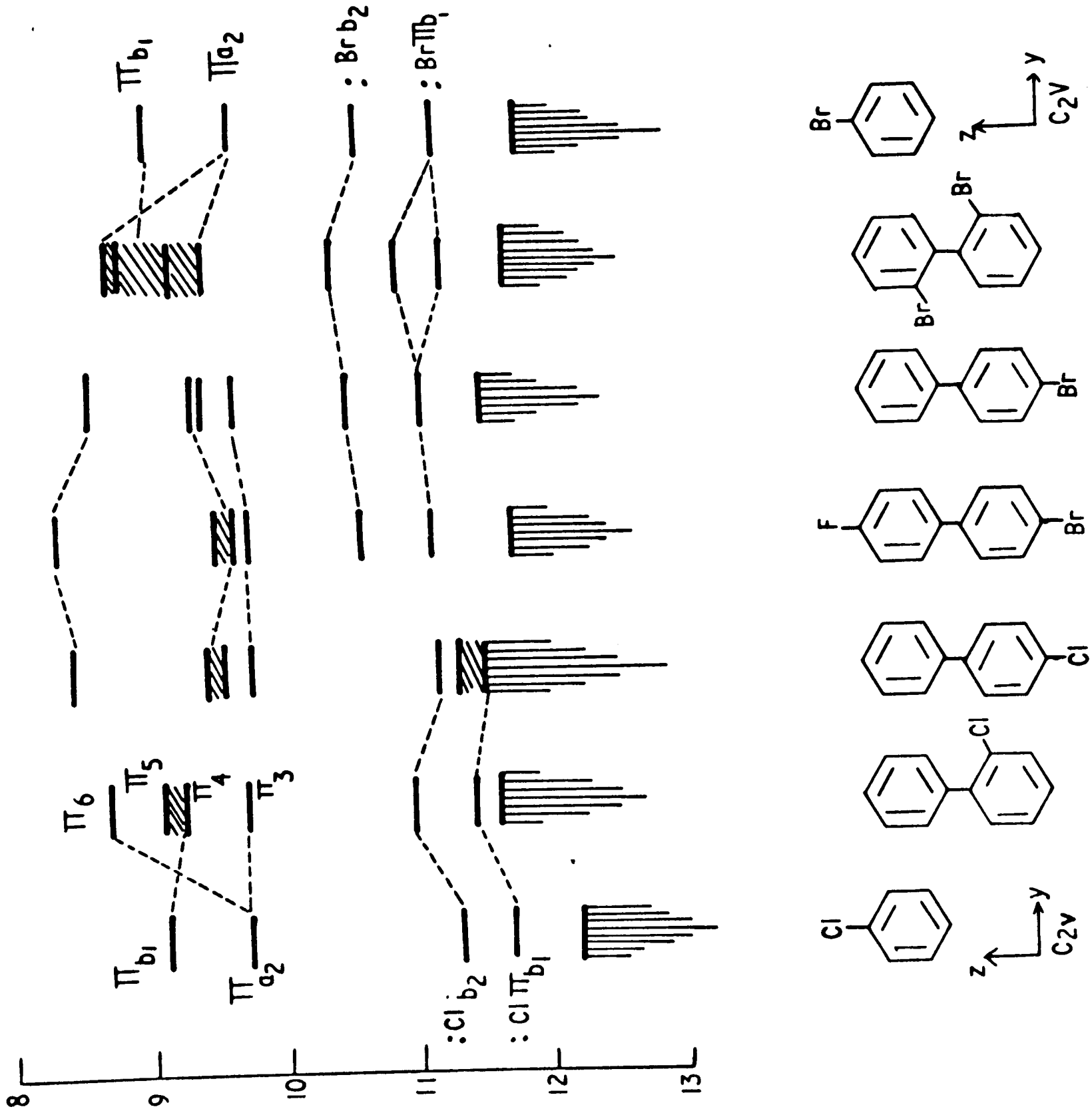


Fig.42 Correlation of ionisation energies

coalescence of two, the new component at (8.12 eV) arising from the anti-symmetric combination of the ethylene pi moiety and π_4 MO. The splitting between first and fourth bands, corresponding to ΔE is 2.0 eV (c.f. fluorene). In contrast the similarity is lost in biphenylene and no such treatment is attempted as strain effects are important.

CHAPTER VI

PHENYL ETHYLENES

6.1 Outline of Related Studies.

Together with biphenyls, stilbenes provide classical examples of steric inhibition of resonance. Through dipole moment studies[150.] and absorption spectroscopy[151.] it was realised qualitatively that in cis-stilbene and 1,1'-diphenylethylene, in contrast to trans-stilbene, the planes of the two benzene rings are rotated from coplanarity with the ethylene carbon atoms to avoid excessive overcrowding of the hydrogen atoms. In styrenes, however, few determinations of the dihedral angle* have been carried out. Specifically, it has been shown that in polymerisation of styrenes[152.] steric considerations are predominant factors. They are also important in the control of reactivity in general and studies of reaction rates[153.] were correlated with the size of the hindering substituents.

Optical activity,[129.] and spectroscopic work in the infra-red[154.] and n.m.r.[155.] fields, have also indicated the importance of steric interference but no precise determinations of dihedral angle were possible.

The only quantitative inference of their dihedral angles have been provided by absorption spectroscopy in the u.v. region[156,157.] and by semi-empirical calculations.[158.] In Table 14 these values are summarised. As pointed out in previous Chapter phase considerations are important when comparing the u.v. results obtained from solution

---

* Footnote: The dihedral angle is the angle defined by the planes of the ethylenic and benzene carbon atoms; zero in the coplanar case.

TABLE 14

Dihedral angles (θ) of substituted phenyl ethylenes

	This work		Other workers	
Phenyl ethylene derivative	(a)	(b)	(c)	(d)
phenyl ethylene	0	0	26	26
trans-β-methyl	0	0	26	26
O-methyl	22	31, 33[e]		
α-methyl	38	33	32	36
O,O'-methyl	55	54,50		
trans-β-phenyl	0	0	17	17
cis-β-phenyl	35	28	43	34
α-phenyl	40	43	33	49
O,O'-dichloro	46			
pentafluoro	28			
n = 2*	0	0		
n = 3	0	0	20[e]	
n = 4	60		40[e]	

(a) See text for estimated uncertainty

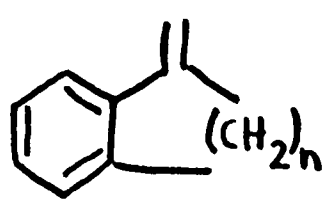
(b) Ref. 157 - Absorption spectroscopy

(c) Ref. 158 - semi-empirical calculation

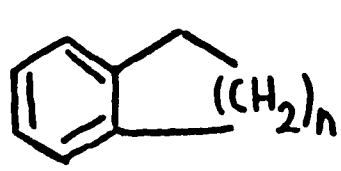
(d) Ref. 158 - Reinterpretation of data Ref. 10

(e) Ref. 156 - Scale models

* In Tables 14, 15, 17 these integer values refer to



and in Table 16 to



studies with calculations, which refer to isolated molecules.

6.2 Results.

The photoelectron spectra of the substituted phenyl ethylenes are shown in Figs. 43-47. The alkyl benzenes spectra required to complete the discussion are collected in Fig. 48. There are points of similarity between all the spectra, and in general they possess certain of the characteristics associated with the P.E. spectrum of benzene[47]. and are conveniently subdivided into corresponding groups of bands as in biphenyls (5.3). The weak band often seen at 16-18 eV is characteristic of the benzene skeleton.

In Tables 15 and 16 the observed I.E. data is collected. The assignment of the P.E. bands are summarised concisely in the correlation diagrams (Figs. 49-52).

Vibrational fine structure

In a number of the spectra, especially for those of planar molecules, certain bands of the first group show evidence of ionic vibrations. This usually takes the form of a short series of up to three quanta, in which case the presumption is that only one mode of vibration is strongly excited. In the absence of a full assignment for the vibrational fundamentals in the parent molecules, assignment is not attempted here though the ΔG interval on the third band is often close enough in magnitude to that expected for a C=C vibration for this assignment to be probable.

The values of $\Delta G\ cm^{-1}$ inferred from the P.E. spectra are listed below. The relevant band (in notation used in discussion) is noted in parentheses. Styrene - 1200 (π_4), 550 (π_3), 1000 (π_2); pentafluorostyrene - 1450 (π_2); 1-methylenebenzocyclopentane - 1400 (π_4), 1000 (π_3), 1400 (π_2); 1-methylenebenzocyclohexane -

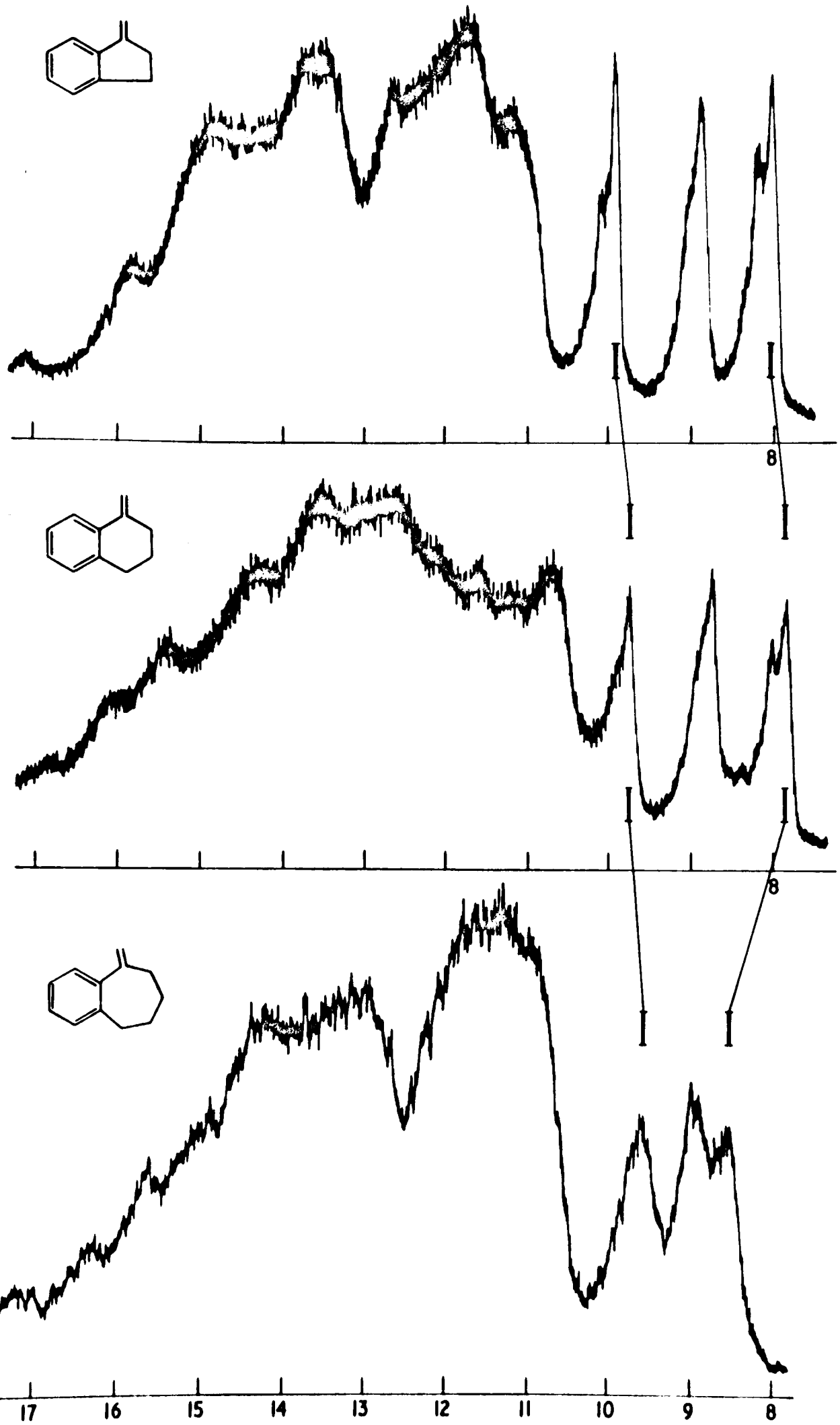


Fig.43 He I (21.22 eV) photoelectron spectra of 1-methylenebenzocycloalkanes

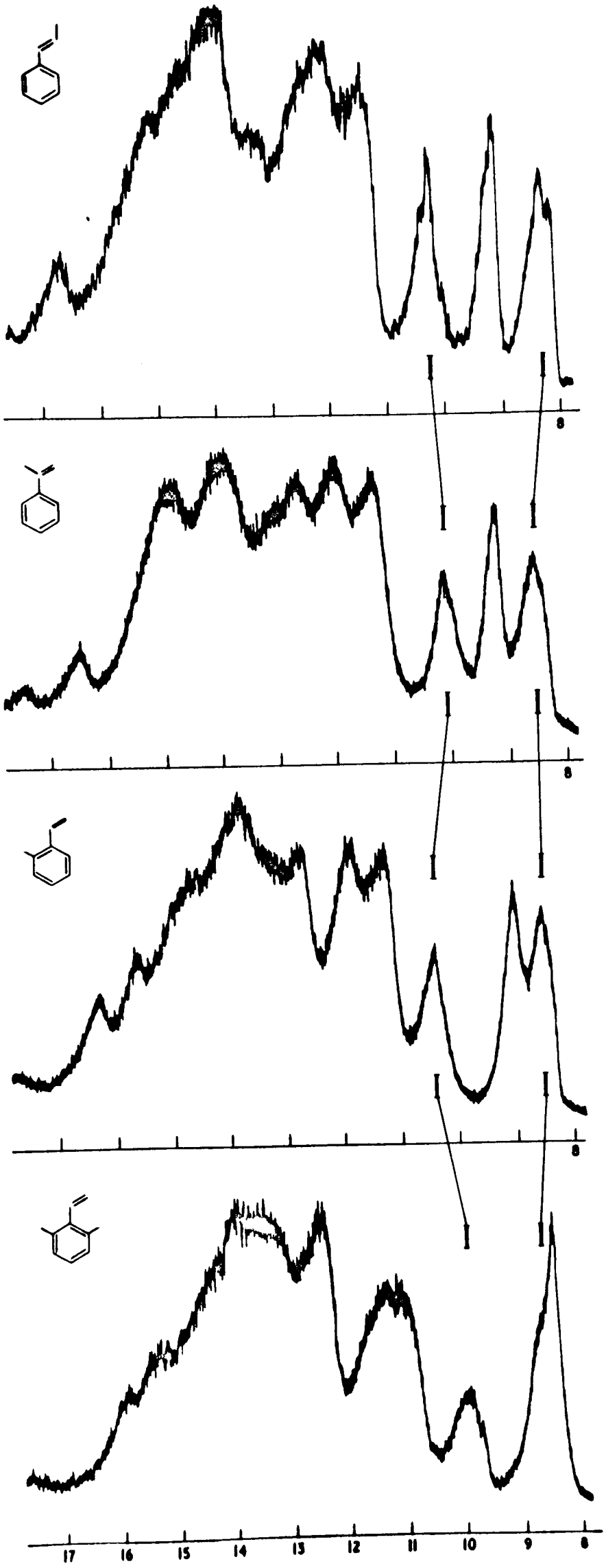


Fig.44 He I (21.22 eV) photoelectron spectra of phenyl ethylenes

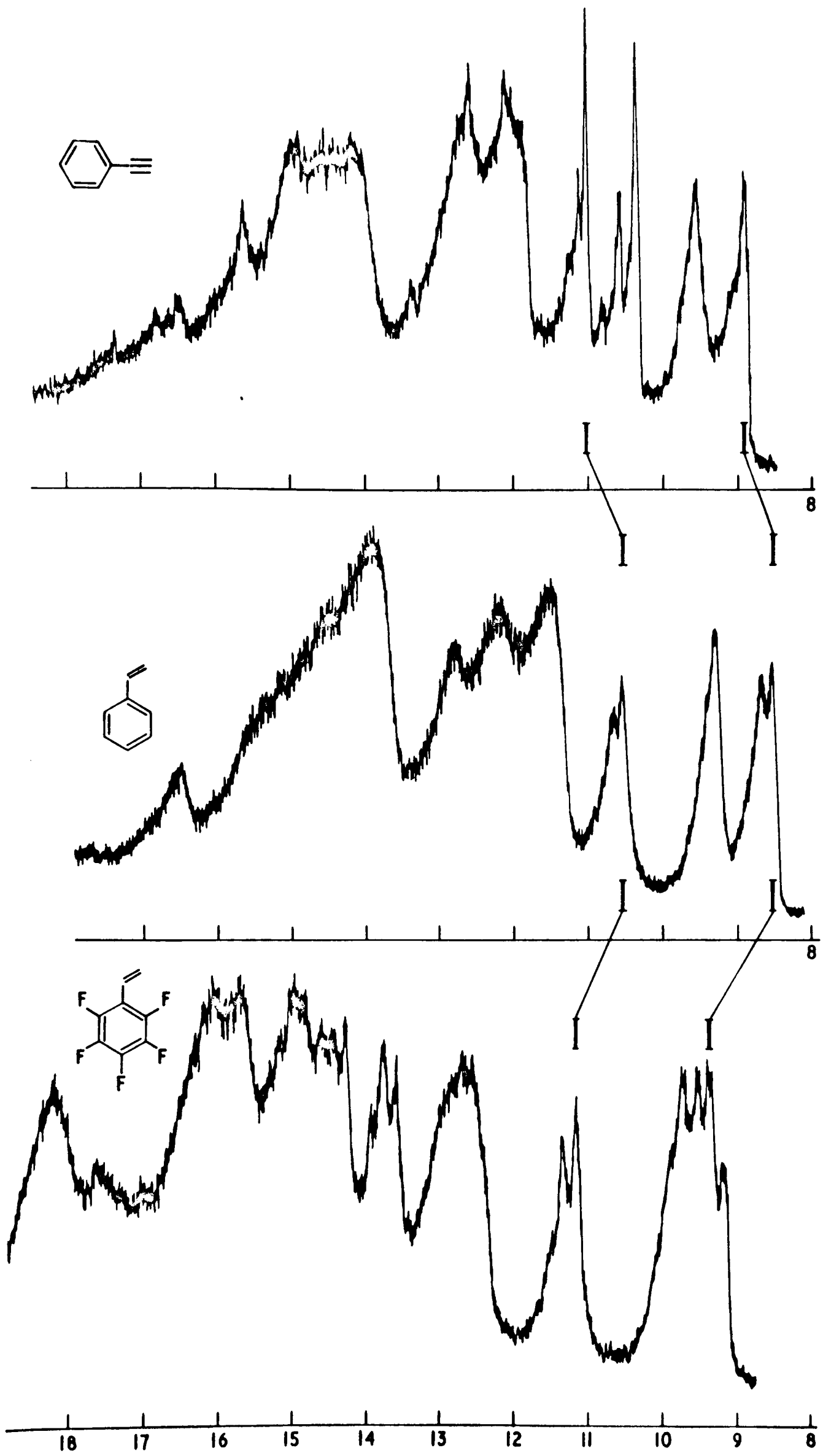


Fig.45 He I (21.22 eV) photoelectron spectra of phenyl ethylene and related molecules

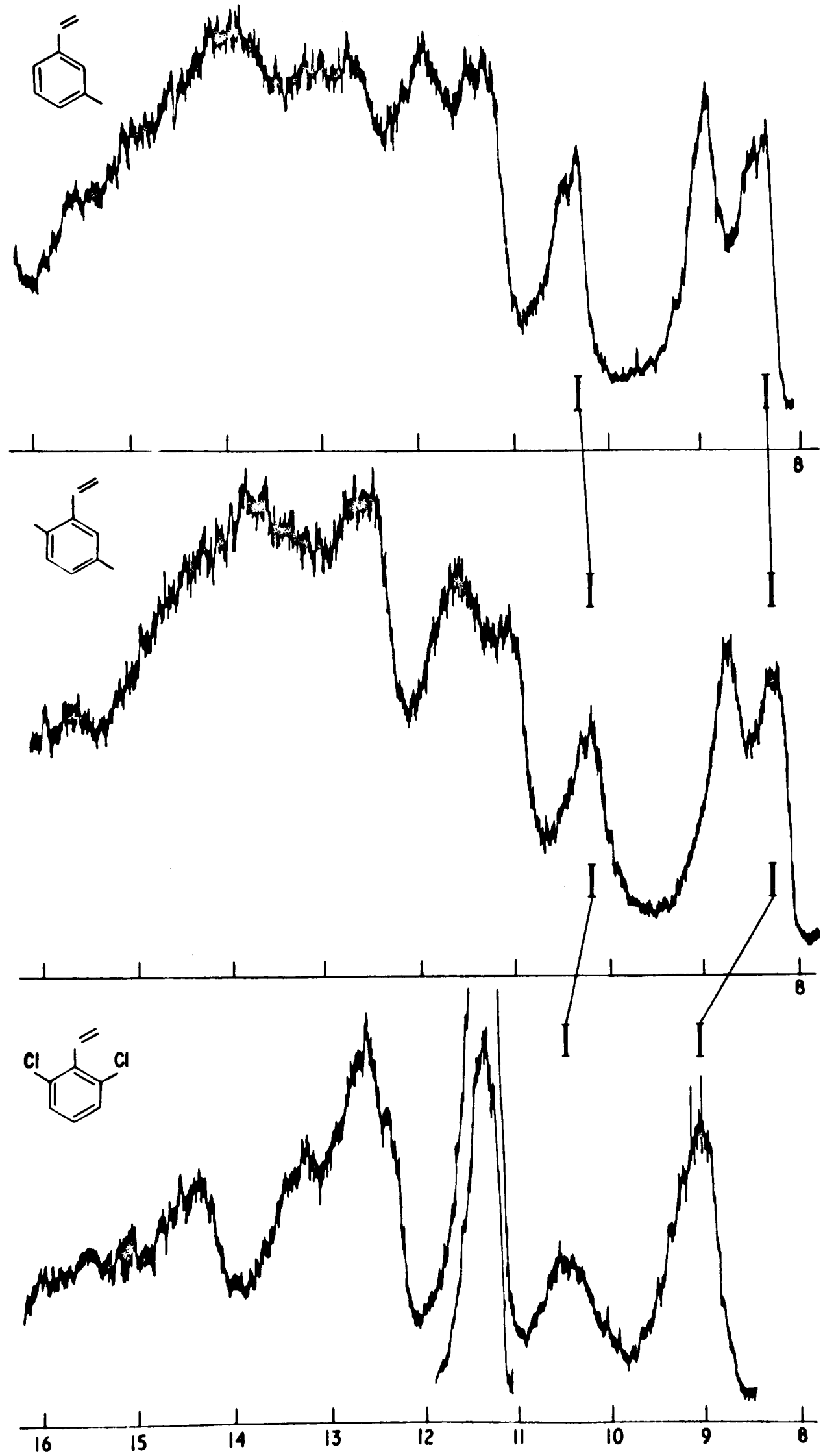


Fig.46 He I (21.22 eV) photoelectron spectra of phenyl ethylenes

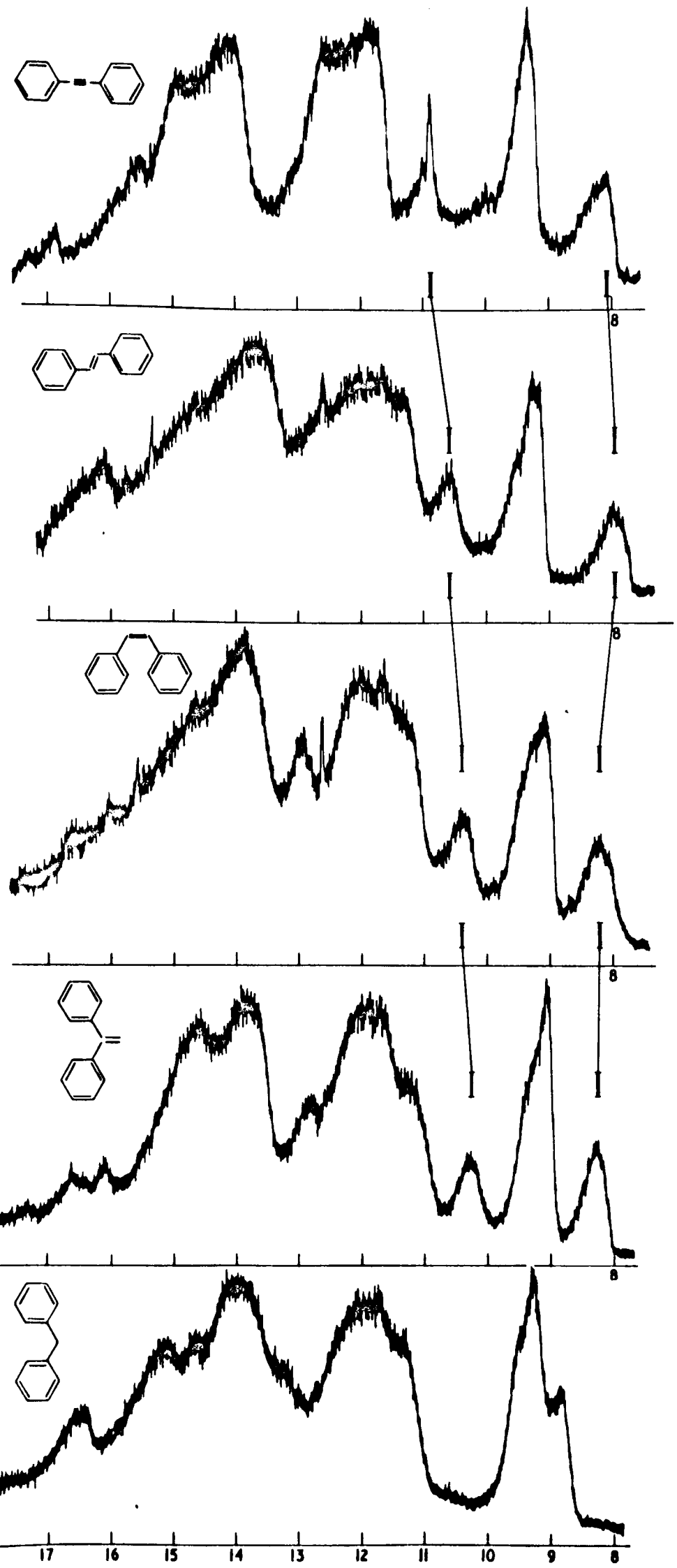


Fig.47 He I (21.22 eV) photoelectron spectra of diphenylethylenes and related molecules

TABLE 15

Observed ionisation energies (eV)

Phenylethylene derivative	$I_1(\Pi_4)$	$I_2(\Pi_3)$	$I_3(\Pi_2)$	I_4
Phenyl ethylene	8.50(8.40)	9.30	10.55(10.30)	11.5(11.2)
o-methyl	8.50(8.20)	9.00	10.40(9.90)	11.3(11.0)
m-methyl	8.36(8.15)	8.97	10.33(10.10)	11.3(11.0)
o,m'-dimethyl	8.30(8.00)	8.76	10.23(9.90)	11.1(10.8)
o,o'-dimethyl	8.45(8.10)(Π_3)	8.65(Π_4)	9.95(9.60)	11.0(10.65)
trans-β-methyl	8.37(8.20)	9.14	10.25(9.95)	11.4(10.9)
α-methyl	8.50(8.20)	9.13(8.90)	10.00(9.70)	11.2(10.8)
n = 2	8.00	8.86	9.91	10.9(10.7)
n = 3	7.90	8.80	9.80	10.7(10.4)
n = 4	8.45	8.90	9.55	10.9(10.4)
o,o'-dichloro	9.05(8.70)	9.30	10.50(10.05)	11.35(11.1) (:Cl)
pentafluoro	9.36(9.18)	9.73	11.15	12.60(12.2)
phenylacetylene	8.88	9.57	10.38($\Pi_{C\equiv c}$)	11.05(Π_2)
trans-β-phenyl	8.00(7.70)(Π_7')	9.25,9.55	10.60(10.30) (Π_3')	11.35(11.0)
cis-β-phenyl	8.20(7.80)(Π_7')	9.08,9.40	10.35(10.10) (Π_3')	11.3(10.9)
α-phenyl	8.25(8.00)(Π_7')	9.05,9.20	10.25(9.95) (Π_3')	11.2(10.8)
tolan	8.06(7.90)(Π_7')	9.30,9.55	10.87(Π_3')	11.7(11.5)

I_1 and I_3 values $\pm$ .02 eV, I_2 and I_4 $\pm$ .05 eV.

a) I_5 12.80, I_6 13.80, I_7 14.30.

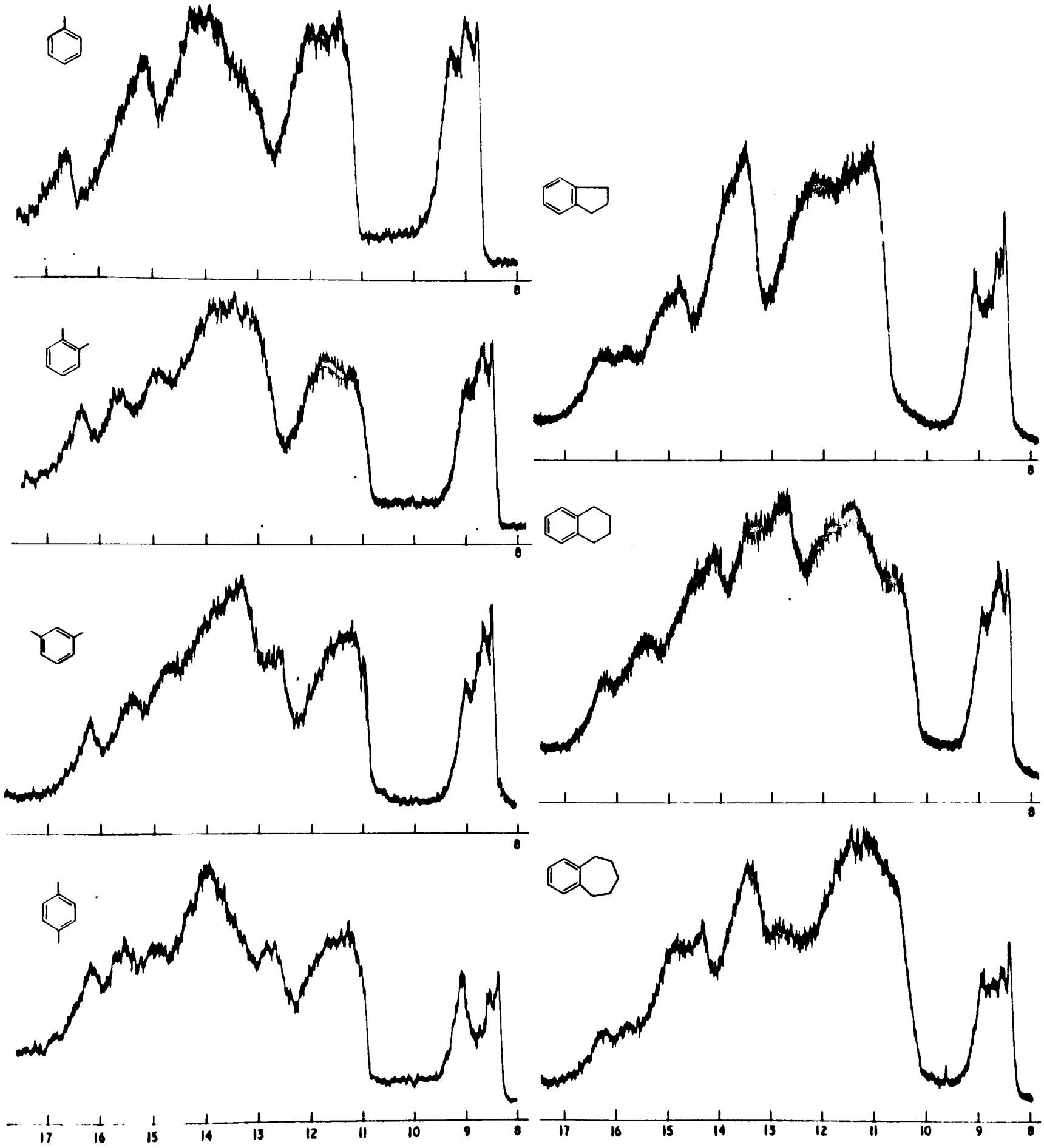


Fig.48 He I (21.22 eV) photoelectron spectra of alkyl substituted benzenes

TABLE 16

Observed ionisation energies (eV)

	I_1	I_2	I_3
Toluene	8.78	9.00	11.3 (11.0)
O-xylene	8.45	8.90	11.0 (10.8)
m-xylene	8.50	9.00	11.0 (10.8)
p-xylene	8.37	9.05	11.1 (10.8)
n = 2	8.45	9.05	11.1 (10.8)
n = 3	8.45	8.95	10.6 (10.1)
n = 4	8.40	8.95	10.5 (10.1)
Diphenylmethane	8.80	9.25	11.3 (10.9)

1300 (π_4), 800 (π_3), 1300 (π_2); values $\pm$ 100 cm^{-1}.

6.3 Discussion.

It was shown in the previous Chapter how in the biphenyls steric hindrance is reflected in the I.E.s of the occupied Π energy levels. Thus by the introduction of substituents in strategic positions, non-bonded interactions between these substituents and adjacent hydrogen atoms, become dominant. In phenyl ethylenes the most efficient means of reducing a similar adverse contribution to the total potential energy is by rotation of the conjugating, ethylene moiety about the linking C-C bond (i.e. 1-α bond).[159] The P.E. spectra of 1-methylenebenzocycloalkanes (Fig. 43) are important in this comparison since the dihedral angle is fixed and the ethylene moiety is then held at a preferred orientation to the benzene ring. This effect depends on the size of the cycloalkane ring.

In the P.E. spectra, the first group of bands (Figs. 43-47) show changes which seem to reflect gross changes in hindrance. As was the case in biphenyls, it is a separation between two levels (here bands 1 and 3) which seems most characteristic. Here as also in the biphenyls, the P.E. spectral pattern seems simpler than the rigorous calculations might suggest. These changes can again be accounted for on a less rigorous basis which is still useful. The fundamental concepts within the framework of a simple semi-empirical approach are as outlined in 5.4.

The interaction pattern of the Π energy levels on rotation of one (styrenes) or two (stilbenes) phenyl groups about the bond linking to the ethylene group is considered. The basis set are the semi-localised orthogonal Π MOs of the phenyl groups; $\Pi_{a_{2u}}$, $\Pi_{e_{1g}}$ (b_1) and $\Pi_{e_{1g}}$ (a_2) labelled Ψ_i i = 1 – 3 respectively and $\Psi_{C=C}$ of the ethylene moiety. Again Ψ_3 is excluded from the interaction scheme from its symmetry. The "experimental" matrix elements A_i and B

$$A_i = \langle \Psi_i | H | \Psi_i \rangle$$

$$B = \langle \psi_i | H | \psi_{C=C} \rangle \quad i = 1,2$$

are so defined. On rotation from coplanarity, it is assumed that the non-zero off-diagonal matrix elements (B_θ) vary as

$$B_\theta = B \cos \theta$$

where B is the standard interaction parameter. There will be some π-σ mixing however, and as for biphenyls this is ignored for the present purpose in dealing with the first group of bands.

The solution of the secular equations leads to the eigenvalues of the MOs which are related via Koopmans' theorem to the experimental I.E.s. The eigenvectors are labelled Π_i i = 1,2,4 for styrenes and Π'_i = 1,2,3,6,7 for stilbenes, in order of increasing orbital energy. In the former the basis MO Ψ_3 becomes Π_3 and in the latter Π'_4, Π'_5.

In styrenes, the direct through space overlap, predominantly between Ψ_2 and $\Psi_{C=C}$, gives rise to the splitting (ΔE) between the MOs Π_2 and Π_4. In diphenyl ethylenes this interaction between two Ψ_3 and the $\Psi_{C=C}$ moieties gives rise to the MOs Π'_3, Π'_6, Π'_7; the corresponding splitting between Π'_3 and Π'_7 is $\Delta E'$.

In the P.E. spectra of styrenes (Figs. 43-46) the first three bands (in increasing I.E.) are then associated with the ejection of electrons from the MOs Π_4, Π_3, Π_2 respectively. The second band seems not to vary upon rotation of the ethylenic moiety, (Figs. 43,44), as expected for the Π_3 MO. In the P.E. spectra of diphenyl ethylenes (Fig. 47), Π'_7 and Π'_3 are associated with first and third photoelectron bands while the second band comprises photoelectrons ionised from the Π'_4, Π'_5 and Π'_6 MOs.

Computations to evaluate the splittings ΔE and $\Delta E'$ as a function of dihedral angle (θ) indicate that the second order perturbation of the basis function Ψ_1 on the splittings (ΔE and $\Delta E'$) is small, and the latter are omitted from the basis set. Thus the secular equations are simplified and the solution leads to the expressions

$$\Delta E = \varepsilon(\Pi_4 - \Pi_2) = \left[(A_{C=C} - A_2)^2 + 4B_\theta^2\right]^{\frac{1}{2}}$$

and

$$\Delta E' = \varepsilon(\Pi'_7 - \Pi'_3) = \left[(A_{C=C} - A_2)^2 + 8B_\theta^2\right]^{\frac{1}{2}}$$

The neglect of all non-nearest neighbour interactions means that the effective symmetry is C_{2v} and D_{2h} for styrene and stilbene respectively. Thus the P.E. spectra of phenylacetylene and tolan provide a useful comparison; almost analogous to a superposition of planar and orthogonal styrene, and stilbene, respectively. The P.E. of phenylacetylene has been discussed previously[160]. and the appreciation of the fine structure on the third and fourth bands (Fig. 45) confirms the assignment (Fig. 49). The splitting between the first and fourth bands ($\equiv \Delta E$) is as would be predicted from the expression given, including B variation with the bond length (see 5.4). In tolan, the splitting between the first and third band ($\Delta E'$) is accounted for in the same way. Similarly, the variation of the splitting ΔE in styrene, trans-β-methyl styrene, 1-methylene-indane can be accounted for solely by bond length and basis set changes.

This formalism can be used to determine the dihedral angles by the manipulation of the equations for ΔE and $\Delta E'$. For the biphenyls, electron diffraction data was available to define the relationship between ΔE and cos θ. Here, however, such reference data is lacking. Therefore a regression is defined, which is assumed to be linear, with two sets of coordinates, at $\theta = 0^\circ$ and $\theta = 90^\circ$. At $\theta = 0^\circ$, the experimental ΔE (or $\Delta E'$) of a coplanar system is used and for $\theta = 90^\circ$, the $A_{C=C} - A_2$ value determined from the basis set of the reference molecules (Table 17).

Formally analogous systems are grouped together, differing only in the B_θ parameter as a result of deviations from coplanarity; e.g. trans, cis-stilbene and 1,1'-diphenyl ethylene. From the experimental splitting, ΔE or $(\Delta E')^*$, in the sterically hindered molecules the dihedral angle is inferred from the regression. These values are listed in Table 14.

In the biphenyls, the purely empirical regression did not pass through the origin as the simple theory predicts. Accordingly, the dihedral angles inferred from the deduced expression (lacking the electron diffraction data), would have been $\sim 4 - 6^\circ$ too low over the range $0\text{-}70^\circ$. Consequently, the values of the dihedral angles obtained here are probably the lower limit of an estimated error of $\sim 5^{\circ **}$, comparable to the uncertainty in the Franck-Condon envelopes.

The choice of A_2 values is appreciated from consideration of the symmetry of the Π MOs of the substituted benzene basis moiety; seen on examination of the correlation diagrams (Figs. 49-52). The $A_{C=C}$ value of the ethylene moiety is obtained from the I.E. of methyl substituted ethylenes. The replacement of hydrogen by a phenyl carbon atom produces the same shift of I.E. of the $\Psi_{C=C}$ MO as does a methyl carbon atom.*** Thus, the electronic perturbation of the substituents is separated from the steric effect by incorporation of the former in the basis parameters. The estimated dihedral angles define the off-diagonal elements B_θ. In Table 17 the calculated eigenvalues are compared to the observed I.E.s. The agreement is fair.

---

* Footnotes: Experimentally ΔE and $\Delta E'$ are defined as $I_3 - I_1$ (eV).

** The error in the choice of the coordinates defining the regression is less.

*** c.f. I.E. of the "in-plane" Π MO ($\Pi_{C=C}$ in Figs. 49,52) of phenyl acetylene and tolan, with the methyl analogues.

TABLE 17. Comparison of calculated and experimental ionisation energies (eV)

Phenyl ethylene derivative	$A_{C=C}$	Calculated A_2	Calculated Π_4	Calculated Π_2	Experimental $\frac{1}{2}(I_1 + I_3)$
phenyl ethylene	9.7	9.3	8.45 (8.50)	10.45 (10.55)	9.53
O-methyl	9.7	9.1	8.5 (8.20)	10.3 (10.40)	9.45
m-methyl	9.7	9.1	8.4 (8.36)	10.4 (10.33)	9.35
O,m'-dimethyl	9.7	9.0	8.4 (8.30)	10.2 (10.23)	9.27
O,O'-dimethyl	9.7	9.0	8.7 (8.65)	9.9 (9.95)	9.30
trans-β-methyl	9.2	9.1	8.2 (8.37)	10.1 (10.25)	9.31
α-methyl	9.2	9.1	8.4 (8.50)	9.9 (10.00)	9.25
n = 2	9.2	8.5	7.9 (8.00)	9.8 (9.91)	8.96
n = 3	9.2	8.5	7.9 (7.90)	9.8 (9.80)	8.85
n = 4	9.2	8.5	8.35 (8.45)	9.35 (9.55)	9.00
O,O'-dichloro	9.7	9.7	9.0 (9.05)	10.4 (10.50)	9.78
phenyl acetylene	10.4	9.6	8.9 (8.88) Π_7' *	11.1 (11.05) Π_3'	9.97 $\frac{1}{2}(I_1 + I_3)$
trans-β-phenyl	9.2	9.3	8.0 (8.00)	10.6 (10.60)	9.30
cis-β-phenyl	9.2	9.3	8.2 (8.20)	10.4 (10.35)	9.28
α-phenyl	9.2	9.3	8.3 (8.25)	10.3 (10.25)	9.25
tolan	9.4	9.6	8.1 (8.06)	10.9 (10.87)	9.47

Values in parentheses are the corresponding experimental I.E.s. * Π_6' will, of course, be $\equiv A_2$

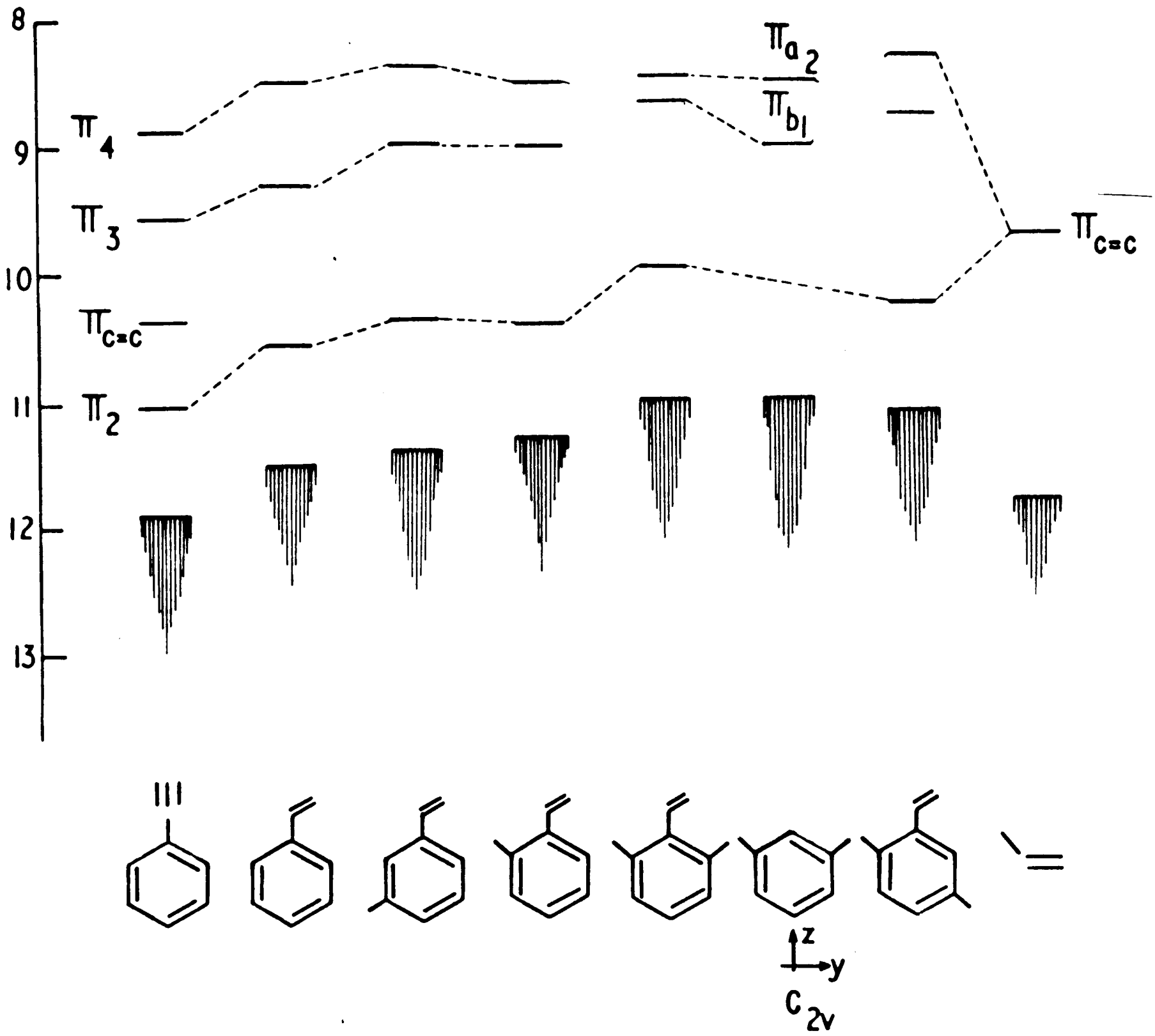


Fig.49 Correlation of ionisation energies

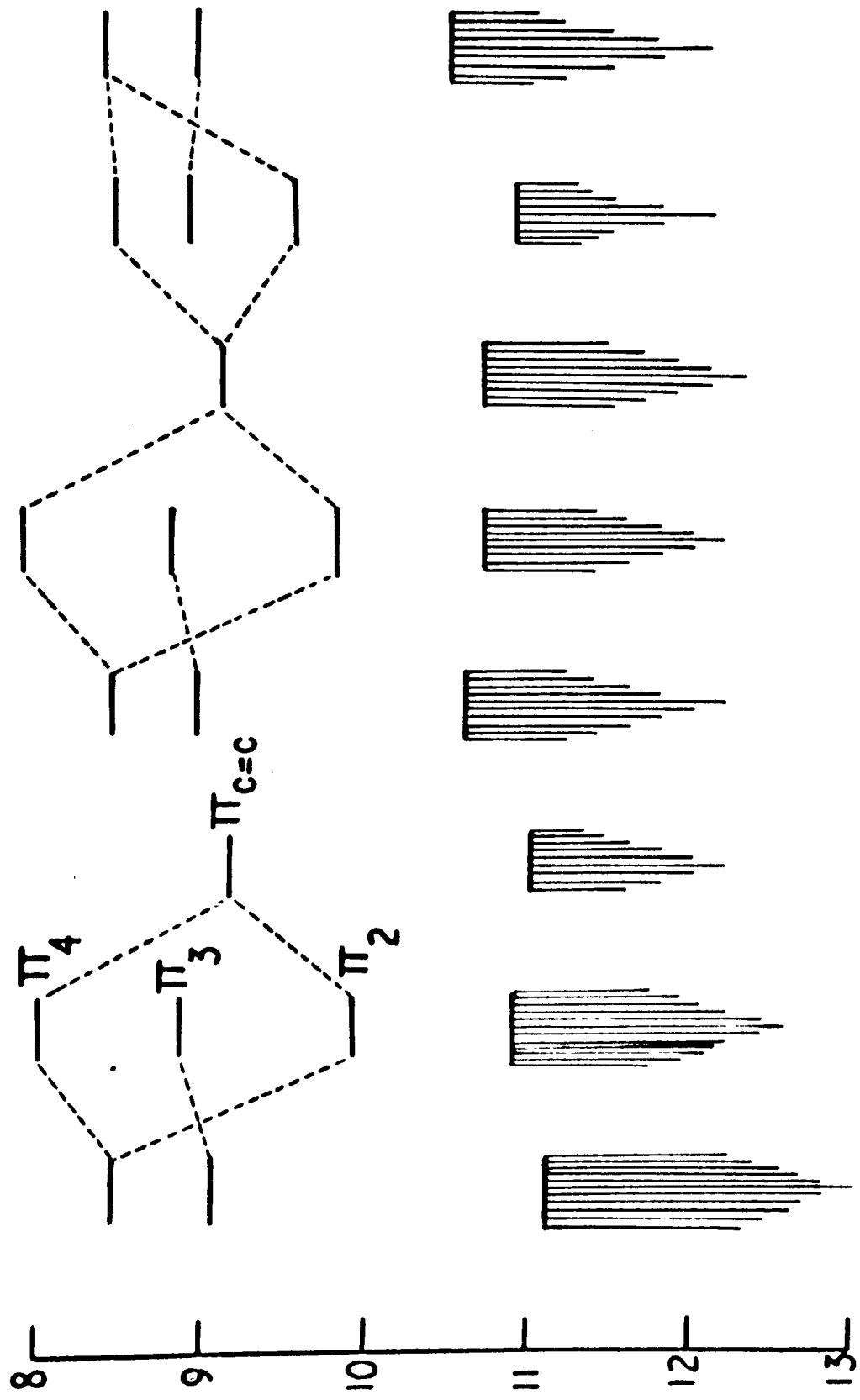
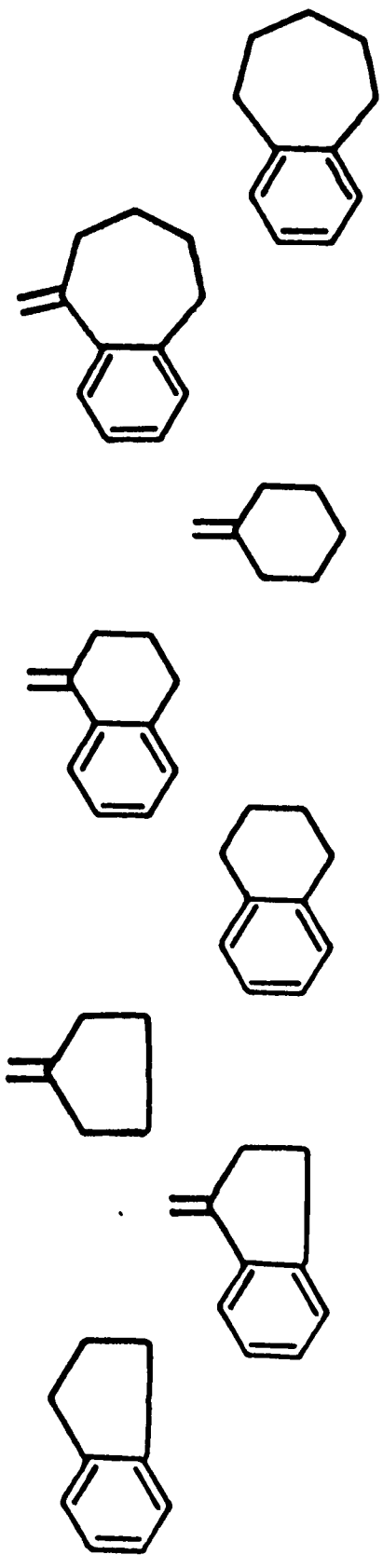


Fig.50 Correlation of ionisation energies



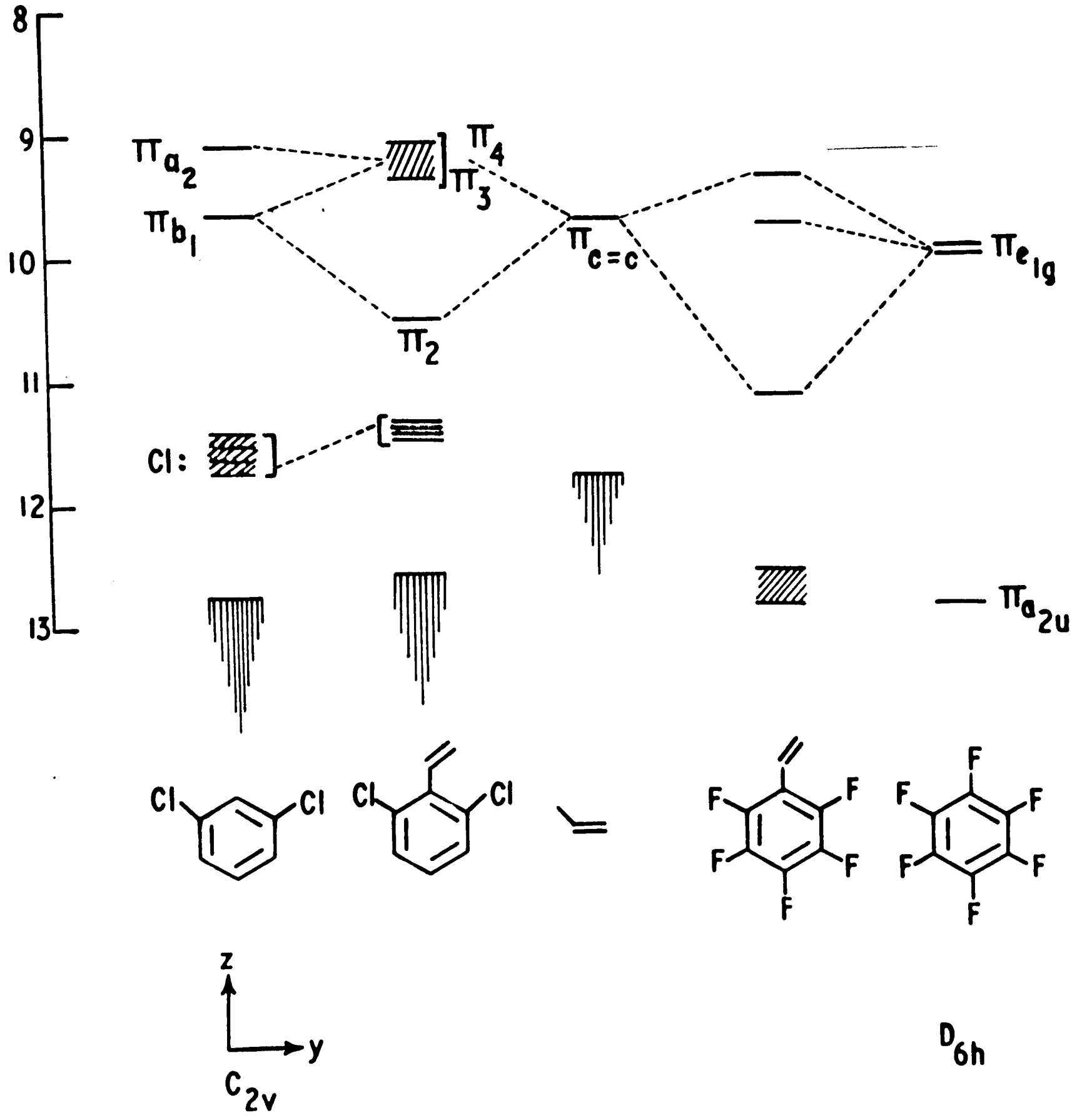


Fig.51 Correlation of ionisation energies

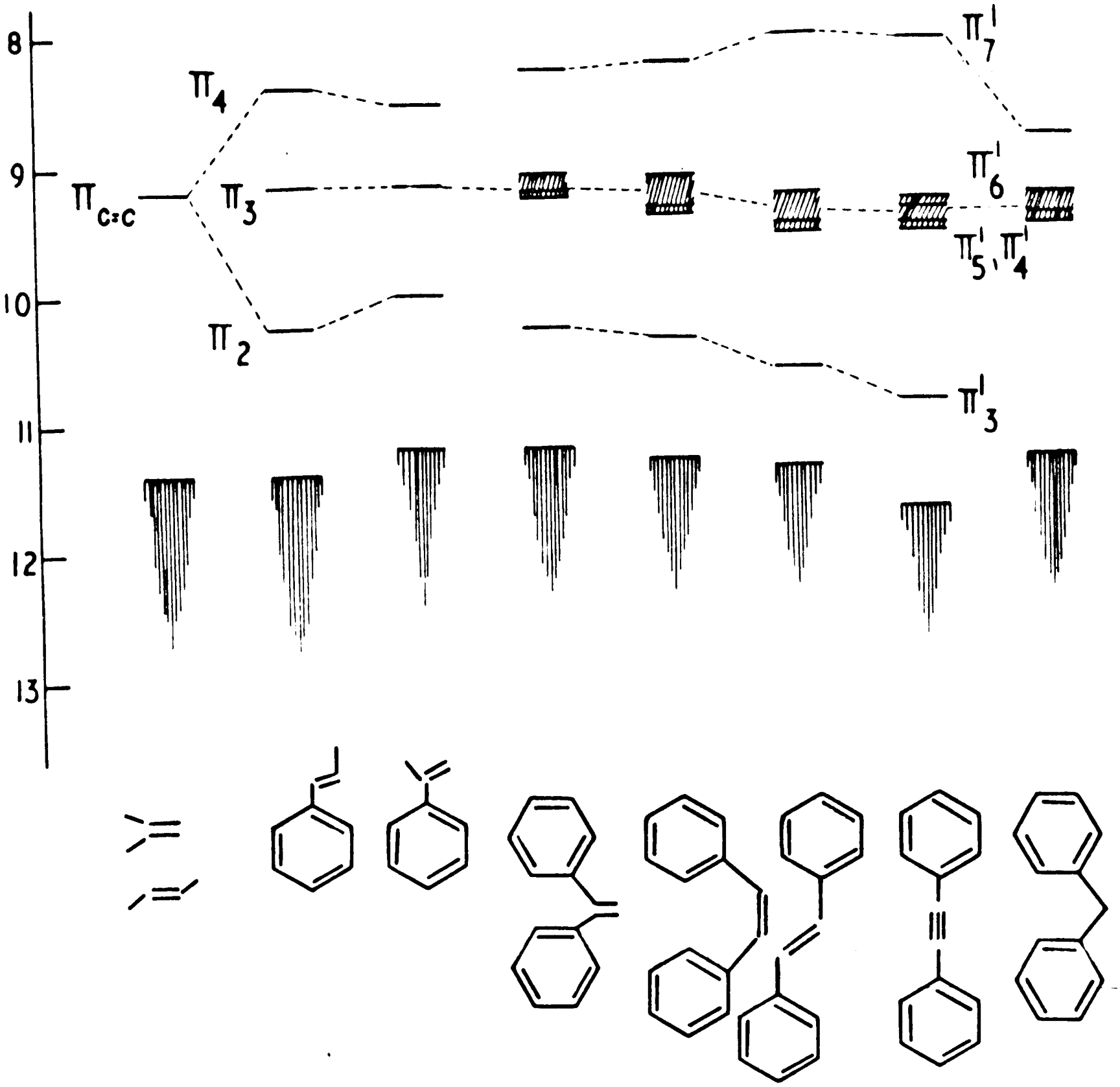


Fig.52 Correlation of ionisation energies

Main features of the P.E. spectra

The P.E. band profile reflects the range of Franck-Condon factors associated with the potential surface of the radical cations. Here, as in biphenyls (5.5) the Franck-Condon envelopes of the first group of bands of the planar molecules display the characteristic prominent O-O transition. In contrast, in the sterically hindered molecules the profiles suggest a change of dihedral angle; nearer to coplanarity on ionisation. This is apparent in the P.E. spectra of 1-methylene benzocycloalkanes for example (Fig. 43). When the methylene group is held coplanar as in a five and six membered cycloalkane ring, as revealed by the splitting ΔE, the first group of bands have Franck-Condon envelopes associated with little, if any, geometrical change on ionization. In the seven membered ring, however, the splitting indicates non-coplanarity and one infers a dihedral angle of $\sim 60^{\circ}$. On ionization it appears that a change of dihedral angle takes place, suggesting that a certain amount of flexibility is possible in a ring of this size.

In the P.E. spectra (Figs. 43-47) the Π_2, Π_4 and Π'_3, Π'_7 bands are correlated and the "size" effect of substituents clearly evident. The presence of one substituent in the ortho position is not sufficient to cause a large deviation from coplanarity; the ethylenic group adopts a favourable conformation with the α-hydrogen on the same side as the ortho substituent. In contrast, an α-substituent causes an appreciable change. This is in agreement with deductions from reaction rates.

It is interesting to note that from these results an approximately linear correlation exists between the dihedral angle and the "size" of hindering substituents, as represented by van der Waals' radius for example, and includes the biphenyls as well as the present molecules. It thus appears justifiable, at least to a first approximation, to ignore other modes of relief of steric strain in balancing conjugation energy changes.

CHAPTER VII

ANILINES , PHENOLS, AND RELATED COMPOUNDS

7.1 Outline of Related Studies.

Amino and oxyaromatic molecules have been prototypes in the reflection of changes of Π-stabilisation energies as consequence of steric hindrance, and in the resulting physicochemical properties.

Dipole moment measurements[161.] gave first indication that non-bonded interactions influence conformations in this series and the effect of the size of ortho substituents was appreciated. Absorption studies also have been important in the development of these concepts.[162,163.] Quantitative analysis of the u.v. bands enabled the estimation of dihedral angles in hindered anilines from band intensities.[164.] Phosphorescence and intramolecular charge transfer studies of the latter have been correlated to the dihedral angles.[165.]

Mass spectral studies[166.] show anomolous results in sterically hindered amino and oxybenzenes, as also do ^{13}C and ^{1}H n.m.r. shifts,[167.] though only qualitative discussion is feasible. The n.m.r.[168.] and microwave[169.] studies have been primarily concerned with the determination of barriers to intramolecular rotation about the hetero-phenyl carbon atoms bond. These barriers show a dependence on the size of ortho substituents.

Quantitative measure of intramolecular interactions can be obtained from i.r. intensities,[170.] and dihedral angles have been inferred in amino and oxybenzenes. Examples of steric effects on chemical equilibria, reaction rates and other physical properties are numerous and

have been amply reviewed.[164.]

As in phenyl ethylenes, absolute structure determinations are scarce. Electron diffraction data is available only for N,N'-dimethyl-aniline,[171.] where the angle at the nitrogen is 116°. Vibrational u.v. spectroscopic study[172.] and microwave analysis of aniline,[173.] indicate the angle at nitrogen of similar magnitude.

7.2 Results.

The P.E. spectra are shown in Figs. 53-60. As in phenyl ethylenes (6.2) the P.E. spectra are conveniently subdivided into four groups of bands. The first group, I.E. ~ 7-11 eV is distinctive as was the case in biphenyls and phenyl ethylenes. In the amino and oxybenzenes this group generally comprises of three and two bands respectively. These are the Π-photoelectrons and as previously, are important in the discussion.

In Tables 18 and 19, the I.E.s obtained from the P.E. spectra are collected. The correlation diagrams (Figs. 61-63) summarise the assignments of the P.E. bands using the nomenclature used in the discussion.

Vibrational fine structure

In a number of cases, vibrational fine structure is often evident in the first group of bands. In the aminobenzenes the structure is complex and analysis is not attempted. In the phenols, the inferred intervals (ΔG cm^{-1}) on the first band are 600 and 1100 cm^{-1}, on the second band 1100 cm^{-1}. In the anisoles, the intervals are 600 and 900 cm^{-1} on the first, 1100 cm^{-1} on the second and 900 cm^{-1} on the third.* Complete analysis of the ground state of the molecules is necessary for assignments and is lacking in most cases.

---

*Footnote: ΔG values $\pm$ 80 cm^{-1}.

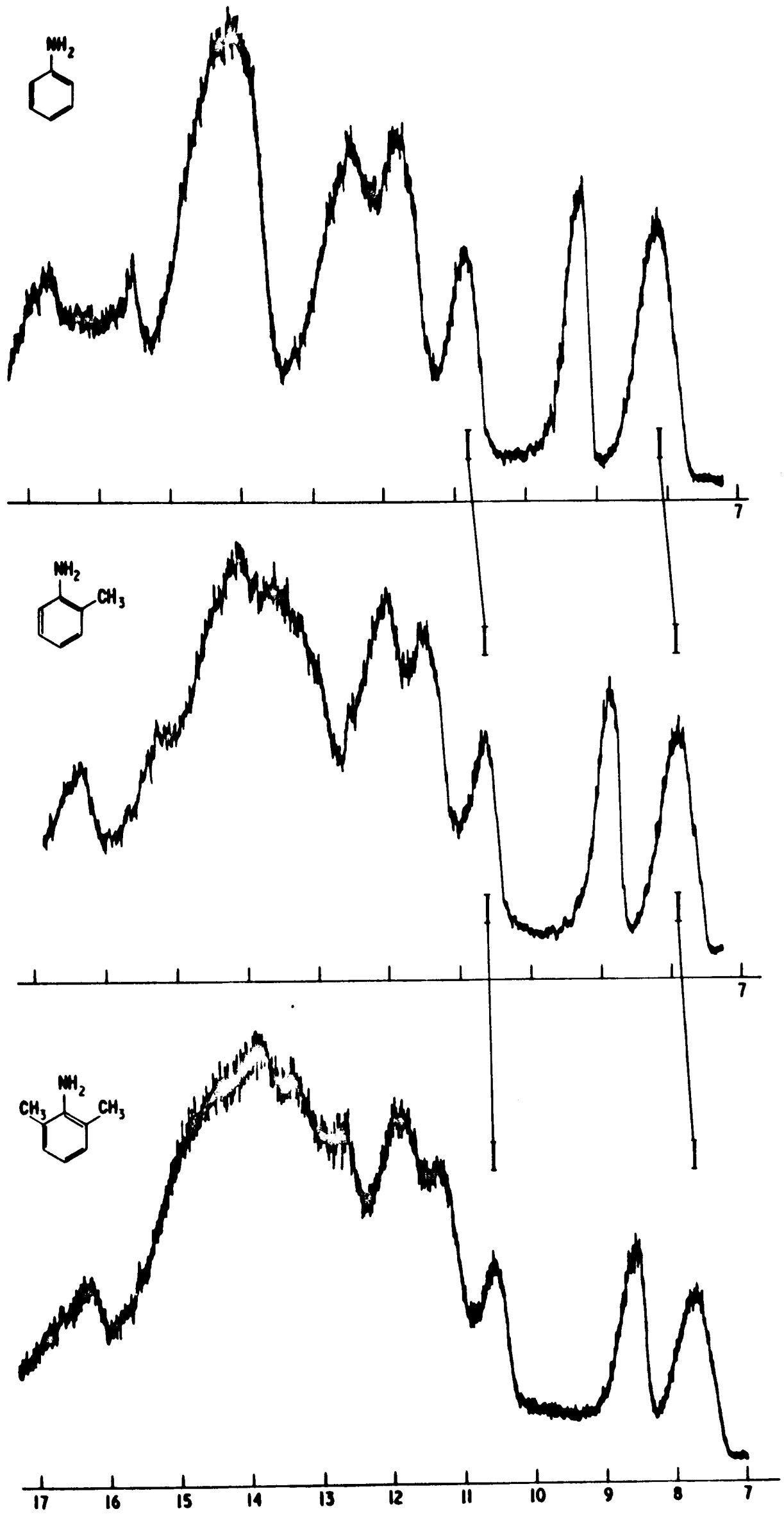


Fig.53 He I (21.22 eV) photoelectron spectra of anilines

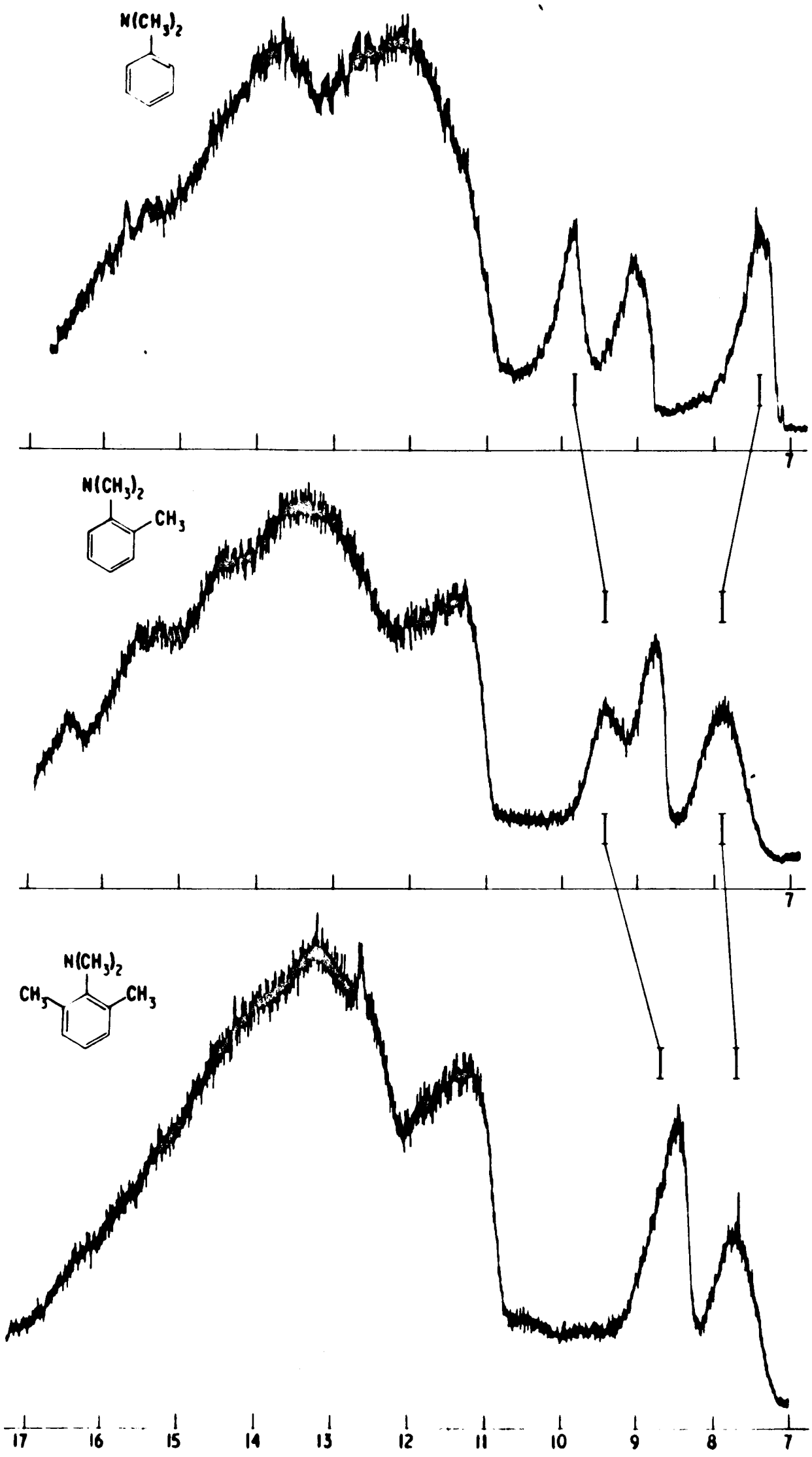


Fig.54 He I (21.22 eV) photoelectron spectra of N,N'-dimethylanilines

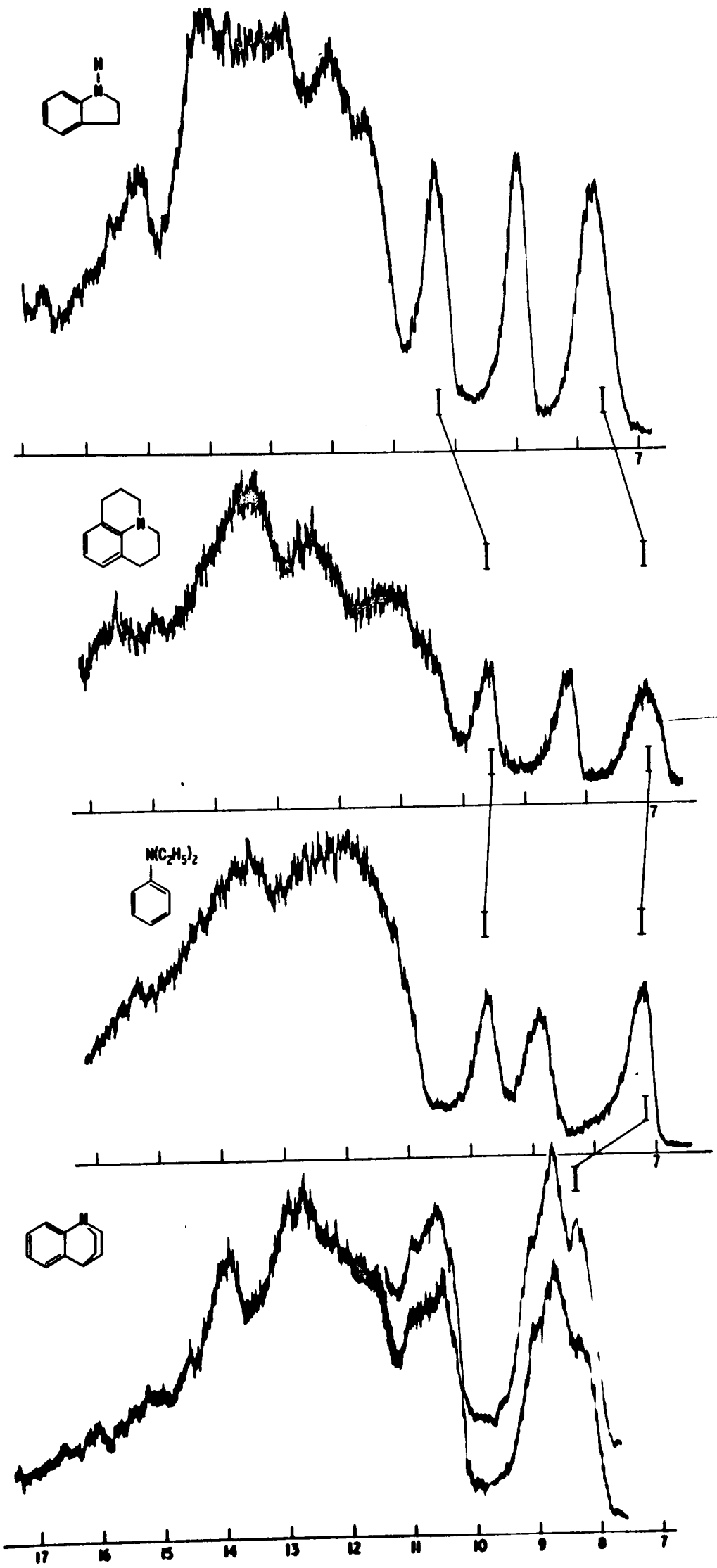


Fig.55 He I (21.22 eV) photoelectron spectra of aminobenzenes and related molecules

TABLE 18 Observed ionisation energies (eV)

Aniline derivative	$I_1(\Pi_4)$	$I_2(\Pi_3)$	$I_3(\Pi_2)$	I_4	I_5
aniline	8.10(7.65)	9.18(8.90)	10.80(10.45)	11.70	12.40
2-methyl	7.90(7.45)	8.85(8.60)	10.63(10.35)	11.45(11.10)	12.1
2,6-dimethyl	7.75(7.30)	8.50(8.35)	10.55(10.20)	11.30	11.7
2,6-dichloro	8.20(7.60)	9.10(8.85)	11.10(10.50)	11.47(Cl:)	12.5
pentafluoro	8.95(8.40)	9.75	11.50(11.20)	13.1	13.65
N-methyl	7.65(7.35)	9.05(8.80)	10.20(10.00)	11.5(11.0)	12.0
N,N'-diethyl	7.20(6.95)	8.90(8.60)	9.70(9.45)	11.2(10.7)	
N,N'-dimethyl	7.45(7.10)	9.00(8.70)	9.85(9.65)	11.4(10.8)	12.1
" " 2-methyl	7.90(7.40)	8.78(8.55)	9.40	11.3(10.9)	
" " 2,6-dimethyl	7.85(7.30)	8.60	8.85	11.2(10.75)	
indoline	7.67(7.15)	8.90(8.60)	10.25(9.95)	11.3(10.9)	11.9
1,2,3,4-tetrahydroquinoline	7.50(7.00)	8.75(8.45)	10.10(9.85)	11.0(10.6)	11.5
julolidine	7.05(6.65)	8.30(8.05)	9.60(9.30)	10.5(10.1)	11.0
benzoquinuclidine	8.35(7.85)	8.70	9.05	10.55(10.10)	11.00

I_{1-3} values $\pm$ .02eV I_4 values $\pm$ .05eV CH_3NH_2 - I_1 9.45(8.80), I_2 12.2(11.45), I_3 12.9

$(CH_3)_2NH$-I_1 8.93(8.25), I_2 12.5(11.85), I_3 13.2 $(CH_3)_3N$-I_1 8.54(7.83), I_2 12.4(11.5) I_3 12.9

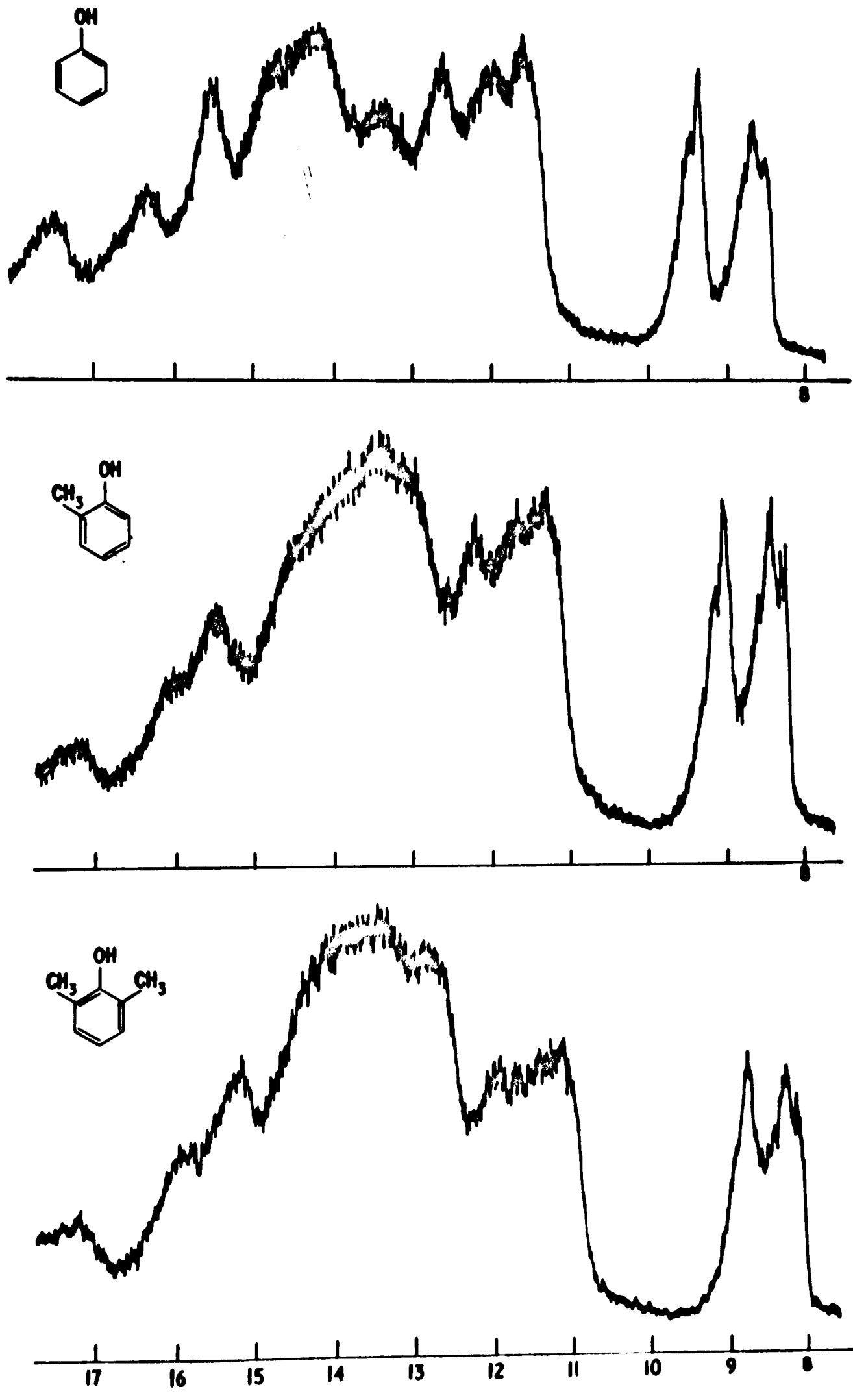


Fig.56 He I (21.22 eV) photoelectron spectra of phenols

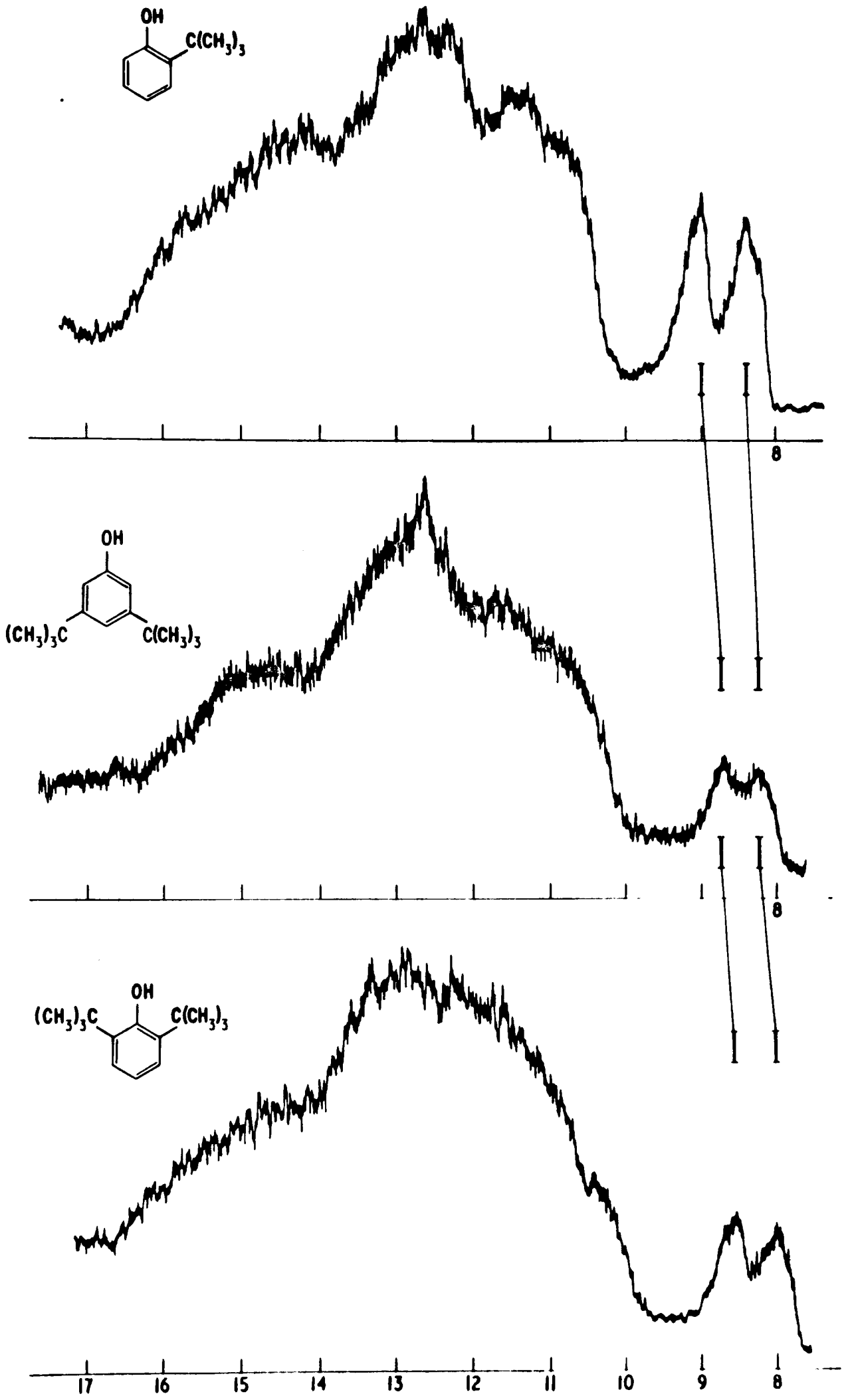


Fig.57 He I (21.22 eV) photoelectron spectra of phenols

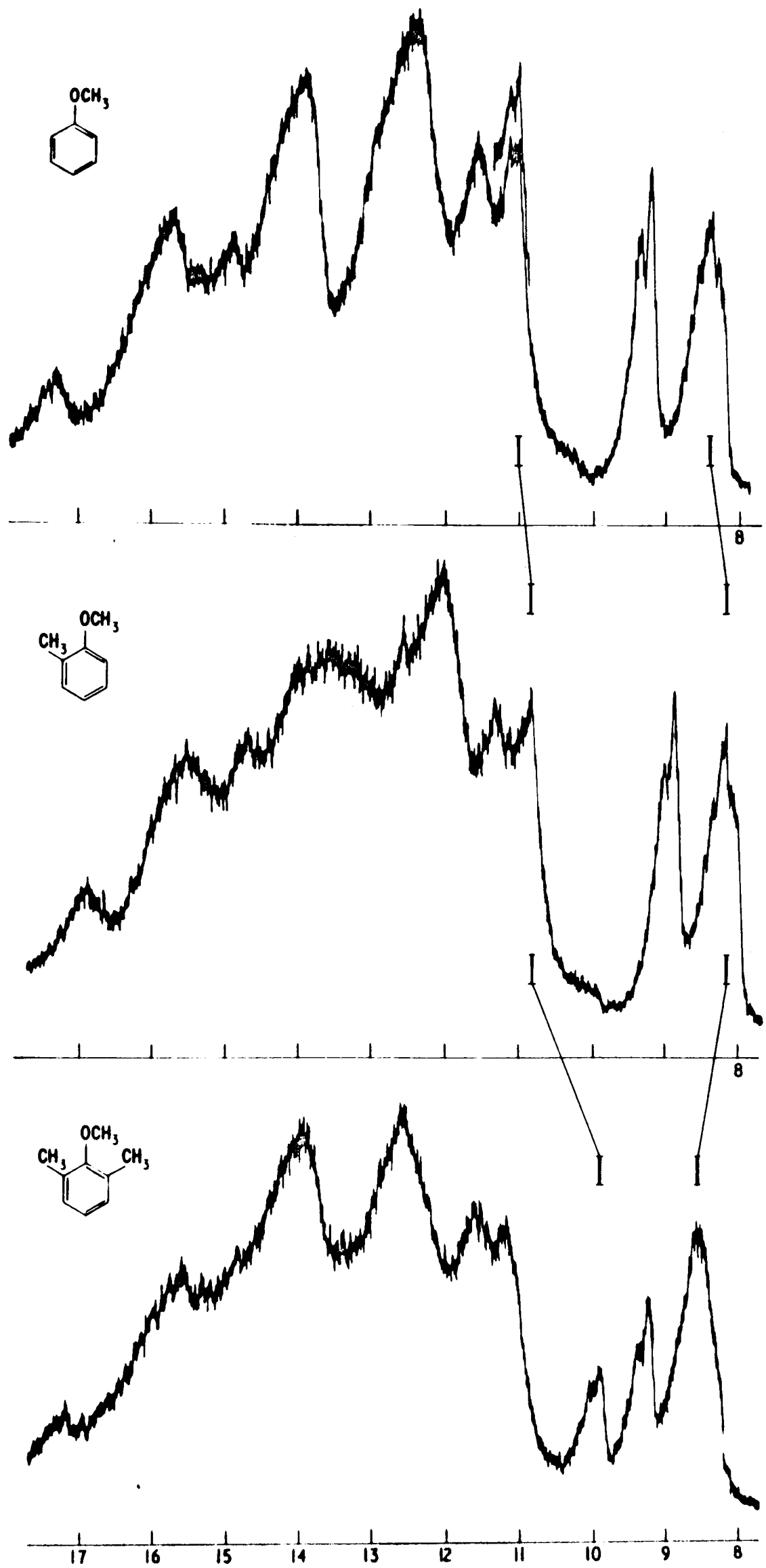


Fig.58 He I (21.22 eV) photoelectron spectra of anisoles

TABLE 19. Observed ionisation energies (eV)

Phenol derivative	$I_1(\pi_4)$	$I_2(\pi_3)$	$I_3(\pi_2)$	I_4	I_5	I_6
phenol	8.67(8.47)	9.36	11.50(11.20)	12.0	12.6	13.3
2-methyl	8.43(8.24)	9.05	11.30(11.00)	11.7	12.2	13.0
2,6-dimethyl	8.23(8.05)	8.73	11.10(10.80)	11.4	12.0	12.7
2,-t-butyl	8.40(8.10)	9.00	10.60(10.10)			
2,6-di-t-butyl	8.05(7.70)	8.60	10.35(9.85)			
3,5-di-t-butyl	8.25(7.90)	8.70	10.5(10.0)			
2,6-dichloro	8.93(8.65)	9.33	11.38(Cl:)	11.95(π_2)	12.50	13.0
pentafluoro	9.73(9.20)	9.90	12.23(12.05)	13.80(13.20)	14.2	14.6
Anisole derivative						
anisole	8.42(8.20)	9.21	11.02(10.60)	11.60	12.4	
2-methyl	8.20(8.03)	8.90	10.90(10.50)	11.35	12.0	
2,6-dimethyl	8.50(8.10)(π_3)	9.20(π_4)	9.85(π_2)	11.15	11.5	12.3
pentafluoro	9.80(9.10)		11.35(10.95)	12.35(12.05)	13.20	13.8

I_{1-3} values $\pm$ .02 eV; I_{4-6} values $\pm$ .05 eV

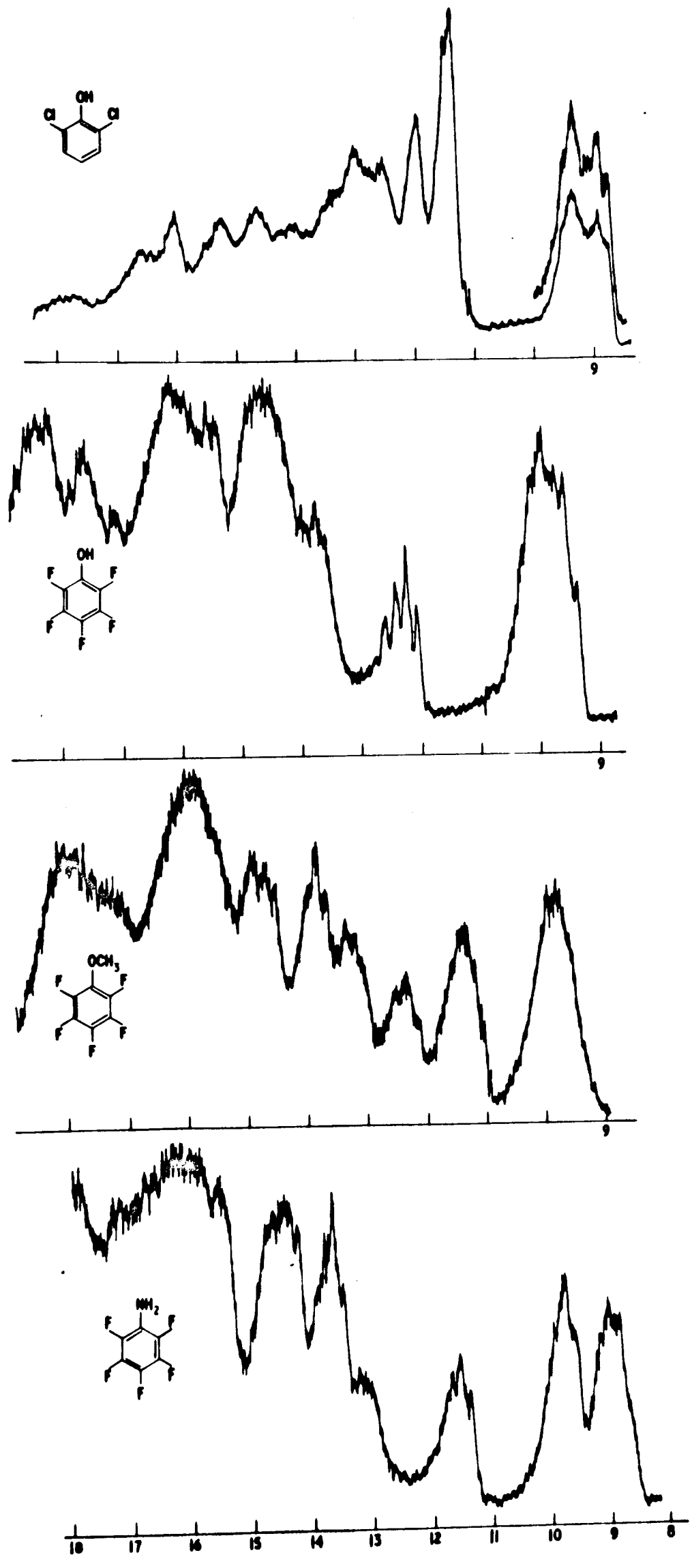


Fig.59 He I (21.22 eV) photoelectron spectra of pentafluorophenol, anisole, aniline and 2,6-dichlorophenol

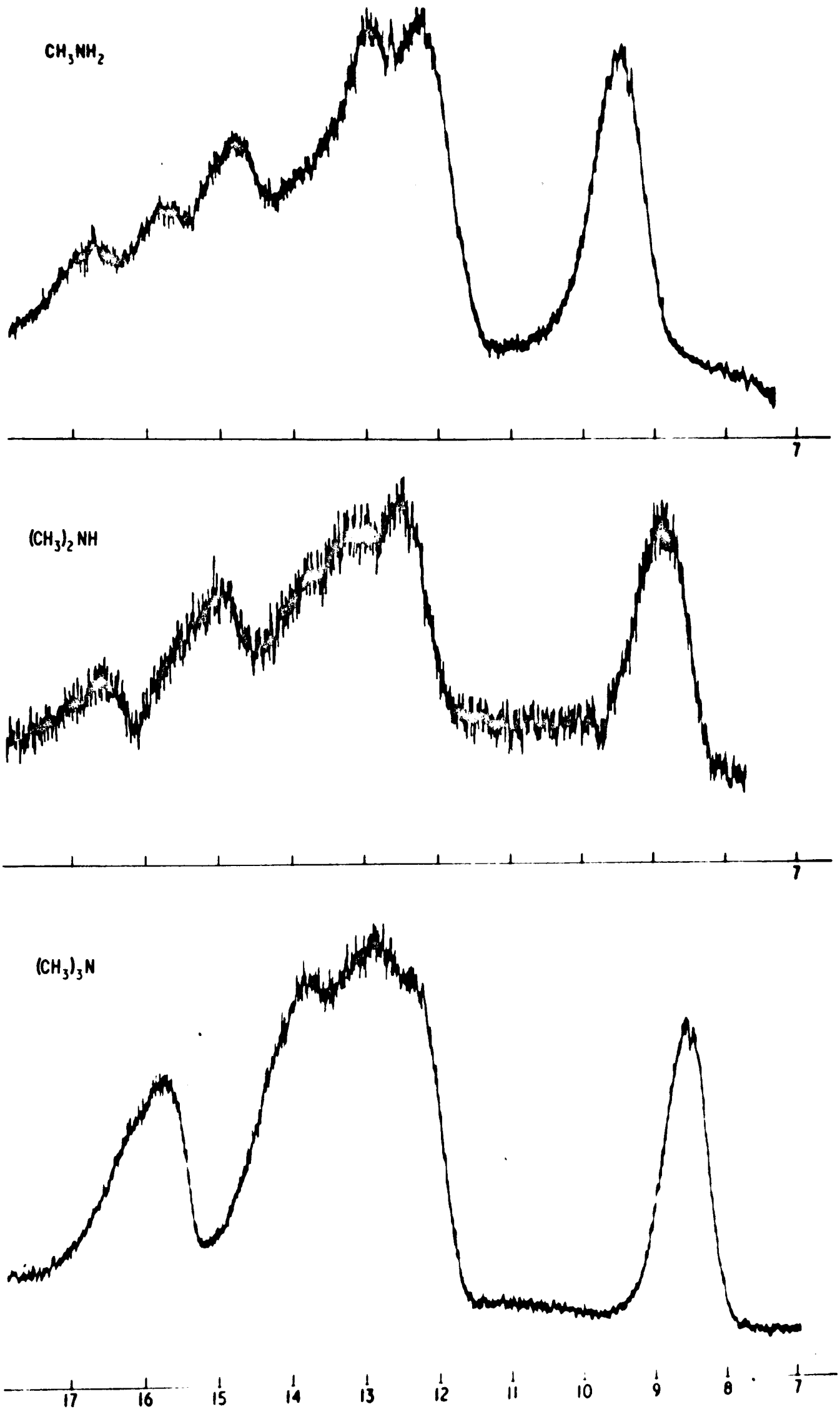


Fig.60 He I (21.22 eV) photoelectron spectra of methyl,-dimethyl,- and trimethyl-amine

In the pentafluoro derivatives, fine structure is more extensive, as is generally the case of fluorinated benzenes. The P.E. spectra of these were reported earlier,[47] but not with vibrational fine structure discernible. The analysis of the latter is included in the discussion (vide infra).

7.3 Discussion.

In the present series as in the earlier biphenyls and phenyl ethylenes, systematic changes are seen in the first group of bands (Figs. 53-58). The other groups exhibit extensive overlapping and correlation though the series of spectra is uncertain. Thus the spectral pattern is most conveniently rationalised in part only in terms of the semi-empirical framework of interaction π-moieties, which was formulated in Chapter V.

The interaction scheme is as outlined for phenyl ethylenes (6.3). The basis orbitals are the appropriate phenyl π-moieties, ψ_i (i=1-3), and the π symmetry MO of the heteroatom, $\psi_{x:}$ (x=N:,O:), i.e. nitrogen or oxygen "lone-pair". The secular equations are set up under the constraints previously introduced and the eigenvectors are again labelled π_i (i=1-4) in increasing energy; π_3 is essentially the basis orbital ψ_3. The eigenvalues are related to the experimental I.E.s via Koopmans' theorem.[1] Thus in the P.E. spectra the first group of bands is associated (in increasing I.E.) with the electronic states of the radical cations corresponding to the ejection of photoelectrons from the π MOs; In the case of aminobenzenes (Figs.53-55) π_i (i=2-4), and for oxybenzenes (Figs.56-58) π_i (i=3,4).

In the P.E. spectra of substituted anilines and anisoles there are striking differences in the first group of bands where non-bonded interactions are important. The considerable mixing between the basis orbitals precludes the identification of a band as the "lone-pair", though we may associate a band with an orbital possessing "a lot of $\psi_{x:}$ character". As the degree of interaction between the π-moieties decreases, these

"lone-pair" MOs, π_4 in N,N'-dimethyl anilines, π_2 in anisoles, acquire more basis orbital ($\psi_{x:}$) character and the I.E. tends towards the aliphatic basis value. In the aminobenzenes, in the extreme case of benzoquinuclidine (Fig. 55), the first band (I.E. = 8.35 eV) is associated with the nitrogen "lone-pair" (cf. quinuclidine[174]. I.E. 8.02 eV). In the case of 2,6-dimethyl anisole, an additional band (I.E. = 9.85 eV), π_2, appears in the first group as result of steric hindrance. These trends are best perceived in the correlation diagrams (Figs. 61,62).

In the interaction scheme, σ -orbitals are excluded. Intramolecular twisting destroys strict $\pi - \sigma$ distinction, however, the σ - effect on the first group of bands is a second order correction, and it was shown in Chapters V and VI that the exclusion is a reasonable approximation. In the phenyl ethylenes the matrix elements, corresponding here to $A_{x:}$, were close in magnitude to A_2 and, thus even ψ_1 could be omitted from the scheme as the effect on ΔE was not important. These are reasonable approximations only for the aminobenzenes as computations show. The splitting ΔE ($\equiv I_3 - I_1$) between the MOs Π_2 and Π_4, arises predominantly from the direct through space overlap between ψ_2 and $\psi_{N:}$, and can be used to determine the dihedral angles (θ).* The secular equations can again be simplified to yield

$$\Delta E = \varepsilon (\Pi_4 - \Pi_2) = \left[(A_{N:} - A_2)^2 + 4B_\theta^2 \right]^{\frac{1}{2}}$$

where

$$B_\theta' = B' \cos\theta \text{ and } B' = \langle \psi_{N:} | H | \psi_2 \rangle$$

The conformations are then inferred from the regressions which are defined as in Chapter VI using purely experimental data. In Table 20 the

---

*Footnote: θ is the angle between the planes containing the "lone-pair" and the phenyl carbon atoms.

dihedral angles are listed and compared to previous estimates. The agreement is good. Furthermore, it is inferred from the splitting ΔE, that in all the aminobenzenes studied, with the exception of the two in Table 20 (and benzoquinuclidine), no appreciable steric inhibition of resonance takes place.

In the oxybenzenes, the limitations of such a quantitative determination of conformations are realised. In the interaction scheme Ψ_1 must be included and the correct choice is now critical. These parameters, unlike Ψ_2 are not identified with certainty in the P.E. spectra of both the component molecules (ψ_1) and in the oxybenzenes(Π_1). On deviations from coplanarity $\pi - \sigma$ interaction is also more important. Thus a quantitative treatment is not attempted, but one can nevertheless discuss the steric factors qualitatively from comparison of P.E. spectra of corresponding molecules, e.g. 2,6 and 3,5-di-t-butyl phenols (Fig.57). It is inferred that in all phenols studied the hydroxyl group and benzene ring are coplanar, or nearly so. Similarly, in the anisoles only for the 2,6-dimethyl derivative is steric inhibition of resonance important.

In the oxybenzenes, the first band of the second group is assigned to the Π_2 MO. This is supported by analysis of the pentafluoro derivatives and 2,6-dichlorophenol (vide infra). In 2,6-dimethyl anisole the I.E. (9.85 eV) of the Π_2 band is low (c.f. I.E. of $(CH_3)_2O$=10.05 eV). In the hindered anilines (Table 18) such deviations on increase of non-coplanarity are also apparent. These deviations are probably the consequence of through-space interactions with the adjacent methyl groups, more pronounced in the oxygen and nitrogen than carbon Π -type orbitals, repelling the Π MOs to lower I.E.s in the former.

The stereochemistry of trivalent nitrogen atom in the aromatic amines has of long been of interest. The recent experimental evidence does unambiguously indicate that in aniline and N,N'-dimethyl aniline, the nitrogen atom is pyramidal. In Fig.55 the P.E. spectra of some

TABLE 20. Dihedral angles (θ) of substituted N,N'-dimethylanilines

N,N'-dimethylaniline derivative	E(eV)*	This work (deg)**	Other workers (deg)			
			a		d	e
N,N'-dimethylaniline	2.40	0				
2-methyl	1.50	55	50	60[b]	75	56
2,6'-dimethyl	1.00	69	68	65[c]	75	90

* $\pm$ .05 eV ** Estimated uncertainty $\pm 5^{o}$

$A_N \sim 8.5$ $A_2 \sim 9.0$

a Ref. 164 - Absorption Spectroscopy

b Ref. 163 - " "

c Ref. 170 - I.r. of Durenes

d Ref. 163 - Scale models, planar nitrogen

e Ref. 163 - Scale models, pyramidal nitrogen

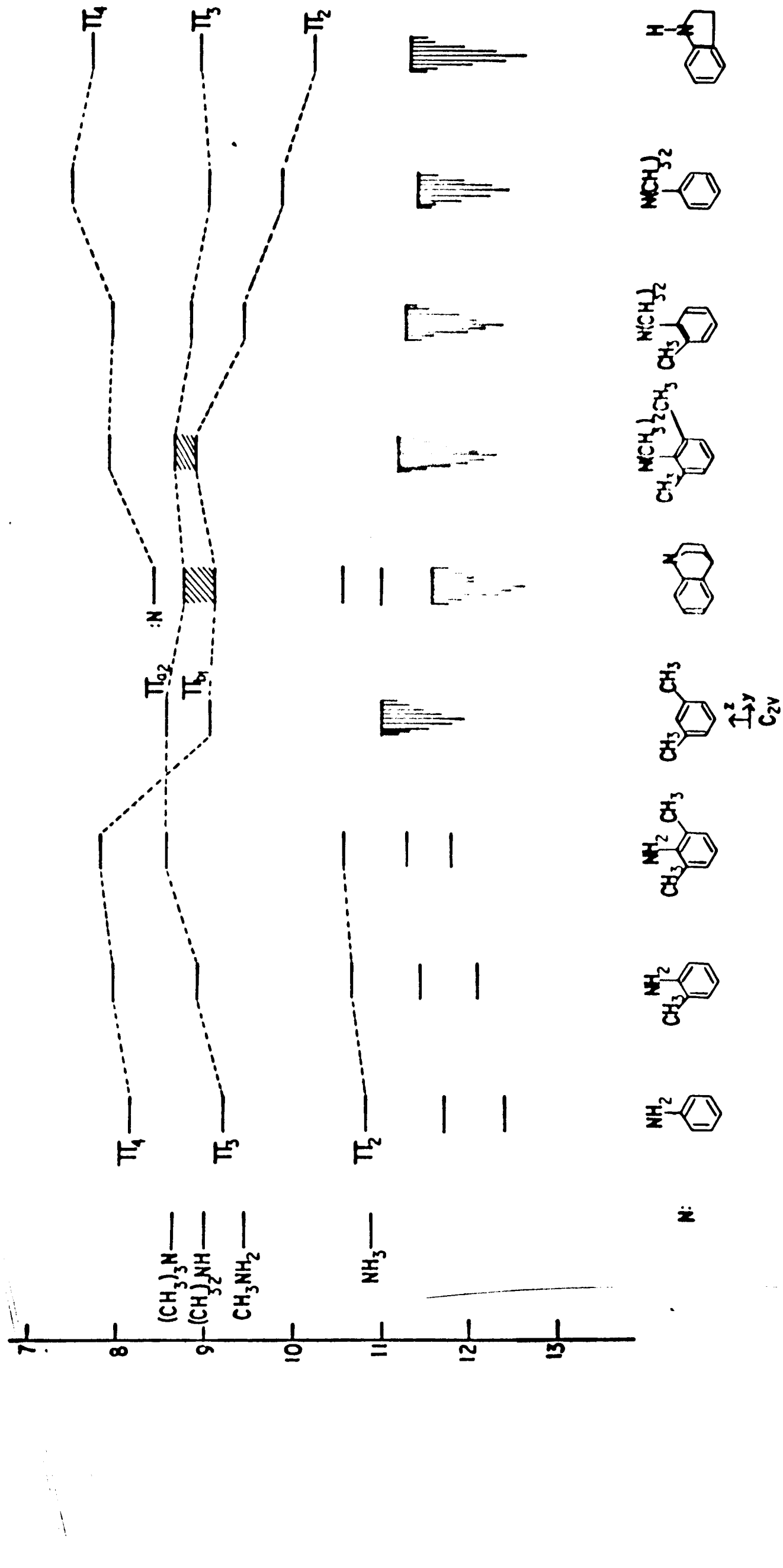
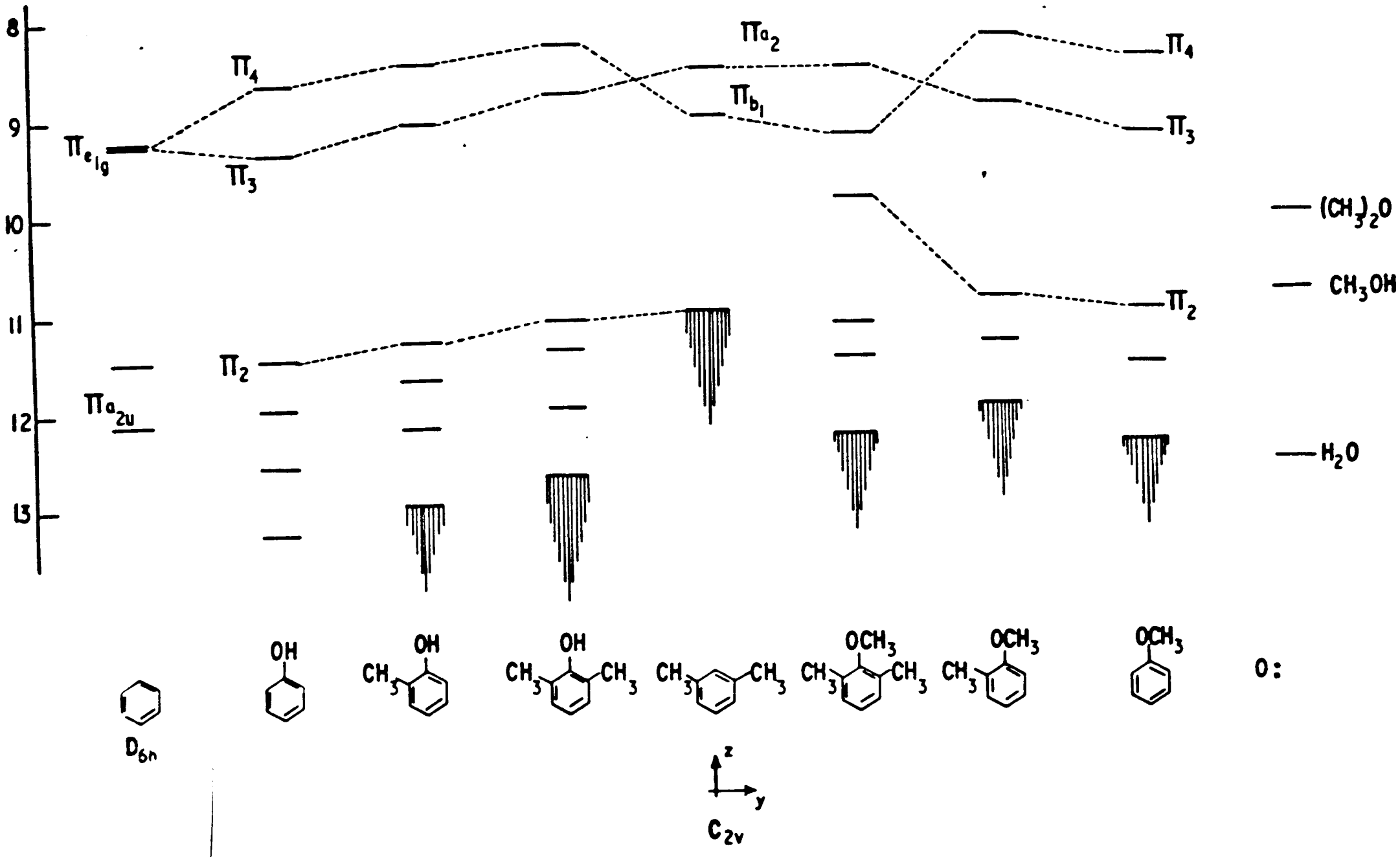


Fig.61 Correlation of ionisation energies

Fig.62 Correlation of ionisation energies



rigidly held aminobenzenes are shown. The constancy of the splittings ΔE (Table 18), incorporating basis set changes, suggest that even in systems where the nitrogen is held rigid, as in indoline, the geometry around the nitrogen is pyramidal, as in N,N'-dimethyl aniline.*

In the biphenyls and phenyl ethylenes the most efficient mode of steric strain relief is by angular rotation about the interannular bond. In the oxy and aminobenzenes, angular relief of strain is important, as indicated by the P.E. spectra. In the aminobenzenes one can evaluate approximately the distortion necessary for relief of strain by change of geometry at the nitrogen only.[175.] A small CNC angle ($\ll 90^{o}$) would be necessary, energetically unfavourable. Nevertheless, after twisting of the amino group the nitrogen may achieve further stabilisation by becoming more pyramidal. In the determination of the dihedral angles by this approach outlined above, this is neglected.

Such changes are reflected in the Franck-Condon envelopes. The latter often give an indication of the character of the orbital associated with those P.E. bands. Thus, "lone-pairs" have usually sharp bands (e.g. first band in water), if however, geometry change takes place on ionisation, as is the case in ammonia, the band is broad.[47.] In all the aminobenzenes studied (Figs. 53-55), the Franck-Condon profile of the first (Π_4) and third (Π_2) bands is broad, while of the second band (Π_3) is relatively sharper, as is the case of the first group of bands in oxybenzenes. It seems that the geometry change at the nitrogen on ionisation is important; the potential surfaces of the ground and ionic states will differ resulting in broad Franck-Condon envelopes.

---

* Footnote: Dewar derives an equation for the resonance integral (B') as function of the geometry at the nitrogen atom.[175.] Incorporating this into the expression for ΔE indicates that the difference between a planar (120^{o}) and experimental (116^{o}) geometry should be readily apparent.

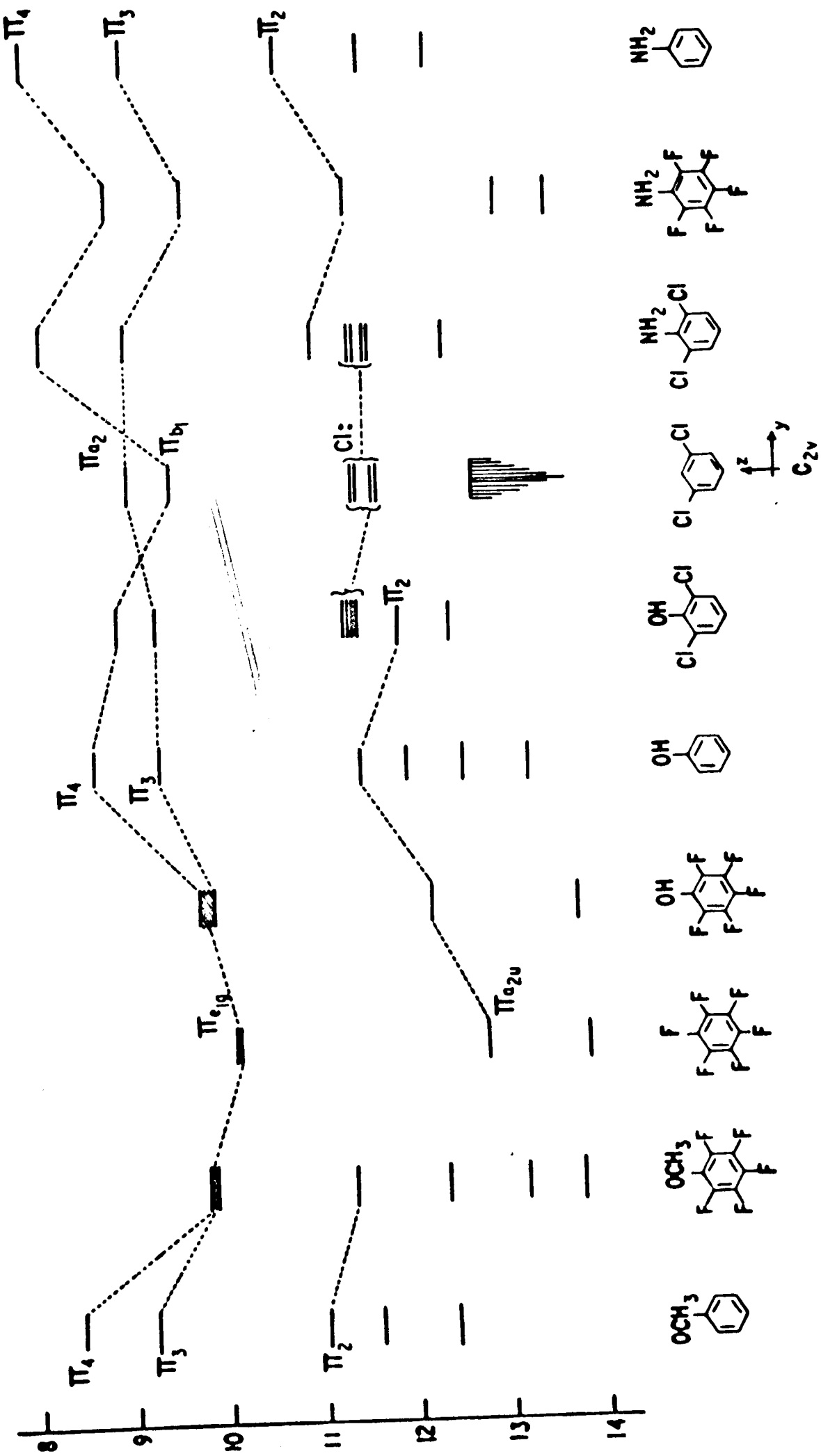


Fig.63 Correlation of ionisation energies

Pentafluoro derivatives

Fluorinated benzene derivatives often assist in the interpretation of the P.E. spectra. Vibrational fine structure is usually more extensive and the effect of substitution of hydrogen by fluorine results in much greater stabilisation of σ orbitals than π .[176.]

In the P.E. spectra (Fig. 59) one can identify the π_2 MO (Fig. 63) as a result of the "perfluoroeffect" and the Franck-Condon profile. The band bears a good deal of resemblance to the $\pi_{a_{2u}}$ band in the P,E. spectrum of hexafluorobenzene.[47.] In pentafluorophenol, three vibrational progressions are discernible on this band (I.E.=9.90 eV), ΔG=1450, 1100, and 600 cm^{-1}. The first band also has vibrational spacing of 1450 cm^{-1} discernible. In pentafluoroanisole and -aniline, all first three bands show evidence of excitation of vibrational quanta 1200 cm^{-1}. In all three pentafluoro molecules, several of the P.E. bands (I.E. $>$ 14 eV) show the quanta $\sim$1500 cm^{-1}. Comparison to hexafluorobenzene suggests that the vibrations excited are probably the C-F modes; 1488 and 559 cm^{-1} the totally symmetric stretch and breathing mode.

7.4 Concluding Remarks on Chapters V-VII.

It has been shown, that armed with the knowledge of the energy levels variation in a set of all combinations of structurally related molecules, electronic and steric effects can be separated and the relative importance of the latter demonstrated.

The simple theoretical framework developed was found satisfactory to explain the main features of the P.E. spectra and enabled the estimation of dihedral angles. The validity of this semi-empirical treatment is demonstrated in the reproducibility of the data using essentially the same parameters as apply to much simpler molecules.

Thus, photoelectron spectroscopy was indeed found the ideal tool for the investigation of steric inhibition of resonance, as these three Chapters show.

APPENDIX

1. In the Hückel-like scheme implemented in Chapters V-VII, the basis sets are the linear combinations of the semi-localised orthogonal π -MOs (LCMO). In the case of biphenyls, these are the phenyl moieties of the separated rings, R and S, labelled $\Psi i = 1-3$. (see 5.4). The LCMO are used as trial eigenfunctions in the variational treatment. The coefficients are adjusted to minimise the total energy subject to the condition that the resultant MOs are orthogonal. The coefficients are given by the set of simultaneous equations

$$\Sigma_i \quad C_{ij}[H_{ij} - \varepsilon \delta_{ij}]$$

and the eigenvalues by the solution of the determinant,

$$\left\| H_{ij} - \varepsilon \delta_{ij} \right\| = 0$$

within the framework of the Hückel approximations

$$H_{ij} = \varepsilon_i \delta_{ij} \text{ and } S_{ij} = \delta_{ij}.$$

For the biphenyl, the solution is facilitated by symmetry; the π -MOs are classified (S or A) w.r.t. the two symmetry planes σ_{xy} and σ_{xz} (Fig. 27) respectively. The Γ (SS) determinant becomes

$$\left\| \begin{matrix} A_1 + B - \varepsilon & B \\ B & A_2 + B - \varepsilon \end{matrix} \right\| = 0$$

yielding the eigenvalues of π_1 and π_3 (Fig. 27a) and the Γ (SA) determinant

$$\left\| \begin{matrix} A_1 - B - \varepsilon & - B \\ - B & A_2 - B - \varepsilon \end{matrix} \right\| = 0$$

yielding the π_2 and π_6 eigenvalues. The matrix elements A_i and B were defined in 5.4.

The eigenvectors will be of the form

$$\pi_1 = \frac{a}{\sqrt{2}} \left[\psi_1^R + \psi_1^S \right] + \frac{b}{\sqrt{2}} \left[\psi_2^R + \psi_2^S \right]$$

$$\pi_3 = \frac{b}{\sqrt{2}} \left[\psi_1^R + \psi_1^S \right] - \frac{a}{\sqrt{2}} \left[\psi_2^R + \psi_2^S \right]$$

where $a \gg b$ $(a^2 + b^2 = 1)$, and similarly for π_2 and π_6.

Thus for all practical purposes the resultant MOs will be very much as the π_i $i = 1 - 6$ MOs shown schematically in Fig. 27a. In, say, the case of biphenyl ($B \sim .7$), the coefficients are

$$\frac{a}{\sqrt{2}} \sim .69 \text{ and } \frac{b}{\sqrt{2}} \sim .16$$

When σ orbitals are included in the treatment, the second order perturbation on the π_i $i = 3$-6 levels will be

$$\frac{\left[B_{\pi-\sigma} \sin\theta \right]^2}{|A_\sigma - A_\pi|}$$

The data in Table 13 shows that this is not significant for the molecules listed. However, it was found that for the other biphenyls studied (Table 10), in particular the halobiphenyls, the treatment did not yield as consistent data; $\pi - \sigma$ mixing is then important.

11. Extended Hückel calculations were carried out using a standard program with parameters as used by Hoffmann.[177] This technique was initially chosen as the most convenient in view of the size of the molecules considered.

Calculations were carried out on biphenyl as function of the

dihedral angle and for number of the methyl substituted derivatives in their equilibrium conformation. A reasonable linear regression was obtained between the calculated eigenvalues of the π_i $i = 3 - 6$ MOs and the experimental I.E.s only for the molecules planar or near planarity. Calculation of ΔE for biphenyl as function of dihedral angle (θ) failed to reproduce the linear relationship between ΔE and cos θ observed experimentally. The calculations over-emphasise $\pi - \sigma$ mixing as the σ orbitals are predicted too high in energy.

Variation of the total energy as function of θ gave a shallow minimum in the vicinity of $\theta \sim 60^{\circ}$ for biphenyl; however, if the hydrogen exponent is changed to 1.3 a minimum around $\theta \sim 45^{\circ}$ is obtained.[178.] With 4,4'-bipyridyl a similar trend was observed. In 2,2'-bipyridyl, two minima were obtained; the equilibrium geometry in the trans co-planar conformation, with a subsidiary minimum at $\theta \sim 40 - 60^{\circ}$ cis conformation.

REFERENCES

1. T. Koopmans, Physica, 1934, 1, 104.
2. P.E. Cade, K.D. Sales and A.C. Wahl, J.Chem.Phys., 1966, 44, 1973.
3. W.G. Richards, Int.J.Mass Spectr. Ion Physics, 1969, 2, 419.
4. J. Franck, Trans.Faraday Soc., 1925, 21, 536.
5. E.U. Condon, Phys,Rev., 1928, 32, 858.
6. H. Eyring, J. Walter,G.E. Kimball, "Quantum Chemistry", Wiley, New York, 1944.
7. H. Sponer and R. Teller, Rev.Mod.Phys., 1941, 13, 75.
8. G. Herzberg, "Spectra of Diatomic Molecules", van Nostrand, New York, 1950.
9. G. Herzberg, "Infra-red and Raman Spectra", van Nostrand, New York, 1945.
10. G. Herzberg, "Electronic Spectra of Polyatomic Molecules", van Nostrand, New York, 1966.
11. D.W. Turner, Ann.Rev.Phys.Chem., 1970, 21, 107.

12a. J.A.R. Samson, "Techniques of Vacuum u.v. Spectroscopy", Wiley, New York, 1967.

12b. J.A.R. Samson, Appl.Optics, 1967, 6, 403.

13. D.C. Frost and C.A. McDowell, Proc.Roy.Soc., 1957, A241, 194.
14. L.J. Kieffer and G.H. Dunn, Rev.Mod.Phys., 1968, 38, 7.
15. S. Geltmann, Phys.Rev., 1956, 102, 171.
16. W.A. Chupka, J.Chem.Phys., 1959, 30, 191.
17. R.E. Fox, W.M. Hickam, W.M. Grove, D.J. and J.Kjeldaas, Rev.Sci.Instr., 1955, 26, 1101.

18a. E.N. Lassettre, A.S. Berman, S.M. Silverman and M.E. Krasnow, J.Chem.Phys., 1964, 40, 1232.

18b. E.N. Lassettre, A. Skerbele, M.A. Dillon and K.J. Ross, J.Chem.Phys., 1968, 48, 5066.

19. V.Y. Foo, C.E. Brion and J.B. Hasted, Proc.Roy.Soc., 1971, A322, 535.

20a. O. Klemperer, Reports Prog.Phys., 1965, 28, 77.

20b. R.S. Berry, Ann.Rev.Phys.Chem., 1969, 20, 357.

21a. K. Watanabe and E.C.Y. Inn, J.Opt.Soc.Amer., 1953, 43, 32.

21b. K. Watanabe, J.Chem.Phys., 1957, 26, 542.

22. M. Krauss, J.A. Walker and V.H. Dibeler, J.Res.Nat.Bur.Stand., 1968, A72, 281.

23a. G.R. Cook and P.H. Metzger, J.Chem.Phys., 1964, 41, 321.

23b. G.R. Cook, P.H. Metzger and M.Ogawa, J.Chem.Phys., 1966, 44, 2936.

24a. N.W. Reid, Int.J.Mass Spectr.Ion Physics, 1971, 6, 1.

24b. D.W. Turner, Adv.Phys.Org.Chem., 1966, 4, 31.

25. V. Cermak and Z. Herman, Coll.Czech.Chem.Comm., 1965, 30, 169.

26. H. Hotop and A. Niehaus, Int.J.Mass Spectr.Ion Physics, 1970, 5, 415.

27. V. Cermak, "Electron Spectroscopy", ed. D.A. Shirley, North-Holland, Amsterdam, 1972, 385.

28. E. Lindholm, Adv.in Chemistry, 1966, 58, 1.

29. F.I.Vilesov, B.L. Kurbatov and A.N. Terenin, Dokl.Acad.Nauk. SSSR, 1961, 138, 1329.

30a. D.W. Turner and M.I. Al-Jobury, J.Chem.Phys., 1962, 37, 3007.

30b. M.I. Al-Jobury and D.W. Turner, J.Chem.Soc., 1963, 5141.

31. A.J. Blake and J.H. Carver, J.Chem.Phys., 1967, 47, 1038.

32. D. Villarejo, J.Chem.Phys., 1968, 48, 4014.

33a. B. Brehm and E. von Puttkamer, Advan.Mass Spectrometry, 1968, 4, 591.

33b. A. Harvey, M-de-L.F.Monteiro and R.I.Reed, Int.J.Mass Spectr.Ion Physics, 1970, 4, 365.

33c. J.H.D. Eland, Int.J.Mass Spectr.Ion Physics, 1972, 8, 143.

34. D.L. Ames, J.P. Maier, F. Watt and D.W. Turner, Discuss. Faraday Soc., 1972, 54.

35. D.L. Judge and G.L. Weissler, J.Chem.Phys., 1968, 48, 4590.

36. B.S. Schneider and A.L. Smith, "Electron Spectroscopy", ed. D.A. Shirley, North-Holland, Amsterdam, 1972, 335.

37. J. Daintith, R. Dinsdale, J.P. Maier, D.A. Sweigart and D.W. Turner, "Molecular Spectroscopy", Institute of Petroleum, London, 1971, 16.

38. G. Herzberg, Quart.Rev., 1971, 25, 201.

39. K. Siegbahn, C. Nordling, A. Fahlman, R. Nordberg, K. Hamrin, J. Hedman, G. Johanson, T. Bergmark, S. Karlsson, I. Lindgren and B. Lindberg, "Electron Spectroscopy for Chemical Analysis", Nova Acta Regiae Societalis Scientiorum Uppsaliensis Ser.IV, Vol.20, 1967.

40. K. Siegbahn, C. Nordling, G. Johansson, J. Hedman, P.F. Heden, K. Hamrin, U. Gelius, A.J. Bergmark, L.O. Werme, R. Manne and Y. Baer, "ESCA Applied to Free Molecules", North Holland, Amsterdam, 1969.

41a. C.R.Brundle, Appl.Spectroscopy, 1971, 25, 8.

41b. "Electron Spectroscopy", ed. D.A. Shirley, North Holland, Amsterdam, 1972.

41c. J.M. Hollander and W.L. Jolly, Accounts Chem.Res., 1970, 3, 193.

42. C.R. Brundle, "Surface and Defect Properties of Solids", ed. M.W. Roberts and J.M. Thomas, The Chemical Society, London, 1972, 1, 171.

43a. D.M. Hercules, Anal.Chem., 1970, 42, 20.

43b. A.D. Baker, C.R. Brundle and M. Thompson, Chem.Soc.Rev., 1972, 1, 355.

43c. K. Siegbahn, Phil.Trans., 1970, A268, 33.

44. D.S. Urch, Quart.Rev., 1971, 25, 343.

45. K. Siegbahn, "Electron Spectroscopy", ed. D.A. Shirley, North-Holland, Amsterdam, 1972, 15.

46. C.C. Chang, Surface Science, 1970, 23, 283.

47. D.W. Turner, A.D. Baker, C. Baker and C.R. Brundle, "Molecular Photoelectron Spectroscopy", Wiley, London, 1970.

48a. P.A. Cox and A.F. Orchard, Chem.Phys.Letters, 1970, 7, 273.

48b. P.A. Cox, S. Evans and A.F. Orchard, ibid., 1972, 13, 386.

49. L.L. Lohr and M.B. Robin, J.Amer.Chem.Soc., 1970, 92, 7241.

50. G.V. Marr, "Photoionization Processes in Gases", Academic Press, London, 1967.

51. J.A.R. Samson, Phil.Trans., 1970, A268, 141.

52. U. Gelius, "Electron Spectroscopy", ed. D.A. Shirley, North-Holland, Amsterdam, 1972, 311.

53a. W. Thiel and A. Schweig, Chem.Phys.Letters, 1971, 12, 49.

53b. W. Thiel and A. Schweig, ibid., 1972, 16, 409.

54. L.L. Lohr, "Electron Spectroscopy", ed. D.A. Shirley, North-Holland, Amsterdam, 1972, 245.

55. W.C. Price, A.W. Potts and D.G. Streets, ibid., 187.

56. F. Wuilleumier and M.O. Krause, ibid., 259.

57. H.A. Bethe and E.E. Salpeter, "Quantum Mechanics of One and Two-Electron Atoms", Academic Press, New York, 1957.

58a. J.W. Cooper and R.N. Zare, J.Chem.Phys., 1968, 48, 942.

58b. R.S. Berry, B.J. Dalton and J.C. Tully, Phys.Rev., 1968, 176, 95.

58c. S.T. Manson, and J.W. Cooper, Phys.Rev.(A), 1970, 2, 2170.

59. A.D. Buckingham, B.J. Orr and J.M. Sichel, Phil.Trans., 1970, A268, 147.

60. F.A. Grimm, "Electron Spectroscopy", ed. D.A. Shirley, North-Holland, Amsterdam, 1972, 199.

61. J.A.R. Samson, J.Opt.Soc.Amer., 1972, 62, 856.

62. T.A. Carlson and A.E. Jonas, J.Chem.Phys., 1971, 55, 4913.

63a. J.W. McGowan, D.A. Vroom and A.R. Comeaux, J.Chem.Phys., 1969, 51, 5626.

63b. H. Harrison, J.Chem.Phys., 1970, 52, 901.

64. T.A. Carlson, G.E. McGuire, A.E. Jonas, K.L. Cheng, C.P, Anderson, C.C. Lu and B.P. Pullen, "Electron Spectroscopy", ed. D.A. Shirley, North-Holland, Amsterdam, 1972, 207.

65. A.E. Jonas, G.K. Schweitzer and F.A. Grimm, J.Elect.Spectr., 1972, 1, 29.

66. A. Niehaus and M.W. Ruf, Chem.Phys.Letters, 1971, 11, 55.

67. J.M. Sichel, Mol.Phys., 1970, 18, 95.

68. W.C. Price, "Molecular Spectroscopy", Institute of Petroleum, London, 1968, 221.

69a. A.J. Blake, J.L. Bahr, J.H. Carver and V. Kumar, Phil.Trans., 1970, A268, 159.

69b. A.L. Smith, Phil.Trans., 1970, A268, 169.

70. R.N. Dixon and S.E. Hull, Chem.Phys.Letters, 1969, 3, 367.

71. J. Raftery and W.G. Richards, Int.J.Mass Spectr.Ion Phys., 1971, 6, 269.

72. O. Edqvist, E. Lindholm, L.E. Selin and L. Åsbrink, Physica Scripta, 1970, 1, 25.

73. J.C. Lorquet and M. Desouter, Chem.Phys.Letters, 1972, 16, 136.

74. D.A. Shirley, Adv.Chem.Phys., 1972, in press.

75. J.A.R. Samson, Phys.Rev.Letters, 1969, 22, 693.

76. C.R. Brundle and D.W. Turner, Proc.Roy.Soc., 1968, A307, 27.

77a. H.M. Rosenstock, Int.J.Mass Spectr.Ion Phys., 1971, 7, 33.

77b. J.M. Hollas and T.A. Sutherley, Molec.Phys., 1971, 22, 213.

77c. R.N. Dixon, G. Duxbury, M. Horan and J. Rostas, Molec.Phys., 1971, 22, 977.

78. D.W. Turner, Phil.Trans., 1970, A268, 7.

79. L. Åsbrink, Chem.Phys.Letters, 1970, 7, 549.

80. H.A. Jahn and E. Teller, Proc.Roy.Soc., 1937, A161, 220.

81. A.D. Baker, C. Baker, C.R. Brundle and D.W. Turner, Int.J.Mass Spectr.Ion Phys., 1968, 1, 285.

82. H.J. Lempka, A.W. Potts, D.G. Streets and W.C. Price, Phil. Trans., 1970, A268, 59.

83. W.E. Bull, B.P. Pullen, F.A. Grimm, W.E. Moddemann, G.K. Schweitzer and T.A. Carlson, Inorg.Chem., 1970, 9, 2474.

84a. R. Renner, Z.Physik, 1934, 92, 172,

84b. G. Herzberg and E. Teller, Z.Physik.Chem., 1933, B21, 410.

85. J.C. Green, M.L.H. Green, P.J. Joachim, A.F. Orchard and D.W. Turner, Phil.Trans., 1970, A268, 111.

86. E. Heilbronner, XXIII Int.Cong.Pure and Appl.Chem., Butterworths, London, 1971, 7, 9 and refs. cited therein.

87. A. Hamnett and A.F. Orchard, "Electronic Structure and Magnetism of Inorganic Compounds", The Chem.Soc., London, 1972, 1, 1.

88. S.D. Worley, Chem.Revs., 1971, 71, 295.

89a. C.R. Brundle and M.B. Robin, "Determination of Organic Structures by Physical Methods", ed. F. Nachod and G. Zuckerman, Academic Press, New York, 1971, 3, 1.

89b. A.D. Baker, Accounts Chem.Res., 1970, 3, 17.

90a. M.I. Al-Jobury and D.W. Turner, J.Chem.Soc., 1964, 4434.

90b. M.I. Al-Jobury, D.P. May and D.W. Turner, J.Chem.Soc., 1965, 616.

90c. M.I. Al-Jobury, D.P. May and D.W. Turner, J.Chem.Soc., 1965, 6350.

90d. T.N. Radwan and D.W. Turner, J.Chem.Soc(A)., 1966, 85.

90e. M.I. Al-Jobury and D.W. Turner, J.Chem.Soc.(B)., 1967, 373.

91a. L. Åsbrink, O. Edqvist, E. Lindholm and L.E. Selin, Chem.Phys. Letters, 1970, 5, 192.

91b. D.C. Frost, J.S. Sandhu and D.A. Vroom, Nature, 1966, 212, 604.

92. R.B. Cairns, H. Harrison and R.I. Schoen, Appl.Optics, 1970, 9, 605.

93. A.W. Potts, T.A. Williams and W.C. Price, Discuss.Faraday Soc., 1972, 54.

94. D.E. Eastman, "Electron Spectroscopy", North-Holland, Amsterdam, 1972, 487 and references cited therein.

95a. M.O. Krause, Chem.Phys.Letters, 1971, 10, 65.

95b. M.O. Krause and F. Wuilleumier, Phys.Letters, 1971, A35, 341.

96. D.W. Turner, Proc.Roy.Soc., 1968, A307, 15.

97. J.A.R. Samson and R.B. Cairns, Phys.Rev., 1968, 173, 80.

98. D.W. Turner and D.P. May, J.Chem.Phys., 1966, 45, 471.

99. W.N. Delgass, T.R. Hughes and C.S. Fadley, Catalysis Rev., 1970, 4, 179.

100. O. Klemperer, "Electron Optics", Cambridge University Press, 1953.

101. J.H.D.Eland and C.J. Danby, J.Sci.Instrum., 1968, 1, 406.

102a. J.A. Simpson, Rev.Sci.Instrum., 1964, 35, 1968.

102b. D.A. Sweigart and J. Daintith, Sci.Prog.Oxf., 1971, 59, 325.

102c. G.R. Branton, D.C. Frost, T. Makita, C.A. McDowell and I.A. Stenhouse, Phil.Trans., 1970, A268, 77.

103. R.G. Albridge, "Physical Methods of Chemistry", ed. A. Weissberger and B.W. Rossiter, Wiley, 1972, Vol.1, Part I, and references cited therein.

104. J. Berkowitz, J.Chem.Phys., 1972, 56, 2766.

105. J.A.R. Samson, Rev.Sci.Instrum., 1969, 40, 1174.

106. L. Åsbrink and J.W. Rabalais, Chem.Phys.Letters, 1971, 12, 182.

107a. D.W. Turner, Nature, 1967, 213, 795.

107b. D.W. Turner, "Molecular Spectroscopy", ed. W. Hepple, Institute of Petroleum, London, 1968, 209.

108. D.R. Lloyd, J.Phys.(E), 1970, 3, 629.

109. D. Gokhale and W.L. Jolly, Inorg.Synth., 1967, 9, 56.

110. W.C. Price and T.R. Passmore, Discuss.Faraday Soc., 1963, 35, 232.

111. H. Basch, M.B. Robin, N.A. Keubler, C. Baker and D.W. Turner, J.Chem.Phys., 1969, 51, 52.

112. C.M. Humphries, A.D. Walsh and P.A. Warsop, Discuss.Faraday Soc., 1963, 35, 148.

113. I.H. Hillier and V.R. Saunders, Trans.Faraday Soc., 1970, 66, 2401.

114. Y.P. Varshni, Rev.Mod.Physics, 1957, 29, 664.

115. W.S. Benedict and E.K. Plyler, Can.J.Phys., 1957, 35, 1235.

116. R.E. Weston Jr., J.Amer.Chem.Soc., 1954, 76, 2645.

117. J.M. Lehn and B. Munsch, Molec.Phys., 1972, 23, 91.

118a. A.D. Walsh, J.Chem.Soc., 1953, 2296.

118b. J.A. Pople and G.A. Segal, J.Chem.Phys., 1966, 44, 3289.

119. W.L. Smith and P.A. Warsop, Trans.Faraday Soc., 1968, 64, 1165.

120. A.D. Walsh and P.A. Warsop, Trans.Faraday Soc., 1961, 57, 345.

121. D.B. Boyd and W.N. Lipscomb, J.Chem.Phys., 1967, 46, 910.

122. A.W. Potts and W.C. Price, Proc.Roy.Soc., 1972, A326, 181.

123. G.R. Branton, D.C. Frost, C.A. McDowell and I.A. Stenhouse, Chem.Phys.Letters, 1970, 5, 1.

124. R. Moccia, J.Chem.Phys., 1964, 40, 2176.

125. P.J. Bassett, D.R. Lloyd, I.H. Hillier and V.R. Saunders, Chem.Phys.Letters, 1970, 6, 253.

126. J.C. Green, D.I. King and J.H.D. Eland, Chem.Comm., 1970, 1121.

127. Y. Wada and R.W. Kiser, Inorg.Chem., 1964, 3, 174.

128. C.G. Brundle, M.B. Robin and G.R. Jones, J.Chem.Phys., 1970, 52, 3383.

129. See, for example, E.L. Eliel, "Stereochemistry of Carbon Compounds", McGraw-Hill, New York, 1962.

130. K. Mislow, Trans.New York Acad.Sci., 19(4), 298.

131. K. Mislow, Ann.New York Acad.Sci., 1961, 93, 459.

132. A. Unanue and P. Bothorel, Bull.Soc.Chim.France, 1966, 1640.

133. S. Brownstein, J.Amer.Chem.Soc., 1958, 80, 2300.

134. N. Boden, J.W. Emsley, J. Feeney and L.H. Sutcliffe, Molec. Phys., 1964, 8, 467.

135. R.M. Barrett and R. Steele, J.Molec.Structure, 1972, 11, 105.

136. G.H. Beaven and D.M. Hall, J.Chem.Soc., 1956, 4637.

137. H. Suzuki, Bull.Chem.Soc., Japan, 1959, 32, 1340, and references listed therein.

138. C.E. Castro, L.J. Andrews and R.M. Keefer, J.Amer.Chem.Soc., 1958, 80, 2322.

139. E.A. Johnson, "Steric Effects in Conjugated Systems", ed. G.W. Gray, Butterworths, London, 1958, 174.

140. "Tables of Interatomic Distances", ed. L.E. Sutton, Chem.Soc., 1958.

141. A. Almeningen and O. Bastiansen, Kgl.Norske, Vid.Selsk.Skr., 1958, No.4.

142. A. Golebiewski and A. Parczewski, Z.Naturforsch., 1970, 25A, 1710 and references cited therein.

143. A. Almeningen, A.O. Hartmann and H.M. Seip, Acta.Chem. Scand., 1968, 22, 1013.

144. A.D. Baker, D.P. May and D.W. Turner, J.Chem.Soc.B., 1968, 22.

145. J.P. Maier and D.W. Turner, unpublished work.

146. F. Brogli and E. Heilbronner, Theor.Chim.Acta, in press.

147. A. Streitwieser, Jr., "Molecular Orbital Theory for Organic Chemists", Wiley, New York, 1961.

148. M.J.S. Dewar, E. Haselbach and S.D. Worley, Proc.Roy.Soc.A. 1970, 315, 431.

149. J.H.D. Eland, Int.J.Mass Spectr.Ion Physics, 1969, 2, 471.

150. G.E. Coates and L.E. Sutton, J.Chem.Soc., 1942, 567.

151. R.N. Jones, J.Amer.Chem.Soc., 1943, 65, 1818.

152. G.B. Bachman and R.W. Finholt, J.Amer.Chem.Soc., 1948, 70, 622.

153. L.H. Schwartzman and B.B. Corson, J.Amer.Chem.Soc., 1956, 78, 322.

154. W.G. Fateley, G.L. Carlson and F.E. Dickson, Appl.Spectroscopy, 1968, 22, 650.

155. Gurudata, J.B. Stothers and J.D. Talman, Canad.J.Chem., 1967, 45, 731.

156. E.A. Braude and F. Sondheimer, J.Chem.Soc., 1955, 3773.

157. H. Suzuki, Bull.Chem.Soc.Japan, 1960, 33, 619.

158. G. Favini and M. Simonetta, Theor.Chim.Acta, 1963, 1, 294.

159. J.N. Murrell, "Theory of the Electronic Spectra of Organic Molecules", Chapman and Hall, London, 1971.

160. J. Daintith, J.P. Maier, D.A. Sweigart and D.W. Turner, "Electron Spectroscopy", North-Holland, Amsterdam, 1972, 289.

161. J.W. Smith, "Steric Effects in Conjugated Systems", ed. G.W. Gray, Butterworths, London, 1958, 141., and references cited therein.

162. W.R. Remington, J.Amer.Chem.Soc., 1945, 67, 1838.

163. H.B. Klevens and J.R. Platt, J.Amer.Chem.Soc., 1949, 71, 1714.

164. B.M. Wepster, "Progress in Stereochemistry", Butterworths, London, 1958, 2, 99.

165a. E.C. Lim and S.K. Chakrabarti, J.Chem.Phys., 1967, 47, 4726.

165b. M. Kasha and H.R. Rawls, Photochem.and Photobiol., 1968, 7, 561.

166. M.M. Bursey and M.K. Hoffman, J.Amer.Chem.Soc., 1969, 91, 5023.

167a. P.C. Lauterbur, J.Amer.Chem.Soc., 1961, 83, 1846.

167b. I. Yamguchi, Bull.Chem.Soc.,Japan, 1961, 34, 744.

168. J. Heidberg, J.A. Weil, C.A. Janusonis and J.K. Anderson, J.Chem.Phys., 1964, 41, 1033.

169. T. Kojima, J.Phys.Soc., Japan, 1960, 15, 284.

170. A.R. Katritzky and R.D. Topsom, Ang.Chem.internat.edit., 1970, 9, 87.

171. L.V. Vilkov and T.P. Timasheva, Dokl.Akad.Nauk.SSSR., 1965, 161, 351.

172. J.C.D. Brand, D.R. Williams and T.J. Cook, J.Mol.Spectry., 1966, 20, 359.

173. D.C. Lister and J.K. Tyler, Chem.Comm., 1966, 152.

174. P. Bishof, J.A. Hashmall, E. Heilbronner and V. Hornung, Tetrahedron Letters, 1969, 46, 4025.

175. M.J.S. Dewar, "The Molecular Orbital Theory of Organic Chemistry", McGraw Hill, New York, 1969.

176. C.R. Brundle, M.B. Robin and N.A. Kuebler, J.Amer.Chem.Soc., 1972, 94, 1466.

177a. R. Hoffmann, J.Chem.Phys., 1963, 39, 1397.

177b. R. Hoffmann and W.N. Lipscomb, J.Chem.Phys., 1962, 36, 2179 and 3489.

178. A. Imamura and R. Hoffmann, J.Amer.Chem.Soc., 1968, 90, 5379.